UNIVERSIDADE DE SÃO PAULO
Instituto de Ciências Matemáticas e de Computação

On the application of Machine Learning and Complex Networks to Neuroscience

Caroline Lourenço Alves

Tese de Doutorado do Programa de Pós-Graduação em Ciências de Computação e Matemática Computacional (PPG-CCMC)

ICMC USP SÃO CARLOS

Caroline Lourenço Alves

On the application of Machine Learning and Complex Networks to Neuroscience

Doctoral dissertation submitted to the Instituto de Ciências Matemáticas e de Computação – ICMC-USP, in partial fulfillment of the requirements for the degree of the Doctorate Program in Computer Science and Computational Mathematics. *EXAMINATION BOARD PRESENTATION COPY*

Concentration Area: Computer Science and Computational Mathematics

Advisor: Prof. Dr. Francisco Aparecido Rodrigues

USP – São Carlos
March 2023

Ficha catalográfica elaborada pela Biblioteca Prof. Achille Bassi
e Seção Técnica de Informática, ICMC/USP,
com os dados inseridos pelo(a) autor(a)

L892o

Lourenço Alves, Caroline
On the application of Machine Learning and Complex Networks to Neuroscience / Caroline Lourenço Alves; orientador Francisco Aparecido Rodrigues. -- São Carlos, 2023.
211 p.

Tese (Doutorado - Programa de Pós-Graduação em Ciências de Computação e Matemática Computacional) -- Instituto de Ciências Matemáticas e de Computação, Universidade de São Paulo, 2023.

1. Machine Learning and deep learning. 2. Complex Network . 3. Mental disorders . 4. Psychedelics. 5. EEG and fMRI data. I. Rodrigues, Francisco Aparecido , orient. II. Título.

Bibliotecários responsáveis pela estrutura de catalogação da publicação de acordo com a AACR2:
Gláucia Maria Saia Cristianini - CRB - 8/4938
Juliana de Souza Moraes - CRB - 8/6176

Caroline Lourenço Alves

Aplicações de aprendizagem de máquina e redes complexas à neurociência

Tese apresentada ao Instituto de Ciências Matemáticas e de Computação – ICMC-USP, como parte dos requisitos para obtenção do título de Doutora em Ciências – Ciências de Computação e Matemática Computacional. *EXEMPLAR DE DEFESA*

Área de Concentração: Ciências de Computação e Matemática Computacional

Orientador: Prof. Dr. Francisco Aparecido Rodrigues

USP – São Carlos
Março de 2023

With much love, to my parents: my heroes;
With great affection my sister and brother-in-law, whose strength have always inspired me;
And for my nephew, whose smile brightens my day.

ACKNOWLEDGEMENTS

I want to thank my supervisor, Professor Francisco, who has been supervising me since I graduated with my Master's degree, to whom I owe everything I have learned since then, and for all the suggestions, support, and conversations about this work. I admire his work and person very much and am very grateful to have known him. He has changed my path for the better.

I want to thank Professor Thielemann, a woman I greatly admire for her strength and work, which allowed me to work in a renowned laboratory in Germany, which was undoubtedly the most significant opportunity in my career. I owe her fruitful suggestions for my work and incentives to learn new subjects.

I want to thank my friend Manuel Ciba from the Biomens lab. I appreciate him for his person and the suggestions, the support, the ideas in my work and also for encouraging me to include research on psychedelics in my work, a topic to which I have developed a real fascination. And also for all the help and friendship during my stay. I will always be very grateful to him for that.

I want to thank my dear sister, of whom I am very proud and admire. Despite a hectic schedule, she helped me to correct this work.

I want to thank my parents, Itamar and Eunice, for constantly investing in my education and supporting me throughout my life. They are my heroes, and I consider myself lucky to have them as my parents.

I want to thank my friend Aruane who has helped me a lot in my work and I would like to work with her in the future. I would also like to thank her for her support and friendship throughout my thesis.

I want to thank also like to thank Kirstin Rooster for her suggestions and help with the present work and I would like to work with her in the future.

I want to thank Thaise, who contributed to this work's biological interpretation, and Joel for their help. Although I met them only briefly, I already consider them friends and intend to do further work with them.

I want to thank Professor Eduardo Pondé de Sena for all the help, and I hope to do further work with him.

I want to thank Dr. Patricia de Carvalho Aguiar for all the help and the opportunity to be part of the dystonia FAPESP project, which I'm delighted about.

I want to thank my friend Nahid for kindly receiving me in Germany.

I would like to thank Nathalie Zech, who helped me a lot herein Germany. With all of its hurdles, the stay was only feasible with her.

I want to thank Guilherme Ferraz Arruda for his help and suggestions at the beginning of this research.

I want to thank Professor João do Espírito Santo Batista Neto, who supervised me at the beginning of this Ph.D.

I want to thank all my friends, in particular Xavante and Pluie, for all the support that they gave me during these years.

I want to thank all the teachers and professors who contribute to my education.

I want to thank CAPES for my Ph.D. scholarship and the Aschaffenburg University of Applied Sciences for their support during my Ph.D. and my stay in Germany.

Finally, I want to thank all the employees of the University of São Paulo and the Aschaffenburg University of Applied Sciences.

"In the midst of hate, I found there was, within me, an invincible love.
In the midst of tears, I found there was, within me, an invincible smile.
In the midst of chaos, I found there was, within me, an invincible calm.
I realized, through it all, that…
In the midst of winter, I found there was, within me, an invincible summer.
And that makes me happy.
For it says that no matter how hard the world pushes against me, within me, there's something stronger – something better, pushing right back. "
(Albert Camus)

RESUMO

ALVES, C. L. **Aplicações de aprendizagem de máquina e redes complexas à neurociência**. 2023. 211 p. Tese (Doutorado em Ciências – Ciências de Computação e Matemática Computacional) – Instituto de Ciências Matemáticas e de Computação, Universidade de São Paulo, São Carlos – SP, 2023.

A mineração de dados e a descoberta de conhecimentos é uma área de estudo, com aplicações em diferentes áreas, tais como na medicina, e seus métodos têm provado ser muito eficazes na realização de diagnósticos automatizados, ajudando na tomada de decisões pelas equipes médicas. Para além da utilização da extração de dados, os dados médicos podem ser representados por redes complexas. Por exemplo, no caso do cérebro, as regiões corticais podem representar vértices num gráfico e as ligações podem ser definidas através de atividades corticais. Assim, podemos comparar a estrutura cerebral de pacientes saudáveis com a de pacientes com distúrbio mental, a fim de definir métodos de diagnóstico e de obter conhecimentos sobre a forma como a estrutura do cérebro está relacionada com mudanças comportamentais e neurológicas. O presente trabalho visava desenvolver um modelo de previsão capaz de melhorar o diagnóstico de doenças mentais como a esquizofrenia, a doença de Alzheimer e o transtorno do espectro autista , utilizando séries temporais obtidas a partir do eletroencefalograma e da ressonância magnética funcional. E, além disso, verificar se essa mesma metodologia é capaz de detectar automaticamente alterações nas redes funcionais cerebrais induzidas pela ayahuasca e pela N,N-Dimetiltriptamina, uma vez que os psicodélicos podem ter um potencial terapêutico para algumas doenças mentais .

Em geral, o modelo preditivo desenvolvido para as doenças aqui estudadas foi superior ao encontrado na literatura. Quanto ao estudo dos psicodélicos, foram adquiridos novos conhecimentos sobre os seus mecanismos. Além disso, a metodologia do presente trabalho determinou quais medidas de redes complexas são mais eficazes na captura de alterações cerebrais, incluindo novas métricas desenvolvidas pelo autor. E estas novas métricas foram fundamentais no estudo do transtorno do espectro autista e das substâncias psicodélicas. Finalmente, a mesma metodologia aqui aplicada pode ser útil na interpretação de séries temporais de eletroencefalograma e ressonância magnética funcional de outras doenças e de sujeitos que consumiram outros psicodélicos ou outros medicamentos (tais como antidepressivos) e podem ajudar a obter uma compreensão detalhada nas alterações das redes funcionais cerebrais resultantes da administração de medicamentos.

Palavras-chave: Aprendizado de máquina, Aprendizado profundo, Redes complexas, Doenças neurológicas, psicodélicos, Eletroencefalograma, Ressonância magnética funcional.

ABSTRACT

ALVES, C. L. **On the application of Machine Learning and Complex Networks to Neuroscience**. 2023. 211 p. Tese (Doutorado em Ciências – Ciências de Computação e Matemática Computacional) – Instituto de Ciências Matemáticas e de Computação, Universidade de São Paulo, São Carlos – SP, 2023.

Data mining and knowledge discovery is a research area with applications in various fields, such as medicine. Data mining methods have proven to be very effective in making automated diagnoses and help medical teams in decision making. In addition to using data mining, medical data can be represented by complex networks. In the case of the brain, for example, brain regions can be represented as vertices of a graph and the neural activity between the regions define the connection.

In this way, we can compare the brain structure of healthy patients with that of patients with mental disorders to define diagnostic methods and gain insights into how brain structure is related to behavioral and neurological changes.

The aim of the present work is to develop a predictive model that can improve the diagnosis of mental disorders such as schizophrenia, Alzheimer's disease, and autism using electroencephalogram and functional magnetic resonance imaging data. In addition, it is to be tested whether the same workflow is capable of automatically detecting the influence of neurally active substances on functional changes in network structure. Because psychedelics are thought to have therapeutic potential for some mental disorders, data from experiments with ayahuasca and N,N-dimethyltryptamine were considered as examples.

In general, the predictive models developed for the diseases were not only able to automatically detect the functional changes, but were also superior to the models presented in the literature.

Regarding the investigation of psychedelics, it could be shown that the same workflow is equally suitable to automatically detect functional changes. Furthermore, by interpreting the models and metrics, new insights into the mechanisms of action of the substances could be gained.

In addition, the present work determined which complex network measures are most effective in detecting brain changes, including new metrics developed by the author. The new metrics proved to be relevant to the studies of autism and psychedelics. It is likely that the methodology used here can be applied to other diseases and substances (e.g., antidepressants) due to its flexibility and adaptability to EEG and fMRI time series data.

Keywords: Machine learning, deep learning, Complex Networks, Neurological Diseases, psychedelics, Electroencephalogram, Functional magnetic resonance imaging.

LIST OF FIGURES

LIST OF TABLES

LIST OF ABBREVIATIONS AND ACRONYMS

2-MTHBC	2-methyl-tetrahydro-beta- carboline
5-MeO-DMT	5-methoxy-DMT
ABIDE	Brain Imaging Data Exchange
Acc.	Accuracy
AD	Alzheimer's disease
ADHD	Attention-Deficit/Hyperactivity Disorder
APL	average path length
ASD	Autism Spectrum Disorders
AUC	Area under the ROC curve
BA	Brodmann Areas
BASC	Bootstrap Analysis of Stable Clusters
BC	betweenness centrality
BM	Biweight Midcorrelation
BOLD	Blood Oxygenation Level Dependent
CC	closeness centrality
CNN	Convolution Neural Networks
COBRE	The Centers of Biomedical Research Excellence
DL	deep learning
DMN	Default Mode Network
DMT	N,N-Dimethyltryptamine
DMT-NO	DMTN-oxide
DSM	*Diagnostic and Statistical Manual of Mental Disorders*
DTI	Diffusion Tensor Imaging
EBC	Edge betweenness community
EC	eigenvector centrality
ED	entropy degree
EEG	electroencephalogram
EPSCs	excitatory postsynaptic currents
ER	endoplasmic reticulum
FC	Fastgreedy community
fMRI	functional magnetic resonance imaging

GC	Granger causality
GL	Graphical Lasso method
IAA	indoleacetic acid
IC	Infomap community
ICA	independent component analysis
ICD-10	*International Statistical Classification of Diseases and Related Health Problems* (10th Revision)
Infomax	maximum information
Knn	average degree of nearest neighbors
L-BFGS	Limited-memory Broyden Fletcher Goldfarb Shanno
LPC	Label propagation community
LR	logistic regression
LSD	lysergic acid diethylamide
LSP	Left Superior Parietal Lobe
LSTM	Long Short-Term Memory neural networks
LW	Ledoit-Wolf shrinkage
MC	Multilevel community
MDMA	3,4-methylenedioxymethamphetamine
MI	Mutual Information
ML	Machine Learning
MLP	multilayer perceptron
MSE	Mean Square Error
NB	Naive bayes
NINCDS-ADRDA	Related Disorders Association
NMT	N-methyltryptamine
PC	Pearson Correlation
PCC	Posterior Cingulate Cortex
PCP	Preprocessed Connectomes Project
PFC	prefrontal cortex
PMC	Primary Motor Cortex
PTSD	Post-Traumatic Stress Disorder
RBF	gaussian
RF	Random forest
ROC	receiver operating characteristic
ROI	Brain regions of interest
SC	Spearman Correlation
SCC	Sparce Canonical Correlation analysis

SGD	stochastic gradient descent with linear models classifier
SHAP	SHapley Additive ExPlanations
Sig-1R	sigma 1 receptor
SMA	Supplementary Motor Area
SMD	second moment degree
SPC	Spinglass community
SPECT	single photon emission computed tomography
SVM	support vector machine
TD	typical development
TE	Transfer Entropy
THH-OH	7-hydroxy-tetrahydroharmine
UPR	Protein Response
XGBoost	extreme Gradient Boosting classifier

CONTENTS

CHAPTER

1

INTRODUCTION

"We dream the flight but we fear the height. To fly one needs to have the courage to face the void. The flight can only happen in the void. The void is the space for freedom, the absence of certainties. But that is what we fear: not having certainties. That is why we change the flight for cages. Cages are the place where certainties live"

— Fyodor Dostoyevsk, *Brothers Karamazov*

From these studies, MD (mainly depressive and anxiety disorders) has appeared in the classification of the leading causes of DALY in the world (WHITEFORD *et al.*, 2013; VIGO; THORNICROFT; ATUN, 2016; BONADIMAN *et al.*, 2017). For more details on the measures used in this study, see Appendix A.

Overall, in the 2019 GBD (NAGHAVI *et al.*, 2017), more than one billion people worldwide have been affected by MD, representing about 16% of the world's population (REHM; SHIELD, 2019). This amount of the population can be seen in Figure 1, below is a map with the percentage of people with MD around the world.

Furthermore, during the coronavirus pandemic, the number of reported cases of mental illness in India, for example, increased by 20% (LOIWAL, 2020; KUMAR; NAYAR, 2021), affecting the mental health of individuals in many other nations (LIU *et al.*, 2020; EZPELETA *et al.*, 2020; BÄUERLE *et al.*, 2020) due to social isolation and fear in the face of a worldwide epidemic.

Moreover, most mental illnesses are associated with an increased risk of attempted suicide (HOERTEL *et al.*, 2015). For example, in (CAVANAGH *et al.*, 2003), through analysis of medical repositories of autopsy studies of suicide-related deaths, they suggest that up to 90% of suicides occur due to underlying mental health or substance use disorder. In (FERRARI *et al.*, 2014), based on the review of several meta-analysis studies, the authors estimated that 68% of suicides in China, Taiwan, and India were attributed to mental health problems and substance use. In their estimations of the total attributable disease burden, the authors also concluded that

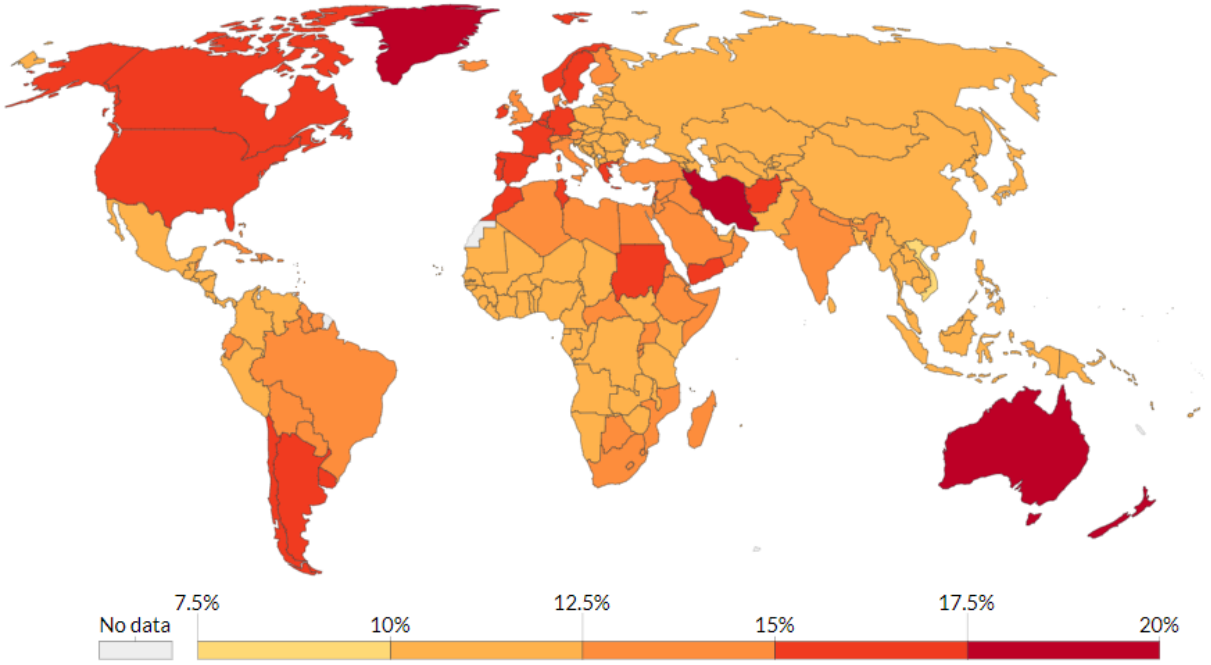

Figure 1 – **The proportion of the population with MD in 2016 -** Figure containing a proportion of the population with any mental health disorder or substance use, including depression, anxiety, bipolar, eating disorders, disorders related to alcohol or drug use, and schizophrenia. Due to the broad and subjective diagnosis, the presented estimation uses a combination of sources, including medical and national records, epidemiological data, research data, and meta-regression models (WHITEFORD; FERRARI; DEGENHARDT, 2016; RITCHIE; ROSER, 2019).

mental health and substance use disorders accounted for 62% of total suicide DALYs.

One way of treating depression is by prescribing antidepressant drugs. In (CIPRIANI *et al.*, 2018), 21 antidepressant drugs were analyzed in different repositories, and in terms of effectiveness, all antidepressants were more effective than placebo. However, in terms of acceptability, it measures the proportion of patients who have withdrawn from treatment for any reason (a recurring reason would be the side effects of the antidepressant medication [1]), only agomelatine and fluoxetine were associated with fewer withdrawals from treatment than placebo. At the same time, clomipramine was worse than placebo (the measure for this study was the *Odds ratio*[2]). Therefore, it is clear that a wrong diagnosis can lead to the prescription of medications with significant side effects. Thus, a precise and accurate diagnosis of mental illnesses is strongly recommended. In the following section, we describe the formal diagnosis of mental diseases and their limitations.

[1] In Brazil, all of these drugs are only sold through a prescription. They are psychotropic drugs, which can cause dependence and bring many side effects and contraindications.

[2] *Odds ratio*, is a measure that expresses risk and assesses the relationship between the chance of an exposed individual to have the condition of interest, compared to the unexposed (FRANCISCO *et al.*, 2008).

1.1 Limitations in the standard approaches for diagnosis of mental disorders

According to the 2001 global health report (ORGANIZATION, 2001), the correct diagnosis of a mental illness is an essential requirement for adequate intervention at the individual level and epidemiology and rigorous monitoring at the community level. The clinical diagnosis is based on diagnostic manuals like the *Diagnostic and Statistical Manual of Mental Disorders* (DSM) and *International Statistical Classification of Diseases and Related Health Problems* (10th Revision) (ICD-10), based on the presence of specific symptoms. However, this practice has not been very effective in psychiatry because certain diseases have overlapping symptoms (BORSBOOM; CRAMER, 2013). An example is a patient with hypothyroidism (an endocrinological illness related to underacting thyroid) who may be misdiagnosed with depression because of tiredness and fatigue, symptoms in both diseases. Other theoretical and psychometric limitations are described in (BORSBOOM, 2008).

Since this standard diagnostic method is subjective (PONDÉ, 2018), it causes social and mental damage to the patient, who often remains mistakenly treated and diagnosed for a long time. An alternative way of conceptualizing mental disorders to these old latent models of diagnosis is the network approach (JONES; HEEREN; MCNALLY, 2017; BORSBOOM, 2017), as we describe as following.

1.2 Data-driven diagnosis of mental disorders

Since the first application of networks in Neuroscience, made by Watts and Strogatz (WATTS; STROGATZ, 1998) for analyzing the nematode worm nervous system *C. elegans*, the use of networks has enabled a better understanding of the organization of the brain (SPORNS, 2011; STAM, 2014). Network models have been providing insights into how structural and functional connectivity of the human brain are related to cognitive symptoms of some mental diseases (BASSETT; ZURN; GOLD, 2018). An increasing number of studies have focused on examining possible functional disconnectivity affects the neurologic brain disorders (HEUVEL; POL, 2010), including Autism Spectrum Disorders (ASD) (HERNANDEZ *et al.*, 2015; WELCHEW *et al.*, 2005; PETERS *et al.*, 2013), Attention-Deficit/Hyperactivity Disorder (ADHD) (QIAN *et al.*, 2018; CAO *et al.*, 2014; MAZAHERI *et al.*, 2010), SZ (CHENG *et al.*, 2015; LIU *et al.*, 2008; SIGURDSSON *et al.*, 2010; GARRITY *et al.*, 2007; WANG *et al.*, 2015), Alzheimer's disease (AD) (GREICIUS *et al.*, 2004; SANZ-ARIGITA *et al.*, 2010; FRANZMEIER *et al.*, 2020), dementia (CHASE, 2014; ROMBOUTS *et al.*, 2009; HAFKEMEIJER; GROND; ROMBOUTS, 2012) and Major Depression (GREICIUS *et al.*, 2007; KAISER *et al.*, 2016; WISE *et al.*, 2017; HAMILTON *et al.*, 2018).Thereat network approach to mental disorders has been considered a more accurate alternative to latent diagnostic models (which, as previously described, has limitations) (FRIED *et al.*, 2017).

Nevertheless, there is a vast number of methods to build networks based on functional connectivity (BASTI *et al.*, 2020) and choosing one of them is a challenge. An example is connections of brain regions of interest are typically measured by Pearson Correlation (PC). However, taking the average across voxels results in biased connectivity estimate (GEERLIGS; HENSON *et al.*, 2016); an alternative is Granger causality (GC), but these methods do not perform well on typical functional magnetic resonance imaging (fMRI) data (KAUFMANN *et al.*, 2017).

Due to the increase in the volume of data related to the health area, such as medical records and exams of patients, and hospital resources, there were greater applicability of Machine Learning (ML) algorithms (HOSSEINI *et al.*, 2018) mainly for medical diagnosis (SONG; JUNG; CHUNG, 2019; MOZAFFARINYA *et al.*, 2019; ILYASOVA *et al.*, 2018; HOSSEINI *et al.*, 2018; KOH; TAN *et al.*, 2011) in order to offer more accurate and automatic investigations of several diseases (BELLAZZI; ZUPAN, 2008). Compared to traditional statistical techniques, this approach has the advantage of not relying on prior assumptions (such as adequate distribution, observation independence, absence of multicollinearity, and interaction problems). It is suited to automatically analyze and capture complex non-linear relationships in data (LI *et al.*, 2020; RAJULA *et al.*, 2020). As brain data are characterized by high complexity and highly correlated brain regions, ML algorithms have been widely used to detect acute and permanent abnormalities in the brain (FONG; SCHEIRER; COX, 2018; KRAGEL; LABAR, 2016; BOUTET *et al.*, 2021). On the other hand, ML needs more interpretability and a black-box nature that is an especially disadvantageous general limitation when it comes to an understanding medical data (RUDIN, 2019; EKANAYAKE; MEDDAGE; RATHNAYAKE, 2022).

In recent years, new techniques have emerged to help interpret machine learning results. Most notable is the SHapley Additive ExPlanations (SHAP) values method (LUNDBERG; LEE, 2017). This metric enables the identification and prioritization of features and can be used with any machine learning algorithm (BOWEN; UNGAR, 2020; RODRÍGUEZ-PÉREZ; BAJORATH, 2019; SPADON *et al.*, 2019). Furthermore, in this area of biomedical research, conventional machine learning techniques have been used depending on a specialist with prior knowledge to design the construction of a pattern recognition system (ESTEVA *et al.*, 2019). However, the space of characteristics of this type of learning deals with raw data scales badly and misses the opportunity to discover new patterns (MIOTTO *et al.*, 2017). An alternative approach is the representation-based learning method capable of automatically discovering the representations necessary to predict raw data (BENGIO; COURVILLE; VINCENT, 2013). In this context, an alternative is to use deep learning, a set of algorithms with multiple levels of representation obtained by the hierarchical composition of simple mathematical functions (each associated with a layer) (LECUN; BENGIO; HINTON, 2015). Furthermore, *Deep learning* models have been widely used for medical image analysis in different application domains (MUNIASAMY *et al.*, 2019), as diagnosing brain-related (PINAYA *et al.*, 2016; BROSCH *et al.*, 2014), heart (WANG *et al.*, 2017a; BERNARD *et al.*, 2018) and cancer (XU *et al.*, 2014; BYCHKOV *et al.*, 2016;

SCHAUMBERG; RUBIN; FUCHS, 2018) diseases.

1.3 Research Objective

This thesis aims to improve the methods of diagnosing mental illnesses and offer an approach that tries to quantify the differences between healthy brains and people with different types of mental illnesses, considering electroencephalogram (EEG) and fMRI data. The diseases considered here were SZ, AD, and ASD.

For this purpose, network measures will be used, including new measures developed for the authors related to network communities. To discriminate between the two classes (patient and non-patient), machine learning algorithms will generate models (classification) to predict whether a patient has a mental illness. In addition, it is intended to find out which network measures most contribute to the model's performance and how the diseases are correlated. Moreover, through the use of the SHAP theoretic approach, it was intended to give a biological interpretation to the ML model.

A second goal of this thesis is to apply the same workflow developed for diagnosing mental diseases to EEG data considering subjects who had used ayahuasca and DMT. The aim was to verify how these substances alter the brain since they have been used successfully in treating some mental diseases. Recently, the interest in the medical use of psychedelics has increased significantly. Only last year, in (PERKINS *et al.*, 2021), it was identified that about 100 psychedelic clinical trials are currently being conducted worldwide. This shows an increase in clinical trials compared to 43 assisted psychedelic therapy clinical trials conducted since 1999.

One example is the psychedelic 3,4-methylenedioxymethamphetamine (MDMA), which is already in phase 3 clinical trials for the treatment of Post-Traumatic Stress Disorder (PTSD) (MITCHELL *et al.*, 2021) and major depression with positive results (ANDREWS; WRIGHT, 2022). Another notable example is psychedelic psilocybin, whose therapeutic use in the U.S. has become a revolutionary therapy for treatment-resistant depression and major depressive disorder (NICHOLS, 2020). These first promising results suggest that other psychedelic substances, such as lysergic acid diethylamide (LSD) (MITCHELL *et al.*, 2021), ibogaine hydrochloride, salvia divinorum, 5-MeO-DMT, ayahuasca, and N,N-Dimethyltryptamine (DMT), which have been less studied so far, should be investigated in more detail (SIEGEL *et al.*, 2021). Therefore, understanding how these drugs affect our brains is essential for new drug developments.

In summary, in this thesis, EEG and fMRI data are used to achieve the proposed goals, and their time series are extracted and preprocessed. Each time series came from an area of the brain, and through different correlation measures, we constructed the connectivity matrices. These matrices generate networks where each node represents an area of the brain, and the edges of these areas are connected. Finally, the connectivity matrix and the measures of complex networks are used to feed several ML algorithms to verify which results in better performance,

the best brain connections, and the best measures of complex networks found by the ML model. Figure 2 contains the schema for the methodology used here.

1.4 Contributions of this thesis

The main contributions provided work are the following:

- Developed a predictive model workflow capable automatic diagnosing mental disorders.
- Detect changes in the functional network structure induced by DMT and ayahuasca using ML to obtain new insights into the mechanisms of action of these psychedelics using ML in combination with SHAP values.
- Determine which complex network measures are most effective for capturing brain changes (in mental disorders and under the effect of psychedelic drugs).
- Advancing state of the art in the field of mental illness diagnosis.

1.5 Thesis organization

This monograph is organized as follows items:

- **Chapter 2 - EEG functional connectivity and deep learning for automatic diagnosis of brain disorders: Alzheimer's disease and schizophrenia**, containing a workflow developed for EEG data from Alzheimer's and schizophrenia patients using a deep learning model and testing different correlation measures used to obtain the connectivity matrix, to ascertain the best measure for each of these diseases and to improve the accuracy of their diagnosis.
- **Chapter 3- Application of machine learning and complex network measures to an EEG dataset from ayahuasca experiments**, containing a workflow developed for EEG data from subjects who have used the psychedelic ayahuasca aiming to investigate how this substance alters the functional connectivity of the brain.
- **Chapter 4- Application of machine learning and complex network measures to an EEG dataset from DMT experiments**, containing a workflow developed for EEG data from subjects who have used the psychedelic substance DMT intending to discover how this substance causes changes in functional connectivity in the brain and which insights into its mechanism of action can be inferred from them.
- **Chapter 5- Analysis using fMRI data from ASD patients**, containing a workflow developed for fMRI data from patients with autism aimed at obtaining an ML algorithm

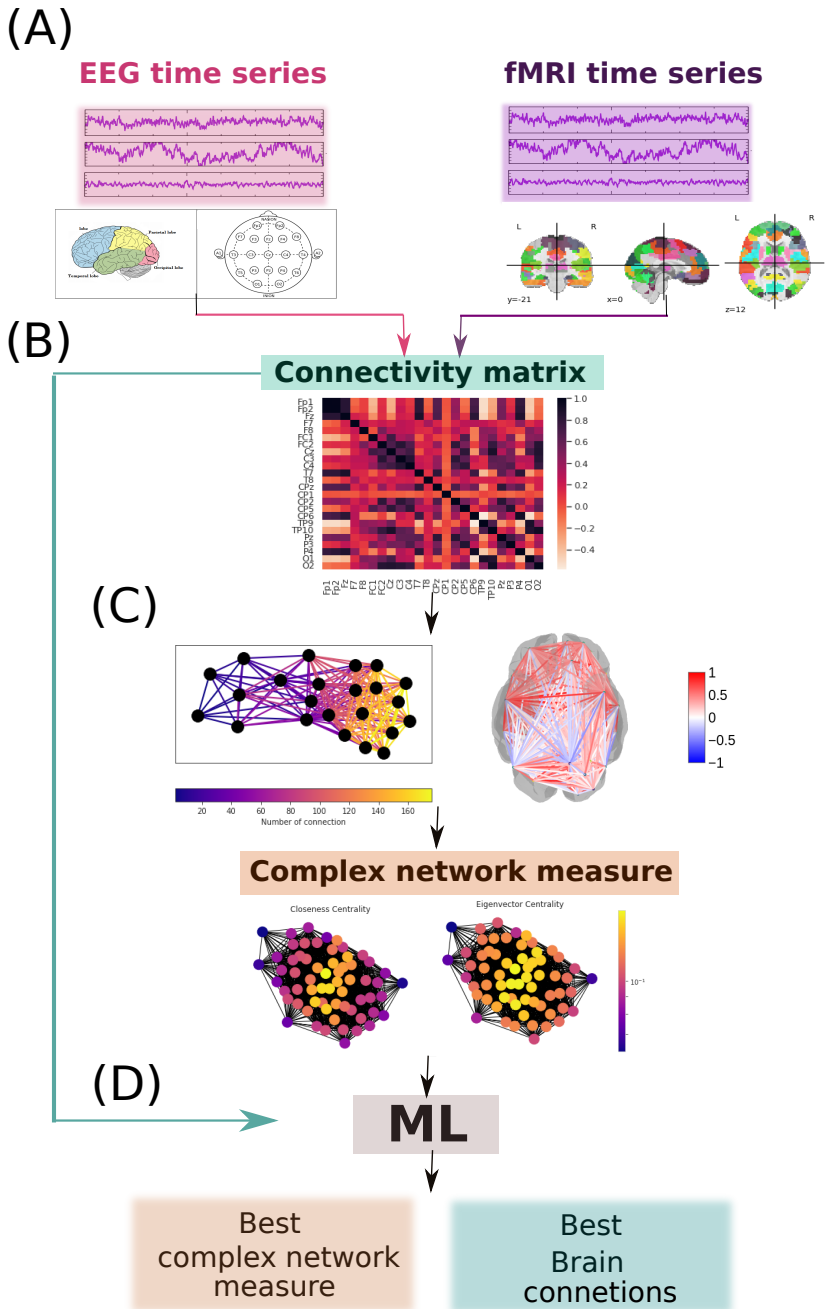

Figure 2 – **Scheme for methodology used-** From the scheme, in (A), time series of EEG and fMRI data where each time series belongs to a region of the brain (in the case of EEG data represents the regions collected by the scalp, in Figure the 10-20 EEG system, and in the case of fMRI data represents the regions of interest, in the Figure represented by Smith's map). Correlating these time series gives the connectivity matrix, depicted in Figure (B), by the connectivity matrix obtained for the EEG database of the DMT experiments. From these matrices, networks are generated (see Figure (C), the graph generated from the EEG data of the experiments using DMT and the brain with the graph of connections to the fMRI database of patients with ASD). From them, measures of complex networks are extracted (in Figure (C), illustrated by the graph obtained from the EEG data of the ayahuasca experiments, depicting the measures of closeness centrality and eigenvector centrality whose values for each node are illustrated in the color bar). Thus, both the connectivity matrices and the complex network measures feed the ML algorithms to verify the best complex network measures and brain connections (see Figure in (D)).

to improve the diagnosis of this disorder, including the best correlation measure, the best measures of complex networks and the most important brain connections capable of capturing the brain changes due to this disease.

- **Chapter 6- Analysis of functional connectivity using machine learning and deep learning in multimodal data from patients with Schizophrenia**, applying the workflow developed here for fMRI and EEG dataset in a multimodal fashion for evaluating connectivity matrices and measures of complex networks to establish an automated diagnosis and comprehending the topology and dynamics of brain networks in schizophrenia patients.

- **Chapter 7- Conclusions and future work**, containing the conclusions of this study and future work.

CHAPTER

2

EEG FUNCTIONAL CONNECTIVITY AND DEEP LEARNING FOR AUTOMATIC DIAGNOSIS OF BRAIN DISORDERS: ALZHEIMER'S DISEASE AND SCHIZOPHRENIA

'If you can dream—and not make dreams your master. If you can think—and not make thoughts your aim. If you can meet with Triumph and Disaster and treat those two impostors just the same. If you can bear to hear the truth you've spoken. Twisted by knaves to make a trap for fools, or watch the things you gave your life to, broken, and stoop and build 'em up with worn-out tools.. Yours is the Earth and everything that's in it.."

— Rudyard Kipling, *If*

Published 13 April 2022 by IOP Publishing Ltd *Journal of Physics: Complexity*.

COLLABORATING AUTHORS

Aruane M. Pineda
Universidade de São Paulo (USP)

Kirstin Roster
Universidade de São Paulo (USP)

Christiane Thielemann
Aschaffenburg University of Applied Sciences (UAS)

Francisco A. Rodrigues
Universidade de São Paulo (USP)

Abstract

MD are among the leading causes of disability worldwide. The first step in treating these conditions is to obtain an accurate diagnosis. ML algorithms can provide a possible solution to this problem, as we describe in this work. We present a method for the automatic diagnosis of mental disorders based on the matrix of connections obtained from EEG time series and deep learning. We show that our approach can classify patients with AD and SZ a with a high level of accuracy. The comparison with the traditional cases, that use raw EEG time series, shows that our method provides the highest precision. Therefore, the application of deep neural networks on data from brain connections is a very promising method for the diagnosis of neurological disorders.

2.1 Introduction

Neurological disorders, including AD and SZ, are among the main priorities in the present global health agenda (ORGANIZATION, 2006). AD is a type of dementia that affects primarily elderly individuals and is characterized by the degeneration of brain tissue, leading to impaired intellectual and social abilities (DOLGIN, 2016). Currently, around 25 million people live with AD and, in the US, nearly six million individuals are affected by AD, with incidence projected to increase more than two-fold to 13.8 million by 2050 (RODRIGUEZ *et al.*, 2021). Individuals with SZ have symptoms such as hallucinations, incoherent thinking, delusions, decreased intellectual functioning, difficulty in expressing emotions, and agitation (JAHMUNAH *et al.*, 2019; GOTTESMAN; SHIELDS, 1982). According to the WHO, SZ affects around 26 million people worldwide (FLEISCHHACKER *et al.*, 2014).

The base for successful treatment of AD and SZ is the correct diagnosis. However, both the diagnosis and the determination of the stage of AD and SZ are based primarily on qualitative interviews, including psychiatric history and current symptoms, and the assessment of behaviour. These observations may be subjective, imprecise, and incomplete (BORSBOOM; CRAMER, 2013; FRIED *et al.*, 2017; BORSBOOM, 2008; DAUWELS; VIALATTE; CICHOCKI, 2010). To provide a quantitative evaluation of mental disorders, methods based on MRI, CT (JR *et al.*, 2009), PET (DING *et al.*, 2019; WALHOVD *et al.*, 2010) has been used to aid professionals in the diagnostic process (GUERRA *et al.*, 2018). However, the use of multiple imaging devices can be expensive to implement and the fusion of images from different devices can have poor quality due to motion artifacts.

To overcome these restrictions, EEG data is a viable candidate to support the diagnosis of SZ and AD (TAIT *et al.*, 2020). Although EEG has a low spatial resolution, it has a comparatively low cost, good temporal resolution and is easily available in most contexts. Nonetheless, visual analysis of EEG data is time-consuming, requires specialized training, and is error-prone (TRAMBAIOLLI *et al.*, 2011; FALK *et al.*, 2012; PIUBELLI *et al.*, 2021). However, we can consider automatic evaluation of EEG time series using modern classification algorithms, which

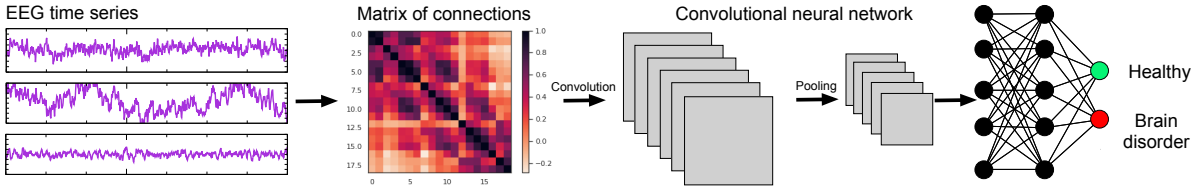

Figure 3 – Illustration of the method for automatic diagnosis of mental disorders based on EEG time series. Time series are collected and the correlation between electrodes are calculated yielding the matrices of connections, which encompass the functional connectivity between brain regions. Finally, the CNN is adjusted to enable the automatic classification of individuals.

can help to improve the efficiency and accuracy of AD and SZ diagnosis, as verified in previous works (PINEDA *et al.*, 2020; OH *et al.*, 2019; AHMADLOU; ADELI; ADELI, 2011; BUETTNER *et al.*, 2020).

Moreover, instead of using raw EEG time series, it is possible to encompass the connections between brain regions by constructing cortical complex networks (SPORNS, 2002). In this case, we build cortical networks for healthy and individuals with neurological disorders. To distinguish between them, we use network measures to describe the network structure, as described in a previous work of ours (ARRUDA *et al.*, 2014) (see also (COSTA *et al.*, 2007; COSTA *et al.*, 2010) for a description of the methodology used in network classification). Therefore, each network is mapped into a d dimensional space, where d is the number of measures adopted for network characterization. This process of building a set of features to represent the input data is called feature engineering. After extracting the network features for the two classes of networks, i.e. healthy and individuals with mental disorders, supervised learning algorithms are adjusted to perform automatic classification. Previous works verified that this approach enables the diagnosis with accuracy higher than 80% in the case of childhood-onset schizophrenia (ARRUDA *et al.*, 2014).

Although this methodology has been used for many different diseases (e.g. (PINEDA *et al.*, 2020; ARRUDA *et al.*, 2014; DIYKH; LI; WEN, 2017; ROCCA *et al.*, 2020)) the performance of the algorithm depends on the measures selected to describe the network structure. The network properties included in the model could represent just a subset of the information necessary to get the best performance of the supervised model. Therefore, the network representation can be incomplete, restricting the accuracy of the classifiers. One possible solution to this problem is the use of a matrix of connections in combination with deep neural networks (GOODFELLOW; BENGIO; COURVILLE, 2016), as we show in the present paper. In this case, instead of extracting the network measures, the matrix of connections is considered as input to train a deep neural network. This matrix encodes all the information necessary to represent the network structure and avoid the choice of network measures.

In this work, the metrics used to construct the matrices also have restrictions. A limitation of the pairwise matrices used in this study is the possible loss of information when reducing the raw EEG time series. However, our study suggests that the amount of information retained is

sufficient for the classification of AD and SZ and represents a more computationally efficient approach that is more practical in a clinical setting. In this work, the metrics used to construct the matrices also have restrictions. As an example, PC considers only linear correlations, on the other hand, Spearman Correlation (SC) is limited when there are many observations with the same order, and GC considers the series stationary. Nevertheless, we aim here to develop an efficient method to classify patients and not to make a comparison of methods.

Therefore, we consider the matrix of connections between brain areas and deep neural networks to distinguish individuals with AD and SZ from healthy controls. Other than previous works, where only raw time series are adopted as input for the neural network(ACHARYA *et al.*, 2018b; KASHIPAREKH *et al.*, 2019; ISLAM; ZHANG, 2018; DUNEJA *et al.*, 2019; ACHARYA *et al.*, 2018a; OH *et al.*, 2018; YILDIRIM; BALOGLU; ACHARYA, 2018), we do not ignore the connections between the electrodes used to record the time series. We construct the matrix of connections by using GC, PC, and SC correlations (BASTOS; SCHOFFELEN, 2016; SETH; BARRETT; BARNETT, 2015; BONITA *et al.*, 2014). We verify that this information about the connections is fundamental and improves the classification, compared to the previously mentioned approaches that use only raw EEG time series.

In summary, in this work we achieve the following contributions:

- We propose a method to classify EEG time series from healthy and patients presenting AD and SZ. With a matrix of connections as input for a tuned Convolution Neural Networks (CNN) model, the accuracy obtained is close to 100 % for both disorders. Our results are more accurate than those observed in previous works that consider only raw EEG time series, reinforcing the importance of the network structure on the diagnosis of mental disorders.

- We show that the method to infer the matrices of connections influences the quality of the classification results. For SZ, the GC provides the most accurate classification, whereas, for AD, the PC yields the highest accuracy.

- Our framework is general and can be used in EEG data from any brain disorder. It allows to determine the best cortical network representation and adjust the CNN to optimize the accuracy.

In the next sections, we outline the data set, present the CNN architecture and show our results, comparing them with more common approaches that do not consider the connections between brain areas.

2.2 EEG data

The AD data set considered here is composed of EEG time series recorded at a sampling frequency of 128 Hz and a duration of eight seconds for each individual and at 19 channels (F_{p1}, F_{p2}, F_7, F_3, F_z, F_4, F_8, T_3, C_3, C_z, C_4, T_4, T_5, P_3, P_z, P_4, T_6, O_1, and O_2). The letters F, C, P, O, and T refer to the respective cerebral lobes frontal (F), central (C), parietal (P), occipital (O), and temporal (T). The data is divided into two sets. The first one consists of 24 healthy elderly individuals (control group; aged 72 11 years) who do not have any history of neurological disorders. The second one is made of 24 elderly individuals with AD (aged 69 16 years) diagnosed by the National Institute of Neurological and Communicative Disorders and Stroke, the AD and Related Disorders Association (NINCDS-ADRDA), following the DSM-III-R criteria ((PINEDA *et al.*, 2020; PRITCHARD; DUKE; COBURN, 1991)).

The data set used for diagnosis of SZ contains 16-channel EEG time series recorded at a sampling frequency of 128 Hz over one minute, including F_7, F_3, F_4, F_8, T_3, C_3, C_z, C_4, T_4, T_5, P_3, P_z, P_4, T_6, O_1, and O_2. Notice that both data set come from studies of 16 common brain regions, with the AD data set having three more regions analyzed. Furthermore, it also includes two sets, (i) one of 39 healthy young individuals (control group; aged 11 to 14 years) and (ii) one of 45 teenagers individuals (aged 11 to 14 years) with symptoms of schizophrenia.

Both data sets are freely available at (PINEDA; ALVES, 2022).

2.3 Concepts and Methods

Our framework to perform the automatic diagnosis of AD and SZ is illustrated in Figure 3. In a first step, EEG time series, which are free of artifacts, are used to construct the matrices of connections. The strength of the connections between two brain regions is quantified by three different methods: (i) GC test (GRANGER, 1969), (ii) the PC (BENESTY *et al.*, 2009) and (iii) SC (LUBINSKI, 2004) correlation measures.

In our work, we have the following null hypothesis: the coefficients of the corresponding past values are zero (one EEG channel does not influence the other). The rows are the response variables and the columns are the predictors. We calculate the p-values, if these p-values are less than 0.05 (significance level) this implies that the null hypothesis can be rejected. Therefore, the p-value analyzes whether one brain region influences the other. If $p < 0.05$ we assign the value 1 because we reject the null hypothesis, i.e. it is true that one EEG channel influences another. This influence is related to having a high correlation.

Therefore, matrices are calculated for AD data sets (19 EEG channels) and for SZ data sets (16 EEG channels) filled with “1” if $p < 0.05$ and “0” if $p \geq 0.05$. These matrices are inserted in a CNN to discriminate healthy individuals from individuals diagnosed with AD and SZ (see Figure 3). Notice that the use of different methods to infer the brain areas is necessary

because there is no general method to infer functional connectivity (BASTOS; SCHOFFELEN, 2016; SETH; BARRETT; BARNETT, 2015; BONITA *et al.*, 2014; COMIN *et al.*, 2020). Indeed, choosing the best metric to infer these connections between brain areas is a current challenge in network neuroscience (e.g. (SHANDILYA; TIMME, 2011; LUSCH; MAIA; KUTZ, 2016)).

2.3.1 CNN

CNN is a type of neural network (MILLSTEIN, 2020) with three types of layers and masked parameters, as proposed in (HUBEL; WIESEL, 1962; LÓPEZ-RISUEÑO *et al.*, 2002). The convolutional layer performs the mathematical operation called convolution, which is done in more than one dimension at a time. The weights of the artificial neurons are represented by a tensor called kernel (or filter). The outputs from the convolutional layer include the main features from the input data. The convolution process between neurons and kernels produces outputs called feature maps.

The pooling layer reduces the dimensionality and operates similarly to the convolutional layer. The difference is that pooling kernels are weightless and add aggregation functions to their input data, such as a maximum or mean function (LECUN *et al.*, 1989; LECUN; BENGIO; HINTON, 2015). The max-pooling function is used here to return the highest value within an area of the tensor, which reduces the size of the feature map. The fully connected layer categorizes input data into different classes, based on an initial set of data used for training. The artificial neurons in the max pooling and fully connected layers are connected, as the output predicts precisely the result of the input EEG data as healthy and unhealthy (OH *et al.*, 2019).

Two approaches for the CNN architectures are proposed here, one using a tuning method (CNN_{tuned}) and another without this optimization step ($\text{CNN}_{untuned}$). Tuning is an optimization method used to find the values of hyperparameters to improve the performance of the CNN model (HUTTER; LÜCKE; SCHMIDT-THIEME, 2015). Three tuning techniques are used in the present work: (i) random search (BERGSTRA; BENGIO, 2012), (ii) hyper-band (ROSTAMIZADEH *et al.*, 2017) and (iii) Bayesian optimization (DOKE *et al.*, 2020). The traditional way to optimize the hyperparameters is exhaustive searching through a manually specified parameters search space and evaluating all possible combinations of these parameter values. However, this approach has a high computational cost. An alternative method is to select the values of parameters in the search space at random until maximize the objective function (here, this objective function is the maximization of accuracy).

The idea of hyper-band optimizations is to select different possible models (with different hyperparameters values), train them for a time, and discard the worst one at each iteration until a few combinations remain. In contrast, Bayesian optimization is a global optimization method that uses the Bayes Theorem to direct the search to find the minimum or maximum of a certain objective function (GOODFELLOW; BENGIO; COURVILLE, 2016).

Table 1 – Best hyperparameters and layer configurations obtained for the CNN_{tuned} model.

Type of Layer	Tuning hyperparameter	Value
Convolutional	—	—
Convolutional	dropout	[0.00, 0.05, 0.10, 0.15, 0.20, 0.25, 0.30, 0.35, 0.40, 0.45, 0.50]
Convolutional	—	—
Convolutional	number of filters	[32, 64]
Max Pooling	dropout	[0.00, 0.50, 0.10, 0.15, 0.20]
Flatten	—	—
Dense	- units -activation	[32, 64, 96....512] [relu, tanh, sigmoid]
Dropout	rate	[0.00, 0.50, 0.10, 0.15, 0.20]
Adam optimization compile	learning rate	$min-value = 1e^{-4}$ $max-value = 1e^{-2}$ sampling= LOG

Table 2 – The network architecture for the CNN_{tuned} model used in the AD and SZ data sets.

Type of Layer	Output Shape (AD)	Output Shape (SZ)	Parameter
Convolutional	(None, 17, 17, 16)	(None, 14, 14, 16)	160
Convolutional	(None, 15, 15, 16)	(None, 12, 12, 16)	2320
max-pooling	(None, 7, 7, 16)	(None, 6, 6, 16)	0
dropout	(None, 7, 7, 16)	(None, 6, 6, 16)	0
Convolutional	(None, 5, 5, 32)	(None, 4, 4, 32)	4640
Convolutional	(None, 3, 3, 32)	(None, 2, 2, 32)	9248
max-pooling	(None, 1, 1, 32)	(None, 1, 1, 32)	0
dropout	(None, 1, 1, 32)	(None, 1, 1, 32)	0
flatten	(None, 32)	(None, 32)	0
dense	(None, 160)	(None, 160)	5280
dropout	(None, 160)	(None, 160)	0
dense	(None, 2)	(None, 2)	3

In the CNN_{tuned} model, the dropout regularization technique is employed to avoid overfitting (SRIVASTAVA *et al.*, 2014). The layers and range used for hyperparameters are presented in table 30. The best CNN_{tuned} architectures tuned for each data set individually are depicted in table 31. The $CNN_{untuned}$ model presents fewer layers and therefore lower computational costs. The parameters used in our analysis are described in table 32.

2.3.2 Evaluation

For evaluation, we consider the Recall, Precision, Accuracy (Acc.), F1 score, receiver operating characteristic (ROC) and Area under the ROC curve (AUC).

Table 3 – The network architecture for the $CNN_{untuned}$ model used in the AD and SZ data sets.

Type of Layer	Output Layer (AD)	Output Layer (SZ)	Kernel
Input Layer	19 x 19 x 1	16x16x1	-
Convolution	18 x 18 x 32	15 x 15 x 32	4
Max pooling	18 x 18 x 32	15 x 15 x 32	2
Convolution	17 x17 x 16	14 x 14 x 16	4
Max pooling	17 x17 x 16	14 x 14 x16	2
Flatten	17 x17 x 16	3136	-
Fully connected	10	10	-
Fully connected	1	1	-

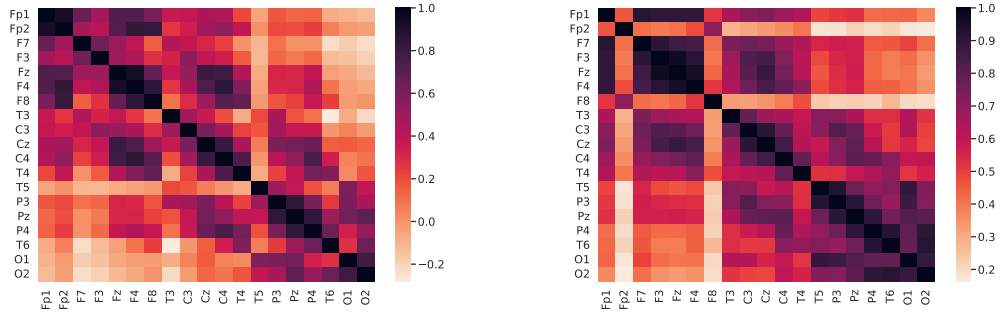

(a) (b)

Figure 4 – Example of matrices of connections calculated with PC for (a) an individual with diagnosed AD and (b) an healthy individual.

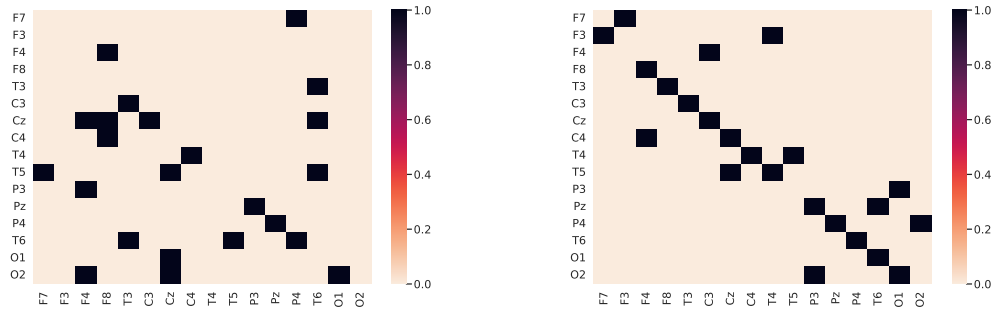

(a) (b)

Figure 5 – Example of matrices of connections calculated with GC test for (a) an individual with diagnosed SZ and (b) an healthy individual.

2.4 Results and discussion

We consider the EEG time series described in section 2.2 to construct the matrices of connections for healthy controls and individuals diagnosed with AD and SZ, following the description in section 2.3. These matrices are built by using the GC test, PC and SC measures for both data sets. In Figures 4 and 5, some examples of such matrices of connections are shown

Table 4 – Classification results for AD using the CNN_{tuned} model (best results are in bold).

Matrices of connections	Hyperparameter	Sample	Acc.	Precision	Recall	AUC
GC	Random Search	Train	0.81	0.81	0.81	0.88
		Test	0.75	0.75	0.75	0.97
	hyper-band	Train	0.65	0.65	0.65	0.65
		Test	0.75	0.75	0.75	0.97
	Bayesian Optimization	Train	0.68	0.68	0.68	0.82
		Test	0.75	0.75	0.75	0.93
PC	Random Search	Train	**0.95**	**0.95**	**0.95**	**0.98**
		Test	**1.00**	**1.00**	**1.00**	**1.00**
	hyper-band	Train	0.86	0.86	0.86	0.90
		Test	1.00	1.00	1.00	1.00
	Bayesian Optimization	Train	0.88	0.88	0.88	0.98
		Test	1.00	1.00	1.00	1.00
SC	Random Search	Train	0.47	0.47	0.45	0.47
		Test	0.75	0.75	0.75	0.75
	hyper-band	Train	0.47	0.47	0.47	0.45
		Test	0.75	0.75	0.75	0.62
	Bayesian Optimization	Train	0.47	0.47	0.47	0.45
		Test	0.75	0.75	0.75	0.68

and differences between them can be noticed visually in both cases.

The matrices of connections are inserted into the CNN by applying the flattening method, which converts the data into a 1-dimensional array that is input to the next layer. Two CNN architectures are considered, i.e. CNN_{tuned} and $CNN_{untuned}$, to evaluate the classification. The CNN_{tuned} is obtained by hyperparameter optimization, whereas the $CNN_{untuned}$ is a simpler model, without using the tuning optimization. The evaluation of both models is done by using the AUC. Nested k-fold cross-validation ($k = 10$) for model selection, adjustment and evaluation is considered here. The training and test sets are selected according to the holdout method, where we include 10% of the observations in the test set. We obtain similar results for other test sizes, as shown in the Appendix A.1.

The results for the CNN_{tuned} model is shown in tables 4 and 5, for AD and SZ, respectively. In all the cases, the CNN_{tuned} model can unambiguously distinguish healthy individuals from individuals diagnosed with a brain disorder. The best results with an accuracy close to 100% are obtained for both AD and SZ in the testing set using random search for hyperparameter tuning.

Concerning the $CNN_{untuned}$ model, the results are shown in tables 6 and 7 for AD and SZ, respectively. For the AD data set, the best results are found using PC with a test accuracy of 92%. Regarding SZ disease, independently of the method used for the construction of the matrices of connections, results are close to the random guessing (see table 7). Therefore, the

Table 5 – Classification results for SZ using the CNN_{tuned} model (best results are in bold).

Matrices of connections	Hyperparameter	Sample	Acc.	Precision	Recall	AUC
GC	Random Search	Train	**0.90**	**0.90**	**0.90**	**0.93**
		Test	**1.00**	**1.00**	**1.00**	**1.00**
	hyper-band	Train	0.73	0.73	0.73	0.77
		Test	0.72	0.72	0.72	0.78
	Bayesian Optimization	Train	0.72	0.72	0.72	0.78
		Test	1.00	1.00	1.00	1.00
PC	Random Search	Train	0.54	0.54	0.54	0.54
		Test	0.50	0.50	0.50	0.50
	hyper-band	Train	0.54	0.54	0.54	0.54
		Test	0.50	0.50	0.50	0.50
	Bayesian Optimization	Train	0.54	0.54	0.54	0.54
		Test	0.50	0.50	0.50	0.50
SC	Random Search	Train	0.53	0.53	0.53	0.53
		Test	0.50	0.50	0.50	0.50
	hyper-band	Train	0.53	0.53	0.53	0.53
		Test	0.50	0.50	0.50	0.50
	Bayesian Optimization	Train	0.53	0.53	0.53	0.53
		Test	0.50	0.50	0.50	0.50

Table 6 – Classification results for AD using the $CNN_{untuned}$ model (best results are in bold).

Matrices of connections	Sample	Acc.	Precision	Recall	AUC
GC	Train	0.97	0.97	0.99	0.99
	Test	0.58	0.57	0.66	0.75
PC	Train	**0.98**	**0.99**	**0.98**	**0.99**
	Test	**0.92**	**1.00**	**0.83**	**1.00**
SC	Train	0.97	0.98	0.97	0.99
	Test	0.83	1.00	0.66	1.00

Table 7 – Classification results for SZ using the $CNN_{untuned}$ model.

Matrices of connections	Sample	Acc.	Precision	Recall	AUC
GC	Train	**0.97**	**0.97**	**0.97**	**0.99**
	Test	**0.52**	**0.53**	**0.73**	**0.55**
PC	Train	0.61	0.58	1.00	0.53
	Test	0.57	0.55	1.00	0.45
SC	Train	0.62	0.59	0.97	0.58
	Test	0.62	0.58	1.00	0.53

CNN_{tuned} model is more accurate for both AD and SZ diagnosis.

Importantly, the overall predictive performance depends on the choice of measure to construct the matrices of connections. In the case of AD, PC provides the best performance in CNN_{tuned} (see table 4). On the other hand, in the case of SZ, GC is superior to the other methods

Table 8 – Classification results for AD using raw EEG time series and the CNN_{tuned} model.

Set	Acc.	Precision	Recall	AUC
Train	0.68	0.61	1.00	0.68
Test	0.75	0.66	1.00	0.75

Table 9 – Classification results for SZ using raw EEG time series and the CNN_{tuned} model.

Set	Acc.	Precision	Recall	AUC
Train	0.62	0.62	1.00	0.50
Test	0.55	0.55	1.00	0.50

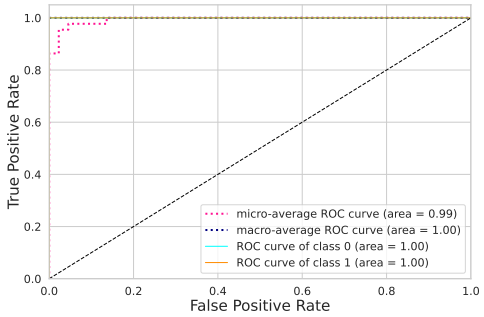

(a) (b)

Figure 6 – ROC curve obtained from the CNN_{tuned} model. The matrices of connections are constructed by (a) PC for AD disease and (b) GC for individuals diagnosed with SZ.

(see table 5). Therefore, there is no general method to infer the connections and obtain the most accurate results. Thus, different methods should be considered to develop an accurate framework for the automatic diagnosis of mental disorders.

For a comparison of our method with the more common approach known from the literature, the classification is performed by applying the raw EEG time series as input for the CNN_{tuned} model (whose performance is the best for both diseases, as discussed before). The results are shown in tables 8 and 9 for AD and SZ, respectively. The Acc. of 75% for AD and 55% for SZ are obtained. This outcome is supported by results available in the literature. Janghel and Rathore (JANGHEL; RATHORE, 2021) obtained an Acc. of 76% for AD, where the authors did not consider the matrices of connections.

As we can see, our proposed method based on a matrix of connections provided as input to a CNN allows for more accurate results. This reinforces the importance of using a data set that encompasses the connections between brain regions. Indeed, the network structure is a fundamental ingredient to differentiate healthy individuals from patients presenting neurological disorders, as verified in many papers (e.g. (ARRUDA *et al.*, 2014; LYNN; BASSETT, 2019; FALLANI *et al.*, 2011a; RODRIGUES; COSTA, 2009; ANTIQUEIRA *et al.*, 2010)).

In Figures 6 we show the ROC curve for the best results, i.e. for AD (using PC) and

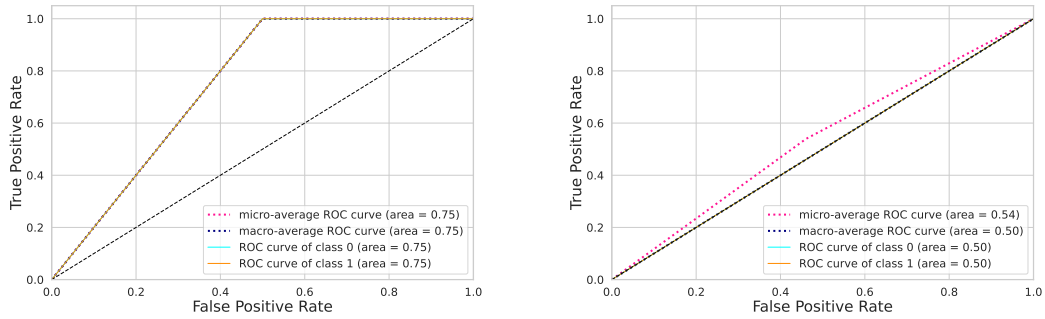

(a) (b)

Figure 7 – ROC curve obtained from raw EEG time series for (a) individuals diagnosed with AD and (b) individuals with SZ.

SZ (using GC test), respectively. For AD, the micro and macro-average ROC curve areas are 0.99 and 1.0, respectively, the micro and macro-average ROC curve areas are 0.92 for both cases. For comparison, Figure 7 shows the ROC curve for AD and SZ using raw times series, where the micro and macro-average AUC are 0.75 for AD and around 0.55 for AZ. Comparing these results, we conclude that the use of the matrix of connections provides the most accurate classifications. Since the databases are small, other classifiers were tested and the results are in the appendix A.1.

2.5 Conclusion

In this paper, we propose a method for automatic diagnosis of AD and SZ based on EEG time series and deep learning. We infer the matrix of connections between brain areas following three different approaches, based on GC, PC and SC. These matrices are included in a convolutional neural network, tunned with the random search, hyper-band, and Bayesian optimization. We verify that this approach provides a very accurate classification of patients with AD and SZ diseases. The comparison with the traditional method that considers raw EEG data shows that our method is more accurate, reinforcing the importance of network topology for the description of brain data. Our method is general and can be used for any mental disorder in which EEG times series can be recorded.

A limitation of our analysis is the relatively small data set, although this is common in other studies on disease classification (OH *et al.*, 2019). However, even with this restriction, our algorithm worked very well, showing that AD and SZ are associated with changes in brain organization. As future work, we suggest considering larger data sets and additional information about the patients, like health conditions and age. A method that provides the level of the evolution of the disease is also an interesting topic to be developed from our study.

CHAPTER

3

APPLICATION OF MACHINE LEARNING AND COMPLEX NETWORK MEASURES TO AN EEG DATASET FROM AYAHUASCA EXPERIMENTS

'It matters not how strait the gate, How charged with punishments the scroll, I am the master of my fate, I am the captain of my soul. "

— William Ernest Henley, *Invictus*

Published 16 December 2022 by *PLOS ONE*.

COLLABORATING AUTHORS

Rubens Gisbert Cury
Universidade de São Paulo (USP)
Kirstin Roster
Universidade de São Paulo (USP)
Aruane M. Pineda
Universidade de São Paulo (USP)
Francisco A. Rodrigues
Universidade de São Paulo (USP)
Christiane Thielemann
Aschaffenburg University of Applied Sciences (UAS)
Manuel Ciba
Aschaffenburg University of Applied Sciences (UAS)

Abstract

Ayahuasca is a blend of Amazonian plants that has been used for traditional medicine by the inhabitants of this region for hundreds of years. Furthermore, this plant has been demonstrated to be a viable therapy for a variety of neurological and mental diseases.

EEG experiments have found specific brain regions that changed significantly due to ayahuasca. Here, we used an EEG dataset to investigate the ability to automatically detect changes in brain activity using machine learning and complex networks. Machine learning was applied at three different levels of data abstraction: (A) the raw EEG time series, (B) the correlation of the EEG time series, and (C) the complex network measures calculated from (B). Further, at the abstraction level of (C), we developed new measures of complex networks relating to community detection.

As a result, the machine learning method was able to automatically detect changes in brain activity, with case (B) showing the highest accuracy (92%), followed by (A) (88%) and (C) (83%), indicating that connectivity changes between brain regions are more important for the detection of ayahuasca. The most activated areas were the frontal and temporal lobe, which is consistent with the literature.

F3 and PO4 were the most important brain connections, a significant new discovery for psychedelic literature. This connection may point to a cognitive process akin to face recognition in individuals during ayahuasca-mediated visual hallucinations.

Furthermore, closeness centrality and assortativity were the most important complex network measures. These two measures are also associated with diseases such as AD, indicating a possible therapeutic mechanism. Moreover, the new measures were crucial to the predictive model and suggested larger brain communities associated with the use of ayahuasca. This suggests that the dissemination of information in functional brain networks is slower when this drug is present.

Overall, our methodology was able to automatically detect changes in brain activity during ayahuasca consumption and interpret how these psychedelics alter brain networks, as well as provide insights into their mechanisms of action.

3.1 Introduction

Ayahuasca is made from a blend of Amazonian herbs (METZNER, 1998). This combination of plants is often associated with rituals of different religions and social groups. Ayahuasca has been used in the Amazon for a couple of hundred years, being part of the traditional medicine of the indigenous population within this region (ARAÚJO, 2019).

Since the use of ayahuasca has spread throughout many countries, it is necessary to study in depth its cerebral mechanisms and its potential clinical implications. In addition,

because it affects brain areas related to emotions, memories, and executive functions, ayahuasca might be used in the treatment of psychiatric disorders, such as drug addiction (BOUSO; RIBA, 2014; FERNÁNDEZ; FÁBREGAS, 2014; GIOVANNETTI *et al.*, 2020), Parkinson's disease (SERRANO-DUEÑAS; CARDOZO-PELAEZ; SÁNCHEZ-RAMOS, 2001; WANG *et al.*, 2010; KATCHBORIAN-NETO *et al.*, 2020; BRIERLEY; DAVIDSON, 2012), and depression (JIMÉNEZ-GARRIDO *et al.*, 2020) (PALHANO-FONTES *et al.*, 2019; SANCHES *et al.*, 2016; PALHANO-FONTES *et al.*, 2021; OSÓRIO *et al.*, 2011; FROOD, 2015; SANTOS *et al.*, 2016). For example, an open-label clinical study found significant therapeutic benefits among patients with treatment-resistant major depressive disorder after the administration of a single dose of ayahuasca (SANCHES *et al.*, 2016). Moreover, a randomized trial showed that ayahuasca doses were associated with reductions in depressive symptoms in patients with major depressive disorder, compared to placebo treatments (PALHANO-FONTES *et al.*, 2019).

Additionally, ayahuasca has been shown to elicit anti-neuroinflammatory properties (SANTOS *et al.*, 2016) and stimulate adult neurogenesis in vitro (MORALES-GARCÍA *et al.*, 2017). In this line, ayahuasca could be helpful for the treatment of several neurological diseases well known to harbor inflammation in its physiopathology (SILVA; DAROS; BITENCOURT, 2020), including chronic degenerative diseases and illnesses related to acute injury, such as cerebral ischemia, multiple sclerosis, and AD (FRECSKA; BOKOR; WINKELMAN, 2016; SANTOS; HALLAK, 2017).

The EEG data studied here are from (SCHENBERG *et al.*, 2015), from subjects who ingested ayahuasca. This study observed slow-gamma power increases at the left Centro-parietal-occipital, left frontotemporal, and right frontal cortices. In contrast, fast-gamma increases were significant at the left Centro-parieto-occipital, left frontotemporal, right frontal, and right parieto-occipital cortices due to ayahuasca ingestion. As a result, this study concentrated solely on the changes in frequency bands caused by the use of the psychedelic substance.

Despite the enormous therapeutic potential of ayahuasca, in most countries, it is an illegal substance and only legalized for religious use, such as in Brazil. Therefore, few studies on human beings are found in the literature, and more research is needed on how this substance alters the brain and its mechanism of action.

The use of graph theory mathematical approaches gave intriguing insights into the intricate network structure of the human brain, which is also related with pathological states (BASSETT; GAZZANIGA, 2011; PINEDA *et al.*, 2020; SPORNS, 2018; BASSETT; ZURN; GOLD, 2018). Notably, complex networks have been employed as biomarkers for a variety of disorders (HAYASHIDA; AKUTSU, 2016; FEKETE *et al.*, 2013). Furthermore, the community detection algorithm (also referred to as the clustering graph) is a fundamental analysis technique that aims to identify densely connected structures within complex networks (NEWMAN, 2012; KIM; LEE, 2015; ZHAO; LIANG; WANG, 2021). Several studies have used complex network measurements and community detection algorithms to detect brain activity in EEG data recently

(LUNG *et al.*, 2016; KHAJEHPOUR *et al.*, 2019; VARLEY *et al.*, 2020).

Because of the increased amount of data related to health, such as medical records, exams of patients, and hospital resources, ML algorithms have become more applicable, primarily for medical diagnosis (SONG; JUNG; CHUNG, 2019; MOZAFFARINYA *et al.*, 2019; ILYASOVA *et al.*, 2018; LI; ASCH; SHAH, 2020), in order to provide more accurate and automatic investigations of various diseases (BELLAZZI; ZUPAN, 2008) and may be an important tool capable of detecting acute and permanent abnormalities in the brain. In addition, many studies have utilized ML algorithms to capture brain activity using raw EEG time series (BUZA, 2020; ABEL *et al.*, 2021), the correlation between electrodes (ALVES *et al.*, 2022b; JAYARATHNE; COHEN; AMARAKEERTHI, 2020), and complex network measures (PINEDA *et al.*, 2020).

Also, in contrast to traditional statistical methods, the ML approach has the advantage that it does not rely on prior assumptions (such as adequate distribution, independence of observations, absence of multicollinearity, and interaction problems) and is also well suited to analyze and capture complex nonlinear relationships in data automatically. Nevertheless, new techniques have emerged to assist in interpreting machine learning results, e.g., SHAP values. Any machine learning algorithm may use this metric for identifying and prioritizing features (BOWEN; UNGAR, 2020; RODRÍGUEZ-PÉREZ; BAJORATH, 2019; SPADON *et al.*, 2019).

The purpose of this study is to determine whether it is possible to automatically detect the changes in brain activity after intake of ayahuasca with machine learning methods using the following data abstraction levels for the input: (A) raw EEG time series, (B) the correlation between the EEG electrodes as used in (A) represented by a connectivity matrix, and (C) complex network measures extracted from (B). In contrast to articles in the literature that use only one of these levels of abstraction, this study uses all three levels. In addition, we define which of these abstraction levels is most appropriate for capturing ayahuasca-induced brain changes. The SHAP value method has also been shown to be more effective than the studies cited above in identifying the best brain regions, the best connections between the brain regions, and the best measures of complex networks, which can be used to interpret the effects of the psychedelic substance on the brain. A final result of this research was the creation of new measures that have never been used before within the literature, which can be used as input to machine learning algorithms to assess the size of community structures.

2 Materials and methods

The python code used for the analysis is available at <https://github.com/Carol180619/Paper-ayahuasca.git>.

2.1 Data

The data used for this study has been made openly available by the Federal University of São Carlos, Brazil (SCHENBERG *et al.*, 2015). Sixteen healthy male and female patients with prior ayahuasca experience (eight women, mean 29.0 years; 12 men, mean 38.5 years) agreed (with written permission) to consume this psychedelic substance while EEG recordings were made [1]. All methodologies for this investigation were approved by the Universidade Federal de São Paulo's Ethical Committee, and the study was carried out in compliance with available criteria for human hallucinogen research safety (JOHNSON; RICHARDS; GRIFFITHS, 2008).

Patients were instructed to close their eyes and remain in a resting condition. A nurse accompanied the experiment for its duration of 225 minutes. The recordings began 25 minutes before ayahuasca consumption and ended 200 minutes afterward. The main compounds in the brew were (SCHENBERG *et al.*, 2015): DMT, DMTN-oxide (DMT-NO), N-methyltryptamine (NMT), indoleacetic acid (IAA), 5-hydroxy-DMT (5-OH-DMT, or bufotenin), 5-methoxy-DMT (5-MeO-DMT), Harmine, Harmol, Harmaline, Harmalol, THH, 7-hydroxy-tetrahydroharmine (THH-OH), and 2-methyl-tetrahydro-beta- carboline (2-MTHBC). All recordings were down-sampled to 500 Hz, bandpass filtered between 0.5 and 150 Hz, and artifacts due to movements were removed. Recordings were made with 62 electrodes, following the EEG electrode positions in the 10-10 system. These channels are: Fp1, Fz, F3, F7, FT9, FC5, FC1, C3, TP9, CP5, CP1, Pz, P3, P7, O1, Oz, P8, TP10, CP6, CP2, C4, T8, FT10, FC6, FC2, F4, F8, Fp2, AF7, AF3, AFz, F1, F5, FT7, FC3, FCz, C1, C5, TP7, CP3, P1, P5, PO7, PO3, POz, PO4, PO8, P6, P2, CPz, CP4, TP8, FC4, FT8, F6, F2, AF4, AF8, O2, P4, C6, and C2 (see in appendix A.2 Fig 51). It is worth mentioning that after using ayahuasca, all individuals experienced notable alterations in their typical state of consciousness.

Further details are given in (SCHENBERG *et al.*, 2015).

2.2 Machine learning algorithm

2.2.1 Classification

In order to classify the (A) EEG time series, (B) the connectivity matrices, and (C) the complex network measures, the support vector machine (SVM) (BOTTOU; LIN, 2007) algorithm was used. SVM has been used with superior results for the classification of complex network measures before by other groups (MAZROOYISEBDANI *et al.*, 2020; DIYKH; LI; WEN, 2017; DEY; RAO; SHAH, 2014) and performed superior in our comparative evaluation. In this analysis, we compared the following machine learning methods to classify the complex network measures: Random forest (RF)(BREIMAN, 2001), SVM (BOTTOU; LIN, 2007), Naive

[1] The following exclusion criteria were used: minors than the age of 21 years, personal history of psychiatric illness, current use of any psychiatric medication, cardiovascular disease, and any neurological disorders or brain damage in the previous year.

bayes (NB) (FRIEDMAN; GEIGER; GOLDSZMIDT, 1997), multilayer perceptron (MLP) (HINTON; RUMELHART; WILLIAMS, 1986), stochastic gradient descent with linear models classifier (SGD) (ZHANG, 2004), logistic regression (LR) (TOLLES; MEURER, 2016) and extreme Gradient Boosting classifier (XGBoost) (FRIEDMAN, 2001). The results can be found in Appendix A.4.

A more robust deep learning (DL) algorithm from (ALVES *et al.*, 2022b) (in which the model was named tuned CNN) was also tested. The results using DL are in the Appendix A.5.

2.2.2 Resampling and evaluation

The dataset was resampled by separating it into training (train) and test sets, with 25% of data composing the test set. Then, for a reliable model, a k-cross validation was used (REFAEILZADEH; TANG; LIU, 2009), with k = 10 (value widely used in the literature (BERRAR, 2019; BENGIO; GRANDVALET, 2004; SHAH; KHAN, 2020; KAWAMOTO; KABASHIMA, 2017; CHAN *et al.*, 2019; KAWAMOTO; KABASHIMA, 2017)). A hyper-parameter optimization called grid search was used here, similar to (SATO *et al.*, 2019; ZHONG *et al.*, 2021; ARCADU *et al.*, 2020; KRITTANAWONG *et al.*, 2021; RASHIDI *et al.*, 2020). The hyper-parameter optimization values used for each classifier models can be found in Appendix A.4.

For evaluation, Acc. was used as the standard performance metrics, as is the state-of-art in the literature (MINCHOLÉ; RODRIGUEZ, 2019; TOLKACH *et al.*, 2020; DUKART *et al.*, 2021; LI; ASCH; SHAH, 2020; PARK; KELLIS, 2015). Since the problem here is a two-class (negative and positive) classification problem, other metrics considered here are the measures of precision and recall, also commonly used in the literature (ITO *et al.*, 2021; KIM *et al.*, 2020; LI *et al.*, 2021; YU *et al.*, 2020). Precision (also called positive predictive value) is the proportion of relevant instances among those retrieved. Whereas recall (also called sensitivity) measures how well a classifier can predict positive examples (hit rate in the positive class), here related with an effect of the ayahuasca. Another measure used here and also used in literature (ZHONG *et al.*, 2021; BERRYMAN *et al.*, 2020; YANG *et al.*, 2019) is the F1 score which is the harmonic mean of the recall and precision (HANNUN *et al.*, 2019). For visualization of these two latter measures, ROC curve is a standard method as it displays the relation between the rate of true positives and false positives. The area below this curve, called the AUC, has been widely used in classification problems (MINCHOLÉ; RODRIGUEZ, 2019; BRACHER-SMITH; CRAWFORD; ESCOTT-PRICE, 2021; PATEL *et al.*, 2021; KRITTANAWONG *et al.*, 2021). The value of the AUC varies from 0 to 1, where the value of one corresponds to a classification result free of errors. $AUC = 0.5$ indicates that the classifier is not able to distinguish the two classes; this result is equal to the random choice. Furthermore, we consider the micro average of the ROC curve, which computes the AUC metric independently for each class (calculate AUC metric for healthy individuals, class zero, and separately calculate for unhealthy subjects, class one), and then the average is computed considering these classes equally. The macro average is also used

in our evaluation, which does not consider both classes equally, but aggregates the contributions of the classes separately and then calculates the average.

Furthermore, we interpret the machine learning results using SHAP values (LUNDBERG; LEE, 2017) to quantify the importance of the complex measures, connections of brain regions, and location of electrodes for the classification result. This metric enables the identification and prioritization of features and can be used with any machine learning algorithm (BOWEN; UNGAR, 2020; RODRÍGUEZ-PÉREZ; BAJORATH, 2019; SPADON *et al.*, 2019).

2.3 Input data for machine learning

The following three data abstraction levels were applied to a classification algorithm as described in subsection 2.2 Machine learning algorithm: (2.3.1 EEG time series) the EEG time series (Fig 8), (2.3.2 Connectivity matrices) the connectivity matrix calculated by means of the Pearson correlation of the EEG time series (Fig 9), and (2.3.3 Complex network measures) the complex network measures calculated from the connectivity matrix (Fig 10).

2.3.1 EEG time series

The data was divided into three "time windows" (see Table 10). The first window (25 minutes before ingestion until 50 minutes after ingestion of ayahuasca) was defined as the "control". This is reasonable as it is known from (SCHENBERG *et al.*, 2015), that the blood plasma concentration of the main psychedelic compound DMT is low until 50 minutes after ingestion. Windows two and three were both defined as thoroughly influenced by ayahuasca. The ayahuasca-influenced time series were divided into two windows to enhance the quantity of data points for the machine learning method. Even though the number of independent samples (subjects) did not change, increasing the data points by splitting the time series is a common machine learning approach (CERQUEIRA; TORGO; MOZETIČ, 2020; BOUKTIF *et al.*, 2018). Even though the number of independent samples (subjects) did not change, increasing the data points by splitting the time series is a standard machine learning approach. Furthermore, in the following classification task, only two classes will be labeled class zero (without ayahuasca) and labeled class one (with ayahuasca). The scheme of this methodology is shown in Fig 8 . All participants' EEG time series were successively combined and stored in a 2D matrix to feed the data into the machine learning algorithm. Each column represents an electrode, and each row represents the amplitude of each time point of the EEG signal. For each of the three time windows, a 2D matrix was constructed.

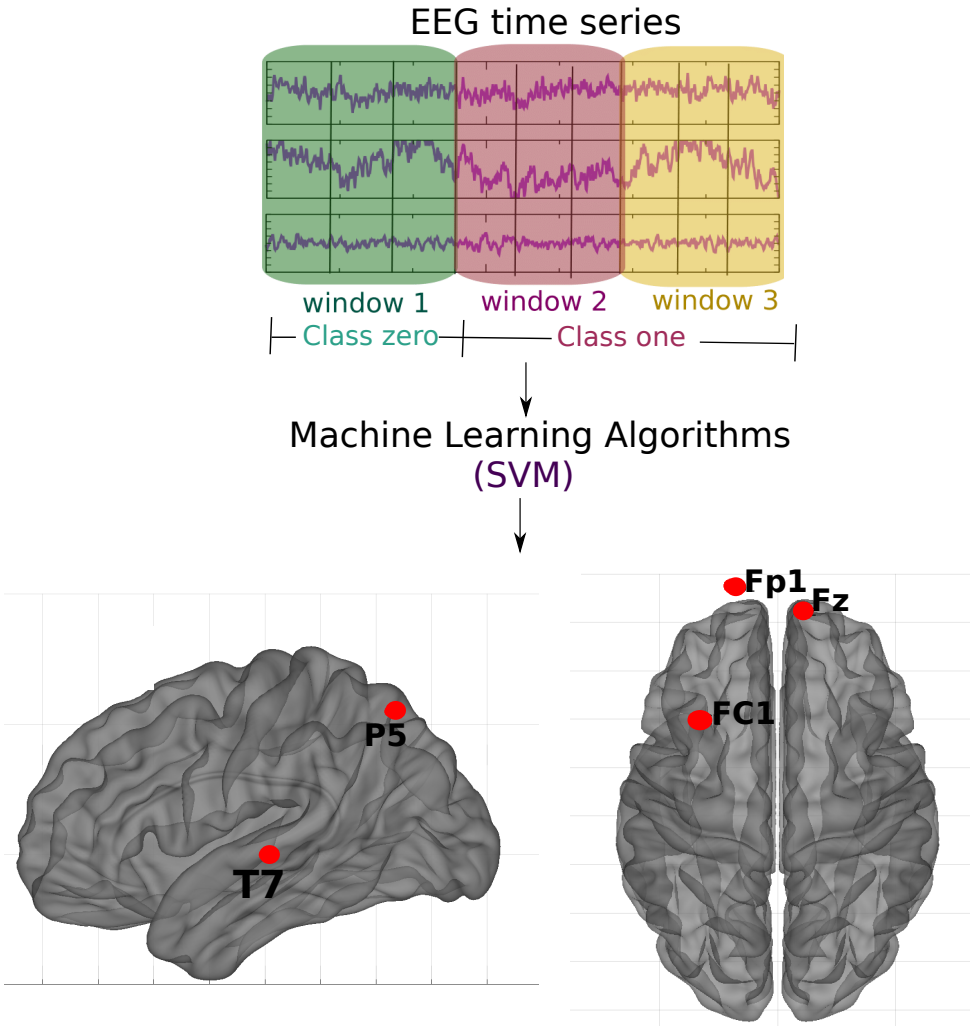

Figure 8 – **Methodology of the subsection 3.1 using raw EEG time series**. For each participant, the EEG time series was split into three parts. Those corresponding to the first window were labeled as class 0 (no effect of ayahuasca) and those corresponding to the second and third windows as class 1 (under the influence of ayahuasca), and then SVM was used. The objective was to determine which brain parts are most influenced by ayahuasca consumption. The crucial areas discovered using the SHAP values approach are emphasized in the illustration.

Table 10 – Definition of time windows of the EEG signal. Window 1 is considered the control (without effect of ayahuasca), window 2 and 3 are considered as recordings under the influence of ayahuasca.

Time window	**Ingestion of ayahuasca at t = 0 minutes**
1	-25 to 50 minutes
2	50 to 125 minutes
3	125 to 200 minutes

2.3.2 Connectivity matrices

The matrices of connectivity were calculated by the well known Pearson correlation. It is a widely used and successfully approved measure to capture the correlation of EEG electrodes (ROJAS *et al.*, 2018; WANG *et al.*, 2017b; JALILI, 2016; HAN *et al.*, 2019; TOKARIEV *et al.*, 2019).

The Pearson correlation was calculated for all electrode pairs resulting in three connectivity matrices per participant (for each time window). Fig 9 illustrates the workflow of this approach. The connectivity matrices were flattened into one vector to input the data into the machine learning algorithm. Then, all vectors were sequentially merged into a 2D matrix. Each column represents a connection between two brain regions, and each row represents a subject. Such a 2D matrix was generated for each of the three time windows.

2.3.3 Complex network measures

For each connectivity matrix (see subsection 2.3.2 Connectivity matrices), a graph was generated to extract different complex network measures. The complex network measures were stored in a matrix to input the data into the machine learning algorithm. Each column represents a complex network measure, and each row a subject. Such a 2D matrix was generated for each of the three time windows. The following complex network measures were calculated: Assortativity (NEWMAN, 2003; NEWMAN, 2002), average path length (APL) (ALBERT; BARABÁSI, 2002), betweenness centrality (BC) (FREEMAN, 1977), closeness centrality (CC) (FREEMAN, 1978), eigenvector centrality (EC) (BONACICH, 1987), diameter (ALBERT; JEONG; BARABÁSI, 1999), hub score (KLEINBERG, 1999), average degree of nearest neighbors (Knn) (EPPSTEIN; PATERSON; YAO, 1997), mean degree (DOYLE; GRAVER, 1977), second moment degree (SMD) (SNIJDERS, 1981), entropy degree (DEHMER; MOWSHOWITZ, 2011), transitivity (WATTS; STROGATZ, 1998; NEWMAN; WATTS; STROGATZ, 2002), complexity, k-core (SEIDMAN, 1983; NEWMAN, 2010), eccentricity (HAGE; HARARY, 1995), density (ANDERSON; BUTTS; CARLEY, 1999), and efficiency (LATORA; MARCHIORI, 2003). Furthermore, newly developed metrics reflecting the number of communities in a complex network are used in this paper.

Furthermore, newly developed metrics reflecting the number of communities in a complex network are used in this paper. We perform the community detection algorithms to find the largest community, then calculate the average path length within this community and receive a single value as a result (that will be used to feed ML algorithm). The community detection algorithms used were:

- Fastgreedy community (FC) is defined in (CLAUSET; NEWMAN; MOORE, 2004) as a hierarchical agglomerative clustering algorithm aimed at maximizing the modularity measure defined in (GIRVAN; NEWMAN, 2002).

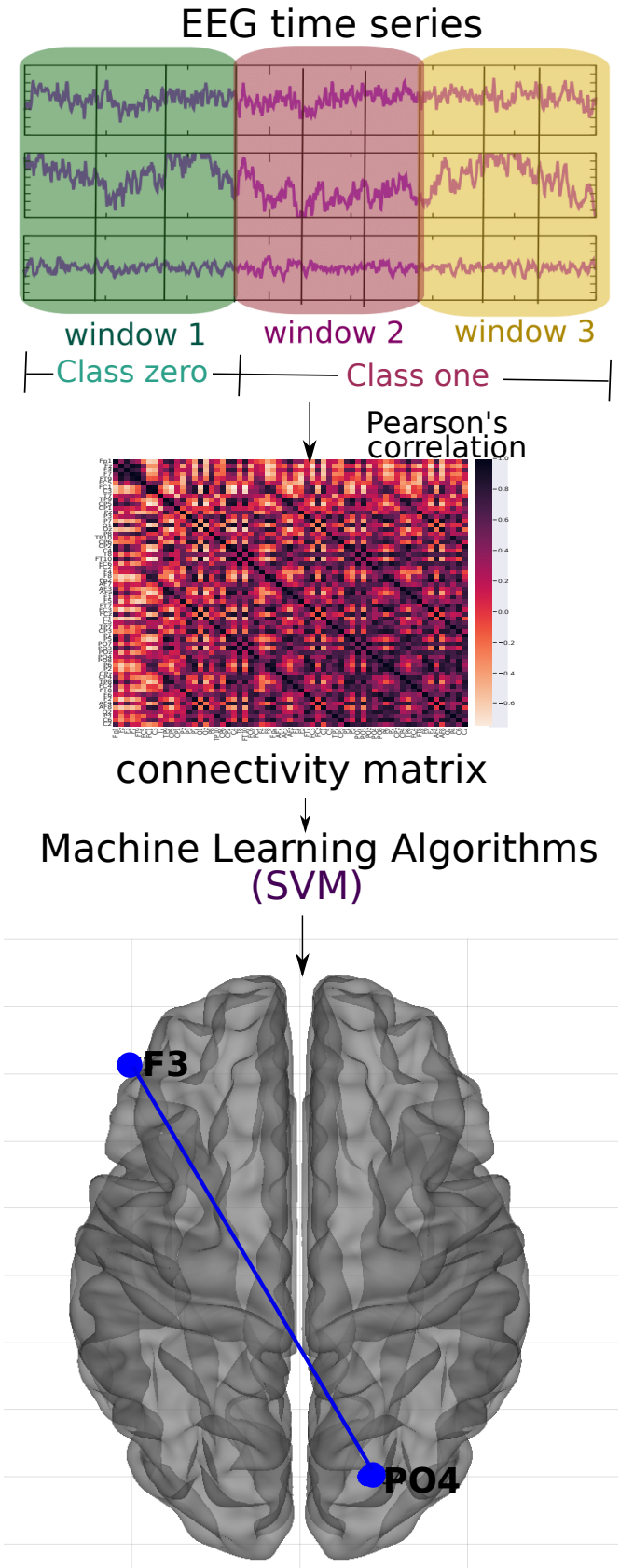

Figure 9 – **Methodology of the subsection 3.1 using connectivity matrices.** For each of the time windows, the Pearson correlation connectivity matrix was generated, and then they were classified with the SVM method considering the first window as zero label (without ayahuasca) and the other two as one label (with ayahuasca). This analysis aimed to verify the best connections of the brain areas used during ayahuasca use. The principal connection discovered using the SHAP value approach is depicted in the picture.

- Infomap community (IC) described in (ROSVALL; AXELSSON; BERGSTROM, 2009), the purpose behind this technique is to exploit the dynamics of random walks. This is accomplished by employing Huffman's method (HUFFMAN, 1952) and then calculating the minimization of the map equation to determine the number of communities (ROSVALL; AXELSSON; BERGSTROM, 2009).

- Leading eigenvector community (LC) is defined in (NEWMAN, 2006). It aims to calculate the eigenvector of the modularity matrix for the largest positive eigenvalue and then separate the vertices into two communities based on the sign of the corresponding element in the eigenvector.

- Label propagation community (LPC) is defined in (RAGHAVAN; ALBERT; KUMARA, 2007). It is an optimization algorithm (BARBER; CLARK, 2009) in which, at first, each node in the network has a label indicating its assignment, and then each node updates its label according to the label with the maximum number in its neighbors. This process is repeated until the network reaches a stable state and nodes with the same class are considered to belong to the same community. (LI *et al.*, 2021).

- Edge betweenness community (EBC) is defined in (GIRVAN; NEWMAN, 2002) is a divisive model based on the BC. At each iteration, this measure is calculated for all edges, and the one with the highest value of this measure is eliminated until the network contains N elements resulting in a hierarchical distribution of communities. The one with the highest modularity is adopted.

- Spinglass community (SPC) is defined in (REICHARDT; BORNHOLDT, 2006) this algorithm considers the spin state of nodes as communities and tries to minimize the spin energy until it finds a ground state of the spin-glass model (CHEJARA; GODFREY, 2017).

- Multilevel community (MC) is a greedy optimization method using modularity and is defined in (BLONDEL *et al.*, 2008).

Since the community detection algorithms were combined with the average path length, we extended the abbreviations by the letter "A" as follows: AFC, AIC, ALC, ALPC, AEBC, ASPC, and AMC.

Figure 10 depicts the entire workflow.

3 Results

The highest classification performance was obtained using the connectivity matrices with an accuracy of 92%, followed by the EEG time series (88%) and the complex network measures (83%) (see Table 11). The following subsections 3.1 EEG time series, 3.2 Connectivity matrices and 3.3 Complex network measures contain the results in more detail.

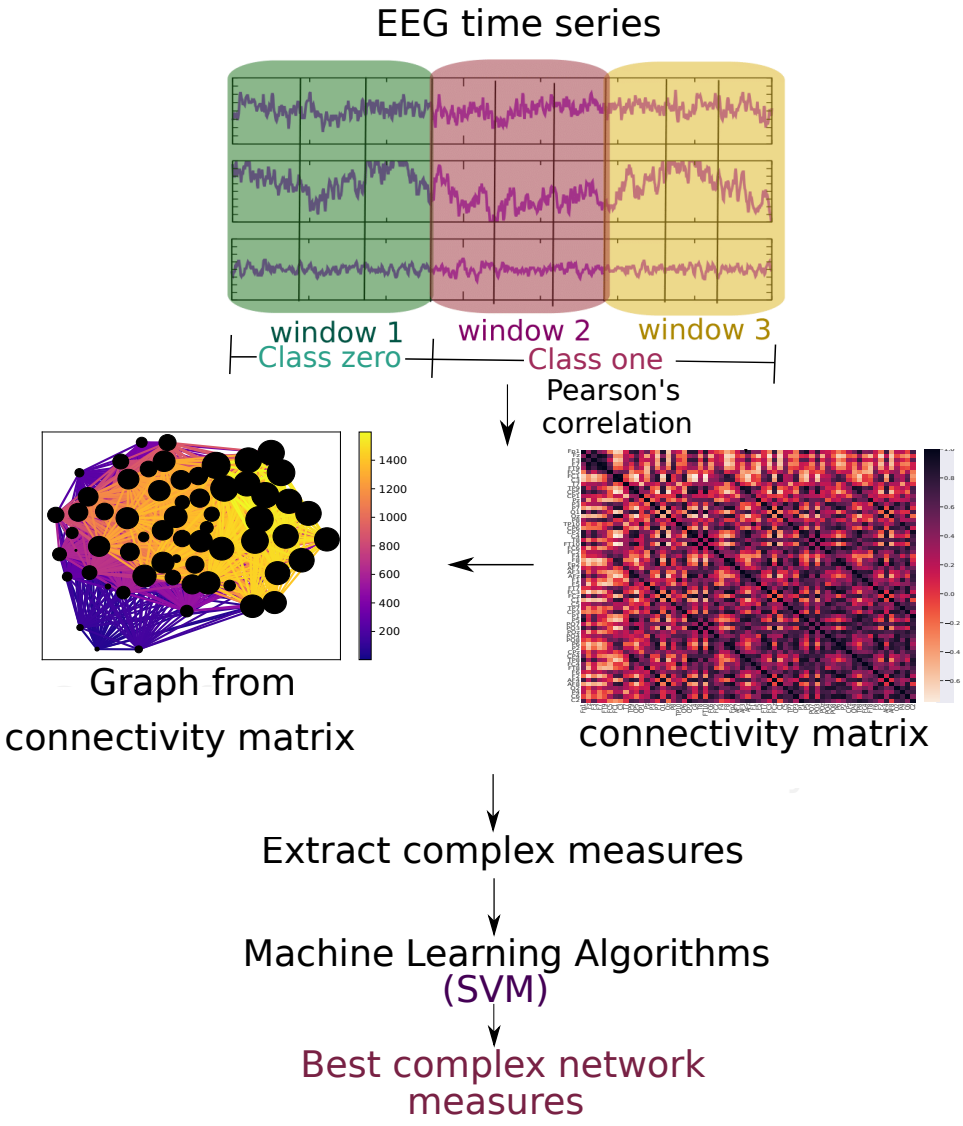

Figure 10 – **Methodology of the subsection 3.1 using complex network measures.** The EEG time series is divided into three parts. For each of them, the Pearson correlation was calculated. For each window, a connectivity matrix was generated (in the Fig, the connectivity matrix of the first window of the first subject containing the 62 electrodes, the color bar containing the connection strength between these electrodes). A graph was formed for each of them (in the Fig, the graph of this connectivity matrix has 62 nodes and the connection strength according to the color bar and the node size according to its number of connections), and complex network measures are extracted from them.

Table 11 – Performances of the SVM classifier for the different data types used in this paper. The best performance is highlighted in bold. The classification of connectivity matrices best captured the changes in the brain due to ayahuasca.

Type of data	Subset	AUC	Acc.	F1 score	Recall	Precision
EEG time series	**Train**	0.87	0.89	0.88	0.87	0.89
	Test	0.85	0.88	0.86	0.85	0.86
Connectivity matrix	**Train**	**0.92**	**0.94**	**0.93**	**0.92**	**0.96**
	Test	**0.88**	**0.92**	**0.90**	**0.88**	**0.94**
Complex measure	**Train**	0.79	0.81	0.79	0.79	0.78
	Test	0.75	0.83	0.78	0.75	0.90

3.1 EEG time series

The performance of the test sample using the EEG time series was mean AUC of 0.85, mean precision of 0.88, mean F1 score of 0.86, mean recall of 0.85, and mean accuracy of 0.86. The precision measure is related to the positive class (with ayahuasca). Since the precision measure was slightly higher than the recall measure, the model can better detect the presence of ayahuasca instead of the absence of it.

In Fig 11, the confusion matrix (Fig 11A), the learning curve (Fig 11B), and the ROC curve (Fig 11C) are plotted.

The learning curve evaluates the predictability of the model by varying the size of the training set (SPADON *et al.*, 2019). Fig 11B shows that the highest accuracy in the test sample can only be achieved when the entire database is used.

Not all electrodes of the EEG recording were equally important for the classification. According to the SHAP values, the most important region for the model was T7, located in the temporal region (see Fig 12). In order of importance, this region was followed by FC1, Fp1, P5, and Fz, located between frontal and central, frontal and parietal, parietal and frontal, respectively (see Fig 13A). In addition, Fig 13B shows details of the impact of each feature on the model. Positive SHAP values are shown when the presence of ayahuasca is detected, and negative SHAP values are shown when the absence of ayahuasca is detected. The colors indicate whether the feature value was low (blue) or high (red). Since the feature consists of the amplitudes of the EEG time series, it can be seen that for T7, the low amplitudes (blue dots) were important to detect the absence of ayahuasca (negative SHAP values), and the high amplitudes (red dots) were important to detect the presence of ayahuasca (positive SHAP values).

3.2 Connectivity matrices

For the connectivity matrices, the test sample performance was a mean AUC of 0.88, mean accuracy of 0.92, mean F1 score of 0.90, mean recall of 0.88, and mean precision of 0.94.

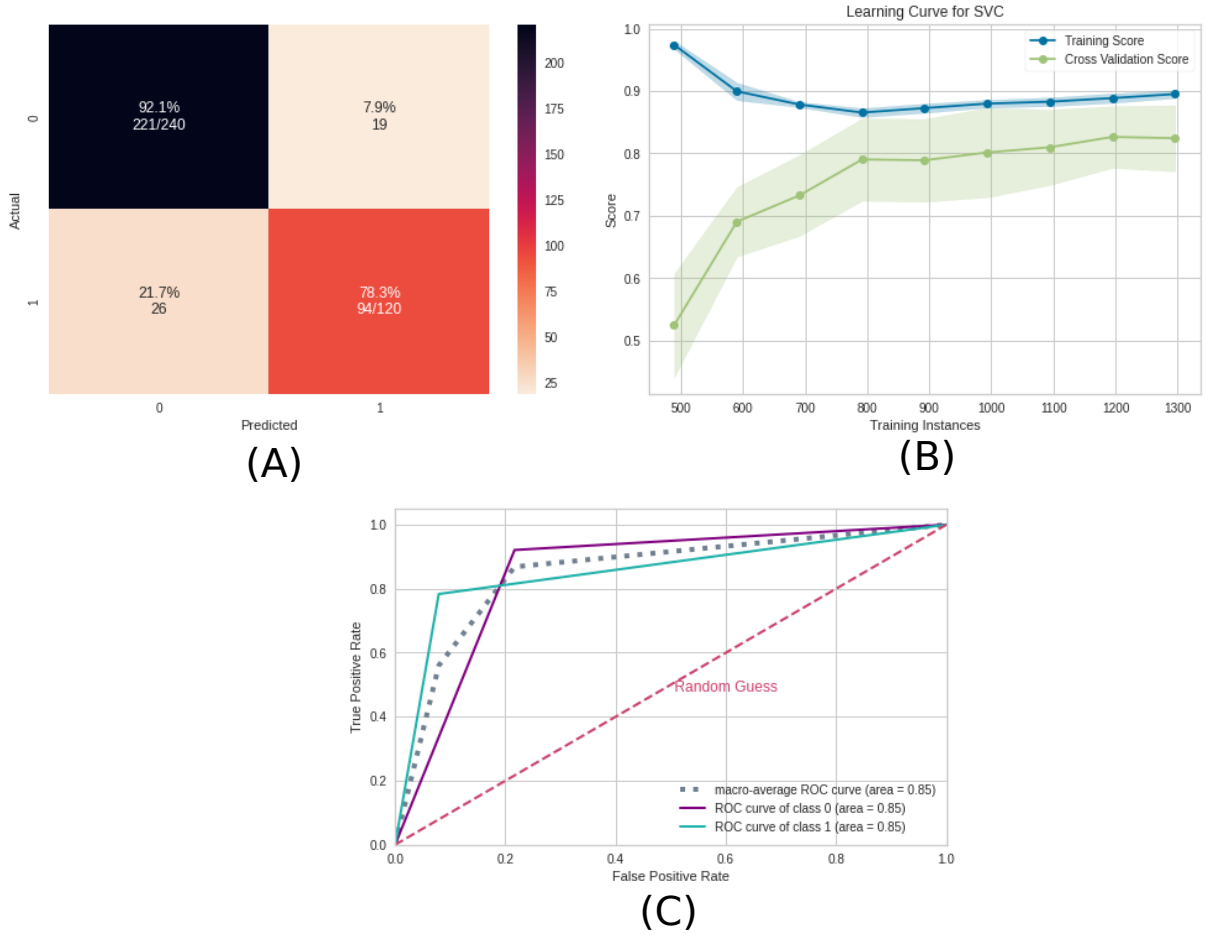

Figure 11 – **Machine learning results using the EEG time series as input data.** A) Confusion matrix indicating a true negative rate of 92.1% (blue according to the color bar) and a true positive rate of 78.3% (orange according to the color bar). B) Learning curve for the training accuracy (blue) and for test accuracy (green). C) ROC curve of class 0 (without ayahuasca) and class 1 (with ayahuasca). The gray dotted curve is the macro-average accuracy (area under curve = 0.85) and the pink one the random classifier.

Similar to the previous subsection 3.1 EEG time series, the precision measure was higher than the recall measure and therefore the model can better detect the presence of ayahuasca. In Fig 14, the confusion matrix (Fig 14A), the learning curve (Fig 14B), and the ROC curve (Fig 14C)are plotted. Similar to EEG time series, the learning curve for the connectivity matrices shows that the highest accuracy in the test sample can only be achieved when the entire database is used.

In order to reveal the importance of the brain connections, the SHAP values were used as in the preview subsection 3.1 EEG time series. The results are shown in Fig 15. From that the most important connection was between F3 (frontal region) and PO4 (between parietal and occipital region). In addition, in Fig 15B it can be seen that for the connection between F3 and PO4, low values of correlation (blue dots) were important for detecting the absence of ayahuasca (negative SHAP values), and high values of correlation (red dots) were important for detecting the presence of ayahuasca (positive SHAP values).

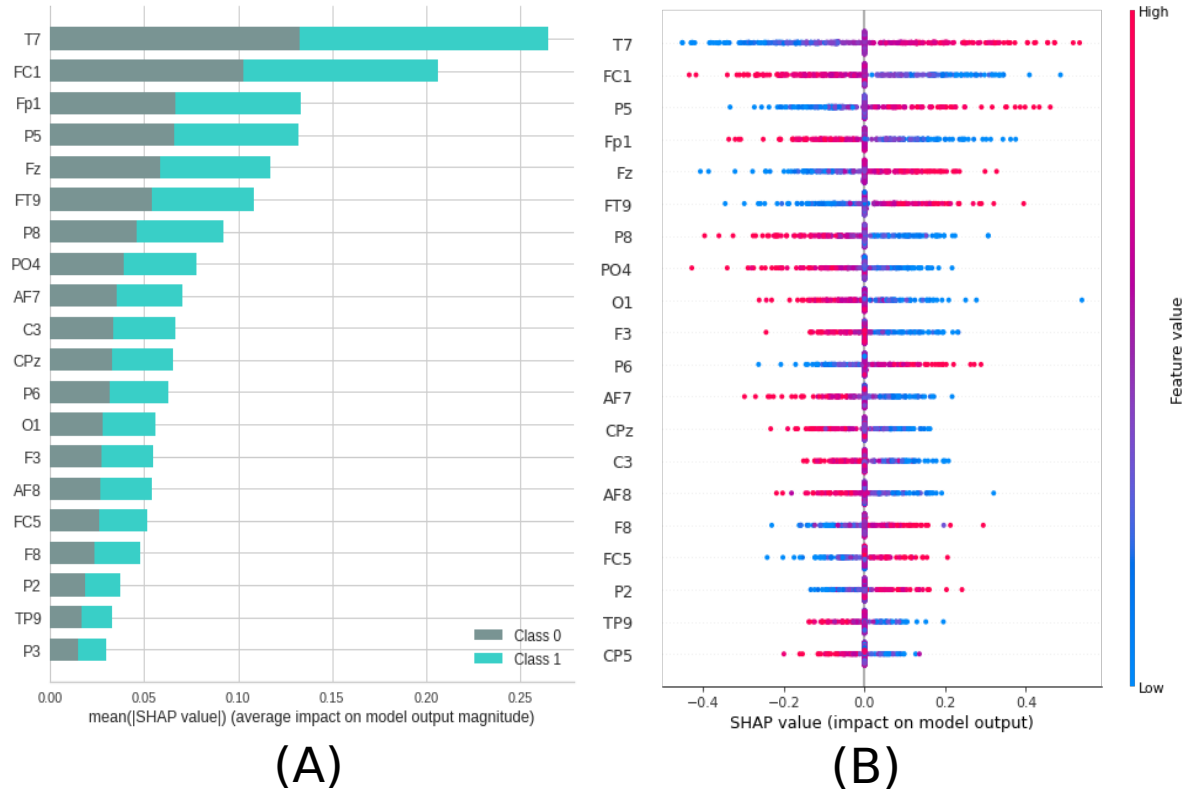

Figure 12 – **Feature importance ranking for SVM classifier being the brain regions ranked in descending order of importance.** Brain region T7 is most important to classify the effect of ayahuasca. A) Feature ranking based on the average of absolute SHAP values over all subjects considering both classes (gray:without ayahuasca, cyan: with ayahuasca). B) Same as A) but additionally showing details of the impact of each feature on the model.

The location in the brain can be seen in Fig 16.

3.3 Complex network measures

The test sample performance using the complex network measures was a mean AUC of 0.75, mean accuracy of 0.83, mean F1 score of 0.78, mean recall of 0.75, and mean precision of 0.90.

Similar to the previous subsections 3.1 EEG time series and 3.2 Connectivity matrices, the precision measure was higher than the recall measure, and therefore the model can better detect the presence of ayahuasca.

In Fig 10, the confusion matrix (Fig 17A), the learning curve (Fig 17B), and the ROC curve (Fig 17C) are plotted. Again, the entire database is necessary in order to get the highest accuracy.

From the SHAP values in Fig 18 it can be seen that the most important measure for the model was the CC, followed by assortativity, and the newly introduced measures ASC and ASPC. In addition, in Fig 18B can be seen that for the CC measure, low values of this metric (blue dots)

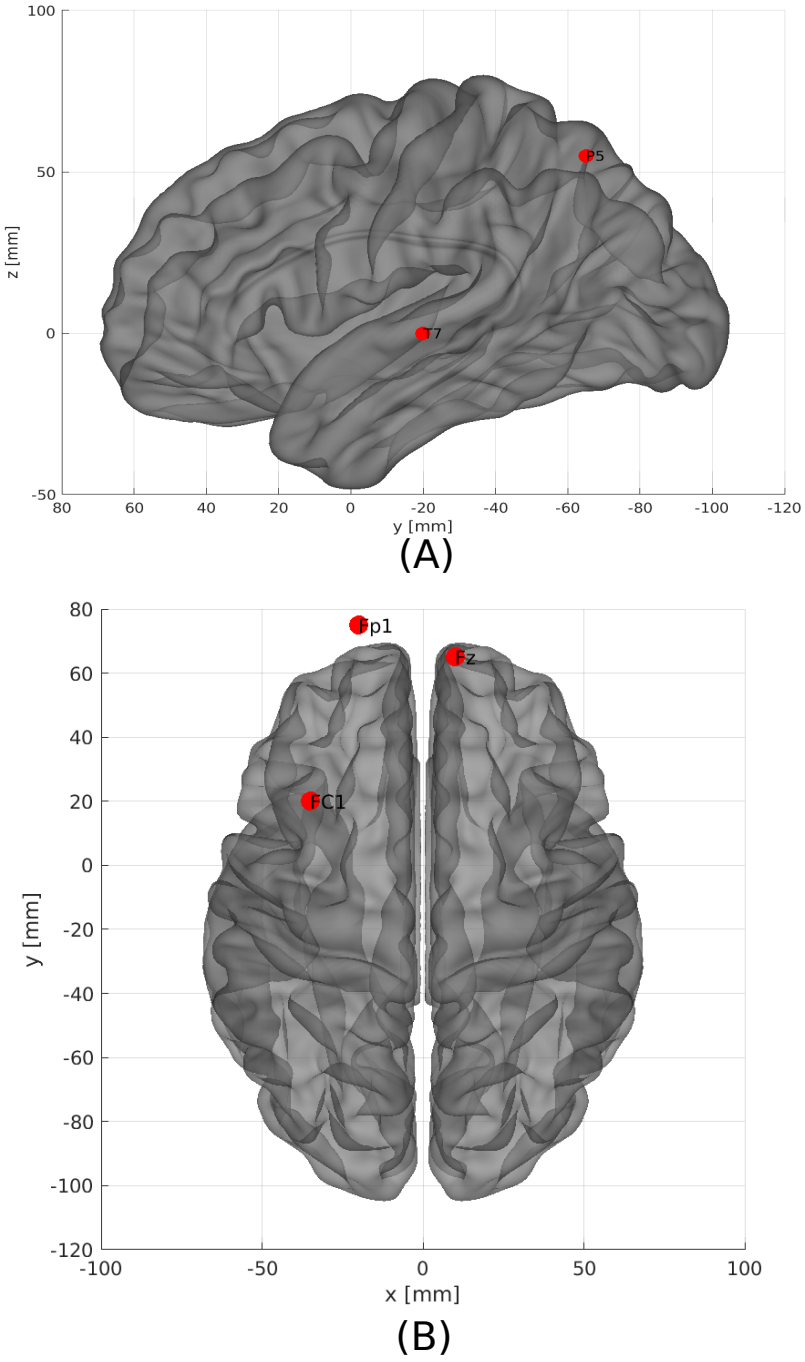

Figure 13 – **The five most important brain regions considering EEG time series as input data.** A) - Sagittal left plane showing the brain region for the channel T7 and P5. B) Axial dorsal plane showing the brain regions Fz, Fp1 and FC1. The brain plot was made using Braph tool (MIJALKOV *et al.*, 2017), based on the coordinates in (MICHEL; BRUNET, 2019; ASHER *et al.*, 2021).

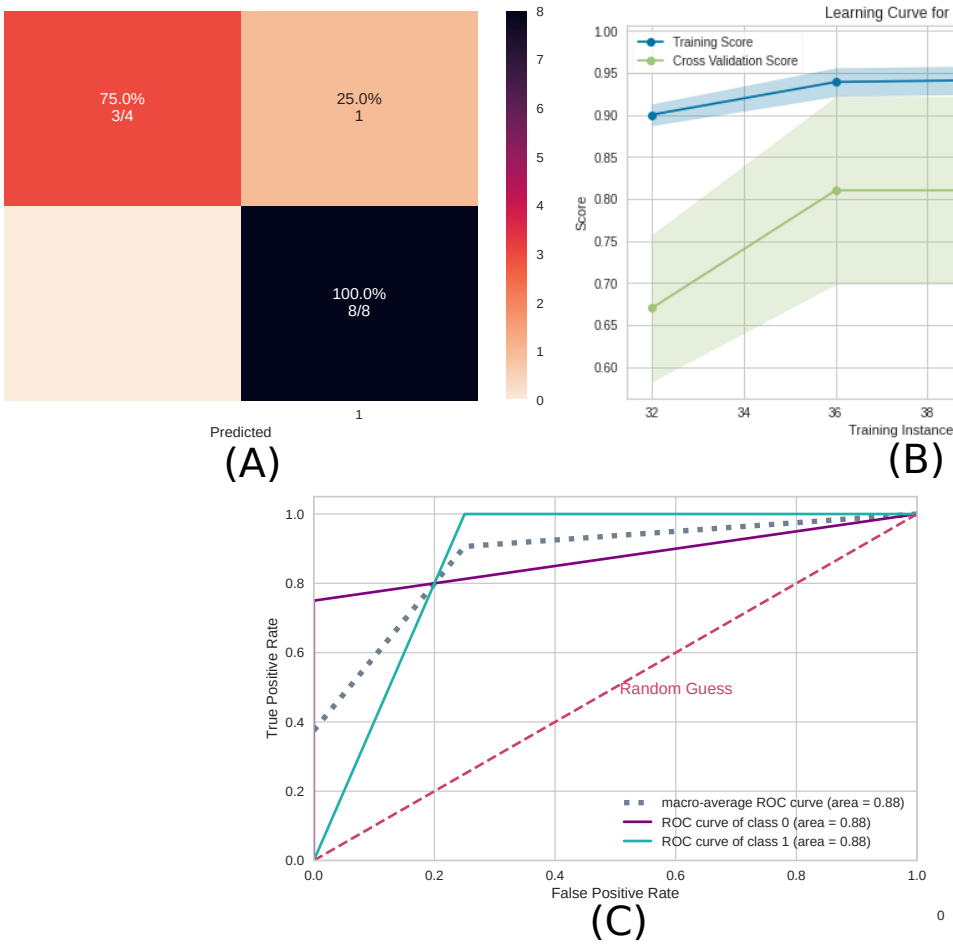

Figure 14 – **Machine learning results using the connectivity matrices as input data.** A) Confusion matrix indicating a true negative rate of 75% (orange according to the color bar) and a true positive of 100% (blue according to the color bar). B) Learning curve for the training accuracy (blue) and for test accuracy (green). C) ROC curve of class 0 (without ayahuasca) and class 1 (with ayahuasca). The gray dotted curve is the macro-average accuracy (area under curve = 0.88) and the pink one the random classifier.

were important for detecting the absence of ayahuasca (negative SHAP values), and high values of this metric (red dots) were important for detecting the presence of ayahuasca (positive SHAP values).

4 Discussion

In this paper, we aimed to answer the question if it is possible to automatically detect brain activity changes due to ayahuasca using machine learning and which features are most important and could act as biomarkers.

Our results show that it is possible to automatically detect the changes due to ayahuasca. The classification accuracy was above 75% for all three data abstraction levels. The classification accuracy of connectivity matrices was higher than the raw EEG time series, suggesting that

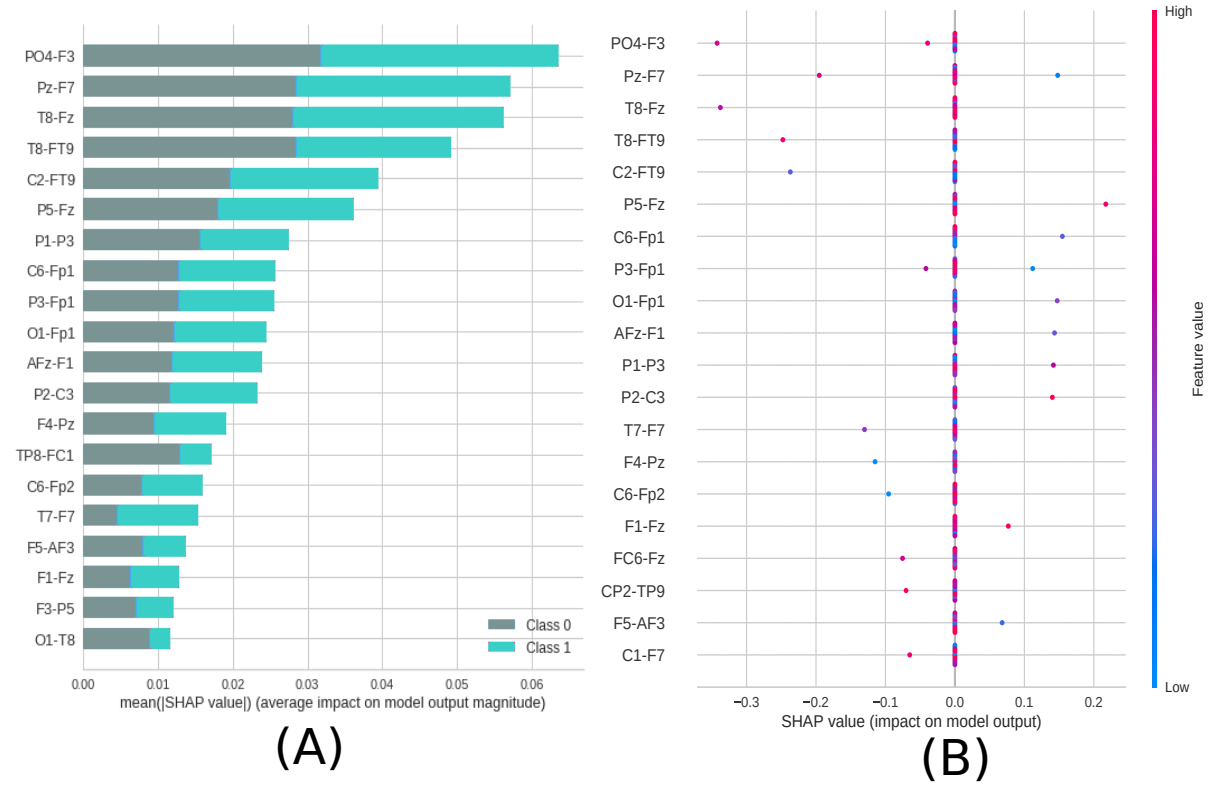

Figure 15 – **Feature importance ranking for SVM classifier being the connections of brain regions ranked in descending order of importance.** The connection between the regions PO4 and F3 is the most important to classify the effect of ayahuasca. A) Feature ranking based on the average of absolute SHAP values over all subjects considering both classes (gray: without ayahuasca, cyan: with ayahuasca). B) Same as A) but additionally showing details of the impact of each feature on the model.

connection changes are more important between brain regions than within brain regions. This result is important since the connectivity matrices improved the accuracy and produced efficiency gains, such as reduced data storage and faster machine learning training. This would be especially useful for larger datasets, where raw time series may be very costly, for example, in hospital diagnosis systems.

4.1 EEG time series

The raw EEG time series analysis revealed that the frontal and the temporal lobe were the most affected brain regions. In line with that, studies using single photon emission computed tomography (SPECT) have reported that ayahuasca increases blood perfusion in the frontal regions of the brain, more specifically, the insula, left nucleus accumbens, left amygdala, parahippocampal gyrus, and left the subgenual area (SANTOS *et al.*, 2016; RIBA *et al.*, 2006). Furthermore, works using functional magnetic resonance imaging have observed activation in the brain's occipital, temporal, and frontal areas (JIMÉNEZ-GARRIDO *et al.*, 2020; ARAUJO *et al.*, 2012). These regions are related to introspection, emotional processing, and the therapeutic

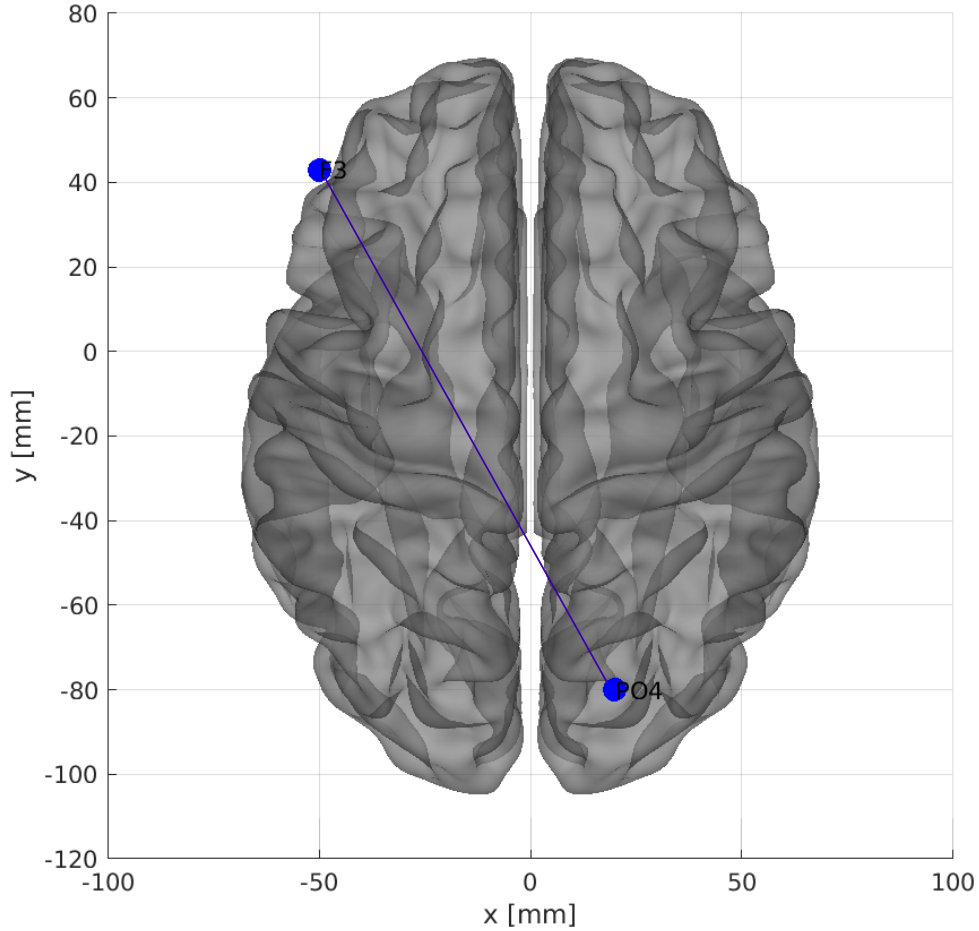

Figure 16 – **The most important connection of brain regions considering connectivity matrices as input data.** Axial dorsal plane showing the brain regions connection between F3 and PO4. The brain plot was made using Braph tool (MIJALKOV *et al.*, 2017), based on the coordinates in (MICHEL; BRUNET, 2019; ASHER *et al.*, 2021).

effects of traditional antidepressants (SANTOS; HALLAK, 2021) and most interestingly, it may also affect motor and cognitive functions in other neurological disorders, such as Parkinson's disease and Alzheimer's disease, respectively (AARSLAND *et al.*, 2017; SMITH *et al.*, 2018).

4.2 Connectivity matrices

The correlation between the left frontal cortex (F3) and right parietal-occipital (PO4) was most important in terms of brain connections.

(RODRIGUEZ *et al.*, 1999) showed that synchronization in the gamma band between the parietal-occipital and frontal cortices was present during face recognition tasks. Since the EEG time series data used in this work only contained the gamma band, the P04-F3 connection could point to similar cognitive processes in the subjects during ayahuasca-mediated visual hallucinations.

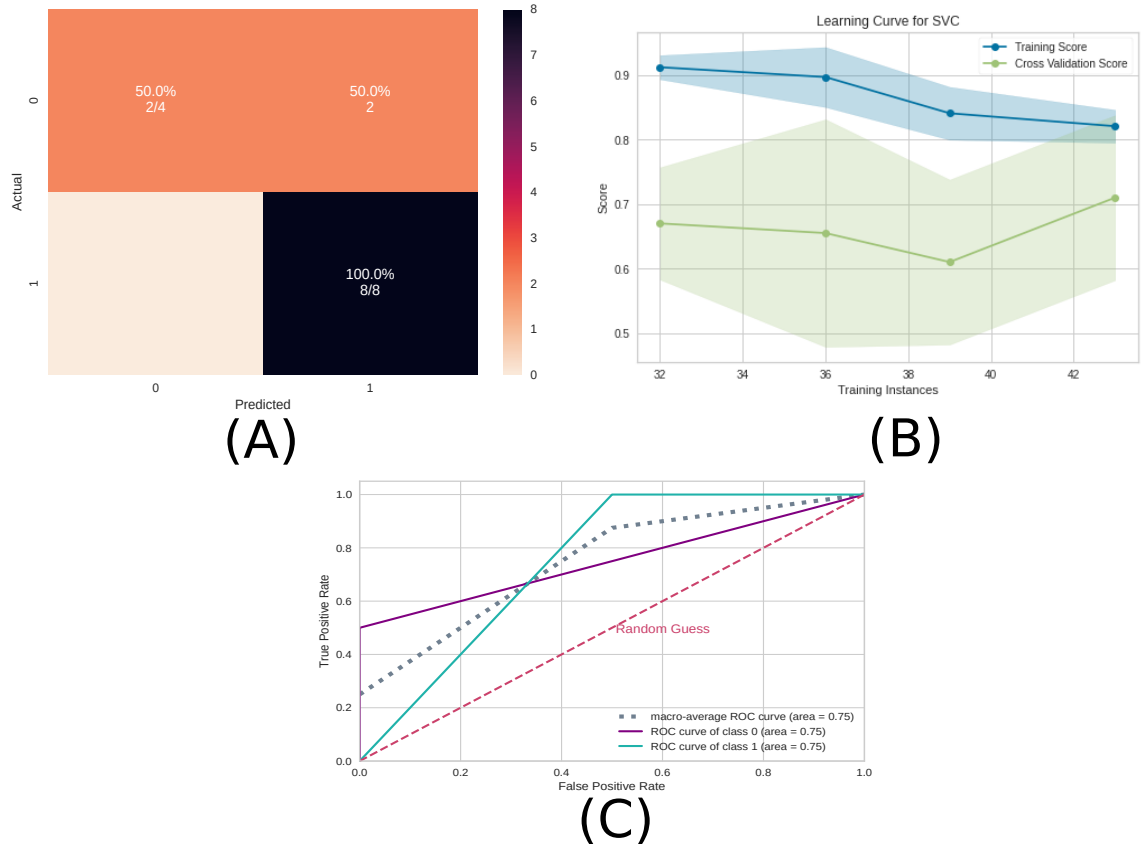

Figure 17 – **Machine learning results using the complex network measures as input data.** A) Confusion matrix indicating a true negative rate of 50% (orange according to the color bar) and a true positive rate of 100% (blue according to the color bar). B) Learning curve for the training accuracy (blue) and for test accuracy (green). C) ROC curve of class 0 (without ayahuasca) and class 1 (with ayahuasca). The gray dotted curve is the macro-average accuracy (area under curve = 0.75) and the pink one the random classifier.

4.3 Complex network measures

The most important complex network measure was CC. CC is a centrality measure that can be defined as the inverse of the average length of the shortest path from one node to all other nodes in the network (RUBINOV; SPORNS, 2010). The idea is that important nodes participate in many shortest paths within a network and, therefore, play an important role in the flow of information in the brain (FREEMAN, 1978). The CC was also the most important measure in other papers related to the differentiation of patients with AD (COPE *et al.*, 2018; PERAZA *et al.*, 2019; EBADI *et al.*, 2017; PEREIRA *et al.*, 2016). In these papers, CC was shown to decrease due to AD disease, while ayahuasca ingestion increased the median value of this measure (see Fig 19).

The second most important complex network measure was assortativity. This measure refers to the resilience of networks (NEWMAN, 2002). A positive assortativity coefficient indicates a network with a resilient core due to the interconnected nodes of high degree (RUBINOV; SPORNS, 2010). This measure was also associated with AD in several works (CONINCK *et al.*,

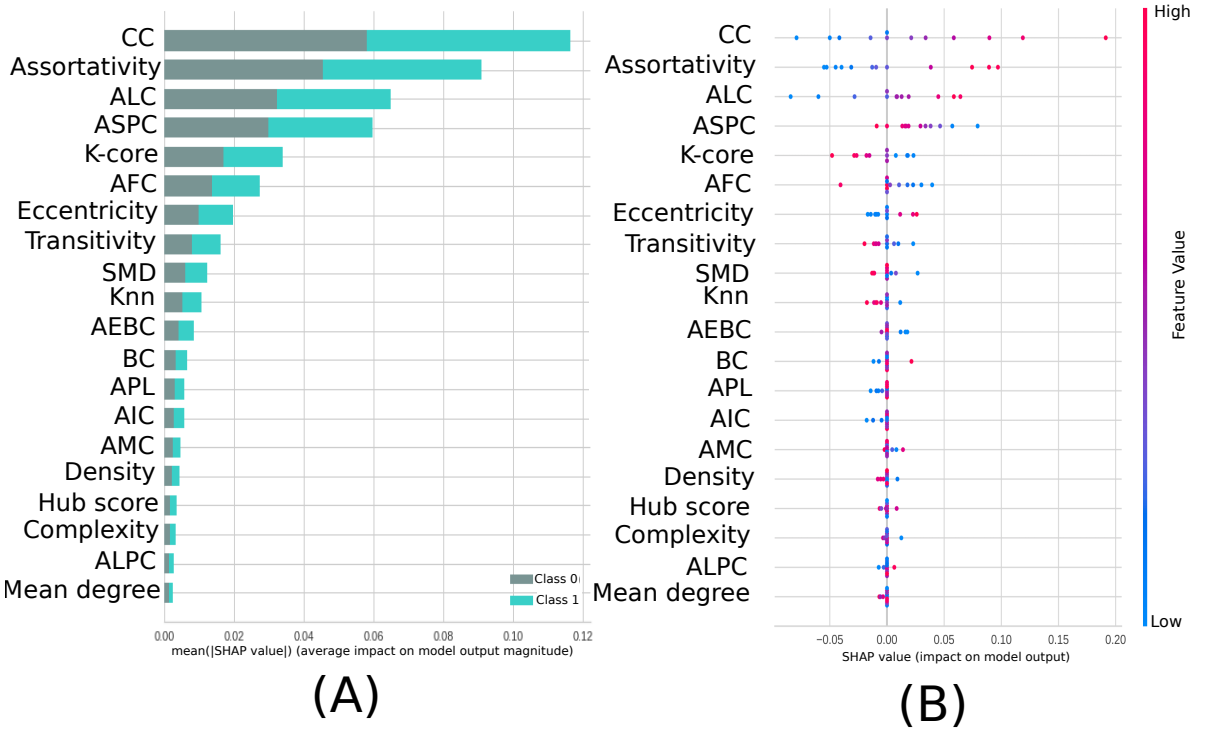

Figure 18 – **Feature importance ranking for SVM classifier being the features ranked in descending order of importance.** The CC measure is the most important to classify the effect of ayahuasca. A) Feature ranking based on the average of absolute SHAP values over all subjects considering both classes (gray: without ayahuasca, cyan: with ayahuasca). B) Same as A) but additionally showing details of the impact of each feature on the model.

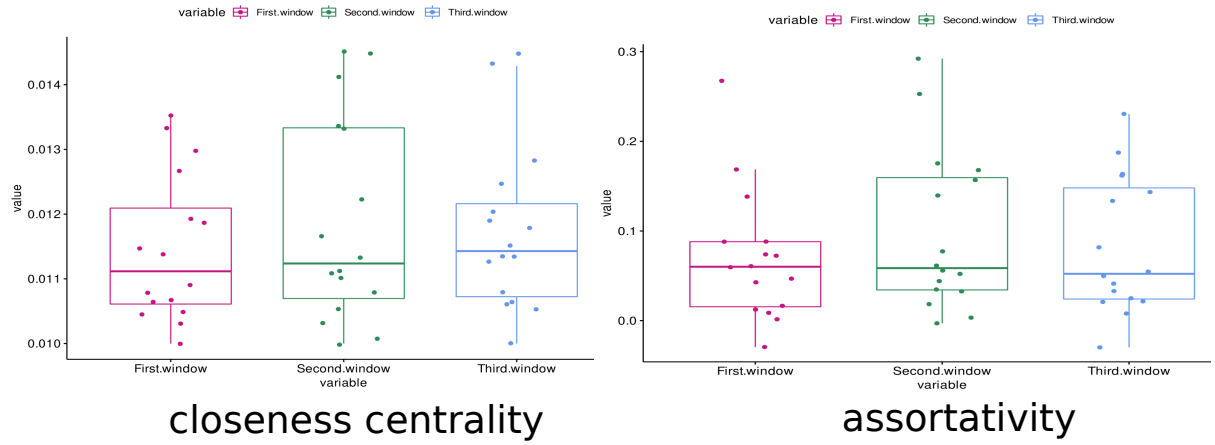

Figure 19 – **Boxplot of the closeness centrality and assortativity measures.** These measures were calculated for all subjects in the first, second and third windows (respectively in pink, green and blue). It can be seen that the median of the closeness centrality measure (central bar in the boxplot) increased with the use of ayahuasca. The median of the assortativity, in contrast, decreased with the use of ayahuasca.

2020; LUO *et al.*, 2021) whose results showed an increase in the assortativity value in contrast to what was found here, where with the use of ayahuasca, the assortativity value (median) decreased (see on Fig 19). It should be noted that although the median value decreased, the upper confidence interval of the distribution increased.

In summary, the results suggest a possible relationship between ayahuasca and AD in terms of the brain network, indicating a therapeutic potential. Indeed, a possible mechanism of how ayahuasca acts against AD was described in (FRECSKA; BOKOR; WINKELMAN, 2016). According to this, the ayahuasca compound DMT agonizes the sigma 1 receptor (Sig-1R) and thereby regulates endoplasmic reticulum (ER) (ER) stress and Unfolded Protein Response (UPR), which are thought to play a crucial role in neuropsychiatric diseases such as AD.

The seven measures developed here concerning community detection are ranked among the twenty most important measures for classification, with ALC ranking third (see Fig 18). ALC is associated with the size of the largest community found by the leading eigenvector community (LC) detection algorithm. This metric shows increased values (compared to controls) in communities with larger path lengths after the use of ayahuasca (Fig18B), indicating communities with larger paths after using this psychedelic. Larger brain communities were also found in (VIOL *et al.*, 2017) after the use of ayahuasca. There are two contrasting concepts in the brains of large vertebrates: functional segregation (or specialization) and integration (or distributed processes)(TONONI; SPORNS; EDELMAN, 1994; SPORNS, 2002). Larger communities also indicate that the balance between functional segregation and integration in the brain was disrupted. This suggests that the distribution of information is slower.

Overall, the classification was successful by considering the complete set of measures rather than just one single measure. As shown in Fig 19, even the most important measures CC and assortativity, did not show much difference between the first window (without ayahuasca) and the other windows (with ayahuasca). Together with the other less important measures, however, the machine learning method was able to distinguish both classes successfully. This leads to the conclusion that a single feature is insufficient as a biomarker, while the different features used in this work may serve as a biomarker.

5 Conclusion

In summary, the results obtained in our study demonstrated that the application of machine learning methods was able to detect changes in brain connectivity during ayahuasca use automatically. Additionally, we demonstrated that the connectivity matrices are the best abstraction level to detect brain changes caused by this psychedelic.

At level abstraction A, our findings suggest that this substance affects important brain regions related to cognitive, psychiatric, and motor functions. These effects may alleviate different symptoms of diseases affecting the brain.

At level abstraction B, the connection between F3 and PO4 is the most important while using ayahuasca according to our classifier model, a significant discovery in psychedelic literature. This connection may point to a cognitive process similar to face recognition in individuals during ayahuasca-mediated visual hallucinations.

Concerning the complex network measures at level abstraction C, CC, assortativity, and one of the new measures developed here, ALC, capture the best brain changes caused by ayahuasca. The new ALC measure inferred that larger communities are associated with this psychedelic and the opposite in its absence. Larger communities suggest that the distribution of information is slower with the use of this substance. Therefore, the present study's findings support that cortical brain activity becomes more entropic under psychoactive substances. (CARHART-HARRIS *et al.*, 2014; CARHART-HARRIS, 2018; PAPO, 2016). There is, however, evidence that psychedelics do not simply make the brain more random, but after the typical organization of the brain is disrupted, strong and topologically far-reaching functional connections emerge which are not present in the natural state of mind.

While our methodology has proven effective, it is focused on the acute evaluation of psychedelics. Consequently, more research is necessary to determine how psychedelics affect the functional connectivity of the brain over the long term using our workflow.

In summary, we have developed a robust computational workflow that provides insights into the mechanism of action of ayahuasca and the interpretability of how it modifies brain networks.

Finally, the same methodology applied here may help interpret EEG time series from patients who consumed other psychedelic drugs, such as pure DMT (PALLAVICINI *et al.*, 2020). In future work, we aim to apply this workflow to recordings from our laboratory using in vitro neuronal networks on microelectrode arrays to study the effects of psychedelics at a single network level. Thus, regardless of the equipment used to collect the data, we would like to verify whether the same method used here can detect changes due to different psychedelics.

CHAPTER

4

ON THE ADVANCES IN MACHINE LEARNING AND COMPLEX NETWORK MEASURES TO AN EEG DATASET FROM DMT EXPERIMENTS

'And those who were seen dancing were thought to be insane by those who could not hear the music."

— Friedrich Nietzsche

Submitted and under review at Springer Journal *Medical & Biological Engineering & Computing*.

COLLABORATING AUTHORS

Thaise G. L. de O. Toutain
Federal University of Bahia (FUB)
Joel Augusto Moura Porto
Universidade de São Paulo (USP)
Aruane M. Pineda
Universidade de São Paulo (USP)
Eduardo Pondé de Sena
Federal University of Bahia (FUB)
Francisco A. Rodrigues
Universidade de São Paulo (USP)
Christiane Thielemann
Aschaffenburg University of Applied Sciences (UAS)
Manuel Ciba
Aschaffenburg University of Applied Sciences (UAS)

Abstract

There is a growing interest in the medical use of psychedelic substances, as preliminary studies using them for psychiatric disorders have shown positive results. In particular, one of these substances is DMT, an agonist serotonergic psychedelic that can induce profound alterations in the state of consciousness.

In this work, we use an exploratory tool to reveal DMT-induced changes in brain activity using EEG data and provide new insights into the mechanisms of action of this psychedelic substance. We used a two-class classification based on (A) the connectivity matrix or (B) complex network measures derived from it as input to a support vector machine.

We found that both approaches could detect changes in the brain's automatic activity, with case (B) showing the highest AUC (89%), indicating that complex network measurements best capture the brain changes that occur due to DMT use.

In the second step, we ranked the features that contributed the most to this result. For case (A), we found that differences in the high alpha, low beta, and delta frequency bands were most important in distinguishing between the state before and after DMT inhalation, which is consistent with the results described in the literature. Further, the connection between the temporal (TP8) and central cortex (C3) and between the precentral gyrus (FC5) and the lateral occipital cortex (P8) contributed most to the classification result. The connection between regions TP8 and C3 has been found in the literature associated with finger movements that might have occurred during DMT consumption. However, the connection between cortical areas FC5 and P8 has not been found in the literature and is presumably related to the volunteers' emotional, visual, sensory, perceptual, and mystical experiences during DMT consumption.

For case (B), closeness centrality was the most crucial complex network measure. Furthermore, we discovered larger communities and longer average path lengths when DMT was used and the converse when not, showing that the balance between functional segregation and integration had been disrupted. These findings support the idea that cortical brain activity becomes more entropic under psychedelics.

Overall, a robust computational workflow has been developed here with interpretability of how DMT (or other psychedelics) modify brain networks and insights into their mechanism of action. Finally, the same methodology applied here may help interpret EEG time series from patients who consumed other psychedelic drugs.

4.1 Introduction

N, N-dimethyltryptamine (DMT) is a substance endogenously produced in various mammals (CHRISTIAN *et al.*, 1977), including humans (SMYTHIES; MORIN; BROWN, 1979), and has serotonin agonist properties. Thus, it can bind to serotonin receptors, simulating

the neurotransmitter (SMITH *et al.*, 1998). In (STRASSMAN, 2001), it was for the first time suggested that the pineal gland produces DMT in stress situations such as birth and death. In (BARKER; MCILHENNY; STRASSMAN, 2012; BARKER *et al.*, 2013), it seems clear that it is produced in small quantities by this gland (NICHOLS, 2018).

The substance was first synthesized in 1931 (MANSKE, 1931), while its psychoactive effects were described for the first time many years later in 1956 by (SZARA, 1956). When administered externally in large quantities, DMT can cause altered states of consciousness (BARKER, 2018), hallucinations (GAUJAC *et al.*, 2013; OTT, 1999; SCHARTNER; TIMMERMANN, 2020) and spiritual experiences such as communication with 'presences' or 'entities', plus reflections on death (TIMMERMANN *et al.*, 2018). Exogenous ingestion can be done by smoking or injecting. Its effect by oral ingestion depends on the inhibition of monoamine oxidase, an enzyme that degrades the alkaloid DMT in the liver and intestine (OTT, 1999). This enzyme and DMT are also present in ayahuasca tea, which has been used in the Amazon for hundreds of years as part of the traditional medicine of the region's inhabitants (ARAÚJO, 2019).

Recently, there has been a surge in interest in the medicinal application of psychedelics. Only last year, in (PERKINS *et al.*, 2021), around 100 psychedelic clinical studies are presently being done globally. This represents increased clinical trials compared to the 43 aided psychedelic treatment clinical studies done since 1999. One example is the psychedelic MDMA which is already in phase 3 clinical trials for the PTSD (MITCHELL *et al.*, 2021) and significant depression with positive results (ANDREWS; WRIGHT, 2022). Another notable example is psychedelic psilocybin, whose therapeutic use in the U.S. has come to be considered a revolutionary therapy for treatment-resistant depression and major depressive disorder (NICHOLS, 2020). These first promising results suggest that other psychedelic substances, such as LSD, ibogaine hydrochloride, salvia divinorum, 5-MeO-DMT, ayahuasca, and DMT, which have been less studied so far, should be investigated in more detail (SIEGEL *et al.*, 2021).

Only a few studies on administering micro- or low-dose DMT to non-human species (predominantly rats) have been published in the scientific literature (BARKER, 2022). In (LY *et al.*, 2018), a low dose of DMT was administered to rats resulting in changes in frequency and amplitude of spontaneous excitatory postsynaptic currents (EPSCs) in the prefrontal cortex (PFC) that lasted long even after the drug was removed from the body. In (CAMERON *et al.*, 2019), it was described that chronic, intermittent, low doses of DMT produced an antidepressant effect and increased fear extinction learning in rats without affecting working memory or social interaction. For a high amount of DMT (10 mg/kg), an increase in the density of the dendritic spines in the prefrontal cortex was found in rodents, and antidepressant and anxiolytic behavioral effects were observed (CAMERON *et al.*, 2018). In humans, a single dose of 0.1 mg/kg of DMT caused an apparent anxiolytic effect shown in (STRASSMAN *et al.*, 1994). However, other studies using inhaled 5-MeO-DMT also observed complete mystical experiences in 75% of volunteers (BARSUGLIA *et al.*, 2018) and improvements in depression and anxiety, which were

associated with greater intensity of mystical experiences, with the spiritual and personal meaning of the experience, when using this substance (DAVIS *et al.*, 2019).

Thus, there is evidence that DMT can help with depression and post-traumatic stress disorder. However, most studies have been conducted on animals and, therefore, only have a reduced power. Therefore, more in-depth studies on DMT, its mechanisms in the brain, and its potential clinical effects in humans are needed since there are few studies investigating the use of DMT in humans through EEG (TIMMERMANN *et al.*, 2019; TAGLIAZUCCHI *et al.*, 2021; ALAMIA *et al.*, 2020) and fMRI (DAUMANN *et al.*, 2008).

Despite DMT's significant therapeutic potential, there are just a few human studies in the literature, and additional study on how this substance modifies the brain and its mechanism of action is required.

Graph theory methods yielded interesting insights into the complex network structure of the human brain. It is known from the literature (SPORNS; ZWI, 2004; DIJK *et al.*, 2010; SCANNELL *et al.*, 1999; HILGETAG *et al.*, 2000; FORNITO; ZALESKY; BULLMORE, 2016; WHITE *et al.*, 1986) that the topology of the brain is a small world network. This type of network has connectivity properties that are intermediate between random and regular graphs, preserving a high degree of connectivity between local neighborhoods while allowing all of its nodes to be connected via remarkably short pathways (SPORNS; ZWI, 2004; WATTS; STROGATZ, 1998). They also preserve a high degree of connectivity between local neighborhoods while allowing all their nodes [1] which to be connected to surprisingly short paths (SPORNS; ZWI, 2004). Altering this topology is also associated with pathological states (BASSETT; GAZZANIGA, 2011; PINEDA *et al.*, 2020; SPORNS, 2018; BASSETT; ZURN; GOLD, 2018), and the use of substances such as psychedelics (NICHOLS; JOHNSON; NICHOLS, 2017; GIRN *et al.*, 2020; VIOL *et al.*, 2017). Notably, complex network parameters have been used as a biomarker for several diseases (HAYASHIDA; AKUTSU, 2016; FEKETE *et al.*, 2013). In addition, complex networks are widely used in EEG to characterize the brain functional networks (BULLMORE; SPORNS, 2009; BARAVALLE *et al.*, 2019; DAS; PUTHANKATTIL, 2020; DIYKH; LI; WEN, 2017).

In this context, ML has been used for more accurate, and automatic medical diagnosis (SONG; JUNG; CHUNG, 2019; MOZAFFARINYA *et al.*, 2019; ILYASOVA *et al.*, 2018; RICHENS; LEE; JOHRI, 2020; LYNCH; LISTON, 2018; ALIZADEHSANI *et al.*, 2019; KEANE; TOPOL, 2018; BHATT *et al.*, 2021). Compared to traditional statistical techniques, this approach has the advantage of not relying on prior assumptions (such as adequate distribution, observation independence, absence of multicollinearity, and interaction problems) and is suited to automatically analyze and capture complex non-linear relationships in data(LI *et al.*,

[1] The network nodes can be representations from of neurons (<1μm, microscale) to brain regions ($\approx$ 10 cm, macro-scale)

2020; RAJULA *et al.*, 2020). As brain data are characterized by high complexity and highly correlated brain regions, ML algorithms have been widely used to detect acute and permanent abnormalities in the brain (FONG; SCHEIRER; COX, 2018; KRAGEL; LABAR, 2016; BOUTET *et al.*, 2021). On the other hand, ML shows a lack of interpretability and a black-box nature that is an especially disadvantageous general limitation when it comes to an understanding medical data (RUDIN, 2019; EKANAYAKE; MEDDAGE; RATHNAYAKE, 2022). In recent years, new techniques have emerged to help interpret machine learning results. Most notable is the SHAP values method (LUNDBERG; LEE, 2017). This metric enables the identification and prioritization of features and can be used with any machine learning algorithm (BOWEN; UNGAR, 2020; RODRÍGUEZ-PÉREZ; BAJORATH, 2019; SPADON *et al.*, 2019).

The present work aims to investigate EEG data using ML as an exploratory tool to detect temporal changes in the brain functionality of participants after DMT consumption. The study raised the following research questions:

- Can we automatically detect changes in the functional network structure induced by DMT using ML?
- Which new insights into the mechanisms of action of DMT can we draw when we use ML in combination with SHAP values?

To answer these questions, we use the same methodology implemented in (ALVES *et al.*, 2022a), which proposes a two-class classification based on (A) the connectivity matrix or (B) complex network measures derived from it as input to a SVM (BOTTOU; LIN, 2007). SVM has been used with excellent results for classifying complex network measures before (MAZROOYISEBDANI *et al.*, 2020; DIYKH; LI; WEN, 2017; DEY; RAO; SHAH, 2014). Furthermore, this ML algorithm can handle problems where the sample size of the data is generally smaller in comparison to the dimensionality of its feature space and is therefore applicable to the study of brain disorders with neuroimaging (PISNER; SCHNYER, 2020), whose data have these characteristics, and also this is the case of the data in this work (the case A with connectivity matrix). Moreover, we determine which abstraction levels are most suited for EEG recording DMT-induced brain changes. In contrast to the previous study (ALVES *et al.*, 2022a), which uses gamma-band frequencies in EEG from ayahuasca experiments. This study advances the methodology used before since different frequency bands are also considered to see the best frequencies to differentiate brain changes due to DMT.

For a biological interpretation of the DMT-induced changes, the SHAP value technique has also been demonstrated to be more successful than the research described above in identifying the best connections between brain areas and the best complex network measures, which helps understand the effects of the psychedelic substance on the brain.

A more robust workflow has also been applied for interpreting brain network modifications due to DMT (or other psychedelics) in these two data abstract levels.

4.2 Data

The data used for this study has been published in (PALLAVICINI *et al.*, 2021) and is publicly available in a raw format [2]. Thirty-five healthy male and female subjects (7 women and 28 men) volunteered to inhale, using pipes, 40 mg of free DMT extracted from the root of Mimosa hostilis. It should be noted that all participants had previous experiences with ayahuasca. Recordings were made with 24 electrodes, following the EEG electrode positions in the standard 10 – 20 location system. These channels are Fp1, Fp2, Fz, F7, F8, FC1, FC2, Cz, C3, C4, T7, T8, CPz, CP1, CP2, CP5, CP6, TP9, TP10, Pz, P3, P4, O1, and O2. In addition, reference and ground electrodes were placed at FCz. The recordings on the subjects started 10 minutes before DMT inhalation, 5 min with eyes closed, and 5 minutes with eyes open. After DMT use, subjects were recorded for about 6 min (6 1.4 min) with eyes closed.

4.3 Methodology

In an earlier work of the authors (ALVES *et al.*, 2022a), ML, in combination with complex network measures, was successfully applied to EEG data recorded after ayahuasca consumption to detect changes in brain activity. For this purpose, different levels of data abstraction were used as input: (a) the raw EEG time series, (b) the correlation of the EEG time series, and (c) the complex network measures calculated from (b). Several ML algorithms were tested, and the best performance was obtained with the SVM at abstraction levels (b) and (c). Based on this result, we decided to use in the present work connectivity matrices (see subsection 4.3.2) and derived complex network measures (see subsection 4.3.3 as input for an SVM).

More details are displayed in Figure 20, which summarizes the methodology workflow. In short, EEG time series were separated by filtering in eight frequency bands. In the next step, preprocessing of the EEG time series was performed to obtain the connectivity matrices for each frequency band (and the unfiltered signal); see Figure 20- A and B with details of this process described in subsection 4.3.1 and 4.3.2. In a second step, complex networks measures are derived from the connectivity matrices as described in subsection 4.3.3, see Figure 20- C, and both types of data sets were used as input to an SVM as described in subsection 4.3.4. Finally, for interpretation of the classification results, the feature ranking algorithm SHAP is finally applied as described in subsection 4.3.5.

[2] Avaiable on Zenodo. <https://doi.org/10.5281/zenodo.3992359>

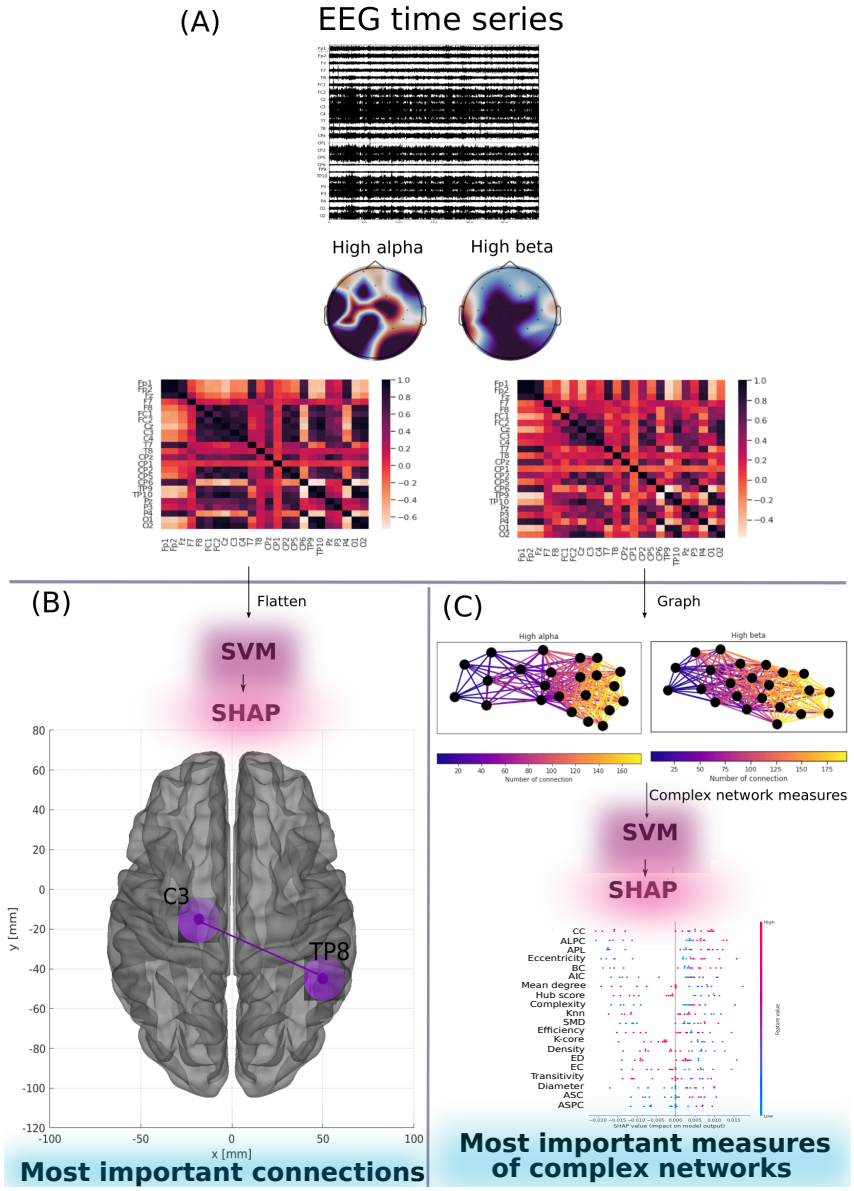

Figure 20 – Diagram showing the methodology used in the present work. In **(A) Data preprocessing**, described in the subsection 4.3.1, the EEG time series are filtered to remove artifacts (in the picture, the time series of a subject at the time the DMT was used) and then separated into the frequency bands high alpha, low alpha, high beta, mid-range beta, low beta, gamma, delta, and theta (as an example in the picture the topographic map for the frequencies high alpha and high beta for the same subject). For each band, the correlation between the channels is calculated using Pearson's correlation to obtain a 24x24 connectivity matrix. In **(B) Connectivity matrices**, described in the subsection 4.3.2, where the connectivity matrices are flattened into a vector that is put into the SVM to verify the most important connections with the use of DMT (in the figure the best performing model, using the high alpha, low beta, and delta bands, found TP8 and C3 as the primary connections). In **(C) complex network measures**, described in the subsection 4.3.3, where the connectivity matrices are analyzed as graphs (in the figure for the same subject, the diagram for the frequencies high alpha and high beta, where the number of connections in each node varies according to the color bar) and from them have extracted measures of complex networks that are applied in the SVM and the best model found for the delta frequency found the closeness centrality as the main measure.

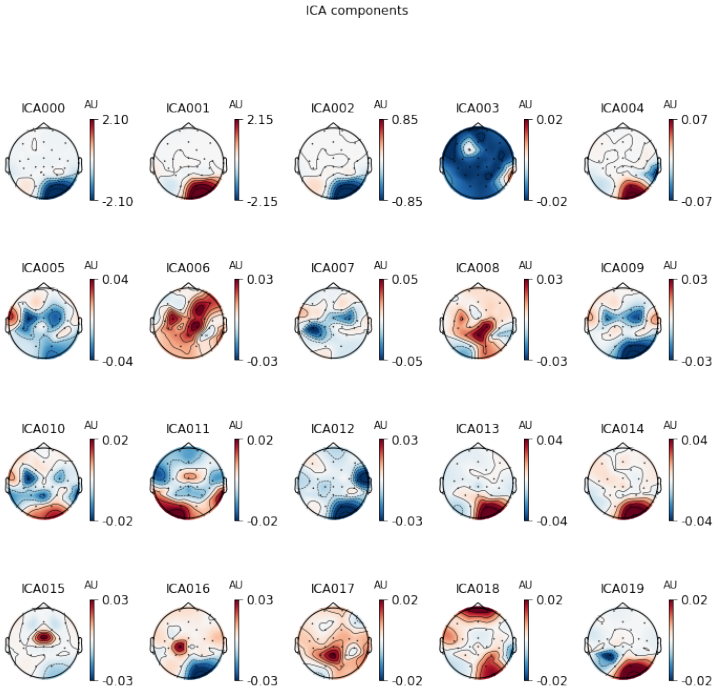

Figure 21 – Scalp topography maps generated by ICA analytics were recorded from a subject shortly after inhalation of DMT. The EEG signal was decomposed into twenty principal components. The component with ocular activity (see ICA018 with activity in the frontal region near the eyes) was removed, and an artifact-free EEG signal was reconstructed.

4.3.1 Data preprocessing

First, a high-pass filter with a cut-off frequency of 0.5 Hz was used to remove artifacts such as electro galvanic signals and motion artifacts (KUMAR *et al.*, 2017). This type of filtering is widely used in the literature (STEVENSON *et al.*, 2019; LOUWERSE; HUTCHINSON, 2012; DAFTARI; SHAH; SHAH, 2022; KLUG; GRAMANN, 2021). To remove eye artifacts, we employed an independent component analysis (ICA) approach in which EEG signals are decomposed to maximize independent components, and those with eye activity are identified and eliminated (JUNG *et al.*, 2000). An example of the ICA analysis for a subject using DMT can be seen in Figure 21. This analysis was done with a python package called MNE (GRAMFORT *et al.*, 2013) using an algorithm based on maximum information (Infomax) perspective (AMARI; CICHOCKI; YANG, 1995).

In the next step, EEG time series were separated by filtering in eight frequency bands: high alpha (10-12 Hz), low alpha (8-10 Hz), low beta waves (12–15 Hz), mid-range beta waves (15–20 Hz), high beta waves (18–40 Hz), gamma (30 - 44 Hz), delta (0.5 – 3 Hz) and theta (4 – 7 Hz).

4.3.2 Connectivity matrices

The well-known Pearson correlation calculated connectivity matrices. It is a widely used and successfully approved measure to capture the correlation of EEG electrodes (ROJAS *et*

al., 2018; WANG *et al.*, 2017b; JALILI, 2016; HAN *et al.*, 2019; TOKARIEV *et al.*, 2019; FALLANI *et al.*, 2011b). The Pearson correlation was calculated for all electrode pairs and all frequency bands (including the unfiltered signal). The connectivity matrices serve as input for the following steps described in subsections 4.3.2 and 4.3.3.

The connection matrices were flattened into a single vector before being fed into the ML algorithm. The vectors were then successively combined into a 2D matrix, with each column representing a link between two electrodes and each row representing a person. For each frequency band, such 2D matrices were created (and the unfiltered signal).

4.3.3 Complex network measures

A complex network graph was generated for each connectivity matrix to extract different measures. To construct the graphs, we normalized the connectivity matrix between 0 and 1, and connections bigger than 0.5 were binarized to 1 and smaller ones to zero. This way, the generated graph is undirected and weightless. This undirected and weightless graph was taken was considered since the Igraph package (CSARDI; NEPUSZ *et al.*, 2006) that we used to extract the complex network measures includes a more significant number of complex network measures for binary graphs, and the ML approach works better with a large number of features.

Furthermore, many recent studies (JALILI, 2016; GOÑI *et al.*, 2013) have excluded weighted edges, turning them into binary edges, since weightless networks are simpler to characterize and there are many more measures, from complex networks to weightless networks. In addition, removing weights still eliminates weak, meaningless edges, which can be seen as noise in functional and effective networks (RUBINOV; SPORNS, 2010).

To feed the data into the ML algorithm, the complex network measures retrieved from the created graphs were stored in a matrix, with each column being a complex network measure and each row representing a subject.

The following complex network measures were calculated: Assortativity (NEWMAN, 2003; NEWMAN, 2002), APL (ALBERT; BARABÁSI, 2002), BC (FREEMAN, 1977), CC (FREEMAN, 1978), EC (BONACICH, 1987), diameter (ALBERT; JEONG; BARABÁSI, 1999), hub score (KLEINBERG, 1999), Knn (EPPSTEIN; PATERSON; YAO, 1997), mean degree (DOYLE; GRAVER, 1977), SMD (SNIJDERS, 1981), entropy degree (ED) (DEHMER; MOWSHOWITZ, 2011), transitivity (WATTS; STROGATZ, 1998; NEWMAN; WATTS; STROGATZ, 2002), complexity, k-core (SEIDMAN, 1983; NEWMAN, 2010), eccentricity (HAGE; HARARY, 1995), density (ANDERSON; BUTTS; CARLEY, 1999), and global efficiency (LATORA; MARCHIORI, 2003). In addition, newly developed metrics (described in detail in (ALVES *et al.*, 2022a)) reflecting the number of communities in a complex network are applied. Community detection (also called clustering graph) is one of the fundamental analyses of com-

plex networks aiming to decompose the network in order to find densely connected structures, so-called communities (NEWMAN, 2012; KIM; LEE, 2015; ZHAO; LIANG; WANG, 2021). However, the community detection measures need to be transformed into a single scalar value to include them in the matrix. To this aim, we perform the community detection algorithms to find the largest community, then calculate the average path length within this community and receive a single value as a result. The community detection algorithms used were: Fastgreedy community (FC) (CLAUSET; NEWMAN; MOORE, 2004), infomap community (IC) (ROSVALL; AXELSSON; BERGSTROM, 2009), leading eigenvector community (LC) (NEWMAN, 2006), label propagation community (LPC) (RAGHAVAN; ALBERT; KUMARA, 2007), edge betweenness community (EBC) (GIRVAN; NEWMAN, 2002), spinglass (SPC) (REICHARDT; BORNHOLDT, 2006), and multilevel community (MC) (BLONDEL *et al.*, 2008). To indicate our approach, we extended the given abbreviations by the letter "A" (for average path length) as follows: AFC, AIC, ALC, ALPC, AEBC, ASPC, and AMC.

4.3.4 Machine learning process

All the parameters of the ML algorithms used in this paper and the metrics used to evaluate the model's performance were based on a recent study (ALVES *et al.*, 2022a). This study assessed whether it could automatically detect changes in functional brain connectivity due to psychedelic ayahuasca, which presents in its composition the substance DMT. Thus, to classify these two levels of data abstraction, namely the connectivity matrix and the complex network measures, the matrices were sampled by separating them into training (train) and test sets, with 25% of the data composing the test set. Then, for a reliable model, k-fold cross validation was used (REFAEILZADEH; TANG; LIU, 2009), with k = 10 (value widely used in the literature (BERRAR, 2019; BENGIO; GRANDVALET, 2004; SHAH; KHAN, 2020; KAWAMOTO; KABASHIMA, 2017; CHAN *et al.*, 2019; KAWAMOTO; KABASHIMA, 2017)). For the training process, the training sets were applied to the SVM. SVM is based on the search for a hyperplane that geometrically divides samples into two classes. Three important hyperparameters of the SVM have been considered in this work:

- Kernel function: also known as kernel trick, has the function of projecting the input vectors in higher dimensions because by increasing the dimension of the problem, the probability of it becoming a linearly separable problem increases, which makes it easier to solve (XU; ZOMER; BRERETON, 2006; AWAD; KHANNA, 2015).
- Regularization parameter C: this is the penalty term of the optimization problem and is an added constant that creates flexible margins concerning the optimal hyperplane found.
- Gamma: defines how much influence a single training example has. When the gamma value is too small, the model is too restricted and fails to capture the complexity of the data.

To find the best parameters, these hyper-parameters were optimized with the grid search method, widely used in the literature (SATO *et al.*, 2019; ZHONG *et al.*, 2021; ARCADU *et al.*, 2020; KRITTANAWONG *et al.*, 2021; RASHIDI *et al.*, 2020). The grid search thoroughly combines all values of the parameters selected for the models using some metrics to evaluate the performance of these combinations, which in the present work was the AUC (for an explanation, see below). Here, we used the following functions as values for the kernel: gaussian (RBF), polynomial (poly), sigmoid and linear. Optimized values for parameters C and gamma are displayed in Appendix A.6.

For evaluation, the standard performance metrics accuracy (Acc.) was used as described in (MINCHOLÉ; RODRIGUEZ, 2019; TOLKACH *et al.*, 2020; DUKART *et al.*, 2021; LI; ASCH; SHAH, 2020; PARK; KELLIS, 2015). As we have a two-class (negative and positive) classification problem, other metrics like Precision and Recall are considered, also typical in the literature (ITO *et al.*, 2021; KIM *et al.*, 2020; LI *et al.*, 2021; YU *et al.*, 2020). Precision (also called specificity) corresponds to the negative class's hit rate (here, no effect induced by DMT). Whereas Recall (also called sensitivity) measures how well a classifier can predict positive examples (hit rate in the positive class), here related to an effect of DMT. Another well-known measure, see (ZHONG *et al.*, 2021; BERRYMAN *et al.*, 2020; YANG *et al.*, 2019), is the F1 score which is the harmonic mean of the Recall and precision (HANNUN *et al.*, 2019).

For visualization of these two latter measures, the ROC curve is a standard method as it displays the relation between the rate of true positives and false positives. The area below this curve called the AUC has been widely used in classification problems (MINCHOLÉ; RODRIGUEZ, 2019; BRACHER-SMITH; CRAWFORD; ESCOTT-PRICE, 2021; PATEL *et al.*, 2021; KRITTANAWONG *et al.*, 2021). The AUC value ranges from 0 to 1, with one corresponding to an error-free classification result. For example, $AUC = 0.5$ indicates that the classifier cannot distinguish the two classes equal to the random choice. Furthermore, we consider the micro average of the ROC curve, which computes the AUC metric independently for each class (calculate the AUC measure for patients before consuming DMT, class zero, and separately for patients after ingesting DMT, class one.) and then the average is computed considering these classes equally. Finally, the macro average is also used in our evaluation, which does not consider both classes equally, but aggregates the classes' contributions separately and then calculates the average.

4.3.5 Feature Ranking

As described in 4.1, the most notable technique for interpreting ML results is the SHAP values, which has its origin in game theory (RODRÍGUEZ-PÉREZ; BAJORATH, 2020; SHAPLEY, 1953), where it aims to assign payoffs to players depending on their contribution to the total payoff in the game. In addition, those who cooperate in a coalition receive a certain

Table 12 – Performances of the SVM classifier. Complex network measures' classification captures the brain's changes due to DMT slightly better than the connectivity matrix. The best performance is highlighted in bold.

Type of data	EEG frequencies band	Subset	AUC	Acc.	F1 score	Recall	Precision
Connectivity matrix	**high alpha, low beta and delta**	**Train**	1.00	1.00	1.00	1.00	1.00
		Test	0.82	0.82	0.82	0.82	0.82
Complex network measures	**delta**	**Train**	**1.00**	**1.00**	**1.00**	**1.00**	**1.00**
		Test	**0.89**	**0.89**	**0.88**	**0.88**	**0.91**

profit from this cooperation (PARRACHINO, 2012). When we apply this method to our ML problem, each feature represents a player in a game, and the prediction represents the reward. Thus SHAP values tell us how to distribute the payoff fairly among the features (MOLNAR, 2020).

Here, we used this methodology to evaluate which complex network measures and which correlation between electrodes (brain regions) contributed most to the classification result allowing for a biological interpretation of the results obtained with our ML algorithms.

4.4 Results

ML was applied for two different levels of data abstraction: (A) the correlation of EEG time series (connectivity matrix) and (B) the complex network measures calculated from (A). We found that both approaches could automatically detect acute changes in brain activity induced by the inhalation of DMT. However, the highest classification performance was obtained for the complex network measures with an AUC of 89% (see Table 12). The following subsections 4.4.1 and 4.4.2 describe the results in more detail.

4.4.1 Connectivity matrix

EEG data recorded from subjects before DMT inhalation (control with eyes closed) and those after inhalation of DMT were filtered and divided into eight frequency bands as described in 4.3.1. Detailed results for each frequency band are given in the appendix A.7.

The best performance was achieved for the low beta frequency band (test sample performance with mean AUC of 0.78, mean precision of 0.78, mean F1 score of 0.78, mean recall of 0.78, and mean Acc. of 0.78) followed by the high alpha and delta frequency bands (test sample performance for both frequency band was a mean AUC of 0.72, mean precision of 0.72, mean F1 score of 0.72, mean recall of 0.72, and mean Acc. of 0.72). Then, these connection matrices from the frequencies that performed best independently were inserted again in the ML approach. Moreover, better results were achieved by combining these frequency bands whose test sample performance had a mean AUC of 0.82, mean precision of 0.82, mean F1 score of 0.82, mean

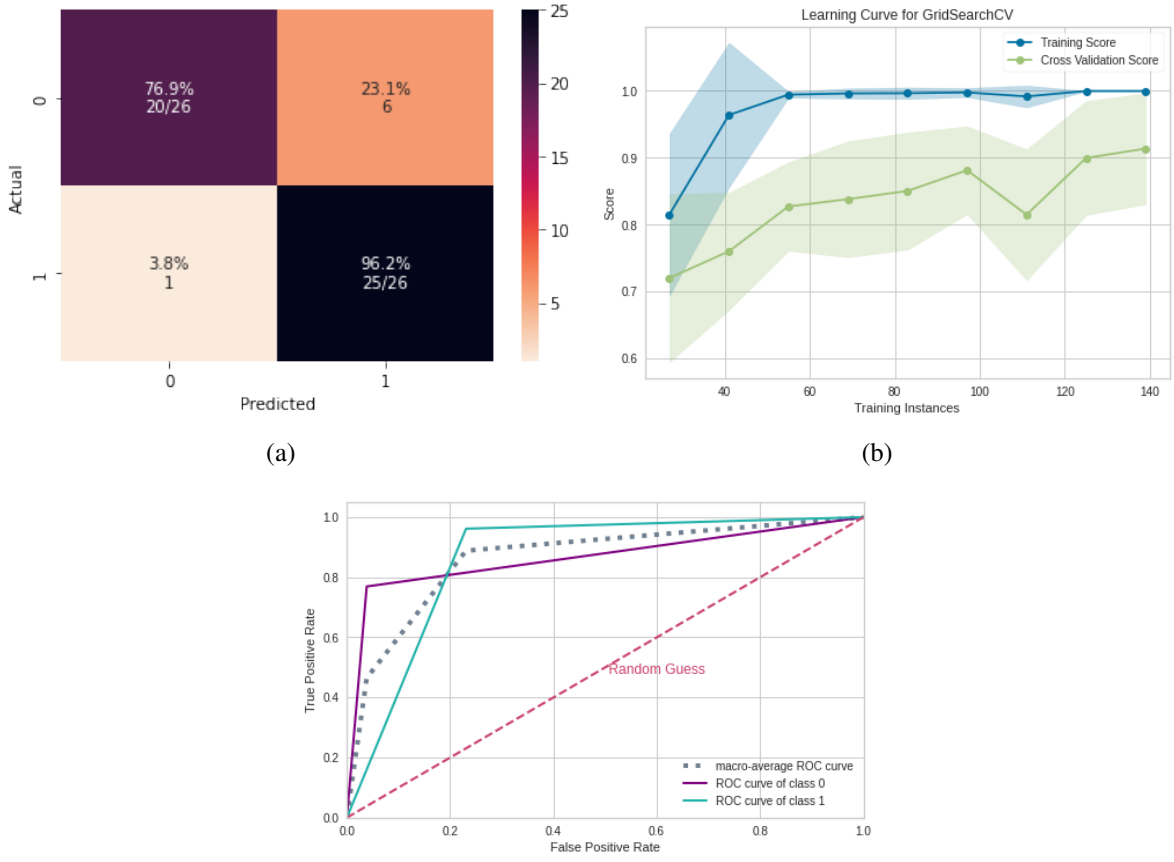

(a) (b)

(c)

Figure 22 – ML results using connectivity matrices. (a) Confusion matrix indicating a true negative rate of 80.8% (purple according to the color bar) and a true positive rate of 84.6% (blue according to the color bar). (b) The learning curve for the training accuracy (blue) and test accuracy (green). (c) ROC curve with class 0 (control) and class 1 (after inhalation of DMT).

recall of 0.82, and mean Acc. of 0.82. Furthermore, see appendix A.9 for the similarity of results obtained for each frequency.

In Figure 22, the confusion matrix (22-(a)), the learning curve (Figure 22-(b)), and the ROC curve (22-(c)) are displayed. The learning curve evaluates the model's predictability by varying the size of the training set (SPADON *et al.*, 2019). Results show that the entire database is required to achieve the highest validation accuracy.

In order to reveal the importance of the connections between electrode pairs (brain connections) by considering the combination of the best EEG frequency bands (high alpha, low beta, and delta), the SHAP values were calculated. The results are shown in Figure 23. The most important connection was between electrodes TP8 (temporal and parietal region) and C3 (central region). In addition, the presentation of the data in Figure 23 shows that for the connection between TP8 and C3, low values of correlation (blue dots) were essential for detecting the presence of DMT (positive SHAP values). High correlation values (red dots) were important for detecting the absence of DMT (negative SHAP values). The second most important connection,

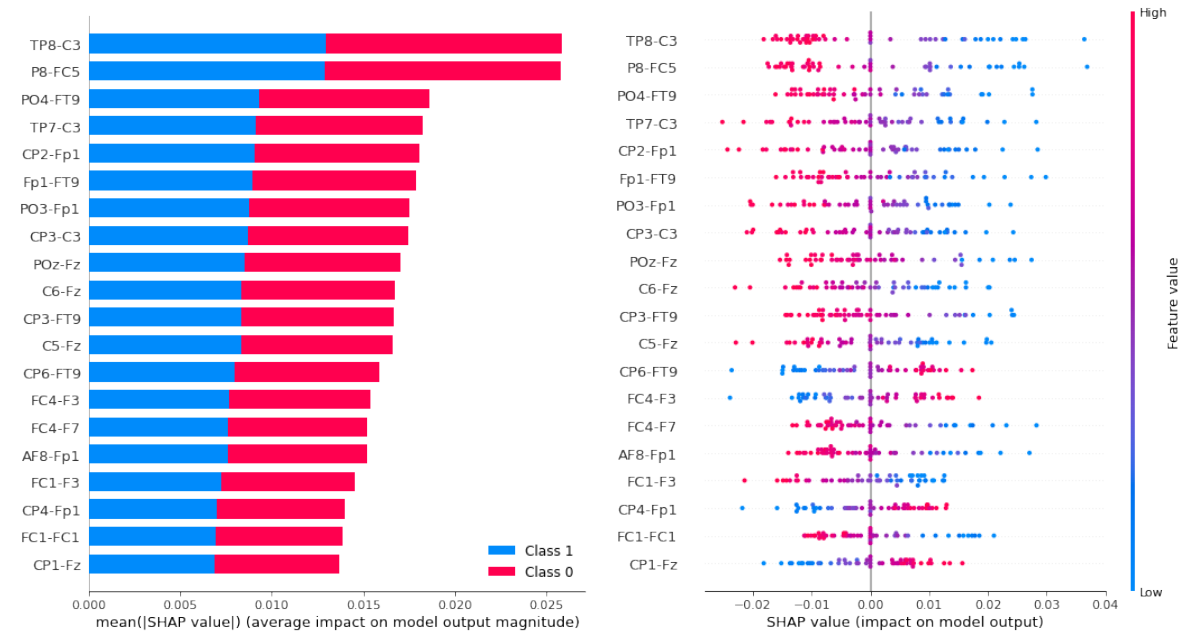

(a) (b)

Figure 23 – Feature importance ranking for the SVM classifier with electrode correlation (brain regions) ranked in descending order of importance by considering the combination of the best EEG frequency bands (high alpha, low beta, and delta). The connection between the regions TP8 and C3 is the most important to classify the effect of DMT. (a) Feature ranking based on the average of absolute SHAP values over all subjects considering both classes (gray: control, cyan: after inhalation of DMT). (b) Same as (a), but additionally showing details of the impact of each feature on the model.

with a similar SHAP value, was between the electrodes FC5 and P8. Figure 24 depicts the corresponding brain regions.

In other words, in Figure 24-B, the positive SHAP values (part to the right of the central zero axis) are associated with the class with DMT. In contrast, the negative SHAP values (part to the left of the central zero axis) are associated with the class without DMT. Each point on the graph represents the Pearson correlation value of that connection obtained for a given subject. For example, for the TP8-C3 connection, subjects had low correlation values in the presence of DMT (blue points on the right region of the central axis) and high correlation values in the absence of DMT (red points on the left region of the axis).

4.4.2 Complex network measures

We received the best performance considering complex network measures for the delta frequency band (test sample performance with mean AUC of 0.89, mean precision of 0.91, mean F1 score of 0.88, mean recall of 0.88 and mean Acc. of 0.89); see Table 12. Furthermore, the precision measure is related to the positive class (with DMT). Thus, since the precision was higher than the recall, we conclude that the model slightly better detects the presence of DMT than its absence. Furthermore, see appendix A.9 for the similarity of results obtained for each

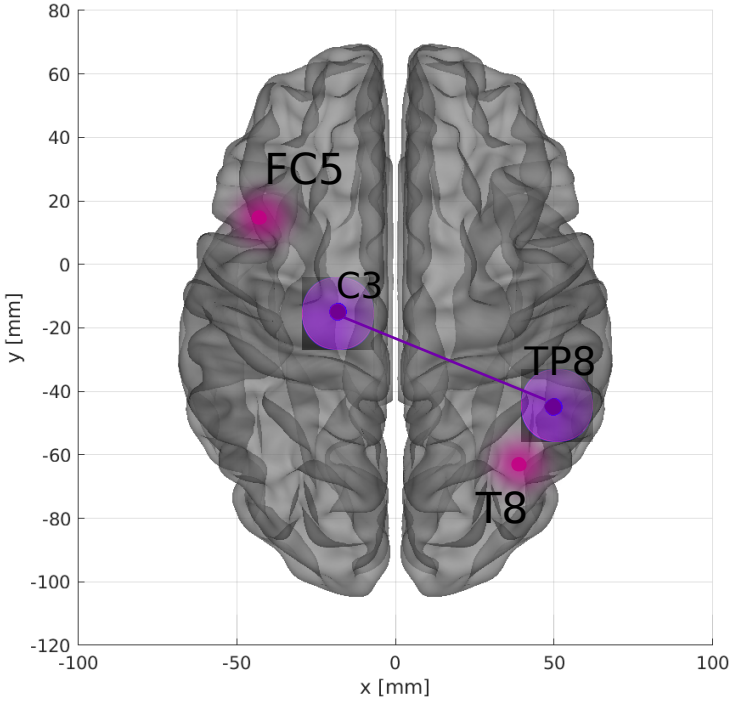

Figure 24 – Brain plot displaying these electrode pairs which contributed most to the classification result based on connectivity matrices. The brain plot was made using the Braph tool (MIJALKOV *et al.*, 2017), based on the coordinates in (MICHEL; BRUNET, 2019; ASHER *et al.*, 2021).

frequency.

In Figure 25, the confusion matrix (Figure 25 (a)), the learning curve (Figure 25 (b)), and the ROC curve (Figure 25 (c)) are plotted. Again, the entire database is necessary to get the highest accuracy. All the other results can be found in Appendix A.8.

Based on the SHAP values in Figure 26, it can be seen that the essential measure for the model was the CC, followed by the ALPC measure and the APL. In addition, high values of the CC measure (pink dots) indicate its importance for the detection of the absence of DMT (negative SHAP values); see Figure 26 (b). In contrast, with the presence of DMT, some subjects have low values of closeness centrality (blue and purple dots).

4.5 Discussion

In the previous sections, we presented a computational workflow, including data preprocessing and an ML algorithm revealing acute differences in brain activity before and after consuming the psychedelic drug DMT. As a result, we achieved a classification accuracy of at least 82%. We further showed that the classification accuracy based on complex network measures (89%) was higher than that based on the connectivity matrix alone (see Table 12), suggesting that these measures are important to capture differences in brain activity.

Further, we searched for descriptive parameters related to changes in the functional network structure by ranking the importance of features that contributed to the classification result.

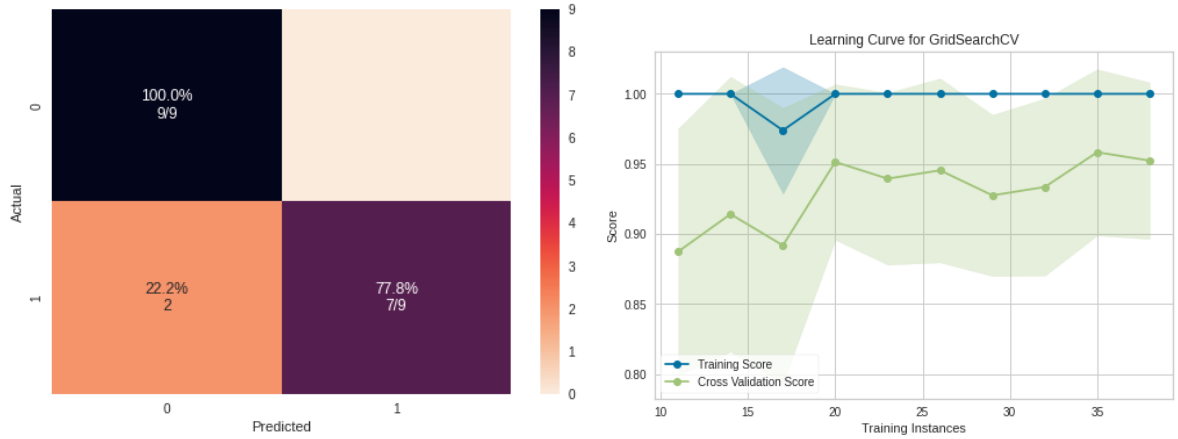

(a) (b)

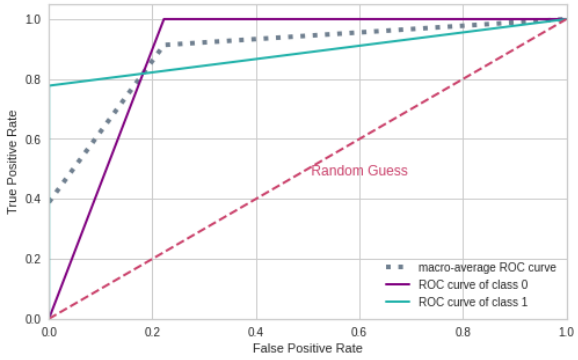

(c)

Figure 25 – ML results using complex network measures. (a) Confusion matrix indicating a true negative rate of 77.8% (purple according to the color bar) and a true positive rate of 100.0% (blue according to the color bar). (b) The learning curve for the training accuracy (blue) and test accuracy (green). (c) ROC curve with class 0 (control) and class 1 (after inhalation of DMT).

The results are discussed in this section to get insights into the effects of DMT consumption on the brain in terms of EEG frequency band (subsection 4.5.1), the connection of the most activated brain regions (subsection 4.5.2), and measures of complex networks (subsection 4.5.3).

4.5.1 Frequency bands

With our workflow, we identified these frequency bands, which were mostly modified after the intake of DMT. Furthermore, we found that classification results received with the connectivity matrices and the complex network measures are strongly based on acute changes in the delta band. Thus, changes in the delta band were most robust for both input data types.

This observation corresponds to what was also found in the literature (PALLAVICINI *et al.*, 2021; TIMMERMANN *et al.*, 2019). Delta band activity is usually associated with states where there is no wakefulness, such as sleep (AMZICA; STERIADE, 1998; BERNARDI *et al.*, 2019) and coma (ARDESHNA, 2016). However, some studies such in (FROHLICH;

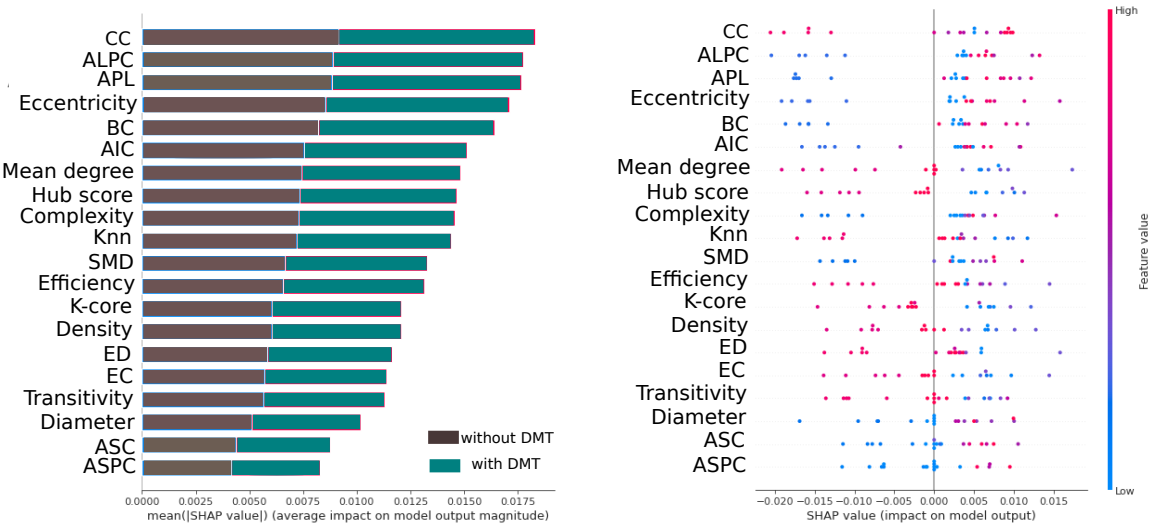

(a) (b)

Figure 26 – Feature importance ranking for SVM classifier with features ranked in descending order of importance. The CC measure is the most important to classify the effect of DMT. (a) Feature ranking based on the average of absolute SHAP values over all subjects considering both classes (gray: control, cyan: after inhalation of DMT). (b) Same as (a) but additionally showing details of the impact of each feature on the model.

TOKER; MONTI, 2021) observed that the delta frequency is present even when there are behavioral responses, such as in propofol anesthesia, postoperative delirium, and in powerful psychedelic states. Moreover, delta band activity has also been detected in studies involving spiritual experiences (BIELLO, 2007; HABIBABAD *et al.*, 2019; BEAUREGARD; PAQUETTE, 2008), and meditation states (BANQUET, 1973; KORA *et al.*, 2021).

Although the increase of delta band activity points clearly to an altered state of consciousness after the inhalation of DMT, other frequency bands were also affected. We found that in addition to delta, high alpha and low beta bands were essential features for the connectivity matrices. This finding is supported by (PALLAVICINI *et al.*, 2021), who describes that inhalation of DMT reduces the alpha band activity while increasing the delta and gamma band at the same time (PALLAVICINI *et al.*, 2020). According to the authors, the increase in gamma is associated with subjective perceptions typical of mystical experiences. In our data, we observed no changes in the gamma band.

4.5.2 Connection between brain regions

With the connectivity matrices, we found that classification results are strongly based on a decreasing correlation between the temporal/parietal (TP8) and the central brain (C3) region after DMT uptake. These brain areas correspond to the occipitotemporal (Right BA37), primary somatosensory cortex, and motor cortex (Left BA01/02) via Brodmann's map (SCRIVENER; READER, 2022). The temporal lobe is associated with the perception and production of speech,

hearing, memory, and emotional processes because it is connected to the amygdala and the limbic system (PATEL *et al.*, 2021). The right temporal region, TP8, is associated with recognizing familiar faces, with participation from the frontal cortex (GAINOTTI, 2007). Furthermore, in humans, the TP8 region contributes to the global processing of visual information (DOYON; MILNER, 1991). The connection between these two regions, TP8 and C3, is involved in visual and tactile perceptions and finger movements (BRAND *et al.*, 2020; PIERNO *et al.*, 2009).

In addition, the correlation between the electrodes FC5 (frontal region) and P8 (parietal region) contributed significantly to the classification result. These regions correspond to Left BA6 and Right BA19 of Brodmann's map, respectively. The frontal region is involved in cognitive processing, planning behavior, and has connections to the somatosensory cortex, motor, and auditory areas (COBIA *et al.*, 2012; CATANI, 2019) and limbic system, and is also involved in emotions. The placement of FC5 electrode encompasses the region of the precentral gyrus in the premotor region, which is responsible for controlling voluntary motor movement of the body. This region also includes a portion of the supplementary motor cortex, responsible for planning the voluntary movement of the limbs (BANKER; TADI, 2021). The P8 region, on the other hand, is located in the lateral occipital cortex, responsible for integrating different types of information so that our interaction with the environment is efficient, forming representational spaces through perception, semantics, through perception, semantics, and motor functions (LINGNAU; DOWNING, 2015).

Studies using other psychedelics, such as LSD, have found reduced functional connectivity in the anterior medial prefrontal cortex, and time-specific effects were correlated with different aspects of subjective experiences under the effect of psychedelics (LUPPI *et al.*, 2021). Psilocybin consumption, on the other hand, was related to decreased functional connectivity between the medial temporal lobe and high-level cortical regions. The changes found in the cortical regions reported above are related to the visual, sensory, perceptual, and motor type experiences experienced by the volunteers during the use of these two psychedelics (LSD and Psilocybin).

Correlating our findings with previous studies, the FC5 and P8 regions also found here are part of the cortical region, and a possible inference is that they are related to the participants' experience with DMT. In the original study from which the data of our study is derived, the authors (PALLAVICINI *et al.*, 2021) applied different scales to evaluate the lived experiences of this study participants. Among the experiences accessed by the volunteers during the use of inhaled DMT, the highest percentages were for elementary imagery (85.27%), blissful (61.77%), complex imagery (50.21%), spiritual experience (49.61%), and disembodiment (47.58%). For the Near-Death Experience scale, it was 60.94% for affect experience. For the Mystical Experience Questionnaire (mystical, positive mood, transcendence of time and space, and ineffability), 46.29% was found. According to authors (PALLAVICINI *et al.*, 2021), 13 of 35 participants (equivalent to 37%) accessed a complete mystical experience. Other studies using inhaled 5-MeO-

DMT also observed complete mystical experiences in 75% of volunteers (BARSUGLIA *et al.*, 2018) and improvements in depression and anxiety, which were associated with greater intensity of mystical experiences, with spiritual and personal meaning, when using 5-MeO-DMT (DAVIS *et al.*, 2019). Although these two cortical regions, FC5 and P8, may be related to the participant's sensory and visual experiences when using DMT, an interpretation of the connectivity between these regions has yet to be obtained since there is no information in the literature.

4.5.3 Complex network measures

Concerning the measures of complex networks, the most important was the CC. CC is a centrality measure defined as the inverse of the average length of the shortest path from one node to all other nodes in the network (RUBINOV; SPORNS, 2010). The idea is that important nodes participate in many shortest paths within a network and, therefore, play an important role in the flow of information in the brain (FREEMAN, 1978).

ALPC was the second important measure associated with the size of the largest community found by the label propagation community (LPC) detection algorithm. Increased values (compared to controls) of this metric are associated with the effect of DMT (see Figure 26 (b)) indicating communities with increased average path lengths after the use of DMT, in other words, larger communities. The third important metric was the APL which is the average of all shortest paths. For example, the shortest path d_{ij} (also known as the geodesic path) between two nodes i and j is defined as the shortest of all possible paths between these vertices. Increased values for APL were associated with the presence of DMT (Figure 26(b)).

In the brain of large vertebrates, there are two contrasting concepts: functional segregation (or specialization) and integration (or distributed processes) (TONONI; SPORNS; EDELMAN, 1994). Anatomical and functional segregation refers to the existence of specialized neurons and brain areas organized in modules (SPORNS, 2002), which correspond to communities where their members have high connectivity among themselves and few connections with members of other modules (SPORNS, 2013). As opposed to segregation, neuron units do not operate in isolation (SPORNS, 2002); there are regions of the brain (distributed system of the cerebral cortex) capable of combining specialized information, characterizing the concept of integration (RUBINOV; SPORNS, 2010). These regions have an executing function, benefiting from a high global efficiency of information transfer throughout the entire network (BULLMORE; SPORNS, 2012). The fact that we found larger communities and a longer average path with the use of DMT and the opposite in its absence indicates a decrease in brain integration, which might slow down the distribution of information. Larger brain communities were also found in (VIOL *et al.*, 2017) after using ayahuasca, a mixture containing DMT.

Furthermore, when looking at the transitivity, which is a measure of the propensity of nodes to be grouped, and global efficiency measure, which is a measure of how effective the exchange of information within a network is, both are also presented in the rank of the most

important measures for the model in Figure 26 (b), the presence of DMT decrease the values of these two measures. The transitivity is a measure of the efficiency of information transfer between all pairs of nodes in the graph (RANGAPRAKASH *et al.*, 2019), and a higher value of these measures indicates more significant active local processing and high segregation (LUO; GREENE; CONSTABLE, 2021). Since we obtained lower values of transitivity associated with DMT, this implicates less segregation in the brain's functional network.

In contrast, higher values of global efficiency indicate greater integration of networks. Since we obtained lower values of transitivity associated with DMT, this implicates less integration in the brain functional network.

Thus, considering the delta frequency, we can infer that the integration and segregation decreased with the use of the DMT. Furthermore, corroborating our findings, a decrease in brain segregation has been found in studies using other psychedelics such as LSD (CARHART-HARRIS *et al.*, 2016). Specifically, in (CARHART-HARRIS *et al.*, 2016), the authors concluded that the use of LSD caused a decrease in the integration and segregation of brain networks, supporting the idea that cortical brain activity becomes more "entropic" under psychedelics (CARHART-HARRIS *et al.*, 2014). However, as pointed out in (NICHOLS; JOHNSON; NICHOLS, 2017), psychedelics not only render the brain more random, but with normal organization disruption, they also produce strong functional and topologically far-reaching connections not seen in the normal state. Thus, even though our results show that integration and segregation have been disrupted, further experiments should be conducted to verify if there have been new long-distance connections, as shown in the literature.

4.6 Conclusion and future work

Our results demonstrated that ML methods could automatically reveal changes in functional brain connectivity induced by DMT consumption, considering a two-class classification based on (A) the connectivity matrix or (B) complex network measures. Moreover, considering these two data abstractions is more robust than the other literature studies.

The workflow developed here is powerful for detecting the brain changes caused due to the psychedelic substance, with case (B) showing the highest AUC (89%), indicating a new finding that complex network measurements best capture the brain changes that occur due to DMT use.

Regarding frequency, the workflow employed here detected that the delta frequency was most associated with DMT use. Although DMT induces an altered state of consciousness with the presence of delta, other frequencies were important for recognizing the pattern of brain activity with this substance, such as high alpha and low beta, through the connectivity matrix. This may suggest that the combination of the brain frequencies may represent an important point to be investigated to define further the altered state of consciousness induced by DMT.

Furthermore, by using the SHAP value, it is possible to interpret the results of the ML algorithms with a biological interpretation associated with the use of DMT on EEG data. The most important connections found with the use of DMT are between the temporal (TP8) and central cortex (C3) regions, followed by the connection between the precentral gyrus (FC5) and the lateral occipital cortex (P8).

The connection between regions TP8 and C3 has been found in the literature associated with finger movements that might have occurred during DMT consumption. However, the connection between cortical regions FC5 and P8 has not been found in the literature, a new finding, and is presumably related to the volunteers' emotional, visual, sensory, perceptual, and mystical experiences during DMT consumption.

Concerning the measures of complex networks similar to what was found with the use of ayahuasca in (ALVES *et al.*, 2022a), the most important is the centrality measure CC.

Furthermore, we find larger communities and a longer average shortest path when DMT is used and the reverse when it is not suggested that the balance between functional segregation and integration has been upset. This suggests that the brain distribution of information using DMT is slower than absence. These findings support that cortical brain activity becomes more entropic under psychedelics. However, from the literature, psychedelics do not simply make the brain more random; after the typical organization is disrupted, strong and topologically far-reaching functional connections emerge that are not present in the normal state. Therefore, since a limitation of our study is that we evaluate the acute effect of this psychedelic, we would like to investigate in the long term how psychedelics change the functional connectivity of the brain using our workflow. Furthermore, although decreased segregation and integration have been found in LSD-related work, this is a new finding for DMT.

Although the results are promising, a limitation of our study is that it is based on only 35 patients at two different times, so in future work, we would like to repeat our methodology in a more extensive dataset. Furthermore, the same methodology applied here may help interpret EEG time series from patients who consumed other psychedelic drugs and can help obtain a detailed understanding of functional changes in the brain neural network due to drug administration. Thus, in future work, we intend to use this methodology on the psychedelic drug called ketamine (FARNES *et al.*, 2020).

Overall, a robust computational workflow has been developed here with interpretability of how DMT (or other psychedelics) modify brain networks and insights into their mechanism of action.

CHAPTER

5

ANALYSIS USING FMRI DATA FROM ASD PATIENTS

'With thunder and heavenly fireworks must one speak to indolent and somnolent senses. But beauty's voice speaketh gently: it appealeth only to the most awakened souls."

— Friedrich Nietzsche, *Thus Spoke Zarathustra*

Submitted and under review at *Scientific Reports*.

COLLABORATING AUTHORS

Thaise G. L. de O. Toutain
Federal University of Bahia (FUB)
Joel Augusto Moura Porto
Universidade de São Paulo (USP)
Aruane M. Pineda
Universidade de São Paulo (USP)
Kirstin Roster
Universidade de São Paulo (USP)
Patricia de Carvalho Aguiar
Hospital Israelita Albert Einstein
Christiane Thielemann
Aschaffenburg University of Applied Sciences (UAS)
Francisco A. Rodrigues
Universidade de São Paulo (USP)

Abstract

ASD is a multifactorial neurodevelopmental disorder with high genetic heterogeneity. Studies of brain networks in autism can provide new insights into the dynamics of information processing

in individuals who suffer from such a condition. This paper proposes a method for automatic diagnosis of autism based on fMRI time series and machine learning algorithms. We verify that the left ventral posterior cingulate cortex region reduces the functional connectivity of the brain area in patients with autism spectrum disorder. Also, the brain networks of patients with autism spectrum disorder show more segregation, lower distribution of information, and less connectivity. Our methodology accurately differentiates control and autistic subjects providing an area under the curve close to higher than 95%.

5.1 Introduction

ASD is a multifactorial neurodevelopmental disorder with a complex genetic component (LORD *et al.*, 2020; AL-BELTAGI, 2021) and usually manifested since childhood (at least in the first three years of life) through deficits in social communication and restricted, repetitive patterns of behaviours or interests (ASSOCIATION *et al.*, 2013). Because ASD varies widely in symptoms and severity, an accurate diagnosis may be difficult. Indeed, there is no medical test to diagnose the disorder, such as a blood test, and diagnosis is based on the observation of the individual's communication, social interaction, and their activities and interests. This approach depends on experienced professional and an incorrect diagnosis can impact families and education, increasing the risk of depression, eating disorders, and self-harm (HOSOZAWA; SACKER; CABLE, 2021). An autism misdiagnosis might occurs because there are many other disorders that have similar symptoms. In this way, it is essential to develop a quantitative and accurate method for autism diagnosis based on physical exams. This paper considers data from functional brain networks and machine learning algorithms to propose a computer-aid diagnostic methodology for autism.

The idea behind our approach is based on previous studies that suggested that autism is a manifestation of changes in the brain organization (BEAUDET, 2007). Abnormal neuronal connectivity has recently become the essential hypothesis for explaining the symptoms associated with autism (BELMONTE *et al.*, 2004). By adopting the fMRI technique, Belmonte and Yurgelun-Todd (BELMONTE; YURGELUN-TODD, 2003) demonstrated that the inputs of the autistic brain regions are cut off, with reduced activation and functional correlations with sensory areas. fMRI data from children with ASD (DERAMUS *et al.*, 2014) suggest a strong activation of the parietal cortex, which is responsible for visuospatial and sensory processing. In a resting state, regions of the medial prefrontal cortex related to the executive function comprised of skills that enable the individual to make decisions, pay attention, and differentiate conflicting thoughts are suppressed (EUSTON; GRUBER; MCNAUGHTON, 2012). Apart from the medial prefrontal region, the rostral anterior cingulate cortex and the posterior cingulate cortex have also been investigated (KENNEDY; REDCAY; COURCHESNE, 2006). The function of the former includes memory recall and learning. In contrast, the posterior cingulate cortex is responsible for cognitive, emotional, and learning processes. Its metabolic activities during rest are deacti-

vated during demanding cognitive tasks. According to Kennedy et al. (KENNEDY; REDCAY; COURCHESNE, 2006), the midline resting network of patients with ASD is not as active as that of the control group, and task deactivation is not significant. In structural terms, Keller at al. (KELLER; KANA; JUST, 2007) suggested the development of the brains of autistic children is atypical, showing an early overgrowth of white matter, followed by its reduction in adolescence and adulthood. Furthermore, Diffusion Tensor Imaging Diffusion Tensor Imaging (DTI) results revealed the disorganization of white matter paths (AOKI *et al.*, 2013).

These studies show that the structure of the autistic brain differs from the control brain. Hence, we hypothesize that it is possible to diagnose autism from data collected from EEG or fMRI experiments. EEG is a relatively inexpensive method readily available in most contexts and has a good temporal resolution. Data from EEG has been used to study brain organization (FALLANI *et al.*, 2011b; ALVES *et al.*, 2022b). On the other hand, fMRI has a low temporal resolution but high spatial one, thus being well suited for analyses of spatial brain dynamics (MENON; CROTTAZ-HERBETTE, 2005; FORMISANO *et al.*, 2003). fMRI scans produce a set of three-dimensional images recorded over time and measure a signal (called BOLD signal [1]. The temporal evolution of the BOLD series is called the hemodynamic response function and is determined by the pixel intensity in fMRI images (STURZBECHER, 2006; BISWAL *et al.*, 1995). Each cube of an fMRI image, called voxel which anatomically maps a position in the brain, has a BOLD time series. Here, we consider BOLD series to develop the classification method for autistic patients.

After mapping the brain, it is possible to classify people with ASD and typical development (TD) using ML methods. ML techniques permit automatically extracting knowledge from a database. Previous studies have evaluated the effectiveness of machine learning in diagnosing ASD with supervised machine learning algorithms that distinguish between two classes, namely ASD and TD. At least 45 articles have focused on supervised machine learning algorithms that aid in ASD diagnosis, where the most used ones are based on SVM (HYDE *et al.*, 2019) (see Table 13 for publications on the use of fMRI for distinguishing between ASD and TD).

Although ML has provided important advances in diagnosing autism, considerable challenges must be addressed. Many methods for classification lack interpretability, which is disadvantageous, especially for the understanding of medical data (RUDIN, 2019; EKANAYAKE; MEDDAGE; RATHNAYAKE, 2022). Also, according to Table 13, (MCBRIDE *et al.*, 2015; YAMAGATA *et al.*, 2019), small data sets are quite common (STEYERBERG *et al.*, 2000; FERGUSON *et al.*, 2014; BAE *et al.*, 2018a; D'SOUZA; HUANG; YEH, 2020), which might cause unreliable results. To overcome the lack of interpretability, we can consider new techniques that have emerged in recent years towards facilitating the interpretation of machine learning results (e.g., SHAP values) (LUNDBERG; LEE, 2017) identify the most important features for a

[1] The decrease in the rate of deoxyhemoglobin can be detected with the increase of the NMR signal. This effect is called Blood Oxygenation Level Dependent (BOLD)

Table 13 – Publications on the use of supervised ML algorithms on fMRI data for distinguishing ASD from TD patients. Based on (HYDE *et al.*, 2019).

Authors	Data size	ML methods	AUC	Acc.	Recall	Precision
(SUBAH *et al.*, 2021)	n = 462 ASD; n =464 TD (ABIDE)	Deep learning	0.96	0.87	0.87	-
(CHEN *et al.*, 2015)	n = 126 ASD; n = 126 TD (ABIDE)	RF	0.91	0.89	0.93	-
(NUNES *et al.*, 2020)	(ABIDE)	SVM	-	0.80	-	-
(YAMAGATA *et al.*, 2019)	n =15 ASD; n =45 TD (ABIDE)	Lasso	0.78	0.75	0.77	0.73
(DEVI *et al.*, 2019)	n = 505 ASD; n = 530 TD (ABIDE)	Deep learning	-	0.70	0.74	0.63
(MCBRIDE *et al.*, 2015)	n= 59 ASD; n= 59 TD	Linear SVM; ridge logistic regression	0.73	-	-	-

model (BOWEN; UNGAR, 2020; RODRÍGUEZ-PÉREZ; BAJORATH, 2019; SPADON *et al.*, 2019)). Moreover, to circumvent the use of small medical data, data augmentation techniques (e.g., sliding windows), which split data (e.g., time series from EEG and fMRI) (LASHGARI; LIANG; MAOZ, 2020; QIANG *et al.*, 2021; LUO *et al.*, 2020), might be adopted. However, one of their limitations is the loss of information during the splitting process, which the overlapping windows technique can solve. Part of the window information is repeated in each subsequent window and used for EEG (CHANG *et al.*, 2013a; LI *et al.*, 2020) and fMRI (CHANG *et al.*, 2013b; JIE *et al.*, 2020) data. In this paper, we consider these methods to develop a new method for diagnosing autism that is interpretable and can be used in small data sets. In summary, our contributions are the following:

- We design a method to classify fMRI time series using a connectivity matrix as input to the ML algorithm, which provides more accurate results than those reported in the literature.
- Complex network measures are used to characterize brain organization, quantifying the differences between ASD and TD patients. We use SHAP values for a biological interpretation of the connections between brain regions and their relation with ASD.
- We adopt a sliding window data augmentation approach to increase the sample size by splitting time series into smaller series with either mutually exclusive sections of time series, or overlapping sections of the sliding windows, in which portions of the sequence are repeated in multiple observations. This approach enables handling small medical data.

In the next sections, we describe the dataset, the methodology and the results.

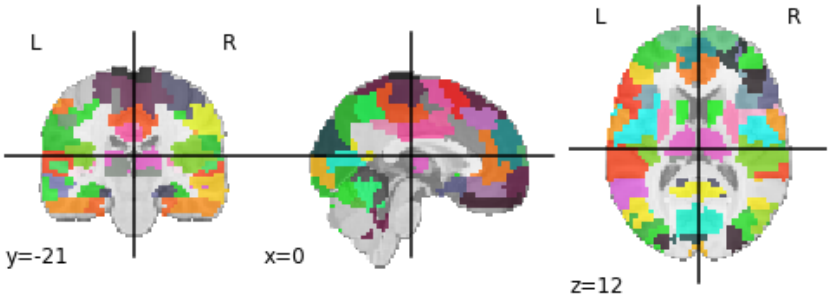

Figure 27 – Figure developed with the use of Python package Nilearn and containing BASC atlas with the 122 ROIs used in the present study.

5.1.1 Data and data preprocessing

We consider the preprocessed version of the Autism Brain Imaging Data Exchange Brain Imaging Data Exchange (ABIDE)[2], which consists of 1112 datasets comprised of 539 ASD and 573 TD with 300s BOLD time series and provided by the Preprocessed Connectomes Project Preprocessed Connectomes Project (PCP) dataset (NIELSEN *et al.*, 2013). The PCP preprocessing pipeline used includes cut time correction, motion correction, intensity normalization, and removal of artifacts such as breathing, heartbeat, and head motion. It is available for use in Nilearn's python package, which is a Python module for neuroimaging data. 242 ASD and 258 TD were used and the preprocessed data were 0.5 Hz band-pass filtered, since recent studies with fMRI have shown fluctuations may exist above that value (TRAPP; VAKAMUDI; POSSE, 2018).

Brain regions of interest (ROI), rather than the entire BOLD time series obtained from each voxel of the brain image, are considered. A brain atlas containing these ROIs is used; therefore, only the BOLD time series voxels of this ROIS were adopted. Among the numerous predefined atlases, Bootstrap Analysis of Stable Clusters (BASC) was chosen, since it was the map with best performance for distinguishing ASD patients by deep learning model, according to (SUBAH *et al.*, 2021). It was proposed in (BELLEC *et al.*, 2010) and generated from group brain parcellation by BASC method, which is a k-means clustering-based algorithm that identifies brain networks with coherent activity in resting-state fMRI (YANG; ZHANG; SCHRADER, 2022). BASC map with a cluster number of 122 ROIs is used here (see figure 27).

A manual use of Yale BioImage Suite Package web application[3] labelled the coordinates of each ROI for the identification of their names. After the extraction of the BOLD time series, the methodology described in Section 5.2 is adopted.

[2] Avaiable in <https://fcon_1000.projects.nitrc.org/indi/abide/>
[3] Avaiable in <https://bioimagesuiteweb.github.io/webapp/mni2tal.html>

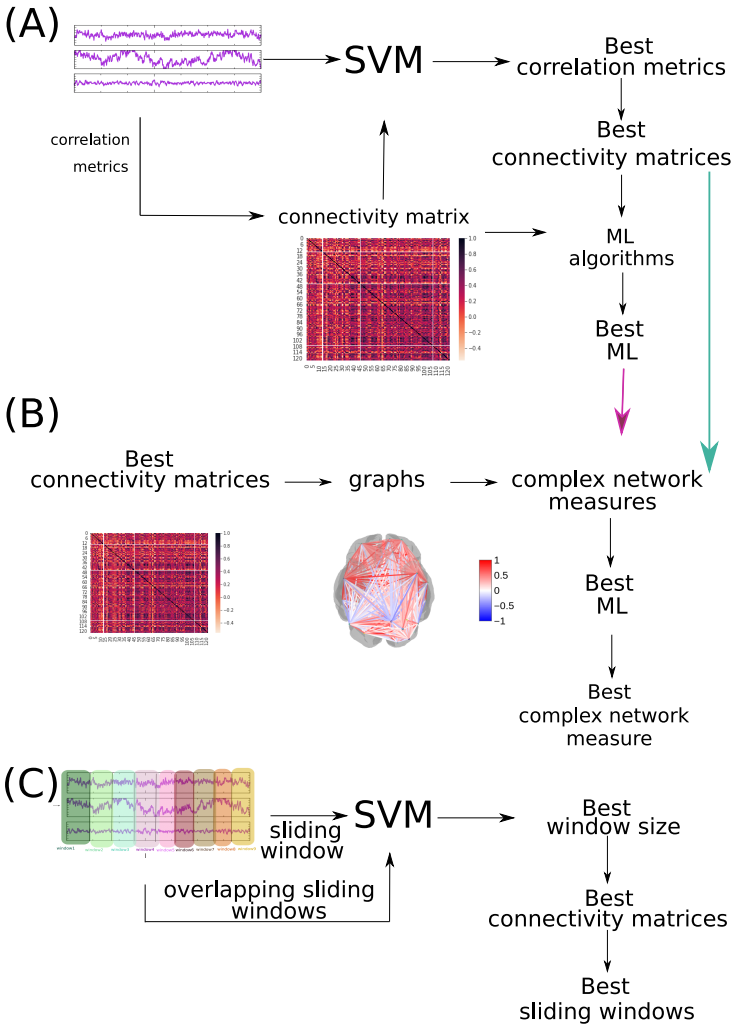

Figure 28 – **The methodology used here for the diagnosis of autism.** (A) methodology described in subsection 5.2.1; (B) methodology reported in subsection 5.2.2; (C) methodology described in subsection 5.2.3.

5.2 Methodology

Figure 28 depicts the methodology workflow used and organized into three parts according to their aim, i.e., the finding of the best connectivity matrix (described in Figure 28-(A) and in subsection 5.2.1), the best measures of complex networks (described in Figure 28-(B) and in subsection 5.2.2), and the best sliding technique for differentiating ASD from TD patients (described in Figure 28-(C) and in subsection 5.2.3.) The python code with the methodology used in this work is available at:

<https://github.com/Carol180619/Paper-autism.git>.

5.2.1 Connectivity matrix

Once the time series for each of the 122 regions had been extracted, they were correlated according to PC (BENESTY *et al.*, 2009), SC (LUBINSKI, 2004), GC (GRANGER, 1969),

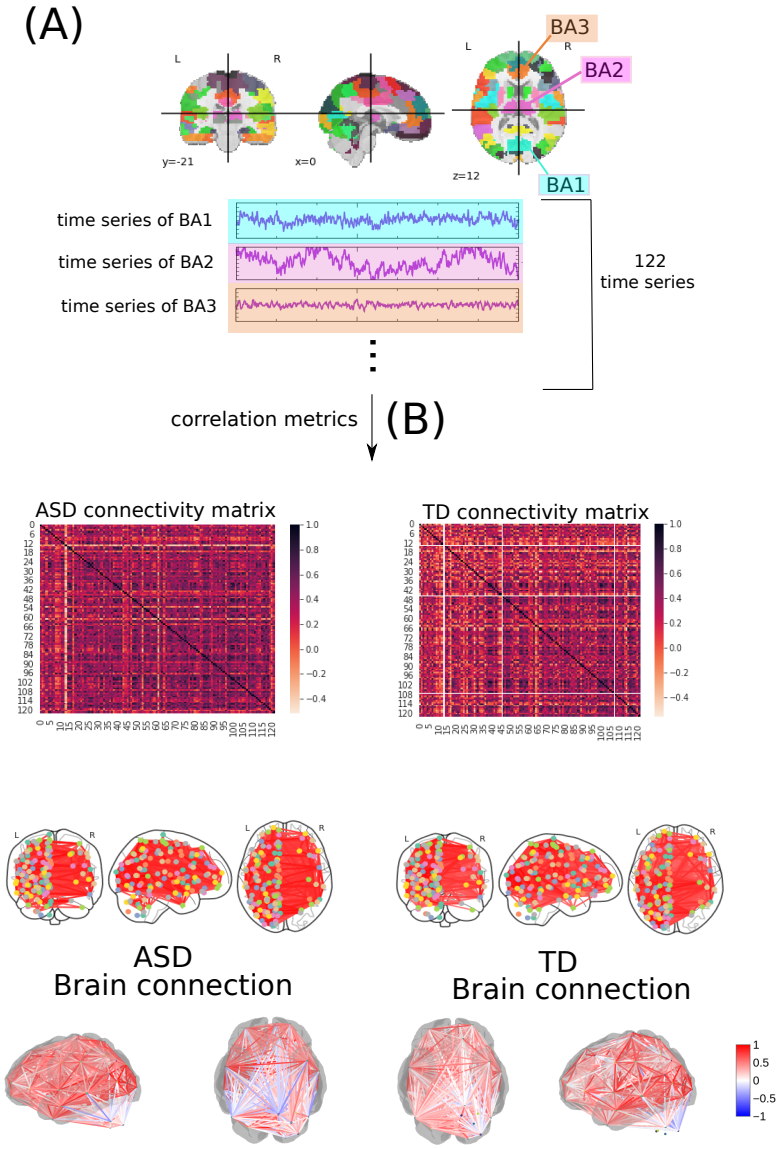

Figure 29 – **Methodology to obtain the connectivity matrices.** In (A), time series of 122 ROI is extracted from fMRI data with the use of BASC BOLD atlas (highlighted in blue, purple, and orange). The time series are correlated, B, by pairwise statistical metrics (Pearson correlation was used in this example) towards forming the connectivity matrices, where each row and column correspond to one of the Brodmann areas for a patient with ASD for one with TD. The same highlighted matrices are arranged in a two-dimensional and three-dimensional brain schematic for better visualization.

Biweight Midcorrelation (BM) (WILCOX, 2011), Sparce Canonical Correlation analysis (SCC) (HARDOON; SHAWE-TAYLOR, 2011), Graphical Lasso method (GL) (SOJOUDI, 2016), Ledoit-Wolf shrinkage (LW) (LEDOIT; WOLF, 2012), Mutual Information (MI) (KRASKOV; STÖGBAUER; GRASSBERGER, 2004), and Transfer Entropy (TE)[4](SCHREIBER, 2000). Figure 29 displays the scheme to generate the connectivity matrices.

[4] For the TE, MI and GL metrics a Min-max normalization and then a thresholding process was performed, with a value of 0.5, since these measures deal best with binary values.

Each matrix was reduced to the size of the vectors used as input to the ML algorithm. The SVM algorithm (BOTTOU; LIN, 2007) was used to select the best methods to construct the correlation and connectivity matrices. We use this method, because is has been considered in studies of ASD (see section 6.1) and has a lower computational cost. The time series of each ROI was used for directly feeding SVM and finding the best connectivity metric that captured the brain changes due to ASD. It also checked whether the use of metrics was better than a direct use of time series – the one of better performance would be chosen. After the best brain connectivity metric had been determined, the following ML classifiers were used: RF (BREIMAN, 2001), NB (FRIEDMAN; GEIGER; GOLDSZMIDT, 1997), LR with L-BFGS Limited-memory Broyden Fletcher Goldfarb Shanno (L-BFGS) solver (NAJAFABADI *et al.*, 2017), MLP (HINTON; RUMELHART; WILLIAMS, 1986), and tuned CNN implemented in (ALVES,). SHAP value method was used for biological interpretation, since it allows to explain individual predictions of each attribute. The same sampling data set was used in all ML algorithms and split into training (train) and test sets, with 25% of data comprising the test set. A k-fold cross validation procedure was employed, with k = 10 — this a very used value for this method (BERRAR, 2019; BENGIO; GRANDVALET, 2004; SHAH; KHAN, 2020; KAWAMOTO; KABASHIMA, 2017; CHAN *et al.*, 2019; KAWAMOTO; KABASHIMA, 2017)). This procedure is used for model selection and a hyper-parameter optimization. We considered the method called grid search, which was used for all ML algorithms, except the untuned CNN model (since deep learning algorithms have a higher computational cost), as done in (SATO *et al.*, 2019; ZHONG *et al.*, 2021; ARCADU *et al.*, 2020; KRITTANAWONG *et al.*, 2021; RASHIDI *et al.*, 2020). The hyper-parameter optimization values for each classifier model are provided in Table 24 in the Appendix A.3. The standard performance metric Acc. (MINCHOLÉ; RODRIGUEZ, 2019; TOLKACH *et al.*, 2020; DUKART *et al.*, 2021; LI; ASCH; SHAH, 2020; PARK; KELLIS, 2015) was employed for evaluation. Due to the two-class (negative and positive) classification problem, other common metrics such as precision and recall were considered (ITO *et al.*, 2021; KIM *et al.*, 2020; LI *et al.*, 2021; YU *et al.*, 2020). Precision (also called positive predictive value) corresponds to the hit rate in the negative class (here corresponding to TD group), whereas recall (also called sensitivity) measures how well a classifier can predict positive examples (hit rate in the positive class), here related to ASD patients. F1 score (ZHONG *et al.*, 2021; BERRYMAN *et al.*, 2020; YANG *et al.*, 2019), another well-known measure, is the harmonic mean of recall and precision (HANNUN *et al.*, 2019). Regarding the visualization of the two latter measures, the ROC curve is a common method that displays the relation between the rate of true and false positives. The area below the curve, called AUC, has been widely used in classification problems (MINCHOLÉ; RODRIGUEZ, 2019; BRACHER-SMITH; CRAWFORD; ESCOTT-PRICE, 2021; PATEL *et al.*, 2021; KRITTANAWONG *et al.*, 2021). The AUC value ranges from 0 to 1- 1 corresponds to a classification result free of errors and 0.5 indicates the classifier cannot distinguish the classes, as in a random choice. The micro average of ROC curve, which computes the AUC metric independently for each class (it calculates AUC for

healthy individuals, class zero, and separately calculates it for unhealthy ones, class one) was also considered. The average is computed considering the classes equally. The macro average was also employed in our evaluation - it does not consider the classes equally, but aggregates their contributions separately and then calculates the average.

5.2.2 Complex network measures

A complex network (or a graph) was generated for each connectivity matrix for the extraction of different measures. Towards inputting data into the ML algorithm, the complex network measures were stored in a matrix of attributes, where each column represents a complex network measure (feature) and each row denotes a subject. 2D matrices were generated for all subjects, as in (ALVES *et al.*, 2022a).

To describe the brain structure, the following complex network measures were calculated: assortativity coefficient (NEWMAN, 2003; NEWMAN, 2002), APL (ALBERT; BARABÁSI, 2002), BC (FREEMAN, 1977), CC (FREEMAN, 1978),EC (BONACICH, 1987), diameter (ALBERT; JEONG; BARABÁSI, 1999), hub score (KLEINBERG, 1999), Knn (EPPSTEIN; PATERSON; YAO, 1997), mean degree (DOYLE; GRAVER, 1977), SMD (SNIJDERS, 1981), ED (DEHMER; MOWSHOWITZ, 2011), transitivity (WATTS; STROGATZ, 1998; NEWMAN; WATTS; STROGATZ, 2002), complexity, k-core (SEIDMAN, 1983; NEWMAN, 2010), eccentricity (HAGE; HARARY, 1995), density (ANDERSON; BUTTS; CARLEY, 1999), and efficiency (LATORA; MARCHIORI, 2003).

Newly developed metrics (described in detail in (ALVES *et al.*, 2022a)) reflecting the number of communities in a complex network were also applied. Community detection algorithms were also used in our study (NEWMAN, 2012; KIM; LEE, 2015; ZHAO; LIANG; WANG, 2021). Since the community detection measures must be transformed into a single scalar value to be included in the matrix, community detection algorithms were applied for finding the largest community. The average path length within the community was then calculated and received a single value as the result. The community detection algorithms used were the FC (CLAUSET; NEWMAN; MOORE, 2004), IC (ROSVALL; AXELSSON; BERGSTROM, 2009), LC (NEWMAN, 2006), LPC (RAGHAVAN; ALBERT; KUMARA, 2007), EBC (GIRVAN; NEWMAN, 2002), SPC (REICHARDT; BORNHOLDT, 2006), and MC (BLONDEL *et al.*, 2008). The abbreviations were extended with letter "A" (for average path length) towards indicating the approach (AFC, AIC, ALC, ALPC, AEBC, ASPC, and AMC).

These network measures were utilized to characterize the brain structure. Thus each observation (which represents the Patient's brain network) is represented by a vector with these metrics. The results are provided in the subsection 5.3.2.

5.2.3 Sliding windows and overlapping sliding windows

Due to the common issue of small datasets in neuroscience, the previously described methodology was expanded by a sliding window data augmentation approach and the sample size was increased by splitting each time series into smaller series. Such an increase can be achieved with either mutually exclusive sections of the time series, or overlapping sections of the sliding windows, in which portions of the sequence are repeated in multiple observations.

A sample with 50 patients (25 ASD and 25 TD) was considered from the initial sample for evaluations by window sliding and overlapping windows sliding techniques. BOLD time series with 300 seconds were divided into windows of 15, 20, 30, 50, and 60 seconds and placed into the SVM for checking the best way to split data.Then, with the best window size, it was also considered overlap sizes of 10%, 15%, 25%, 35%, 45%, and 55% of it. In other words, if the overlapping is 10%, each sliding window size has depicted a repetition of 10% of the previous window. This approach is used to avoid losing information when sliding.

The connection matrices are constructed using the best partitioning technique and the best correlation metric that fed the previously computed best classifier (see figure 28). The same sliding workflow was considered with samplings of 10, 20, 30, 50, 124, and 188 patients. The choice of such different sizes was based on previous neuroscience studies that used fMRI of similar sample sizes, respectively (HAJEBRAHIMI *et al.*, 2022; LIU *et al.*, 2022; PEROVNIK *et al.*, 2022; ASHAR *et al.*, 2022; HACK; ZHANG; WILLIAMS, 2021; POLLI *et al.*, 2016).

Additionally to the performance metrics, a mean square error Mean Square Error (MSE) was obtained for each sampling and for each iteration of the k-fold cross validation, resulting in an error vector. It was compared with the vector of the MSE obtained with the use of the whole sample by statistical Student's paired t-test (WILLIAM, 1908). The results are provided in subsection 5.3.3.

5.3 Results

ML algorithms were applied for three different levels of data abstraction, namely (A) connectivity matrix, (B) the matrix of attributes, whose elements are complex network measures calculated from (A), and (C) sliding data (see Figure 28). The sliding window method was employed as an augmentation technique on small data samples to evaluate whether this methodology is advantageous when dealing with these data sets. We verify that all approaches automatically detected changes in the brain of ASD patients. The highest classification performance was obtained for the connectivity matrix with a 99% mean AUC (Table 14). Subsections 5.3.1, 5.3.2, and 5.3.3 detail the results.

Table 14 – Classification using the connectivity matrix best captured brain changes due to ASD. The best performance is highlighted in bold.

Data abstraction level	Subset	AUC	Acc.	F1	Recall	Precision
Connectivity matrix	**Train**	**1.00**	**1.00**	**1.00**	**1.00**	**1.00**
	Test	**0.99**	**0.99**	**0.99**	**0.99**	**0.99**
Complex network	**Train**	0.93	0.93	0.89	0.88	0.91
	Test	0.98	0.98	0.98	0.98	0.98
Sliding data	**Train**	0.84	0.84	0.84	0.84	0.84
	Test	0.81	0.81	0.81	0.81	0.81

Table 15 – Results from different ML algorithms. The best MLs were RF and LR, whose performances are highlighted.

Measures	Subset	AUC	Acc.	F1	Recall	Precision
Time series	**Train**	0.49	0.51	0.00	0.27	0.35
	Test	0.50	0.51	0.34	0.50	0.26
PC	**Train**	0.67	0.67	0.69	0.67	0.66
	Test	0.60	0.60	0.60	0.60	0.60
SC	**Train**	**0.98**	**0.98**	**0.97**	**0.98**	**0.98**
	Test	**0.98**	**0.98**	**0.98**	**0.98**	**0.98**
GC	**Train**	0.51	0.52	0.00	0.32	0.37
	Test	0.50	0.51	0.34	0.50	0.26
BM	**Train**	0.75	0.75	0.72	0.75	0.75
	Test	0.75	0.75	0.75	0.75	0.75
SCC	**Train**	0.67	0.67	0.65	0.67	0.66
	Test	0.62	0.62	0.62	0.62	0.62
GL	**Train**	0.66	0.66	0.65	0.66	0.66
	Test	0.57	0.58	0.57	0.57	0.57
LW	**Train**	0.66	0.66	0.64	0.66	0.65
	Test	0.58	0.58	0.58	0.58	0.58
MI	**Train**	0.49	0.50	0.40	0.50	0.49
	Test	0.49	0.49	0.49	0.49	0.49
TE	**Train**	0.90	0.90	0.89	0.90	0.90
	Test	0.91	0.91	0.91	0.91	0.91

5.3.1 Results related to connectivity matrix

Table 15 contains the results for each connectivity matrix with different types of pairwise statistical metrics. SVM was used to detected the best one for capturing the brain changes due to ASD.

Spearman correlation coefficient (SC) achieved the best performance, followed by the transfer entropy (TE). The best connectivity matrix was tested with the other ML algorithms for determining the one that best differentiated ASD patients from TD ones. According to Table 16, the best classifiers are the random forest (RF) and logistic regression (LR). Since LR has a lower computational cost, it was chosen for the next steps. Its performance for the test set was equal to

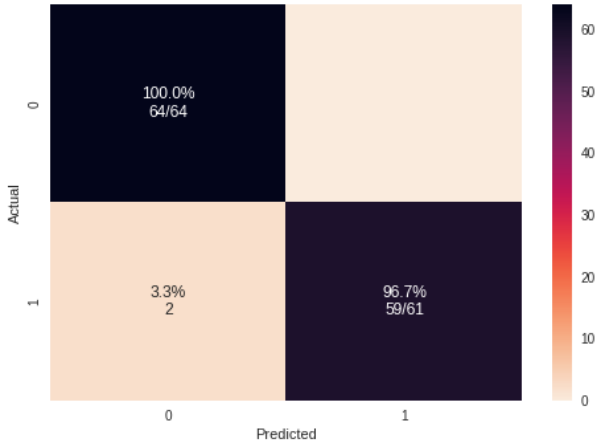

(a) Confusion matrix

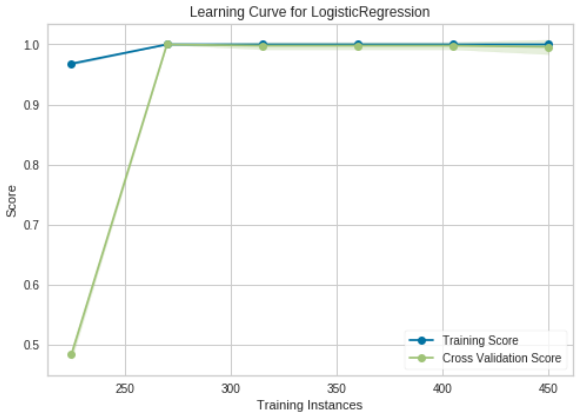

(b) Learning curve

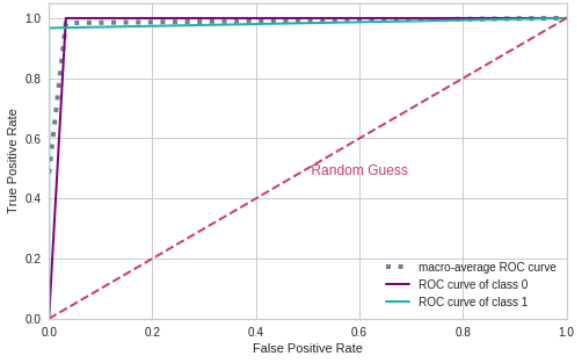

(c) ROC curve

Figure 30 – **ML results from connectivity matrices**. (a) Confusion matrix indicating a 96.7% TN rate (purple, according to the color bar) and a 100% TP rate (blue, according to the color bar). (b) Learning curve for the training Acc. (blue) and for test Acc. (green). (c) ROC curve with classes 0 (TD) and 1 (ASD).

0.99 for the mean AUC, precision, F1, recall and Acc. Figure 30 displays the confusion matrix (30-(a)), the learning curve (Figure 30-(b)), and the ROC curve (30-(c)), respectively.

The learning curve evaluates the predictability of the model by varying the size of the training set (SPADON *et al.*, 2019). The results show the entire database is not necessary for the achievement of a highest validation Acc. Regarding the classification model, TP (related to class 1) was higher than TN, showing that it better detects ASD patients (see confusion matrix in Figure 30- (b)).

SHAP values were calculated to quantify the importance of brain connections for the logistic regression classifier (LR) (see Figure 42 for the results). The area between regions Left-Sec Visual (visual cortex) and Outside defined BAS1 (area outside Brodmann's map), identified as the cerebellum, was clearly the most important connection. According to the data in Figure 42, low correlation values (blue dots) for the connection (Left-Sec Visual and Outside defined BAS1) were important for the detection of ASD patients, and high values of correlation (red dots) were important for the detection of TD ones. The second most important connection

Table 16 – Results from different ML algorithms. The best ML was RF and LR, whose performances are highlighted.

ML algorithm	Subset	AUC	Acc.	F1	Rec.	Pre.
SVM	**Train**	0.99	0.99	0.99	0.99	0.99
	Test	0.98	0.98	0.98	0.98	0.98
RF	**Train**	**1.00**	**1.00**	**1.00**	**1.00**	**1.00**
	Test	**0.99**	**0.99**	**0.99**	**0.99**	**0.99**
NB	**Train**	1.00	1.00	0.99	1.00	0.99
	Test	0.98	0.98	0.98	0.98	0.98
LR	**Train**	**1.00**	**1.00**	**1.00**	**1.00**	**1.00**
	Test	**0.99**	**0.99**	**0.99**	**0.99**	**0.99**
MLP	**Train**	1.00	1.00	1.00	1.00	1.00
	Test	0.98	0.99	0.99	0.99	0.99
untuned CNN	**Train**	1.00	1.00	1.00	1.00	1.00
	Test	0.86	0.87	0.92	0.94	0.90

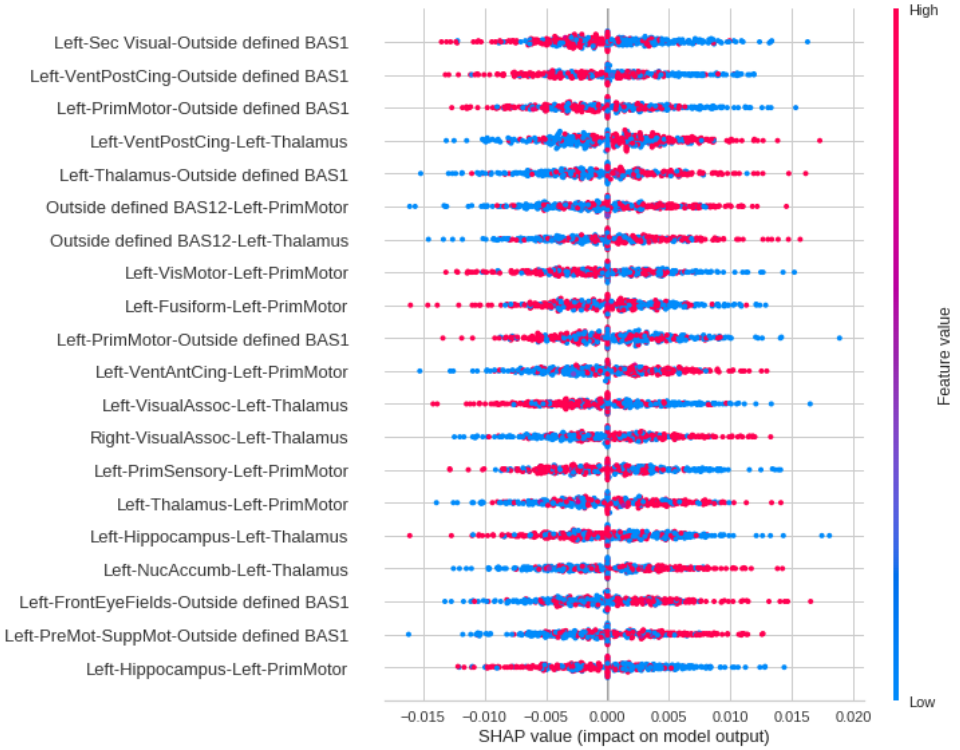

Figure 31 – **Feature importance ranking for the LR classifier with brain regions in a descending order.** The connection between the Left-Sec Visual and Outside defined BAS1 regions is the most important for the classification of ASD patients.

was detected between the Left ventral posterior cingulate cortex (Left-VentPostCing) and, again, the cerebellum (Outside defined BAS1). The corresponding brain regions are depicted in Figure 32.

Since LG was the algorithm that provided the best performance, it was used in the next subsections. Furthermore, since the results were close to 100%, noises were inserted into the ASD and TD time series for further testing the model in this study. Such noises were generated by a

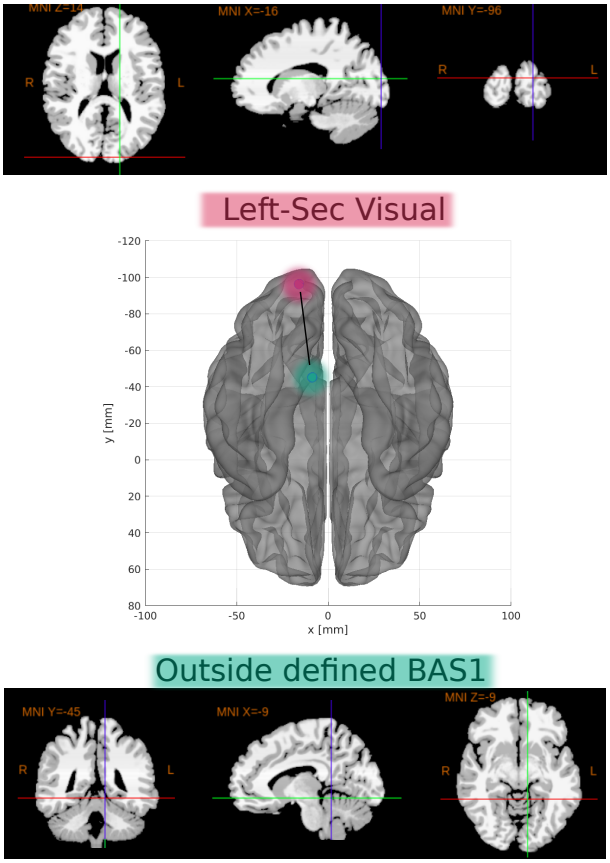

Figure 32 – **The most important connection found.** Two-dimensional schematic (ventral-axis), where the connection between the Left-Sec Visual region (visual cortex, highlighted in pink) and Outsides BAS1 (cerebellum, highlighted in green) is observed in the central region. The brain plot was developed by Braph tool (MIJALKOV *et al.*, 2017) and each region was plotted with the use of Brodmann map from Yale BioImage Suite Package (upper and lower regions in the Figure).

normal distribution with a standard deviation equals to 0.1 and mean on the interval $[0, 10]$. After the introduction of the noises, Spearman's correlation was used to generated the connectivity matrices from the time series. The results of the average AUC calculated on the test set are shown in Table 33. According to Figure 33, the AUC according to the noise follows approximately a decreasing logarithmic function.

5.3.2 Results for complex networks measures

The performance of the test sample considering the complex network yield a mean AUC equals to 0.98, 0.98 for precision, 0.98 for F1 score, 0.98 for recall, and 0.99 for the Acc. Confusion matrix 34, learning curve 34, and ROC curve 34 are shown in Figure 34. The use of the entire dataset was not necessary, since from the Figure 34 with 100 train instances was possible to acquire the best performance. Furthermore, according to the Figure 34, the whole dataset was unnecessary because the best result could be reached with only 100 train instances.

According to the SHAP values in Figure 35, the most important measure for the model

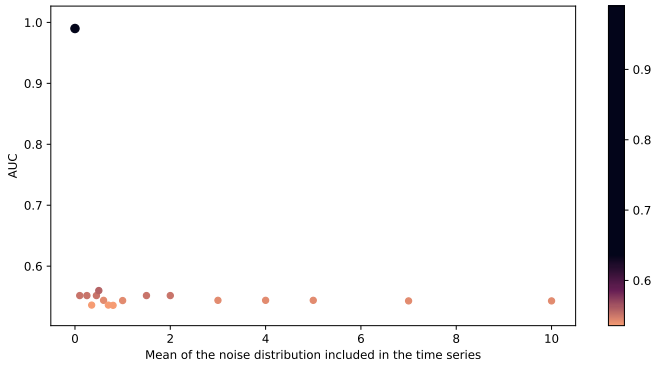

Figure 33 – **Mean AUC of the test obtained with the insertion of noise generated by a normal distribution with 0.1 standard deviation and 0-10 mean range.**

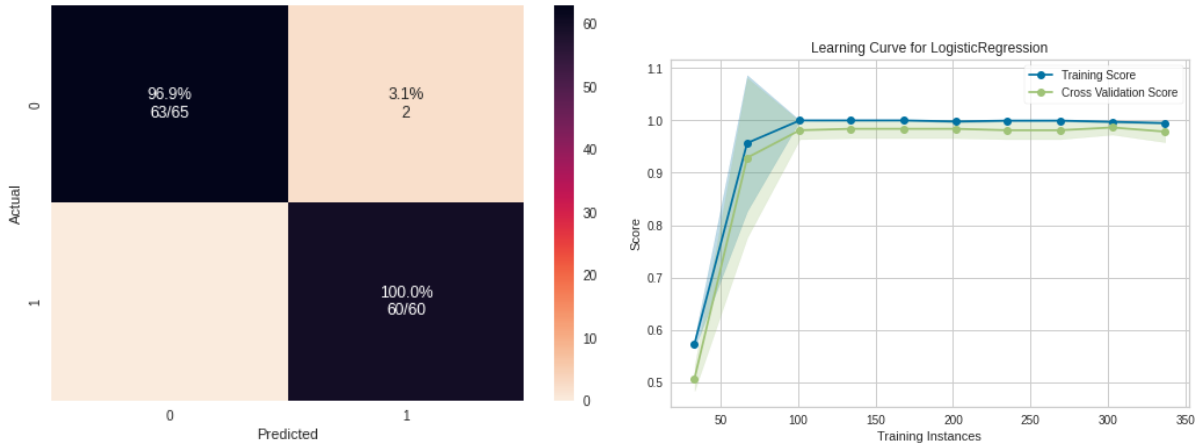

(a) Confusion matrix (b) Learning curve

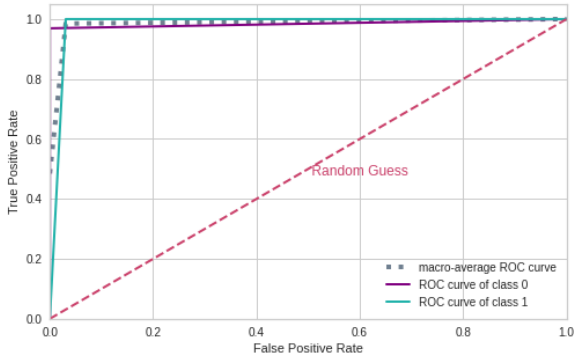

(c) ROC curve

Figure 34 – **ML results from complex network measures.** (a) Confusion matrix indicating a 98.5% TN rate (blue, according to the color bar) and a 98.3% TP rate (purple, according to the color bar). (b) Learning curve for the training Acc. (blue) and for test Acc. (green). (c) ROC curve with classes 0 (TD) and 1 (ASD).

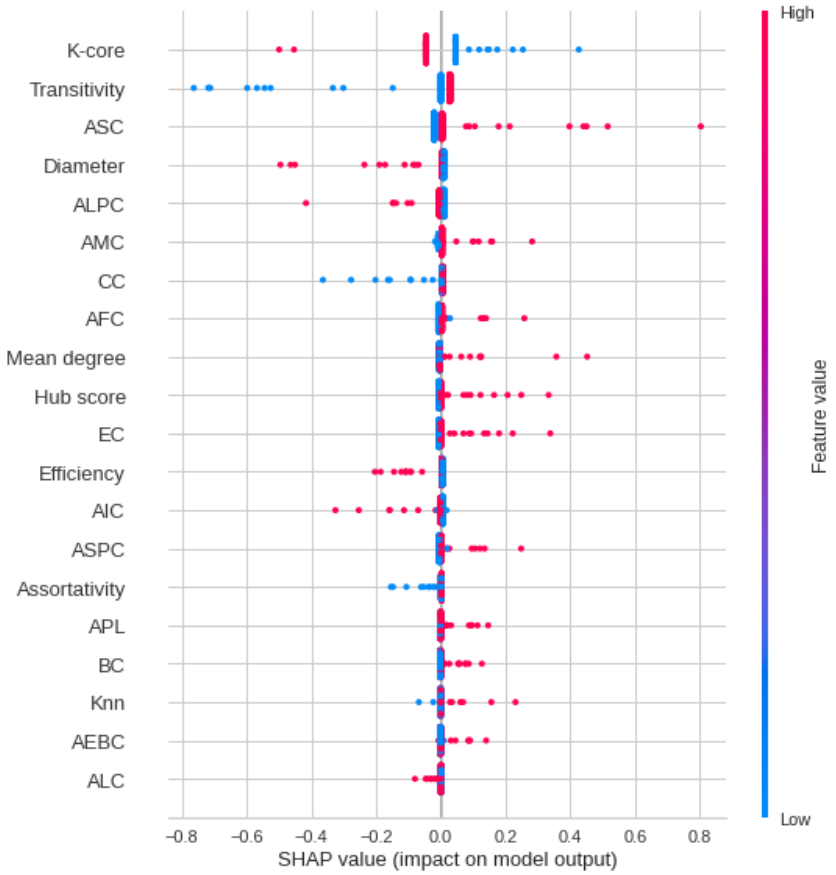

Figure 35 – **Feature importance ranking for LR classifier with features in a descending order.** K-core measure is the most important for the classification of ASD patients, followed by the AEBC measure.

was the k-core, followed by the AEBC, introduced in (ALVES *et al.*, 2022a). High k-core values (pink dots) indicate its importance for the detection of TD and low ones (blue dots) are important for the detection of ASD (Figure 35). Low AEBC values (blue dots) indicate its importance for the detection of ASD and high ones (pink dots) suggest its importance for the detection of TD. Higher values of efficiency were associated with TD patients; higher values of transitivity were associated with ASD and low values indicated TD. Remarkably, the seven measures introduced in (ALVES *et al.*, 2022a) appeared in the ranking of best ones.

5.3.3 Results from sliding windows and overlapping sliding windows

Figure 36- (a) shows the performance of SVM fed by time series divided into different window sizes. The best performance was achieved with the use of a window size of 20 seconds. Figure 36- (b) shows the best performance obtained with no overlapping or with a 10% of the size of time window. Consequently, 10% overlapping was considered for the next step for avoiding loss of information in the sliding process.

The sliding process was used with different sample sizes, and the results are shown in Table 17.

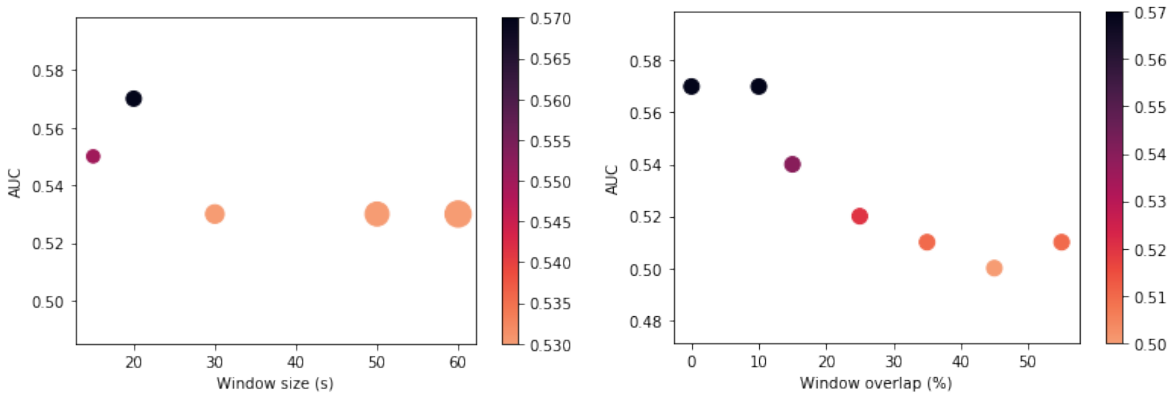

(a) (b)

Figure 36 – **Results of sliding and overlapping window sizes.** (a) Mean AUC test obtained for the different window sizes. The width of the points in the graph corresponds to the window size variation and their colors are indicated in the color bar. (b) Mean AUC test obtained for the different overlapping sizes corresponding to the percentage of the window size. The colors of the points in the graph are depicted in the color bar.

Paired Student's t-test (here called t-test) was also calculated between the sample performance and the performance for the whole data set. The null hypothesis is the performances were statistically different. Therefore, a sample size of only 10 patients was taken as a basis for comparison, given the premise their performance should be statistically different when the entire database is considered for such a small sample size. Only samples for which the null hypothesis could be rejected (p-value greater than or equal to the baseline value for comparison) were considered, i.e., 10 and 20 patients. In other words, the performance of those two sizes showed no statistically significant differences from the data set, but very similar results (Table 17). In other words, the performance of these two sample sizes showed no statistically significant differences from the data set, but very similar results.

Figure 37 shows the confusion matrix (37-(a)) for the sample size of 30 patients, the mean AUC test for each sample size (Figure 37-(b)), and the ROC curve for the sample size of 30 patients (37-(c)). According to Figure 37-(b), ASD and TD patients were differentiated even with different sample sizes, with above 79% AUC and Acc.

5.4 Discussion

The results from the use of the abstraction levels of the connectivity matrix and complex network data were superior to those reported in the literature (see Table 13). Therefore, the workflow developed here is more effective for detecting ASD patients with above 95% mean Acc. and mean AUC, and SC was the measure that best captured brain changes in the patients (as an example, it is more robust for non-linear correlations than PC (WANG *et al.*, 2015)). Since the Pearson correlation coefficient (PC) was not effective to discriminated between the two classes

Table 17 – Performance of the LR algorithm with the use of the sliding process and varied number of samples of TD and ASC patients. The best performance is highlighted in bold and was achieved with 30 patients.

Data abstraction level	Subset	AUC	Acccuracy	F1 score	Recall	Precision	T-test
sample	**Train**	0.79	0.80	0.80	0.77	0.81	7.25 e-07
10	**Test**	0.80	0.80	0.80	0.80	0.80	Threshold p-value
sample	**Train**	0.80	0.80	0.80	0.77	0.80	7.11 e-05
20	**Test**	0.80	0.80	0.80	0.80	0.80	Reject null hypothesis
sample	**Train**	**0.84**	**0.84**	**0.84**	**0.84**	**0.84**	**3.14 e-06**
30	**Test**	**0.81**	**0.81**	**0.81**	**0.81**	**0.81**	**Reject null hypothesis**
sample	Train	0.75	0.75	0.75	0.76	0.75	1.24 e-08
50	Test	0.75	0.75	0.75	0.75	0.75	
sample	**Train**	0.70	0.70	0.70	0.72	0.70	2.77e-09
124	**Test**	0.73	0.73	0.73	0.73	0.73	
sample	**Train**	0.70	0.70	0.70	0.70	0.70	7.60 e-12
188	**Test**	0.74	0.74	0.74	0.73	0.74	

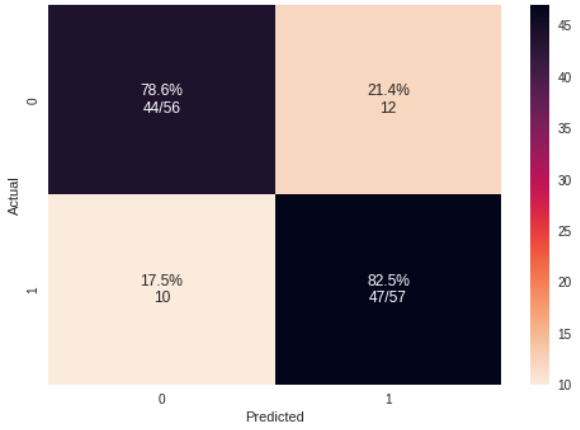

(a) Confusion matrix

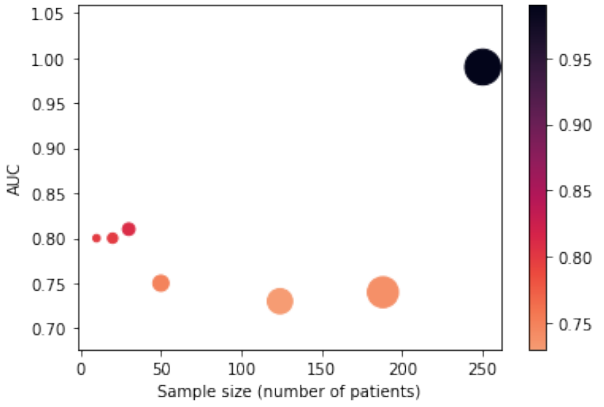

(b) Mean test AUC for the different sample sizes

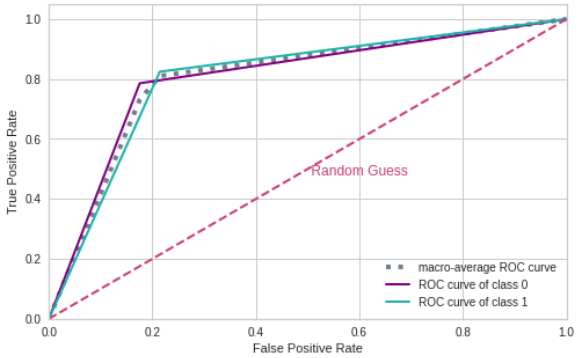

(c) ROC curve

Figure 37 – **Results from connectivity matrices and ML.** (a) Confusion matrix indicating an 82.5% true negative rate (blue, according to the color bar) and a 78.6% true positive rate (purple, according to the color bar). (b) Mean test AUC obtained for the different sample sizes; the width of the points in the graph corresponds to the window size variation, and their colors are depicted in the color bar. (c) ROC curve with classes 0 (TD) and 1(ASD).

(ASD and control subjects), we can conclude that brain changes due to ASD have a non-linear nature. Also, LG provides the best results, being the most suitable machine learning model, with lower computational cost than other ML algorithms used here (such as untuned CNN).

The most important connection in the first five major correlations was clearly observed between Left-Sec Visual (visual cortex) and cerebellum (Outside defined BAS1) regions. Low values of correlation (blue dots) were important for the detection of ASD patients, whereas high values (red dots) indicated TD. The second most important connection was established between the Left- VentPostCing and, again, the cerebellum (Outside de- fined BAS1) regions. Cerebellum (Outside defined BAS1), Left-Thalamus, and Left-Prim Motor appeared in several of the main connections found. Notably, Left-Thalamus has been reported in other studies associated with ASD (MCGRATH *et al.*, 2013; ALAERTS *et al.*, 2014).

Left-Sec Visual (visual cortex) is a part of the cerebral cortex that processes visual information, and a lower connection to the cerebellum (Outside defined BAS1) is more associated with ASD.

Left-VentPostCing corresponds to the upper part of the limbic system, i.e., part of the brain involved in behavioural and emotional responses. According to the literature, reductions in the functional connectivity of that brain area are common in ASD patients (LEECH; SHARP, 2014), which is consistent with our results, since the region is less connected to the Outside BAS1 in ASD patients.

The brain region changes addressed elsewhere have been reported in the ASD literature. As an example, both hyper- and hypo-connectivity were observed in ASD through stepwise functional connectivity in the resting state (MARTÍNEZ *et al.*, 2020). In the same study, hypoconnectivity was related to the parietal and frontal regions of the attention networks, whereas hyperconnectivity was observed for the default mode network, in the visual cortex region. The authors in (CLERY *et al.*, 2013) claimed ASD patients have higher activity in the occipital cortex bilaterally and in the Anterior Cingulate Cortex (ACC), but lower activation in the frontal gyri in comparison with a control group, during automatic identification of visual changes. However, (LEECH; SHARP, 2014) reported reductions in functional connectivity in ACC in ASD patients. The low correlation observed between the posterior cingulate region and the cerebellum (Left-VentPostCing vs Outside BAS1) observed in our study seems to point to a dysfunction, i.e., an alteration in functional communication in ASD. Such a correlation differs from the findings for ASD reported by other researchers, who have pointed to the anterior cingulate as one of the altered brain regions in ASD (LEECH; SHARP, 2014; CLERY *et al.*, 2013; LAIDI *et al.*, 2019) and found cortical thinning for ASD in the right ACC. Such results have led us to hypothesize that not only the ACC, but also other cingulate regions are implicated in ASD. Moreover, our attention has been drawn to both the cingulate region and its relationships with other brain regions. The hypothesis can be reinforced by the findings of (LAU; LEUNG; ZHANG, 2020), who reported an abnormal functional connectivity between the posterior cin-

gulate cortex and the ventromedial prefrontal cortex for ASD, with hypoconnectivity. Other studies have shown ASD patients have altered intra- and inter- network connectivity among the cerebellum, visual networks, and the sensory-motor region. According to (OLDEHINKEL *et al.*, 2019), the connectivity among those regions is related to problems in sensory and visual motor integration present in ASD. Such findings have corroborated our results of a low correlation between visual cortex regions and the cerebellum (first correlation of highest importance) and a correlation between the left primary motor region and the cerebellum (third correlation of highest importance). The cerebellum is associated with both motor functions such as balance maintenance and executive control of movements, and cognitive, behavioral, and language functions (AMORE *et al.*, 2021; MARIËN; BORGATTI, 2018; JEREMY; SCHMAHMANN, 2019; WANG; KLOTH; BADURA, 2014; OVERWALLE *et al.*, 2020). Studies with fMRI have pointed to structural and functional changes in several regions of the cerebellum that are related to ASD. Lesions in the cerebellum compromise the cognitive, perceptual, and motor functioning of those systems (DELGADO-GARCÍA, 2001). (STOODLEY, 2016) claimed abnormalities in the different cerebellar regions would produce behavioral symptoms associated with the functional breakdown of specific cerebrocerebellar circuits, thus compromising the acquisition of certain skills. Moreover, such long-term changes would exert significant impacts on behavior, language, and social cognition, hence dysfunctions in behaviors associated with ASD, dyslexia, and Attention- Deficit/Hyperactivity Disorder (ADHD).

The third most important correlation found in our study was between Left-PrimMotor and the cerebellum. The motor cortex is also associated with alterations in ASD patients. (NEBEL *et al.*, 2014) reported a delayed functional specialization within the motor cortex and alterations in both size and segregation of the primary motor cortex and that the functional sub-networks of the motor control system might be altered in autism. (MOSTOFSKY; BURGESS; LARSON, 2007) observed a low motor ability in ASD related to an increased white matter volume in the primary motor and premotor regions of the left hemisphere. We found a low correlation between Left-PrimMotor and the cerebellum for ASD, which are two important regions for motor control and skill, balance, and executive control of movements. Such a low correlation may cause problems in the overall motor performance, thus interfering with socialization, commonly observed in ASD.

Regarding complex network measures, the most important measure for the model was k-core, followed by the AEBC. K-Core decomposes the graph for finding important highly and mutually interconnected areas (DAIANU *et al.*, 2013; HAGMANN *et al.*, 2008). The k-core average was used for the calculation, which provides the degree of the subgraph in which all nodes have the same degree value, and helps the identification of small contiguous core areas in a network. High k-core values (pink dots) indicate its importance for the detection of TD, whereas low ones (blue dots) suggest ASD patients (Figure 35, hence a weaker network connection among them. In contrast, EBC measures the average size of the largest community found by the edges betweenness method. For AEBC, low scores (blue dots) were important for detecting ASD

and high scores (pink dots) were important for detecting TD. Therefore, smaller communities can be detected by the presence of ASD. Higher values of efficiency were associated with TD patients and a greater integration of networks and distributions of information in them. Therefore, the distribution of information in the functional networks of ASD patients is worse than that in TD. With respect to transitivity, which is a segregation network measure of the propensity of nodes to be grouped together, higher values were associated with ASD and low values indicated TD and presence of more isolated communities clustered together.

The sliding process proved effective in differentiating TD from ASD patients, since 30 patients enabled the achievement of a 0.81 AUC and 0.81 mean Acc. A statistical comparison between data from the sliding process and complete data showed no significant differences. Despite a lower performance with the use of the full database, the technique could distinguish between ASD and TD patients with a significantly reduced amount of data, proving interesting for few data regarding ASD, as in (MCBRIDE *et al.*, 2015; YAMAGATA *et al.*, 2019) (see Table 13).

5.5 Conclusions and future work

The workflow developed with the use of fMRI data could distinguish TD from ASD patients with both Acc. and AUC above 81%. The best pairwise statistical metric that captured brain changes due to the presence of ASD was SC, and the best performing machine learning model was LG. According to the metric and the algorithm, the three most important brain connections with low values were established among Left-Sec Visual (visual cortex), Left-VentPostCing, and Left-PrimMotor with Outside defined BAS1 in ASD.

The functional connectivity of the Left-VentPostCing Posterior cingulate cortex is known to be reduced in ASD patients, which is consistent with our findings, since this region is less connected to the cerebellum (Outside BAS1 region) in patients with ASD. Regarding complex networks, the brain networks of ASD patients showed more segregation, a weaker distribution of information across the network, and less connectivity. The sliding process employed proved effective in differentiating TD from ASD patients, since a sample with 30 patients enabled the achievement of 0.81 mean AUC and mean Acc. A statistical comparison between data from the sliding process and complete data showed no significant differences. Therefore, the methodology is appropriate for cases of data of small sample size.

Future studies may involve the application of the methodology to other fMRI data, as in (BELLEC, 2016) for schizophrenia, and fMRI data from ADHD-200 Global Competition. It can also be adopted with EEG data from patients with dystonia (BALTAZAR *et al.*, 2020). Other methodologies such as the transfer learning method (WAN *et al.*, 2021) may be applied to small databases for comparison purposes.

CHAPTER

6

ANALYSIS OF FUNCTIONAL CONNECTIVITY USING MACHINE LEARNING AND DEEP LEARNING IN MULTIMODAL DATA FROM PATIENTS WITH SCHIZOPHRENIA

'Let nothing limit you, let nothing define you, let nothing hold you.
Let freedom be your own substance, since to live is to be free.
Because someone said, and I agree,
that time heals, sorrow passes, and regret does not kill.
And life always, always continues."

— Simone de Beauvoir

Submitted and under review at *Journal of Neural Engineering*

COLLABORATING AUTHORS

Thaise G. L. de O. Toutain
Federal University of Bahia (FUB)
Joel Augusto Moura Porto
Universidade de São Paulo (USP)
Aruane M. Pineda
Universidade de São Paulo (USP)
Eduardo Pondé de Sena
Federal University of Bahia (FUB)
Francisco A. Rodrigues
Universidade de São Paulo (USP)

Patricia de Carvalho Aguiar
Hospital Israelita Albert Einstein
Christiane Thielemann
Aschaffenburg University of Applied Sciences (UAS)

Abstract

Schizophrenia is a severe mental disorder associated with persistent or recurrent psychosis, hallucinations, delusions, and thought disorders that affect approximately 26 million people worldwide, according to the World Health Organization (WHO). Several studies encompass machine learning and deep learning algorithms to automate the diagnosis of this mental disorder. Others study schizophrenia brain networks to get new insights into the dynamics of information processing in patients suffering from the condition. In this paper, we offer a rigorous approach with machine learning and deep learning techniques for evaluating connectivity matrices and measures of complex networks to establish an automated diagnosis and comprehend the topology and dynamics of brain networks in schizophrenia patients. For this purpose, we employed an fMRI and EEG dataset in a multimodal fashion. In addition, we combined EEG measures, i.e., Hjorth mobility and complexity, to complex network measurements to be analyzed in our model for the first time in the literature. When comparing the schizophrenia group to the control group, we found a high positive correlation between the left superior parietal lobe and the left motor cortex and a positive correlation between the left dorsal posterior cingulate cortex and the left primary motor. In terms of complex network measures, the diameter, which corresponds to the longest shortest path length in a network, may be regarded as a biomarker because it is the most important measure in a multimodal fashion. Furthermore, the schizophrenia brain networks exhibit less segregation and lower distribution of information. As a final result, EEG measures outperformed complex networks in capturing the brain alterations associated with schizophrenia. As a result, our model achieved an AUC of 100%, an accuracy of 98% for the fMRI, an AUC of 95 %, and an accuracy of 95% for the EEG data set. These are excellent classification results. Furthermore, we investigated the impact of specific brain connections and network measures for these results, which helped us better describe changes in the diseased brain.

6.1 Introduction

Schizophrenia is a mental disorder that has plagued individuals for millennia and affects around 26 million people worldwide, according to the WHO. Archaeologists discovered ancient Egyptian inscriptions outlining common signs of this mental disorder (VEAGUE; COLLINS, 2007). However, it was not until the nineteenth century that it was classified as dementia praecox by psychiatrist Emil Kraepelin, who claimed that people with this condition suffered from constant and permanent mental degeneration beginning in childhood. In 1908, the Swiss

physician Eugen Bleuler dubbed this psychiatric condition *schizophrenia* (BLEULER; JUNG, 1908), which means split mind in Greek because one of its symptoms was a loss of mind and awareness unity (SPORNS, 2010). Other symptoms of SZ encompass: persistent or recurring psychosis, hallucinations (mainly auditory voices), delusions, and disordered thinking (HUHN *et al.*, 2019; ANDREASEN; FLAUM, 1991).

Despite centuries of research, it is still unknown what biologically causes schizophrenia (BAE *et al.*, 2018b). The authors in (FRISTON; FRITH, 1995) propose a functional and structural disconnection of brain networks, resulting in a dysfunctional integration of them, reflecting on numerous cognitive and behavioral symptoms of schizophrenia (CALHOUN; EICHELE; PEARLSON, 2009). This large-scale disconnection is reflected in the structural and functional topology of patients with the disorder; thus, network measures have been applied to them (SPORNS, 2010). In (TAN *et al.*, 2006), and (LIU *et al.*, 2008), altered small world properties on these networks are suggested using fMRI data, and in (MICHELOYANNIS *et al.*, 2006), through EEG data, a decrease in these properties is reported. In (RUBINOV *et al.*, 2009), again, using electroencephalogram data and network measurements, such as cluster coefficient and the mean of the shortest paths, it was found in the networks of patients with schizophrenia a decrease in clusters and shorter paths concerning networks of healthy patients. Although the SZ networks still present a small world topology, there is subtle randomization resulting in a disturbance in the balance of brain integration and segregation (SPORNS, 2010).

In the investigation (ZHANG *et al.*, 2021), SZ patients, compared with control patients, had lower segregation and functional connectivity in brain areas such as the bilateral fusiform gyrus, bilateral medial temporal gyrus, left supramarginal gyrus, right amygdala, and left temporal regions. In addition, (TYAGI; SINGH; GORE, 2022) brought attention to the concurrent increases and decreases in Posterior Cingulate Cortex (PCC) connectivity seen in SZ patients, but mostly reduced connectivity between PCC and brain regions linked to the Default Mode Network (DMN). The authors also discovered significant discriminative capacity using machine learning (ML) for categorizing persons with the first episode of schizophrenia compared to control participants, with an average accuracy of 72.28% in test sample data. Furthermore, (DONG *et al.*, 2018) discovered hypoconnectivity in the DMNs in patients with SZ in the thalamus region. Another investigation with SZ patients (NIERENBERG *et al.*, 2005) showed changes in the left angular gyrus brain region. The gray matter volume of this region was 14.8% smaller than the control group in the same research, indicating that this region may represent a neuroanatomical basis for the “expression of schizophrenia". The reversal asymmetry in the inferior parietal lobe, angular gyrus, discovered by (NIZNIKIEWICZ *et al.*, 2000), indicated a significance for this area in cognitive deficiencies, language issues, and thinking disorders in SZ. The authors of (SCHÜRMANN *et al.*, 2007) also emphasize the impairment of motor cognition in SZ patients.

These aforementioned studies show that the structure of the brains of individuals with SZ differs from those of normal controls. Hence, it is possible to diagnose SZ based on data collected

Table 18 – The table comprises machine learning research that used the same database as the current study (COBRE data described in more detail in subsection 6.2.1).

Authors	Data	Data Type	Correlation metrics	ML methods	ROIs	AUC	Acc.	Recall	Precision
(QURESHI *et al.*, 2017)	COBRE data	fMRI	specific method	SVM	102	-	0.99	-	-
(PATEL; AGGARWAL; GUPTA, 2016)	COBRE data	fMRI	Pearson correlation	Deep Learning combined with SVM	116	-	0.92	-	-
(ANDERSON; COHEN, 2013)	COBRE data	fMRI	correlation-based distance metric	SVM	90	-	0.65	-	-
(SAVIO; GRAÑA, 2015)	COBRE data	fMRI	Pearson correlation	SVM	27	-	0.80	-	-
(ZENG *et al.*, 2018)	COBRE data	fMRI	Pearson correlation	SVM	160	-	0.69	0.92	-

by the EEG or experiments. Furthermore, EEG is a low-cost, widely available technology with high temporal resolution. Therefore, EEG data have been used to study brain organization (FALLANI *et al.*, 2011b; ALVES *et al.*, 2022a). fMRI, in contrast, has a poor temporal resolution but a high spatial resolution, which makes it ideal for studying spatial brain dynamics (MENON; CROTTAZ-HERBETTE, 2005; FORMISANO *et al.*, 2003). fMRI scans produce a set of three-dimensional images recorded over time and measure a signal. The temporal evolution of the BOLD series is called the hemodynamic response function and is determined by the pixel intensity in fMRI images (STURZBECHER, 2006; BISWAL *et al.*, 1995). Each cube of an fMRI image, called voxel, which anatomically maps a position in the brain, has a BOLD time series (LOPES *et al.*, 2016).

Previous studies have evaluated the effectiveness of ML in diagnosing SZ with supervised machine learning algorithms that distinguish between two classes, namely SZ and control group (see Table 18). In contrast to traditional statistical methods, the ML approach does not rely on prior assumptions (such as adequate distribution, independence of observations, absence of multicollinearity, and interaction problems). It is well suited to automatically analyze and capture complex nonlinear relationships in data. In addition, new methodologies, such as SHAP values, have evolved to aid in interpreting machine learning outcomes. Any machine learning algorithm may use this statistic to detect and prioritize features (BOWEN; UNGAR, 2020; RODRÍGUEZ-PÉREZ; BAJORATH, 2019; SPADON *et al.*, 2019).

This study aims to determine whether it is feasible to automatically detect brain changes caused by SZ while providing a biological explanation. For that, we consider the BOLD series to develop the classification method for SZ patients, and we also test in EEG data. After the preprocessing of these two data (A), we consider as an input for the machine learning the following data abstraction levels: (B) the correlation between the EEG electrodes and fMRI regions of interest and (C) complex network measures extracted from (B). In contrast to articles in the literature that use only one of these levels of abstraction, this study uses all two levels in both data sets in a multimodal fashion for the first time in literature. In addition, we define

which of these abstraction levels is the most appropriate for capturing SZ brain changes. The SHAP value technique has also been found to be more successful than the previous research (AL-BELTAGI, 2021; ALVES *et al.*, 2022b; ALVES *et al.*, 2022a) in finding the best brain areas, connections between brain regions, and measurements of complex networks that may be utilized to evaluate the effects of the SZ on the brain. As a final result of this research, for the first time in literature, we combine EEG measures extracted from time series and complex network measures as input for the ML method to evaluate which measure is more critical to distinguish SZ from control patients.

6.2 Materials and methods

In the current study, two schizophrenia datasets were used to test our general workflow: one fMRI, described in the subsection 6.2.1, and another EEG, described in the subsection 6.2.2, with different pre-processing for each data. First, the best pairwise metrics for capturing schizophrenia-induced changes in the brain are defined based on the fMRI data workflow. This metric is then validated using EEG data.

Figure 38 depicts the fMRI complete methodology workflow used and organized into three parts according to their aim, i.e., preprocessing and using the best selecting pairwise metrics (described in Figure 38-(A) and in subsection 6.2.1.1), the best brain connection (described in Figure 38-(B) and in subsection 6.2.1.2), and the best complex network measures for differentiating schizophrenia from control group (described in Figure 38-(C) and in subsection 6.2.1.3.)

Further, Figure 39 fully represents the EEG entire method workflow used and organized into three parts accordingly to their aim. First, following preprocessing, the most distinguishing metrics discovered for the fMRI data were used to create a connection matrix (described in Figure 39-(A) and subsection 6.2.2.1), the best brain connection (described in Figure 39-(B) and in subsection 6.2.2.2), and the best complex network measures for differentiating schizophrenia from the control group (described in Figure 39-(C) and subsection 6.2.2.3.)

The python code with the methodology used in this work is available at: <https://github.com/Carol180619/Paper-multimodal-schizophrenia.git>.

6.2.1 fMRI data

6.2.1.1 fMRI data preprocessing and selecting best pairwise metrics

The fMRI data utilized in this study were from The Centers of Biomedical Research Excellence (COBRE) and included raw anatomical and fMRI data from 72 schizophrenia patients and 74 healthy controls (ages 18 to 65 in each group) with 6 minutes resting-state BOLD time series. As exclusion criteria, all the screened patients were excluded if they had a history of

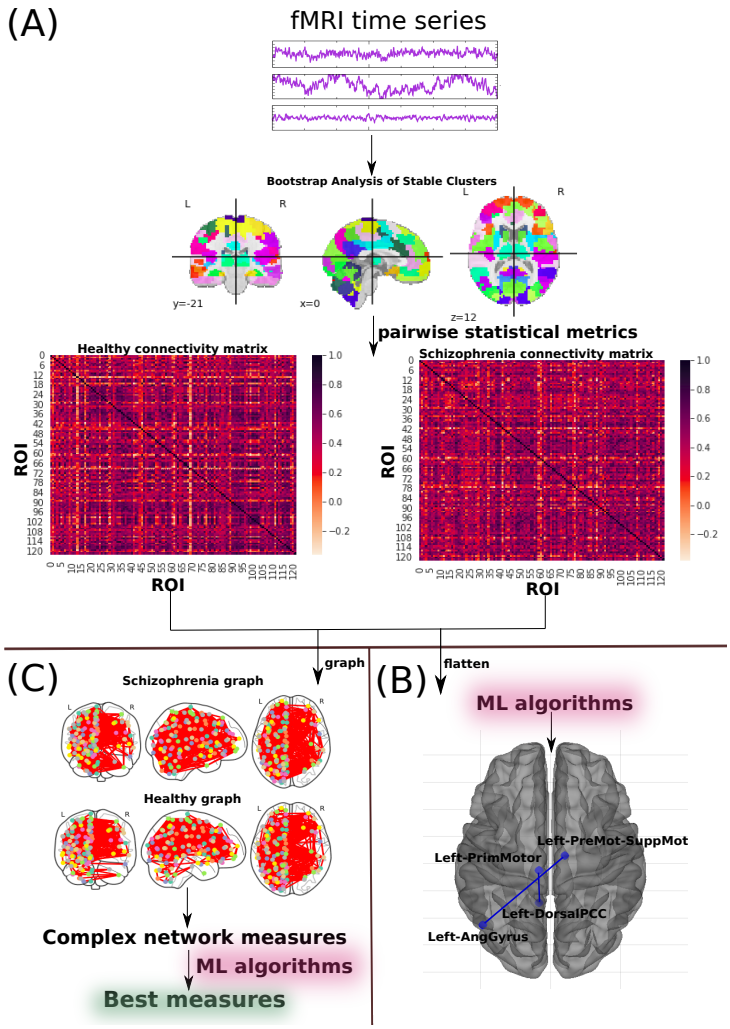

Figure 38 – The methodology for diagnosing schizophrenia using fMRI schizophrenia data is also in subsection 6.2.1. (A) **fMRI preprocessing and selecting best pairwise metrics** methodology described in subsection 6.2.1.1; (B) **Connectivity matrix** methodology reported in subsection 6.2.1.2; (C) **Complex network measure** methodology described in subsection 6.2.1.3.

mental retardation, a neurological condition, severe head trauma with more than 5 minutes of loss of consciousness, or a history of drug dependency or misuse within the previous 12 months. More details can be seen in (CALHOUN *et al.*, 2012). This data was accessed using the Nilearn Python library, in which the images were already preprocessed using the NIAK resting-state pipeline (BELLEC, 2016).

ROIs are considered rather than the whole BOLD time series collected from each voxel of the brain imaging. Because a brain atlas comprising these ROIs is employed, only the BOLD time series voxels of these ROIs were utilized. BASC was chosen from among the several preconfigured atlases since it was the map with the most outstanding performance according to (SUBAH *et al.*, 2021; ALVES *et al.*, 2022). It was proposed in (BELLEC *et al.*, 2010) and obtained via group brain parcellation using the BASC technique, a k-means clustering-based

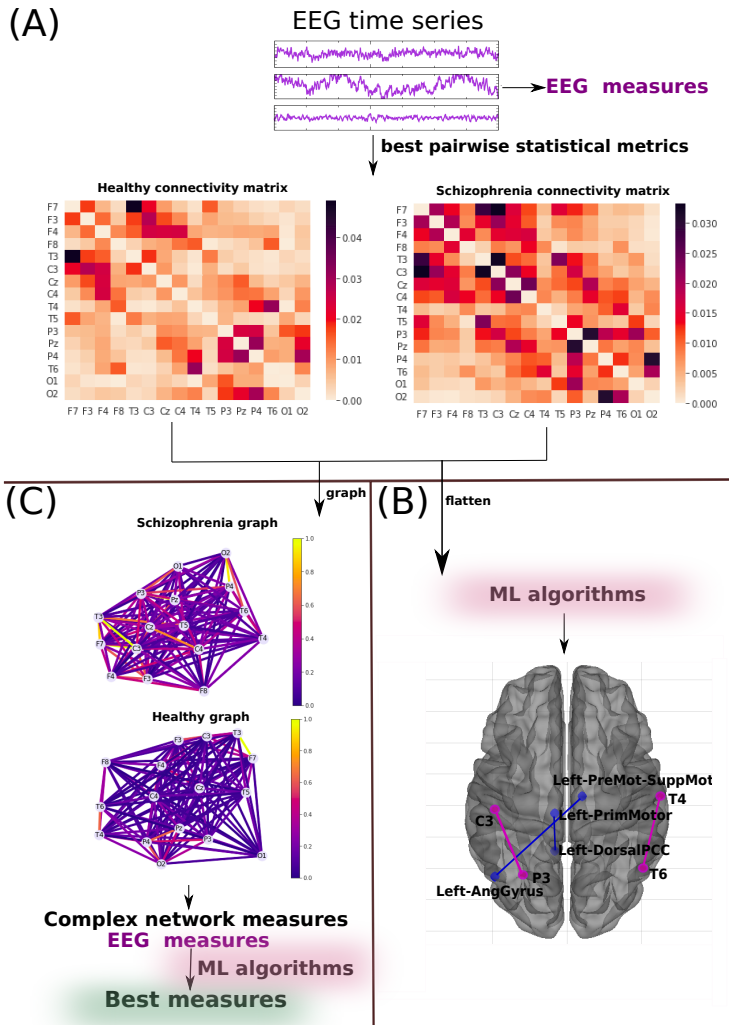

Figure 39 – The methodology used here for the diagnosis of schizophrenia using EEG schizophrenia data in subsection 6.2.2. (A) **EEG preprocessing and selecting best pairwise metrics** methodology described in subsection 6.2.2.1; (B) **Connectivity matrix** methodology reported in subsection 6.2.2.2; (C) **Complex network measure** methodology described in subsection 6.2.2.3.

approach that finds brain networks with coherent activity in resting-state fMRI (YANG; ZHANG; SCHRADER, 2022). BASC map with a cluster number of 122 ROIs is used here (see Figure 38-(A)). Further, manual use of Yale BioImage Suite Package web application[1] labeled the coordinates of each ROIs for the identification of their names.

Once the time series for each of the 122 regions had been extracted, they were correlated according to PC (BENESTY *et al.*, 2009), SC (LUBINSKI, 2004), GC (GRANGER, 1969), BM (WILCOX, 2011), SCC (HARDOON; SHAWE-TAYLOR, 2011), GL (SOJOUDI, 2016), LW (LEDOIT; WOLF, 2012), MI (KRASKOV; STÖGBAUER; GRASSBERGER, 2004), and TE (SCHREIBER, 2000) [2].

[1] Avaiable in <https://bioimagesuiteweb.github.io/webapp/mni2tal.html>

[2] For the TE, MI and GL metrics a Min-max normalization and then a thresholding process was

Each matrix was reduced to the size of the vectors used as input to the ML algorithm. The support vector machine (SVM) algorithm (BOTTOU; LIN, 2007) was used as a classifier to select the most effective method to choose the best methods to construct the correlation and connectivity matrices. We use this method because it has been considered in studies of schizophrenia (see section 6.1) and has a low computational cost, it also checked whether the use of metrics was better than the direct use of time series – the one of better performance would be chosen.

6.2.1.2 Most important brain connection

After the best brain connectivity metric had been determined, the following ML classifiers were used: RF, NB, MLP, tuned CNN (called here CNN_{tuned} and $CNN_{untuned}$) implemented in (ALVES,), and Long Short-Term Memory neural networks (LSTM) (HOCHREITER; SCHMIDHUBER, 1997). In addition to the CNN deep learning used in prior work (ALVES *et al.*, 2022b), the LSTM network is a form of recurrent neural network commonly used to identify patterns in time series. Subsequently, the SHAP value method was used for the biological interpretation, as it explains the predictive power of each attribute. The same sampling data set was used in all ML algorithms and split into training (train) and test sets, with 25% data comprising the test set. was employed, with k = 10 which is a common value for this method (BERRAR, 2019; BENGIO; GRANDVALET, 2004; SHAH; KHAN, 2020; KAWAMOTO; KABASHIMA, 2017; CHAN *et al.*, 2019; KAWAMOTO; KABASHIMA, 2017)). This procedure is applied for model selection and hyper-parameter optimization. It was also considered the grid search method used for all ML algorithms except the untuned CNN and LSMT model, as done in (SATO *et al.*, 2019; ZHONG *et al.*, 2021; ARCADU *et al.*, 2020; KRITTANAWONG *et al.*, 2021; RASHIDI *et al.*, 2020). The hyper-parameter optimization values for each classifier model are provided in Appendix A.3. The standard performance metric accuracy (MINCHOLÉ; RODRIGUEZ, 2019; TOLKACH *et al.*, 2020; DUKART *et al.*, 2021; LI; ASCH; SHAH, 2020; PARK; KELLIS, 2015) was employed for evaluation. Due to the two-class (negative and positive) classification problem, other common metrics such as precision and recall were considered (ITO *et al.*, 2021; KIM *et al.*, 2020; LI *et al.*, 2021; YU *et al.*, 2020). Precision (also called positive predictive value) corresponds to the hit rate in the negative class (here corresponding to the control group), whereas recall (also called sensitivity) measures how well a classifier can predict positive examples (hit rate in the positive class), here related to SZ patients. Regarding the visualization of the two latter measures, the ROC curve is a common method that displays the relation between the rate of true and false positives. The area below the curve, called AUC, has been widely used in classification problems (MINCHOLÉ; RODRIGUEZ, 2019; BRACHER-SMITH; CRAWFORD; ESCOTT-PRICE, 2021; PATEL *et al.*, 2021; KRITTANAWONG *et al.*, 2021). The AUC value ranges from 0 to 1- 1 corresponds to a classification result free of errors, and 0.5 indicates the classifier cannot distinguish the classes, as in a random choice. The micro average of the ROC

performed, with a value of 0.5, since these measures deal best with binary values.

curve, which computes the AUC metric independently for each class (it calculates AUC for healthy individuals, class zero, and separately calculates it for unhealthy ones, class one), was also considered. The average is computed considering the classes equally. The macro average was also employed in our evaluation - it does not consider the classes equally but aggregates their contributions separately and then calculates the average.

6.2.1.3 Best complex network measures

A complex network (or a graph) was generated for each connectivity matrix for the extraction of different measures. Towards inputting data into the ML algorithm, the complex network measures were stored in a matrix of attributes, where each column represents a complex network measure (feature), and each row denotes a subject. 2D matrices were generated for all subjects, as in (ALVES *et al.*, 2022a).

To describe the brain structure, the following complex network measures were calculated: assortativity coefficient (NEWMAN, 2003; NEWMAN, 2002), APL (ALBERT; BARABÁSI, 2002), BC (FREEMAN, 1977), CC (FREEMAN, 1978),EC (BONACICH, 1987), diameter (ALBERT; JEONG; BARABÁSI, 1999), hub score (KLEINBERG, 1999), Knn (EPPSTEIN; PATERSON; YAO, 1997), mean degree (DOYLE; GRAVER, 1977), SMD (SNIJDERS, 1981), ED (DEHMER; MOWSHOWITZ, 2011), transitivity (WATTS; STROGATZ, 1998; NEWMAN; WATTS; STROGATZ, 2002), complexity, k-core (SEIDMAN, 1983; NEWMAN, 2010), eccentricity (HAGE; HARARY, 1995), density (ANDERSON; BUTTS; CARLEY, 1999), and efficiency (LATORA; MARCHIORI, 2003).

Newly developed metrics (described in detail in (ALVES *et al.*, 2022a)) reflecting the number of communities in a complex network were also applied. Community detection algorithms were also used in our study (NEWMAN, 2012; KIM; LEE, 2015; ZHAO; LIANG; WANG, 2021). Since the community detection measures must be transformed into a single scalar value to be included in the matrix, community detection algorithms were applied for finding the largest community. The average path length within the community was then calculated and received a single value as the result. The community detection algorithms used were the FC (CLAUSET; NEWMAN; MOORE, 2004), IC (ROSVALL; AXELSSON; BERGSTROM, 2009), LC (NEWMAN, 2006), LPC (RAGHAVAN; ALBERT; KUMARA, 2007), EBC (GIRVAN; NEWMAN, 2002), SPC (REICHARDT; BORNHOLDT, 2006), and MC (BLONDEL *et al.*, 2008). The abbreviations were extended with letter "A" (for average path length) towards indicating the approach (AFC, AIC, ALC, ALPC, AEBC, ASPC, and AMC).

These network measures were used to characterize the brain's network structure. Thus, each observation representing the network properties of one patent is represented by a vector containing these metrics. The results are provided in subsection 6.3.1.2.

6.2.2 EEG data

6.2.2.1 Preprocessing and selecting best pairwise metrics

The EEG dataset used for diagnosis of SZ, also used in (ALVES *et al.*, 2022b), contains a 16-channel EEG time series recorded at a sampling frequency of 128 Hz over one minute, including F_3, F_4, F_7, F_8, T_3, C_3, C_z, C_4, T_4, T_5, P_3, P_z, P_4, T_6, O_1, and O_2. The study included 39 healthy young people (control group; aged 11 to 14 years) and 45 teenagers (aged 11 to 14 years) with schizophrenia symptoms in a resting state.

From these time series are extracted EEG measurements which are widely used in the literature, as there are spectral entropy (TIAN *et al.*, 2017; VANLUCHENE *et al.*, 2004), Hjorth mobility and complexity (ELBERT *et al.*, 1992; HJORTH, 1975; HJORTH, 1986) and Lempel-Ziv complexity (BAI; LIANG; LI, 2015; LEMPEL; ZIV, 1976).

Further, connectivity matrices were generated with the most successful method evaluated for fMRI data; see section 6.2.1.

6.2.2.2 Most important brain connection

Based on these connectivity matrices, the best ML method is used. With the SHAP value method, most distinguishing brain regions are found.

6.2.2.3 Complex network measures

The same measures of complex networks used in the previous subsection were extracted. Moreover, for the first time in the literature, EEG measures extracted from time series and complex network measures have been put into the ML algorithm to obtain which metric best differentiates EEG data from schizophrenia patients.

6.3 Results

In general, ML algorithms were applied for two different levels of data abstraction, namely (B) the connectivity matrix and (C) the matrix of attributes, whose elements are complex network measures calculated from (B). This approach was used for EEG and fMRI data. However, for EEG, not only the complex network but also EEG measures extracted from time series.

We verified that all approaches automatically detected changes in the brain of SZ patients. The fMRI connectivity matrix obtained the highest classification performance with a 99% mean AUC (see Table 19 and subsections 6.3.1 and 6.3.2.

Table 19 – Summary of all the results obtained in the present work. Classification results using the connectivity matrix best-captured brain changes due to SZ. The best performance is highlighted in bold.

Data abstraction	Data ML	Subset	AUC	Acc.	Recall	Precision
Connectivity matrix	**fMRI CNN**	**Train**	**1.00**	**1.00**	**1.00**	**1.00**
		Test	**0.99**	**0.99**	**1.00**	**0.97**
Connectivity matrix	**fMRI RF**	**Train**	**1.00**	**1.00**	**1.00**	**1.00**
		Test	**0.97**	**0.97**	**0.97**	**0.97**
Complex network	**fMRI RF**	**Train**	1.00	1.00	1.00	1.00
		Test	0.89	0.89	0.89	0.90
Connectivity matrix	**EEG RF**	**Train**	1.00	1.00	1.00	1.00
		Test	0.95	0.95	0.95	0.95
Complex network	**EEG RF**	**Train**	1.00	1.00	1.00	1.00
		Test	0.81	0.81	0.81	0.81

6.3.1 fMRI results

6.3.1.1 Selecting best pairwise metrics

Appendix A.11 contains the results for each connectivity matrix with different types of pairwise statistical metrics. SVM was used to detect the best one for capturing the brain changes due to SZ in fMRI data. TE achieved the best performance. It is worth mentioning that the connectivity matrices outperformed the raw BOLD time series.

Then, the best connectivity matrix was tested with the other ML algorithms to determine the one that best-differentiated SZ patients from control ones. According to Table 20, the best classifiers are the CNN_{tuned} and RF. CNN performance for the test set was equal to 1.00 for the mean AUC and 0.98 for precision, recall, and accuracy. RF performance for the test set was equal to 0.97 for the mean AUC, precision, F1, recall, and accuracy. Figure 41 displays the confusion matrix (41-(a)), the learning curve (Figure 41-(b)), and the ROC curve (41-(c)), respectively, using TE and CNN_{tuned}. The learning curve contains the loss error in each epoch. The loss error is computed on training and validation, and its interpretation is how well the model performs for these two sets. It is the total error committed for each example in these train, and test samples (RASCHKA; MIRJALILI, 2019).

In contrast, Figure 40 displays the confusion matrix (40-(a)), the learning curve (Figure 40-(b)), and the ROC curve (40-(c)), respectively, using TE and RF. The results suggest that the complete database is not required to obtain the best validation accuracy (see learning curve in Figure 40- (b)). Regarding the classification model, TP (related to class 1) was higher than TN,

Table 20 – Results from different ML algorithms. The best ML was CNN_{tuned} and RF for the fMRI dataset, whose performances are highlighted.

ML methods	Subset	AUC	Acc.	Recall	Precision
RF	**Train**	**1.00**	**1.00**	**1.00**	**1.00**
	Test	**0.97**	**0.97**	**0.97**	**0.97**
CNN tunned	**Train**	**1.00**	**1.00**	**1.00**	**1.00**
	Test	**1.00**	**0.98**	**0.98**	**0.98**
CNN untuned	**Train**	1.00	1.00	1.00	1.00
	Test	1.00	0.98	1.00	0.97
LSTM	**Train**	1.00	0.99	0.99	0.99
	Test	0.99	0.97	0.97	0.97
SVM	**Train**	0.99	0.99	1.00	0.99
	Test	0.92	0.92	0.92	0.92
NB	**Train**	1.00	1.00	1.00	1.00
	Test	0.87	0.86	0.88	0.89
MLP	**Train**	0.89	0.85	1.00	0.90
	Test	0.80	0.80	0.80	0.80

showing that it better detects SZ patients (see confusion matrix in Figure 40- (a)). The learning curve for ML assesses the model's predictability by altering the size of the training set (SPADON *et al.*, 2019). Since RF has a lower computational cost, it was chosen for the following steps.

SHAP values were calculated to quantify the importance of brain connections for the RF (see Figure 42 for the results). The connection between the Left-Dorsal Posterior Cingulate Cortex and Left-Primary motor cortex (Left-DorsalPCC – Left PrimMotor1) was the most important, according to Figure 42. Low correlation values (blue dots) for this connection (Left-DorsalPCC – Left PrimMotor1) were essential for the detection of the control group, and high values of this correlation (red dots) were important for the detection of SZ. The second most crucial connection was detected between the Left- Premotor Cortex and Left-angular gyrus (Left-premotor suppmor5 – Left-AngGyrus1). Low correlation values for this connection (blue dots) were associated with SZ patients, and high correlation values (red dots) were essential for detecting control ones. The corresponding brain regions are depicted in Figure 42.

Since RF was the algorithm that provided the best performance, it was used in the following subsections.

6.3.1.2 Complex network

The performance of the test sample considering the complex network yielded a mean AUC of 0.89, 0.90 for precision, 0.89 for F1 score, 0.89 for recall, and 0.89 for accuracy. Confusion matrix Figure 43-(a), learning curve Figure 43-(b), and ROC curve Figure 43-(c). Furthermore, according to Figure 43, the whole dataset was necessary. The results suggested that almost the complete database is required to obtain the best validation accuracy (see learning

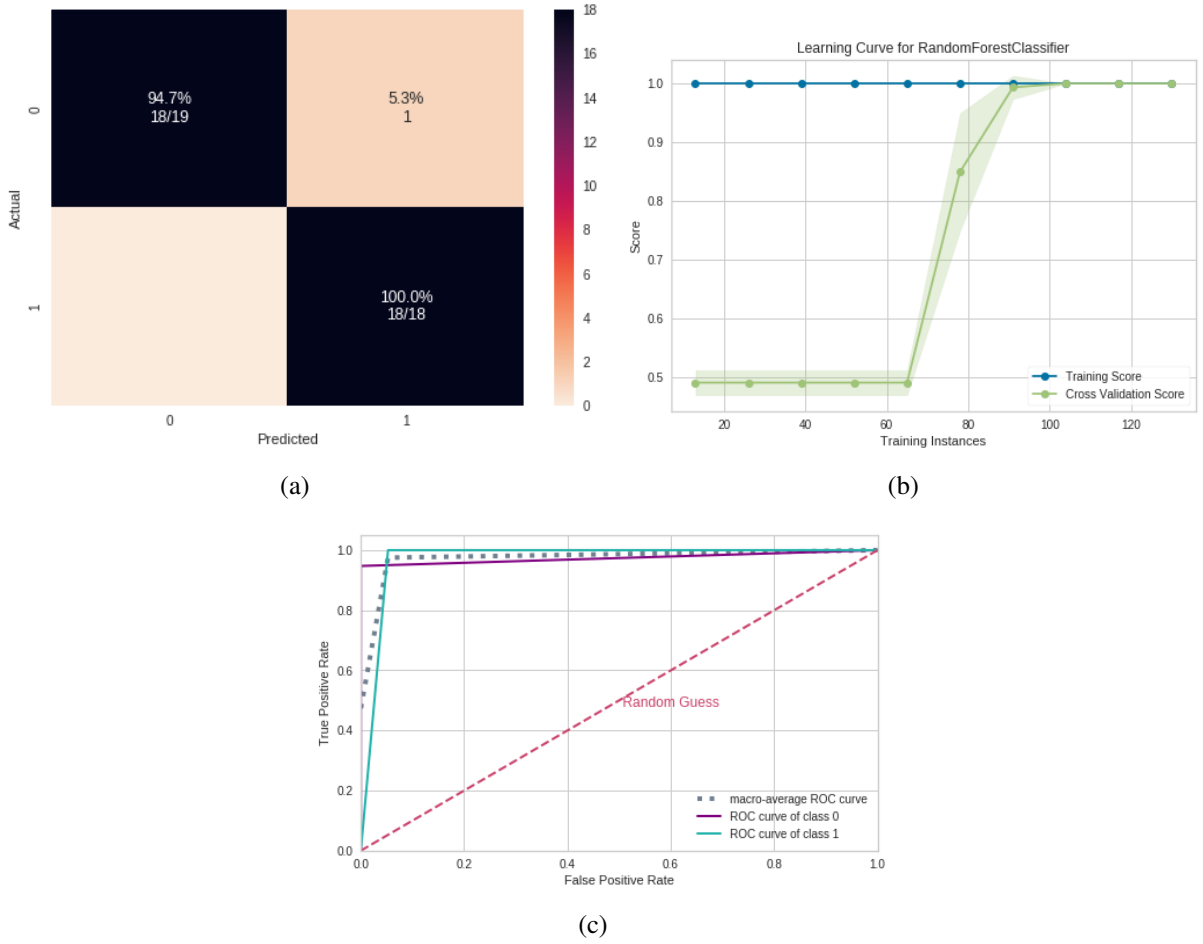

(a) (b)

(c)

Figure 40 – RF results using fMRI connectivity matrices. (a) Confusion matrix indicating a TN rate of 100% (purple, according to the color bar) and a TP rate of 95.2% (blue, according to the color bar). (b) Learning curve for the training Acc. (blue) and test Acc. (green). (c) ROC curve with class 0 (control) and class 1 (with SZ).

curve in Figure 43- (b)).

According to the SHAP values in Figure 44, the most crucial measure for the model was the Diameter, followed by the CC. Furthermore, except for CC, it is difficult to determine whether low or high values of these other measures are related to the presence or absence of schizophrenia from the Figure 44. However, in contrast to the other measures, it is evident that low CC values are associated with the presence of schizophrenia.

6.3.2 EEG dataset

6.3.2.1 Connectivity matrix

As previously stated, the identical approach used in the preceding section was evaluated on the EEG data. Furthermore, the TE measure was utilized to build the connectivity matrices of the EEG data, and RF was used to differentiate SZ patients from the control group. Its performance for the test set was equal to 0.95 for the mean AUC, precision, F1, recall, and

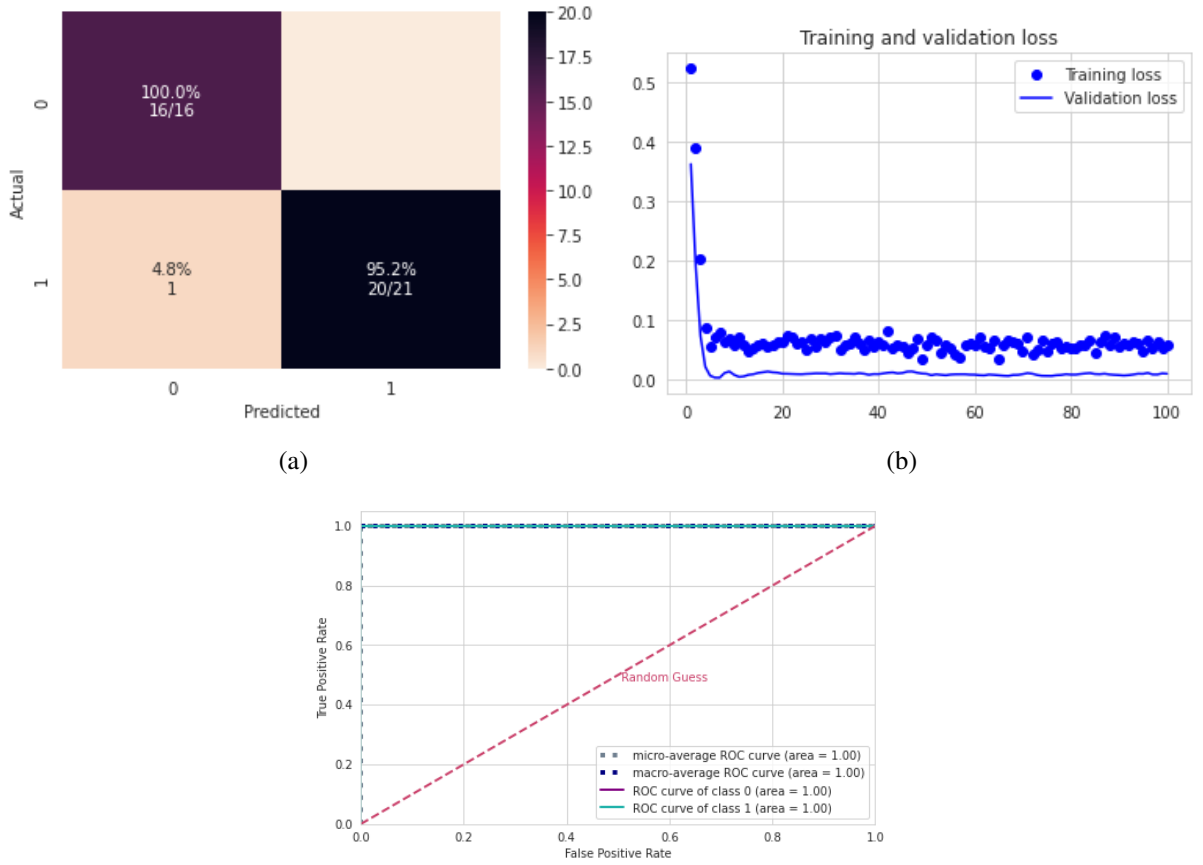

(a) (b)

(c)

Figure 41 – CNN_{tuned} results using fMRI connectivity matrices. (a) Confusion matrix indicating a TN rate of 100% (blue, according to the color bar) and a TP rate of 94.7% (blue, according to the color bar). (b) The learning curve with the Loss for the training (blue dots) and validation (line). (c) ROC curve with class 0 (control) and class 1 (with SZ).

accuracy. Figure 45 displays the confusion matrix (45-(a)), the learning curve (Figure 45-(b)), and the ROC curve (45-(c)), respectively. The results suggest that the complete database is required to obtain the best validation accuracy (see learning curve in Figure 45- (b)).

SHAP values were calculated to quantify the importance of brain connections for the RF (see Figure 46 for the results). The connection between regions P3 and C3 (P3 – C3) was the most important for the RF model. According to the data in Figure 46, high correlation values (red dots) for the connection (P3 – C3) were essential for the detection of SZ patients, and low values of correlation (blue dots) were necessary for the detection of control ones. The second most crucial connection was detected between T6 and T4 (T6 – T3), and this connection's low values were associated with SZ. The corresponding brain regions are depicted in Figure 46

6.3.2.2 Complex network

The performance of the test sample considering the complex network yielded a mean AUC equal to 0.82, 0.85 for precision, 0.81 for F1 score, 0.75 for recall, and 0.81 for accuracy.

Figure 42 – Feature importance ranking for the RF classifier with brain regions ranked in descending order of importance. For example, the connection between the regions Left-DorsalPCC and Left-PrimMotor1 is the most important to classify SZ patients.

Confusion matrix, learning curve, and ROC curve are shown in Figure 47. The results suggest that the complete database is required to obtain the best validation accuracy (see learning curve in Figure 47- (b)). Regarding the classification model, TP (related to class 1) was slightly higher than TN, showing that it better detects SZ patients (see confusion matrix in Figure 47- (a)).

According to the SHAP values in Figure 48, the most relevant measure was spectral entropy, which had a positive correlation with SZ, followed by Hjorth mobility and complexity, which have a negative correlation with the occurrence of SZ. Further, the measures extracted from the EEG time series were more important than the complex network measures. However, the diameter was the most relevant complex network measure, comparable to that found for the fMRI data. Furthermore, the existence of SZ was connected with greater ASPC values, which estimated the size of the communities. As a result, SZ is connected with larger communities.

6.4 Discussion

6.4.1 Connectivity matrix

One aim of this work was to compare the classificatory statements that can be made based on two different SZ datasets, namely fMRI and EEG. The ML workflow used was essentially the same. A comparison of the main results regarding altered connectivity in the neural network

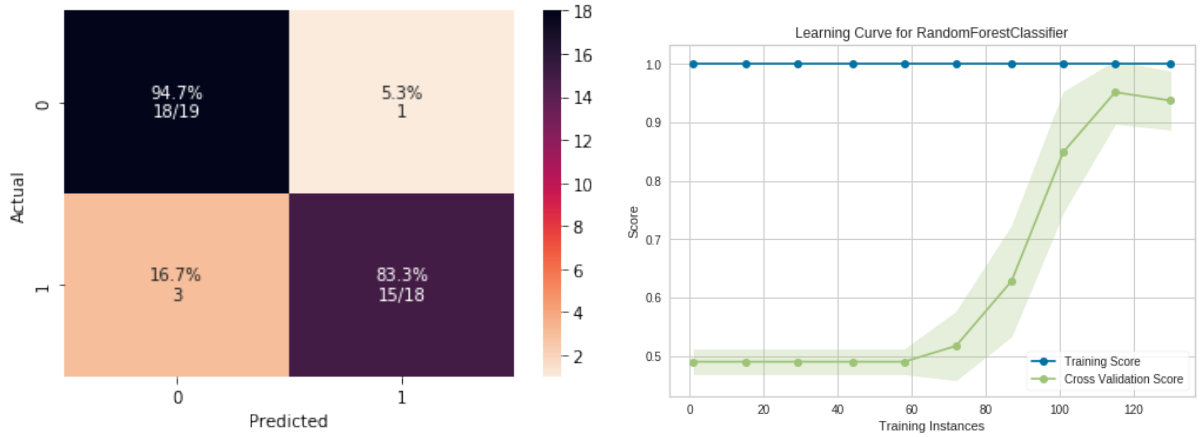

(a)

(b)

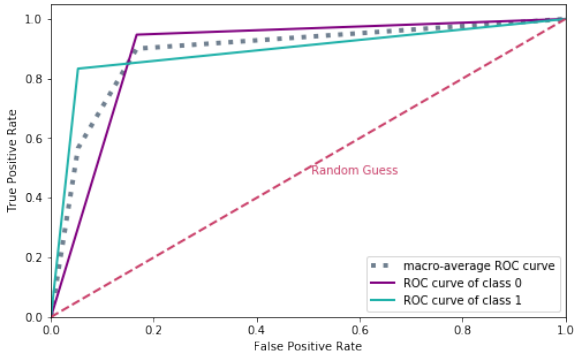

(c)

Figure 43 – ML results using complex networks and fMRI. (a) Confusion matrix indicating a TN rate of (blue, according to the color bar) and a TP rate of (blue, according to the color bar). (b) Learning curve for the training Acc. (blue) and test Acc. (green). (c) ROC curve with class 0 (control) and class 1 (with SZ).

structure of the SZ patients can be found in Figure 49.

Our method identified a positive correlation in the SZ group between the left dorsal PCC and the left primary motor during rest. The posterior cingulate cortex is in the upper region of the limbic system and is associated with Brodmann Areas (BA)) 23 and 31. Researchers (LEECH; BRAGA; SHARP, 2012) suggested that this brain region behaves as a central hub for information exchange and has high connectivity with frontoparietal regions, which is related to the cognitive control of directing attention inside and outside. Furthermore, they observed that the ventral PCC is highly involved in DMN when there is the activation of cognitive activity directed towards the inside focus and when there is recovery and memory planning. On the other hand, dorsal PCC is related to highly complex connectivity directed to the frontal lobe, correlated to the balance of internal/external and broad/ narrow attention (LEECH; BRAGA; SHARP, 2012; LEECH; SHARP, 2014).

In contrast, the Primary Motor Cortex (PMC), BA04, was a brain region positively correlated with PCC in our study, usually activated when the finger is in movement (WINDIS-

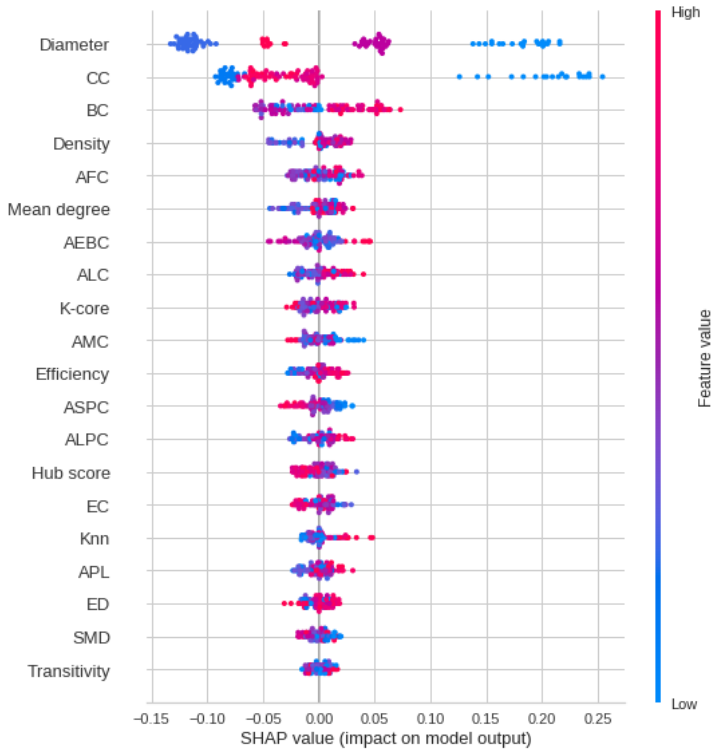

Figure 44 – RF classifier features importance ranking in an fMRI dataset, with factors mentioned in descending order. For the categorization of SZ patients, the spectral entropy measure is the most essential, followed by the Hjorth mobility and complexity measure.

CHBERGER *et al.*, 2003) or when healthy subjects press a button in a given task. However, (YANG; SHU, 2012) suggested that the premotor and primary premotor cortex may be involved in language processing, especially the left premotor cortex, which performs articulation planning (DUFFAU *et al.*, 2003). Considering previously cited studies mentioned here and in the 6.1, the high positive correlation found between PCC and left PMC in our study suggests that activation of DMN-related areas, usually present during rest and reflecting voluntary targeting for inside observation, are also associated with language processing and may reflect problems in production, articulation, and speech expression, such as alterations in thought process manifested in speech, seen by (MOTA *et al.*, 2012) in SZ patients.

The second highest correlation found in our study occurred between the left premotor supplementary (BA6) and angular gyrus (BA39) areas; this time, these areas are negatively correlated. The Supplementary Motor Area (SMA) has been associated with movement control and preparation (WELNIARZ *et al.*, 2019), and patients with left medial SMA lesions showed severe difficulties remembering and reproducing rhythms compared to control subjects. Furthermore, it has been observed that bilateral SMA regions are altered in SZ patients with catatonia, and this hyperperfusion is a marker of current catatonia in schizophrenia, indicating a dysregulation in the motor system, particularly affecting the premotor areas (WALTHER *et al.*, 2017).

The angular gyrus brain region, located in the posterior inferior parietal area, is activated during different tasks, and as shown by (SEGHIER, 2013) as being a hub that receives information

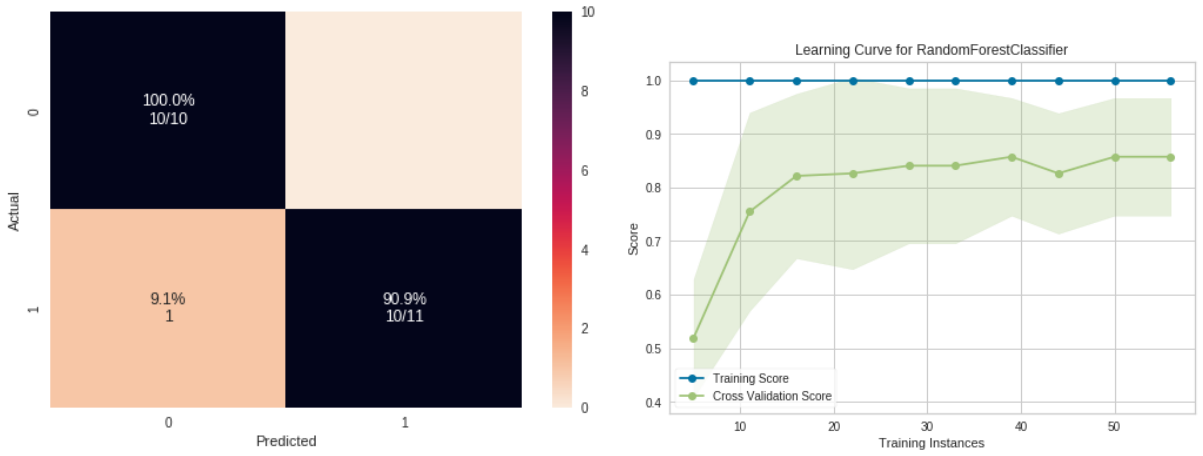

(a) (b)

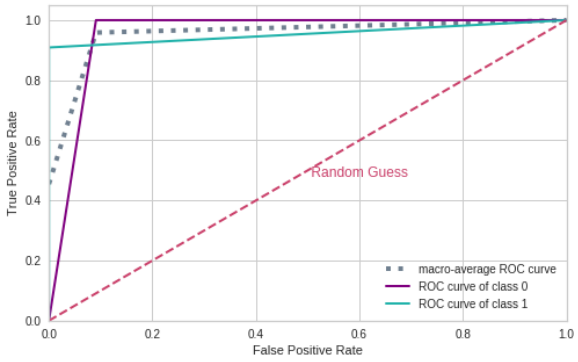

(c)

Figure 45 – ML results using EEG connectivity matrices. (a) Confusion matrix indicating a TN rate of (blue, according to the color bar) and a TP rate of (blue, according to the color bar). (b) Learning curve for the training Acc. (blue) and test Acc. (green). (c) ROC curve with class 0 (control) and class 1 (with SZ).

and integrates it, generating comprehension and reasoning, redirecting attention to relevant information, manipulating mental processes, and problem-solving. Considering the angular gyrus findings described in the 6.1 and through the findings obtained for the negative correlation in our study, in the SZ group compared to the control, between the left premotor supplementary regions and the angular gyrus, we can suggest that this correlation may reflect an altered motor system, with problems related to motor learning with altered coordination; express the cognitive deficits, language and thinking problems, both associated with SZ.

We also observed a high positive correlation between P3 and C3 regions for the SZ group compared to the control group. The P3 region corresponds to the Left Superior Parietal Lobe (LSP), BA07, while the C3 region corresponds to the left motor cortex, BA06 (SCRIVENER; READER, 2022). LSP is activated during the performance of body part localization task (FELICIAN *et al.*, 2004); both right and left parietal regions showed deficits in tests related to working memory information involving mental information (KOENIGS *et al.*, 2009). The motor cortex is usually associated with motor actions. However, (BHATTACHARJEE *et al.*, 2021) highlighted

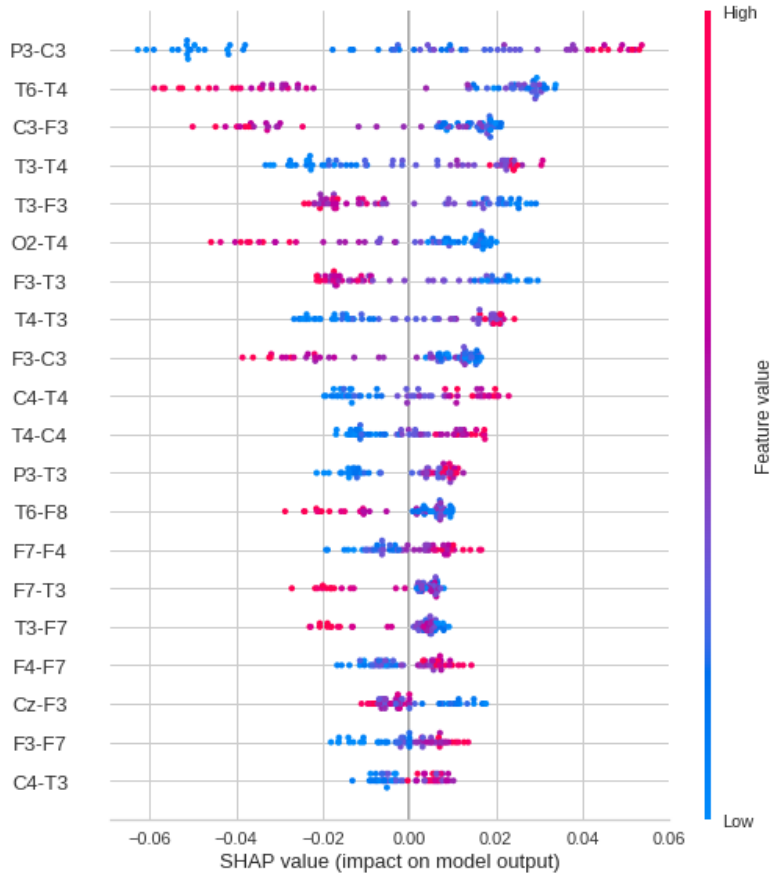

Figure 46 – Feature importance ranking for the RF classifier with brain regions in descending order. The connection between the P3 and C3 is the most important for classifying SZ patients.

its involvement in cognitive processes such as task-directed attention, motor consolidation, integration of multiple sensory inputs, and inhibition of involuntary movements. Therefore, the studies cited in 6.1 and the correlation observed between P3 and C3 regions in our study during resting state may reflect the dysfunctions found in SZ that unfold working memory problems and deficits in motor cognition.

Our study's negative correlation in the right temporal lobe between T6 and T4 electrodes for SZ patients comprises BA 21 and 38. For example, the temporal lobe is associated with speech perception and production, hearing, and episodic memory (PATEL; BISO; FOWLER, 2021). During hallucinatory crises in SZ patients, (SRITHARAN *et al.*, 2005) found increased coherence in the temporal cortices bilaterally, suggesting abnormally increased synchrony in the left and right auditory cortices compared to the time without hallucination. In contrast with this study, we only found a correlation between two electrodes in the right temporal cortex in SZ patients, indicating an inverse activity variation in this region. Furthermore, the hallucinating patients showed reduced alpha coherence in FT7, and FT8 electrodes, compared to the HC and the group of patients without hallucination (HENSHALL *et al.*, 2013). This finding points to the importance of the activity of the temporal region bilaterally with other areas of SZ patients.

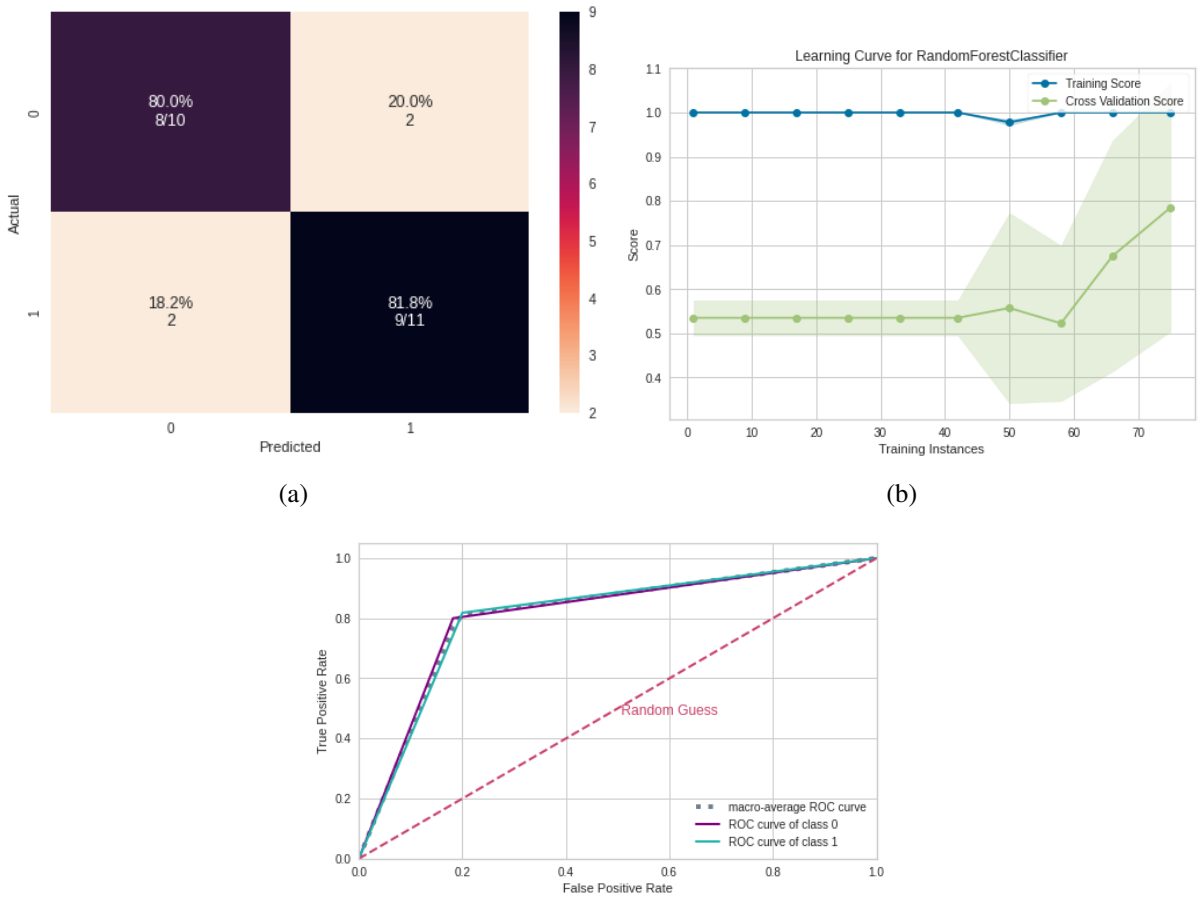

(a) (b)

(c)

Figure 47 – ML results using complex network measures from EEG. (a) Confusion matrix indicating a TN rate of (blue, according to the color bar) and a TP rate of (blue, according to the color bar). (b) Learning curve for the training Acc. (blue) and test Acc. (green). (c) ROC curve with class 0 (control) and class 1 (with SZ).

6.4.2 Complex network and measures extracted from EEG time series

The most important measure found for both data was Diameter, which corresponds to the length of the longest of the shortest path between any two vertices (RYU *et al.*, 2020). Since this measure was observed in two different bases, EEG and fMRI, it may be an indicative biomarker for the diagnosis of schizophrenia.

Regarding the EEG database, for the first time in the literature, we combined measures extracted from EEG time series with measures of complex networks extracted from functional networks of control individuals and schizophrenia patients to verify which measures are more efficient for this type of data. The results suggested that measures extracted from time series were more critical for classifying patients with SZ. The most relevant measure for EEG was spectral entropy, which has a positive correlation with SZ, followed by Hjorth mobility and complexity, which have a negative correlation with the occurrence of SZ.

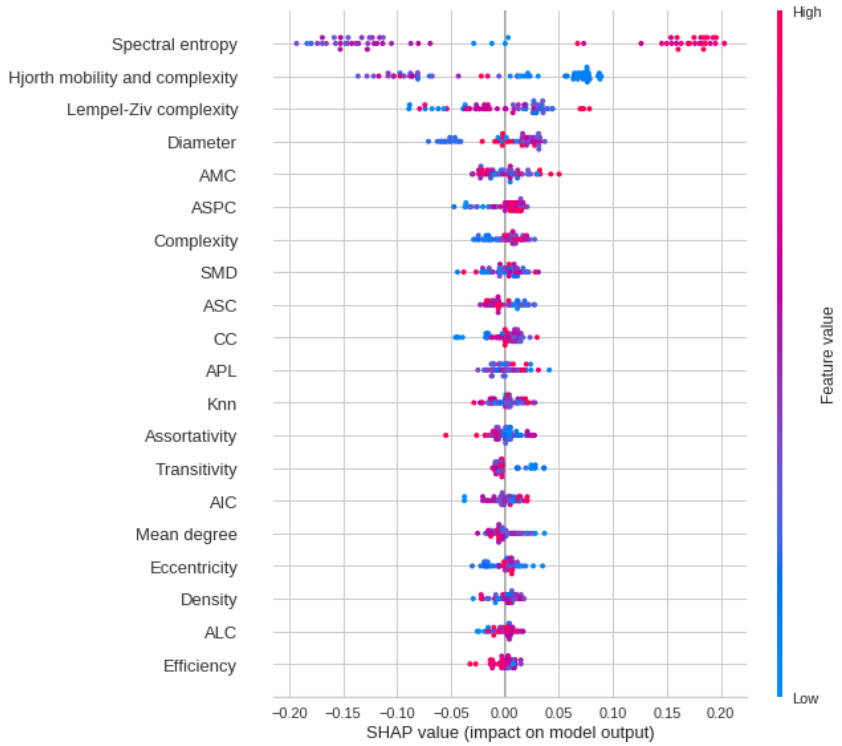

Figure 48 – RF classifier features importance ranking in an EEG dataset, with factors mentioned in descending order. For the categorization of SZ patients, the spectral entropy measure is the most essential, followed by the Hjorth mobility and complexity measure.

Spectral Entropy is an information theory-derived quantity that measures the degree of uncertainty in a signal, with higher values corresponding to a more uniform spectrum and more random frequency content and lower values corresponding to more regular frequencies (DUFF *et al.*, 2013; GOMEZ-PILAR *et al.*, 2018). Spectral Entropy is an information theory-derived quantity that measures the degree of uncertainty in a signal, with higher values corresponding to a more uniform spectrum and more random frequency content and lower values corresponding to more regular frequencies. During the resting condition, we detected greater levels of spectral Entropy associated with SZ, indicating more random frequencies. This conclusion contradicts previous studies (TAKAHASHI *et al.*, 2010; MOLINA *et al.*, 2020; GOMEZ-PILAR *et al.*, 2018) that reported spectral entropy deficiencies in schizophrenia patients executing the P300 activity. We assume this discrepancy because our data were obtained during the rest. The second most important EEG measure was Hjorth mobility and complexity, which illustrates a frequency shift and shows how a signal's form is comparable to a pure sine wave (HJORTH, 1970). The Hjorth mobility and complexity values found for SZ patients were according to the literature (PORTNOVA; ATANOV, 2018).

Furthermore, for EEG data, the existence of SZ was connected with greater ASPC values, which estimate the size of the communities. As a result, SZ is connected with larger communities. Moreover, the discovery of larger communities shows that the brain's equilibrium between functional segregation and integration has been disrupted, implying that information distribution

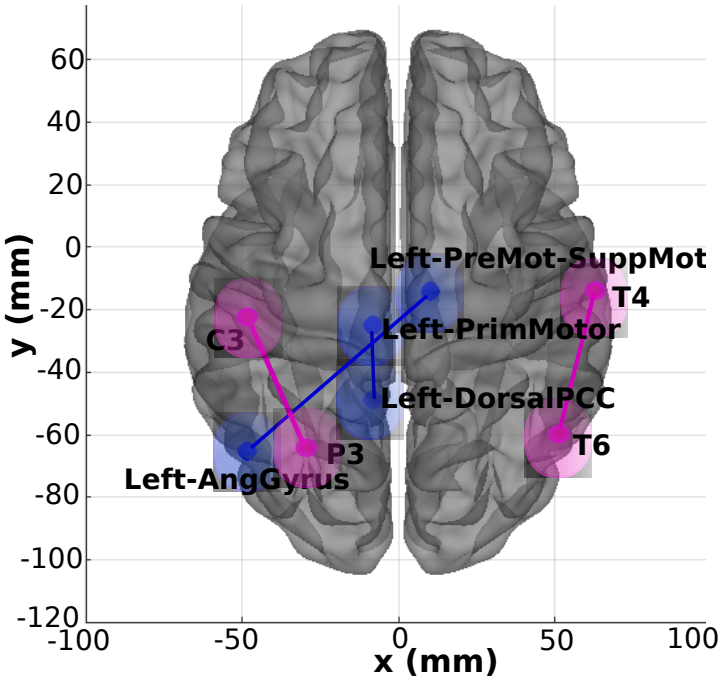

Figure 49 – Plot with the most crucial connections found, in the two-dimensional schematic (ventral-axis), with the essential fMRI connection highlighted in blue and the most critical EEG connection highlighted in pink. The brain plot was developed by Braph tool (MIJALKOV *et al.*, 2017), based on the coordinates in (MICHEL; BRUNET, 2019; ASHER *et al.*, 2021; SCRIVENER; READER, 2022), and each region was plotted using the Brodmann map from the Yale BioImage Suite Package.

is slower than in the control group. These findings support the idea that functional brain networks in SZ patients are more random than the control ones, as described in section 6.1.

Further, lower Transitivity values are related to the existence of SZ. The transitivity is a measure of the efficiency of information transfer between all pairs of nodes in the graph (RANGAPRAKASH *et al.*, 2019), and a lower value of these measures indicates lower segregation (LUO; GREENE; CONSTABLE, 2021). This finding is according to the literature (ANDERSON; COHEN, 2013; BASSETT *et al.*, 2008).

Additionally, for fMRI, CC was the second most crucial measure. The average of the shortest path lengths from the node to every other node in the network, measured as CC, represents how near a node is to all other nodes in the network (GOLBECK, 2013). Therefore, a lower Closeness Centrality score reflects impairment at these nodes (THOMAS *et al.*, 2015), which was also found in previous findings (GRIFFA *et al.*, 2015).

6.5 Conclusions and future work

The workflow developed using fMRI data distinguish control from SZ patients with an accuracy of 98% and AUC of 100%. The best pairwise statistical metric captured brain changes

due to the presence of SZ was TE, and the best-performing machine learning model was RF.

According to the TE and RF, essential brain connections in the SZ group are a positive correlation between the left dorsal PCC and left primary motor at rest and a negative correlation between the left premotor supplementary and angular gyrus areas. Furthermore, in the right parietal lobe, there is a strong positive correlation between the P3 and C3 regions and a negative correlation between the T6 and T4 electrodes, according to the EEG connectivity matrix.

Due to the employment of two databases collected in different groups of SZ patients using two different types of equipment that capture detailed information on brain activity, this study has particular difficulties in comprehending the associations revealed (fMRI and EEG). However, the findings provide a wealth of information about brain activity in SZ patients, which is corroborated by clinical and neurophysiological findings in the literature. We hypothesize that fMRI and EEG correlations in the data point to brain regions involved in motor, cognitive, and sensory processing, internal attention targeting, DMN-related regions, and auditory and language processing. This finding may reflect changes in SZ patients, such as problems with expression, production, and speech articulation, changes in thinking, internal attention targeting, cognition, and hallucinatory episodes.

Concerning the complex network measures, Diameter is recognized as a critical measure for both data, and it may be a suggestive biomarker for the diagnosis of SZ because the same result was obtained with two different equipment and patient groups. This study could be a significant finding, as it reveals a robust biomarker that enables ML-based diagnosis of schizophrenia disease regardless of data modalities. Furthermore, for EEG data, SZ functional networks, compared to the control group, have larger communities and lower. Moreover, SZ functional networks exhibit larger communities and lower Transitivity for EEG data, indicating slower information distribution and less segregation than in the control group. According to the literature, these results mean that our approach with the SHAP value method could predict the primary SZ-related connections and the best complex network measures.

Nevertheless, according to our ML approach, EEG measures extracted from raw time series are more important than complex network measurements in capturing brain alterations in SZ patients.

Finally, future studies may involve the application of the methodology to other fMRI data from ADHD-200 Global Competition. It can also be adopted with EEG data from patients with other neurological disorders, for example, dystonia (BALTAZAR *et al.*, 2020).

CHAPTER

7

CONCLUSIONS AND FUTURE WORKS

'The truth is that we isolate a particular kind of love and appropriate it for the name of love, which really belongs to a wider whole"

— Plato, *The Symposium*

The present work aimed to develop a predictive model capable of improving the diagnosis of mental illnesses such as schizophrenia, AD, and autism. Furthermore, verify if the same workflow can automatically detect changes in the functional network structure induced by DMT and ayahuasca since psychedelics may have a therapeutical potential for some mental illnesses.

In general, the model predictions for the diseases studied here were superior to those found in the literature. Thereby state of art in the field of mental illness diagnosis has advanced.

Regarding the study of psychedelics, it was obtained new insights into the mechanisms of action of ayahuasca and DMT using ML and SHAP values. Moreover, it was determined which complex network measures are most effective for capturing brain changes, including new metrics developed by the author. In addition, these new metrics have been fundamental in the studies of autism and psychedelics.

In further detail, chapter 2 showed a deep learning approach that classifies patients with Alzheimer'sAlzheimer's disease and schizophrenia with a high level of accuracy. Furthermore, the comparison with the classic cases that use raw EEG time series shows that our method provides the highest precision.

In chapter 3, our workflow was able to distinguish brain changes occurring due to ayahuasca, and the most activated areas were the frontal and temporal lobes, which is consistent with the literature. The correlation between F3 and PO4 was the most important in terms of brain connections. This connection may point to a cognitive process similar to face recognition in individuals during ayahuasca-mediated visual hallucinations. Furthermore, closeness centrality and assortativity were the most important complex network measures. These two measures are also associated with AD, indicating a possible therapeutic mechanism.

Specifically, in chapter 4, the ML model using our workflow found that differences in the high alpha, low beta, and delta frequency band were most important to distinguish between the state before and after DMT inhalation, which is consistent with results described in the literature. Furthermore, the connection between the temporal (TP8) and central cortex (C3) and between the precentral gyrus (FC5) and the lateral occipital cortex (T8) contributed most to the classification result. The connection between regions TP8 and C3 has been found in the literature associated with finger movements that might have occurred during DMT consumption. However, the connection between cortical regions FC5 and P8 has not been found in the literature and is presumably related to the volunteers' emotional, visual, sensory, perceptual, and mystical experiences during DMT consumption. In terms of complex networks, closeness centrality was this chapter's most crucial complex network measure. Moreover, we found larger communities and a longer average path length with the use of DMT and the opposite in its absence, indicating that the balance between functional segregation and integration was disrupted. These findings support that cortical brain activity becomes more entropic under psychedelics.

In chapter 5, using fMRI data, the workflow developed here was able to distinguish TD from ASD patients. Important regions include Left-Sec Visual (visual cortex), Left-VentPostCing, Left-prim motor, and Left-VentPostCing Posterior cingulate cortex. Noteworthy, The Left-VentPostCing Posterior cingulate cortex is known from the literature that reductions in functional connectivity of this brain area in ASD patients, and this is consistent with the results found here, in which this region is less connected to the Outside BAS1 region in patients with ASD. In terms of complex networks, the brain networks of ASD patients showed more segregation, less distribution of information across the network, and less connectivity. Regarding the sliding process employed, this technique proved effective for differentiating TD and ASD patients, where with 30 patients, it was possible to achieve a mean AUC and mean accuracy of 0.81. Statistical comparison considering the data from the sliding process and complete data did not show significant differences. Thus, it is an appropriate methodology that can be employed in the case of data with a small sample size.

In chapter 6, we applied our workflow using fMRI and EEG datasets in a multimodal fashion of SZ patients. Besides the previous ML methods, we also consider the deep learning architecture LSTM. Furthermore, for the first time in the literature, we combined EEG measures with complex network measurements to be analyzed in our model. We found that in the right parietal lobe, there is a strong positive correlation between the P3 and C3 regions and a negative correlation between the T6 and T4 electrodes, according to the EEG connectivity matrix. In terms of complex network measures, the diameter, which corresponds to the longest shortest path length in a network, is a biomarker because it is the most important measure in a multimodal fashion. Furthermore, the schizophrenia brain networks exhibit less segregation and lower distribution of information. As a final result, EEG measures outperformed complex networks in capturing the brain alterations associated with schizophrenia. As a result, our model achieved an AUC of 100%, an accuracy of 98% for the fMRI, an AUC of 95%, and an accuracy of 95% for the

EEG data set. Noteworthy that a standard metric for constructing the connectivity matrix that outperformed in the chapters 5 and chapter 6 was the normalized TE.

Although our methodology outperformed the diseases studied to those found in the literature, we analyzed mainly EEG and fMRI during the rest and small data. For a more generalized and robust workflow that could transform into a medical application, it would be necessary to analyze data collected with patients performed some task, i. e. auditory oddball for EEG and a more significant volume of data.

Another limitation is that we considered a binary classification with our workflow, which would be interestingly considered a multiclass approach. Furthermore, it would be interesting to extend our analyses for EEG and fMRI time series from other diseases and patients who consumed other psychedelic drugs. Finally, the same methodology applied here may be useful in interpreting EEG and fMRI time series from other diseases and patients who consumed other psychedelic drugs. The following section 7.1 contains the intended future work.

7.1 Future work

We want to use EEG data and the methods described here to research, in addition to AD, other degenerative disorders such as Parkinson's disease and dystonia (BALTAZAR *et al.*, 2020).

In addition, the methodology will also be applied to other EEG data related to other mental disorders such as major depressive disorder, other schizophrenia dataset(ZHANG, 2019), ASD (FROHLICH *et al.*, 2019), and Attention deficit hyperactivity disorder (ADHD) (NASRABADI *et al.*, 2020). This comparison will also be made considering EEG and fMRI data from ADHD-200 Global Competition for ADHD patients.

Regarding the study of psychedelics, in future work, we intend to use this methodology on EEG data from subjects that used the psychedelic drug called ketamine (FARNES *et al.*, 2020), and fMRI data from that used the psychedelic drug called Lysergic acid diethylamide (LSD) (CARHART-HARRIS *et al.*, 2016).

Moreover, finally, in addition to psychedelics, we would like to test our methodology on other types of drugs such as antidepressants (JAWORSKA *et al.*, 2019).

BIBLIOGRAPHY

AARSLAND, D.; CREESE, B.; POLITIS, M.; CHAUDHURI, K. R.; WEINTRAUB, D.; BALLARD, C. *et al.* Cognitive decline in parkinson disease. **Nature Reviews Neurology**, Nature Publishing Group, v. 13, n. 4, p. 217–231, 2017. Citation on page 73.

ABEL, J. H.; BADGELEY, M. A.; MESCHEDE-KRASA, B.; SCHAMBERG, G.; GARWOOD, I. C.; LECAMWASAM, K.; CHAKRAVARTY, S.; ZHOU, D. W.; KEATING, M.; PURDON, P. L. *et al.* Machine learning of eeg spectra classifies unconsciousness during gabaergic anesthesia. **Plos one**, Public Library of Science San Francisco, CA USA, v. 16, n. 5, p. e0246165, 2021. Citation on page 58.

ACHARYA, U. R.; OH, S. L.; HAGIWARA, Y.; TAN, J. H.; ADELI, H.; SUBHA, D. P. Automated eeg-based screening of depression using deep convolutional neural network. **Computer Methods and Programs in Biomedicine**, Elsevier, v. 161, p. 103–113, 2018. Citation on page 46.

ACHARYA, U. R.; OH, S. L.; HAGIWARA, Y.; TAN, J. H.; ADELI, H. Deep convolutional neural network for the automated detection and diagnosis of seizure using eeg signals. **Computers in Biology and Medicine**, Elsevier, v. 100, p. 270–278, 2018. Citation on page 46.

AHMADLOU, M.; ADELI, H.; ADELI, A. Fractality and a wavelet-chaos-methodology for eeg-based diagnosis of alzheimer disease. **Alzheimer Disease & Associated Disorders**, LWW, v. 25, n. 1, p. 85–92, 2011. Citation on page 45.

AL-BELTAGI, M. Autism medical comorbidities. **World journal of clinical pediatrics**, Baishideng Publishing Group Inc, v. 10, n. 3, p. 15, 2021. Citations on pages 102 and 127.

ALAERTS, K.; WOOLLEY, D. G.; STEYAERT, J.; MARTINO, A. D.; SWINNEN, S. P.; WENDEROTH, N. Underconnectivity of the superior temporal sulcus predicts emotion recognition deficits in autism. **Social cognitive and affective neuroscience**, Oxford University Press, v. 9, n. 10, p. 1589–1600, 2014. Citation on page 119.

ALAMIA, A.; TIMMERMANN, C.; NUTT, D. J.; VANRULLEN, R.; CARHART-HARRIS, R. L. Dmt alters cortical travelling waves. **Elife**, eLife Sciences Publications Limited, v. 9, p. e59784, 2020. Citation on page 82.

ALBERT, R.; BARABÁSI, A.-L. Statistical mechanics of complex networks. **Reviews of modern physics**, APS, v. 74, n. 1, p. 47, 2002. Citations on pages 63, 87, 109, and 131.

ALBERT, R.; JEONG, H.; BARABÁSI, A.-L. Diameter of the world-wide web. **nature**, Nature Publishing Group, v. 401, n. 6749, p. 130–131, 1999. Citations on pages 63, 87, 109, and 131.

ALIZADEHSANI, R.; ROSHANZAMIR, M.; ABDAR, M.; BEYKIKHOSHK, A.; KHOSRAVI, A.; PANAHIAZAR, M.; KOOHESTANI, A.; KHOZEIMEH, F.; NAHAVANDI, S.; SARRAFZADEGAN, N. A database for using machine learning and data mining techniques for coronary artery disease diagnosis. **Scientific data**, Nature Publishing Group, v. 6, n. 1, p. 1–13, 2019. Citation on page 82.

ALVES, C.; THAISE, G. d. O.; AGUIAR, P. de C.; PINEDA, A. M.; ROSTER, K.; THIELEMANN, C.; PORTO, J. A. M.; RODRIGUES, F. A. Diagnosis of autism spectrum disorder based on functional brain networks and machine learning. 2022. Citation on page 128.

ALVES, C. L. **Diagnóstico de doenças mentais baseado em mineração de dados e redes complexas**. Phd Thesis (PhD Thesis) — Universidade de São Paulo. Citations on pages 108 and 130.

ALVES, C. L.; CURY, R. G.; ROSTER, K.; PINEDA, A. M.; RODRIGUES, F. A.; THIELEMANN, C.; CIBA, M. Application of machine learning and complex network measures to an eeg dataset from ayahuasca experiments. **medRxiv**, Cold Spring Harbor Laboratory Press, 2022. Citations on pages 83, 84, 87, 88, 99, 109, 116, 126, 127, and 131.

ALVES, C. L.; PINEDA, A. M.; ROSTER, K.; THIELEMANN, C.; RODRIGUES, F. A. Eeg functional connectivity and deep learning for automatic diagnosis of brain disorders: Alzheimer's disease and schizophrenia. **Journal of Physics: Complexity**, IOP Publishing, v. 3, n. 2, p. 025001, 2022. Citations on pages 58, 60, 103, 127, 130, 132, and 200.

AMARI, S.-i.; CICHOCKI, A.; YANG, H. A new learning algorithm for blind signal separation. **Advances in neural information processing systems**, v. 8, 1995. Citation on page 86.

AMORE, G.; SPOTO, G.; IENI, A.; VETRI, L.; QUATROSI, G.; ROSA, G. D.; NICOTERA, A. G. A focus on the cerebellum: from embryogenesis to an age-related clinical perspective. **Frontiers in Systems Neuroscience**, Frontiers Media SA, v. 15, p. 646052, 2021. Citation on page 120.

AMZICA, F.; STERIADE, M. Electrophysiological correlates of sleep delta waves. **Electroencephalography and clinical neurophysiology**, Elsevier, v. 107, n. 2, p. 69–83, 1998. Citation on page 94.

ANDERSON, A.; COHEN, M. S. Decreased small-world functional network connectivity and clustering across resting state networks in schizophrenia: an fmri classification tutorial. **Frontiers in human neuroscience**, Frontiers Media SA, v. 7, p. 520, 2013. Citations on pages 126 and 144.

ANDERSON, B. S.; BUTTS, C.; CARLEY, K. The interaction of size and density with graph-level indices. **Social networks**, Elsevier, v. 21, n. 3, p. 239–267, 1999. Citations on pages 63, 87, 109, and 131.

ANDREASEN, N. C.; FLAUM, M. Schizophrenia: the characteristic symptoms. **Schizophrenia bulletin**, Oxford University Press, v. 17, n. 1, p. 27–49, 1991. Citation on page 125.

ANDREWS, T.; WRIGHT, K. The frontiers of new psychedelic therapies: A survey of sociological themes and issues. **Sociology Compass**, Wiley Online Library, v. 16, n. 2, p. e12959, 2022. Citations on pages 39 and 81.

ANTIQUEIRA, L.; RODRIGUES, F. A.; WIJK, B. C. van; COSTA, L. d. F.; DAFFERTSHOFER, A. Estimating complex cortical networks via surface recordings—a critical note. **Neuroimage**, Elsevier, v. 53, n. 2, p. 439–449, 2010. Citation on page 53.

AOKI, Y.; ABE, O.; NIPPASHI, Y.; YAMASUE, H. Comparison of white matter integrity between autism spectrum disorder subjects and typically developing individuals: a meta-analysis of diffusion tensor imaging tractography studies. **Molecular autism**, BioMed Central, v. 4, n. 1, p. 1–17, 2013. Citation on page 103.

ARAÚJO, D. B. de. Evidence for the therapeutic effects of ayahuasca. **Advances in psychedelic medicine. State-of-the-art therapeutic applications**, Praeger Santa Barbara, CA, p. 103–23, 2019. Citations on pages 56 and 81.

ARAUJO, D. B. de; RIBEIRO, S.; CECCHI, G. A.; CARVALHO, F. M.; SANCHEZ, T. A.; PINTO, J. P.; MARTINIS, B. S. de; CRIPPA, J. A.; HALLAK, J. E.; SANTOS, A. C. Seeing with the eyes shut: Neural basis of enhanced imagery following ayahuasca ingestion. **Human brain mapping**, Wiley Online Library, v. 33, n. 11, p. 2550–2560, 2012. Citation on page 72.

ARCADU, F.; BENMANSOUR, F.; MAUNZ, A.; WILLIS, J.; HASKOVA, Z.; PRUNOTTO, M. Author correction: Deep learning algorithm predicts diabetic retinopathy progression in individual patients. **NPJ digital medicine**, Nature Publishing Group, v. 3, n. 1, p. 1–6, 2020. Citations on pages 60, 89, 108, and 130.

ARDESHNA, N. I. Eeg and coma. **The Neurodiagnostic Journal**, Taylor & Francis, v. 56, n. 1, p. 1–16, 2016. Citation on page 94.

ARRUDA, G. F. de; COSTA, L. da F.; SCHUBERT, D.; RODRIGUES, F. A. Structure and dynamics of functional networks in child-onset schizophrenia. **Clinical Neurophysiology**, Elsevier, v. 125, n. 8, p. 1589–1595, 2014. Citations on pages 45 and 53.

ASHAR, Y. K.; GORDON, A.; SCHUBINER, H.; UIPI, C.; KNIGHT, K.; ANDERSON, Z.; CARLISLE, J.; POLISKY, L.; GEUTER, S.; FLOOD, T. F. *et al.* Effect of pain reprocessing therapy vs placebo and usual care for patients with chronic back pain: a randomized clinical trial. **JAMA psychiatry**, American Medical Association, v. 79, n. 1, p. 13–23, 2022. Citation on page 110.

ASHER, E. E.; PLOTNIK, M.; GÜNTHER, M.; MOSHEL, S.; LEVY, O.; HAVLIN, S.; KANTELHARDT, J. W.; BARTSCH, R. P. Connectivity of eeg synchronization networks increases for parkinson's disease patients with freezing of gait. **Communications biology**, Nature Publishing Group, v. 4, n. 1, p. 1–10, 2021. Citations on pages 17, 19, 22, 70, 73, 93, and 144.

ASSOCIATION, A. P. *et al.* **American Psychiatric Association: Diagnosti c and Statistical Manual of Mental Disorders, Arlington**. 2013. Citation on page 102.

AWAD, M.; KHANNA, R. Support vector machines for classification. In: **Efficient learning machines**. [S.l.]: Springer, 2015. p. 39–66. Citation on page 88.

BAE, H.-J.; KIM, C.-W.; KIM, N.; PARK, B.; KIM, N.; SEO, J. B.; LEE, S. M. A perlin noise-based augmentation strategy for deep learning with small data samples of hrct images. **Scientific reports**, Nature Publishing Group, v. 8, n. 1, p. 1–7, 2018. Citation on page 103.

BAE, Y.; KUMARASAMY, K.; ALI, I. M.; KORFIATIS, P.; AKKUS, Z.; ERICKSON, B. J. Differences between schizophrenic and normal subjects using network properties from fmri. **Journal of digital imaging**, Springer, v. 31, n. 2, p. 252–261, 2018. Citation on page 125.

BAI, Y.; LIANG, Z.; LI, X. A permutation lempel-ziv complexity measure for eeg analysis. **Biomedical Signal Processing and Control**, Elsevier, v. 19, p. 102–114, 2015. Citation on page 132.

BALTAZAR, C. A.; MACHADO, B. S.; FARIA, D. D. D.; PAULO, A. J. M.; SILVA, S. M. C. A.; FERRAZ, H. B.; AGUIAR, P. de C. Brain connectivity in patients with dystonia during motor tasks. **Journal of Neural Engineering**, IOP Publishing, v. 17, n. 5, p. 056039, 2020. Citations on pages 121, 145, and 149.

BANKER, L.; TADI, P. Neuroanatomy, precentral gyrus.[updated 2020 jul 31]. **StatPearls [Internet]. StatPearls Publishing: Treasure Island (FL)**, 2021. Citation on page 96.

BANQUET, J.-P. Spectral analysis of the eeg in meditation. **Electroencephalography and clinical neurophysiology**, Elsevier, v. 35, n. 2, p. 143–151, 1973. Citation on page 95.

BARAVALLE, R.; GUISANDE, N.; GRANADO, M.; ROSSO, O. A.; MONTANI, F. Characterization of visuomotor/imaginary movements in eeg: An information theory and complex network approach. **Frontiers in Physics**, Frontiers, p. 115, 2019. Citation on page 82.

BARBER, M. J.; CLARK, J. W. Detecting network communities by propagating labels under constraints. **Physical Review E**, APS, v. 80, n. 2, p. 026129, 2009. Citation on page 65.

BARENDREGT, J. J.; BONNEUX, L.; MAAS, P. Van der. Dalys: the age-weights on balance. **Bulletin of the World Health Organization**, World Health Organization, v. 74, n. 4, p. 439, 1996. Citation on page 191.

BARKER, S. A. N, n-dimethyltryptamine (dmt), an endogenous hallucinogen: Past, present, and future research to determine its role and function. **Frontiers in neuroscience**, Frontiers, p. 536, 2018. Citation on page 81.

_____. Administration of n, n-dimethyltryptamine (dmt) in psychedelic therapeutics and research and the study of endogenous dmt. **Psychopharmacology**, Springer, p. 1–15, 2022. Citation on page 81.

BARKER, S. A.; BORJIGIN, J.; LOMNICKA, I.; STRASSMAN, R. Lc/ms/ms analysis of the endogenous dimethyltryptamine hallucinogens, their precursors, and major metabolites in rat pineal gland microdialysate. **Biomedical Chromatography**, Wiley Online Library, v. 27, n. 12, p. 1690–1700, 2013. Citation on page 81.

BARKER, S. A.; MCILHENNY, E. H.; STRASSMAN, R. A critical review of reports of endogenous psychedelic n, n-dimethyltryptamines in humans: 1955–2010. **Drug testing and analysis**, Wiley Online Library, v. 4, n. 7-8, p. 617–635, 2012. Citation on page 81.

BARSUGLIA, J.; DAVIS, A. K.; PALMER, R.; LANCELOTTA, R.; WINDHAM-HERMAN, A.-M.; PETERSON, K.; POLANCO, M.; GRANT, R.; GRIFFITHS, R. R. Intensity of mystical experiences occasioned by 5-meo-dmt and comparison with a prior psilocybin study. **Frontiers in Psychology**, Frontiers, p. 2459, 2018. Citations on pages 81 and 97.

BASSETT, D. S.; BULLMORE, E.; VERCHINSKI, B. A.; MATTAY, V. S.; WEINBERGER, D. R.; MEYER-LINDENBERG, A. Hierarchical organization of human cortical networks in health and schizophrenia. **Journal of Neuroscience**, Soc Neuroscience, v. 28, n. 37, p. 9239–9248, 2008. Citation on page 144.

BASSETT, D. S.; GAZZANIGA, M. S. Understanding complexity in the human brain. **Trends in cognitive sciences**, Elsevier, v. 15, n. 5, p. 200–209, 2011. Citations on pages 57 and 82.

BASSETT, D. S.; ZURN, P.; GOLD, J. I. On the nature and use of models in network neuroscience. **Nature Reviews Neuroscience**, Nature Publishing Group, v. 19, n. 9, p. 566–578, 2018. Citations on pages 37, 57, and 82.

BASTI, A.; NILI, H.; HAUK, O.; MARZETTI, L.; HENSON, R. N. Multi-dimensional connectivity: a conceptual and mathematical review. **NeuroImage**, Elsevier, p. 117179, 2020. Citation on page 38.

BASTOS, A. M.; SCHOFFELEN, J.-M. A tutorial review of functional connectivity analysis methods and their interpretational pitfalls. **Frontiers in Systems Neuroscience**, Frontiers, v. 9, p. 175, 2016. Citations on pages 46 and 48.

BÄUERLE, A.; STEINBACH, J.; SCHWEDA, A.; BECKORD, J.; HETKAMP, M.; WEISMÜLLER, B.; KOHLER, H.; MUSCHE, V.; DÖRRIE, N.; TEUFEL, M. *et al.* Mental health burden of the covid-19 outbreak in germany: predictors of mental health impairment. **Journal of primary care & community health**, SAGE Publications Sage CA: Los Angeles, CA, v. 11, p. 2150132720953682, 2020. Citation on page 35.

BEAUDET, A. L. Autism: highly heritable but not inherited. **Nature Medicine**, Nature Publishing Group, v. 13, n. 5, p. 534–536, 2007. Citation on page 102.

BEAUREGARD, M.; PAQUETTE, V. Eeg activity in carmelite nuns during a mystical experience. **Neuroscience letters**, Elsevier, v. 444, n. 1, p. 1–4, 2008. Citation on page 95.

BELLAZZI, R.; ZUPAN, B. Predictive data mining in clinical medicine: current issues and guidelines. **International journal of medical informatics**, Elsevier, v. 77, n. 2, p. 81–97, 2008. Citations on pages 38 and 58.

BELLEC, P. Cobre preprocessed with niak 0.17-lightweight release. **DOI**, v. 10, p. m9, 2016. Citations on pages 121 and 128.

BELLEC, P.; ROSA-NETO, P.; LYTTELTON, O. C.; BENALI, H.; EVANS, A. C. Multi-level bootstrap analysis of stable clusters in resting-state fmri. **Neuroimage**, Elsevier, v. 51, n. 3, p. 1126–1139, 2010. Citations on pages 105 and 128.

BELMONTE, M. K.; ALLEN, G.; BECKEL-MITCHENER, A.; BOULANGER, L. M.; CARPER, R. A.; WEBB, S. J. Autism and abnormal development of brain connectivity. **Journal of Neuroscience**, Soc Neuroscience, v. 24, n. 42, p. 9228–9231, 2004. Citation on page 102.

BELMONTE, M. K.; YURGELUN-TODD, D. A. Functional anatomy of impaired selective attention and compensatory processing in autism. **Cognitive brain research**, Elsevier, v. 17, n. 3, p. 651–664, 2003. Citation on page 102.

BENESTY, J.; CHEN, J.; HUANG, Y.; COHEN, I. Pearson correlation coefficient. In: **Noise reduction in speech processing**. [S.l.]: Springer, 2009. p. 1–4. Citations on pages 47, 106, and 129.

BENGIO, Y.; COURVILLE, A.; VINCENT, P. Representation learning: A review and new perspectives. **IEEE transactions on pattern analysis and machine intelligence**, IEEE, v. 35, n. 8, p. 1798–1828, 2013. Citation on page 38.

BENGIO, Y.; GRANDVALET, Y. No unbiased estimator of the variance of k-fold cross-validation. **Journal of machine learning research**, v. 5, n. Sep, p. 1089–1105, 2004. Citations on pages 60, 88, 108, and 130.

BERGSTRA, J.; BENGIO, Y. Random search for hyper-parameter optimization. **Journal of Machine Learning Research**, v. 13, n. 2, 2012. Citation on page 48.

BERNARD, O.; LALANDE, A.; ZOTTI, C.; CERVENANSKY, F.; YANG, X.; HENG, P.-A.; CETIN, I.; LEKADIR, K.; CAMARA, O.; BALLESTER, M. A. G. *et al.* Deep learning

techniques for automatic mri cardiac multi-structures segmentation and diagnosis: Is the problem solved? **IEEE transactions on medical imaging**, ieee, v. 37, n. 11, p. 2514–2525, 2018. Citation on page 38.

BERNARDI, G.; BETTA, M.; RICCIARDI, E.; PIETRINI, P.; TONONI, G.; SICLARI, F. Regional delta waves in human rapid eye movement sleep. **Journal of Neuroscience**, Soc Neuroscience, v. 39, n. 14, p. 2686–2697, 2019. Citation on page 94.

BERRAR, D. **Cross-Validation.** 2019. Citations on pages 60, 88, 108, and 130.

BERRYMAN, S.; MATTHEWS, K.; LEE, J. H.; DUFFY, S. P.; MA, H. Image-based phenotyping of disaggregated cells using deep learning. **Communications Biology**, Nature Publishing Group, v. 3, n. 1, p. 1–9, 2020. Citations on pages 60, 89, and 108.

BHATT, C.; KUMAR, I.; VIJAYAKUMAR, V.; SINGH, K. U.; KUMAR, A. The state of the art of deep learning models in medical science and their challenges. **Multimedia Systems**, Springer, v. 27, n. 4, p. 599–613, 2021. Citation on page 82.

BHATTACHARJEE, S.; KASHYAP, R.; ABUALAIT, T.; CHEN, S.-H. A.; YOO, W.-K.; BASHIR, S. The role of primary motor cortex: more than movement execution. **Journal of Motor Behavior**, Taylor & Francis, v. 53, n. 2, p. 258–274, 2021. Citation on page 140.

BIELLO, D. Searching for god in the brain. **Scientific American Mind**, JSTOR, v. 18, n. 5, p. 38–45, 2007. Citation on page 95.

BISWAL, B.; YETKIN, F. Z.; HAUGHTON, V. M.; HYDE, J. S. Functional connectivity in the motor cortex of resting human brain using echo-planar mri. **Magnetic resonance in medicine**, Wiley Online Library, v. 34, n. 4, p. 537–541, 1995. Citations on pages 103 and 126.

BLEULER, E.; JUNG, C. G. Komplexe und krankheitsursachen bei dementia praecox. **Zentralblatt fur Nervenheilkunde und Psychiatrie**, n. XIX, p. 220–227, 1908. Citation on page 125.

BLONDEL, V. D.; GUILLAUME, J.-L.; LAMBIOTTE, R.; LEFEBVRE, E. Fast unfolding of communities in large networks. **Journal of statistical mechanics: theory and experiment**, IOP Publishing, v. 2008, n. 10, p. P10008, 2008. Citations on pages 65, 88, 109, and 131.

BONACICH, P. Power and centrality: A family of measures. **American journal of sociology**, University of Chicago Press, v. 92, n. 5, p. 1170–1182, 1987. Citations on pages 63, 87, 109, and 131.

BONADIMAN, C. S. C.; PASSOS, V. M. d. A.; MOONEY, M.; NAGHAVI, M.; MELO, A. P. S. A carga dos transtornos mentais e decorrentes do uso de substâncias psicoativas no brasil: Estudo de carga global de doença, 1990 e 2015. **Revista Brasileira de Epidemiologia**, SciELO Public Health, v. 20, p. 191–204, 2017. Citation on page 35.

BONITA, J.; AMBOLODE, L.; ROSENBERG, B.; CELLUCCI, C.; WATANABE, T.; RAPP, P.; ALBANO, A. Time domain measures of inter-channel eeg correlations: a comparison of linear, nonparametric and nonlinear measures. **Cognitive neurodynamics**, Springer, v. 8, n. 1, p. 1–15, 2014. Citations on pages 46 and 48.

BORSBOOM, D. Psychometric perspectives on diagnostic systems. **Journal of clinical psychology**, Wiley Online Library, v. 64, n. 9, p. 1089–1108, 2008. Citations on pages 37 and 44.

_____. A network theory of mental disorders. **World psychiatry**, Wiley Online Library, v. 16, n. 1, p. 5–13, 2017. Citation on page 37.

BORSBOOM, D.; CRAMER, A. O. Network analysis: an integrative approach to the structure of psychopathology. **Annual Review of Clinical Psychology**, Annual Reviews, v. 9, p. 91–121, 2013. Citations on pages 37 and 44.

BOTTOU, L.; LIN, C.-J. Support vector machine solvers. **Large scale kernel machines**, Citeseer, v. 3, n. 1, p. 301–320, 2007. Citations on pages 59, 83, 108, 130, and 194.

BOUKTIF, S.; FIAZ, A.; OUNI, A.; SERHANI, M. A. Optimal deep learning lstm model for electric load forecasting using feature selection and genetic algorithm: Comparison with machine learning approaches. **Energies**, Multidisciplinary Digital Publishing Institute, v. 11, n. 7, p. 1636, 2018. Citation on page 61.

BOUSO, J. C.; RIBA, J. Ayahuasca and the treatment of drug addiction. In: **The therapeutic use of ayahuasca**. [S.l.]: Springer, 2014. p. 95–109. Citation on page 57.

BOUTET, A.; MADHAVAN, R.; ELIAS, G. J.; JOEL, S. E.; GRAMER, R.; RANJAN, M.; PARAMANANDAM, V.; XU, D.; GERMANN, J.; LOH, A. *et al.* Predicting optimal deep brain stimulation parameters for parkinson's disease using functional mri and machine learning. **Nature communications**, Nature Publishing Group, v. 12, n. 1, p. 1–13, 2021. Citations on pages 38 and 83.

BOWEN, D.; UNGAR, L. Generalized shap: Generating multiple types of explanations in machine learning. **arXiv preprint arXiv:2006.07155**, 2020. Citations on pages 38, 58, 61, 83, 104, and 126.

BRACHER-SMITH, M.; CRAWFORD, K.; ESCOTT-PRICE, V. Machine learning for genetic prediction of psychiatric disorders: a systematic review. **Molecular Psychiatry**, Nature Publishing Group, v. 26, n. 1, p. 70–79, 2021. Citations on pages 60, 89, 108, and 130.

BRAND, J.; PICCIRELLI, M.; HEPP-REYMOND, M.-C.; ENG, K.; MICHELS, L. Brain activation during visually guided finger movements. **Frontiers in Human Neuroscience**, Frontiers, p. 309, 2020. Citation on page 96.

BREIMAN, L. Random forests. **Machine learning**, Springer, v. 45, n. 1, p. 5–32, 2001. Citations on pages 59, 108, and 194.

BRIERLEY, D. I.; DAVIDSON, C. Developments in harmine pharmacology—implications for ayahuasca use and drug-dependence treatment. **Progress in neuro-psychopharmacology and biological psychiatry**, Elsevier, v. 39, n. 2, p. 263–272, 2012. Citation on page 57.

BROSCH, T.; YOO, Y.; LI, D. K.; TRABOULSEE, A.; TAM, R. Modeling the variability in brain morphology and lesion distribution in multiple sclerosis by deep learning. In: SPRINGER. **International Conference on Medical Image Computing and Computer-Assisted Intervention**. [S.l.], 2014. p. 462–469. Citation on page 38.

BUETTNER, R.; BEIL, D.; SCHOLTZ, S.; DJEMAI, A. Development of a machine learning based algorithm to accurately detect schizophrenia based on one-minute eeg recordings. In: **Proceedings of the 53rd Hawaii International Conference on System Sciences**. [S.l.: s.n.], 2020. Citation on page 45.

BULLMORE, E.; SPORNS, O. Complex brain networks: graph theoretical analysis of structural and functional systems. **Nature reviews neuroscience**, Nature Publishing Group, v. 10, n. 3, p. 186–198, 2009. Citation on page 82.

____. The economy of brain network organization. **Nature Reviews Neuroscience**, Nature Publishing Group, v. 13, n. 5, p. 336–349, 2012. Citation on page 97.

BUZA, K. Asterics: Projection-based classification of eeg with asymmetric loss linear regression and genetic algorithm. In: IEEE. **2020 IEEE 14th International Symposium on Applied Computational Intelligence and Informatics (SACI)**. [S.l.], 2020. p. 000035–000040. Citation on page 58.

BYCHKOV, D.; TURKKI, R.; HAGLUND, C.; LINDER, N.; LUNDIN, J. Deep learning for tissue microarray image-based outcome prediction in patients with colorectal cancer. In: INTERNATIONAL SOCIETY FOR OPTICS AND PHOTONICS. **Medical Imaging 2016: Digital Pathology**. [S.l.], 2016. v. 9791, p. 979115. Citations on pages 38 and 39.

CALHOUN, V. D.; EICHELE, T.; PEARLSON, G. Functional brain networks in schizophrenia: a review. **Frontiers in human neuroscience**, Frontiers Research Foundation, 2009. Citation on page 125.

CALHOUN, V. D.; SUI, J.; KIEHL, K.; TURNER, J.; ALLEN, E.; PEARLSON, G. Exploring the psychosis functional connectome: aberrant intrinsic networks in schizophrenia and bipolar disorder. **Frontiers in psychiatry**, Frontiers Research Foundation, v. 2, p. 75, 2012. Citation on page 128.

CAMERON, L. P.; BENSON, C. J.; DEFELICE, B. C.; FIEHN, O.; OLSON, D. E. Chronic, intermittent microdoses of the psychedelic n, n-dimethyltryptamine (dmt) produce positive effects on mood and anxiety in rodents. **ACS chemical neuroscience**, ACS Publications, v. 10, n. 7, p. 3261–3270, 2019. Citation on page 81.

CAMERON, L. P.; BENSON, C. J.; DUNLAP, L. E.; OLSON, D. E. Effects of n, n-dimethyltryptamine on rat behaviors relevant to anxiety and depression. **ACS chemical neuroscience**, ACS Publications, v. 9, n. 7, p. 1582–1590, 2018. Citation on page 81.

CAO, M.; SHU, N.; CAO, Q.; WANG, Y.; HE, Y. Imaging functional and structural brain connectomics in attention-deficit/hyperactivity disorder. **Molecular neurobiology**, Springer, v. 50, n. 3, p. 1111–1123, 2014. Citation on page 37.

CARHART-HARRIS, R. L. The entropic brain-revisited. **Neuropharmacology**, Elsevier, v. 142, p. 167–178, 2018. Citation on page 77.

CARHART-HARRIS, R. L.; LEECH, R.; HELLYER, P. J.; SHANAHAN, M.; FEILDING, A.; TAGLIAZUCCHI, E.; CHIALVO, D. R.; NUTT, D. The entropic brain: a theory of conscious states informed by neuroimaging research with psychedelic drugs. **Frontiers in human neuroscience**, Frontiers, p. 20, 2014. Citations on pages 77 and 98.

CARHART-HARRIS, R. L.; MUTHUKUMARASWAMY, S.; ROSEMAN, L.; KAELEN, M.; DROOG, W.; MURPHY, K.; TAGLIAZUCCHI, E.; SCHENBERG, E. E.; NEST, T.; ORBAN, C. *et al.* Neural correlates of the lsd experience revealed by multimodal neuroimaging. **Proceedings of the National Academy of Sciences**, National Acad Sciences, v. 113, n. 17, p. 4853–4858, 2016. Citations on pages 98 and 149.

CATANI, M. The anatomy of the human frontal lobe. **Handbook of clinical neurology**, Elsevier, v. 163, p. 95–122, 2019. Citation on page 96.

CAVANAGH, J. T.; CARSON, A. J.; SHARPE, M.; LAWRIE, S. M. Psychological autopsy studies of suicide: a systematic review. **Psychological medicine**, Cambridge University Press, v. 33, n. 3, p. 395–405, 2003. Citation on page 35.

CERQUEIRA, V.; TORGO, L.; MOZETIČ, I. Evaluating time series forecasting models: An empirical study on performance estimation methods. **Machine Learning**, Springer, v. 109, n. 11, p. 1997–2028, 2020. Citation on page 61.

CHAN, J.; REA, T.; GOLLAKOTA, S.; SUNSHINE, J. E. Contactless cardiac arrest detection using smart devices. **NPJ digital medicine**, Nature Publishing Group, v. 2, n. 1, p. 1–8, 2019. Citations on pages 60, 88, 108, and 130.

CHANG, C.; LIU, Z.; CHEN, M. C.; LIU, X.; DUYN, J. H. Eeg correlates of time-varying bold functional connectivity. **Neuroimage**, Elsevier, v. 72, p. 227–236, 2013. Citation on page 104.

CHANG, C.; METZGER, C. D.; GLOVER, G. H.; DUYN, J. H.; HEINZE, H.-J.; WALTER, M. Association between heart rate variability and fluctuations in resting-state functional connectivity. **Neuroimage**, Elsevier, v. 68, p. 93–104, 2013. Citation on page 104.

CHASE, A. Altered functional connectivity in preclinical dementia. **Nature Reviews Neurology**, Nature Publishing Group, v. 10, n. 11, 2014. Citation on page 37.

CHEJARA, P.; GODFREY, W. W. Comparative analysis of community detection algorithms. In: IEEE. **2017 Conference on Information and Communication Technology (CICT)**. [S.l.], 2017. p. 1–5. Citation on page 65.

CHEN, C. P.; KEOWN, C. L.; JAHEDI, A.; NAIR, A.; PFLIEGER, M. E.; BAILEY, B. A.; MÜLLER, R.-A. Diagnostic classification of intrinsic functional connectivity highlights somatosensory, default mode, and visual regions in autism. **NeuroImage: Clinical**, Elsevier, v. 8, p. 238–245, 2015. Citation on page 104.

CHENG, W.; PALANIYAPPAN, L.; LI, M.; KENDRICK, K. M.; ZHANG, J.; LUO, Q.; LIU, Z.; YU, R.; DENG, W.; WANG, Q. *et al.* Voxel-based, brain-wide association study of aberrant functional connectivity in schizophrenia implicates thalamocortical circuitry. **npj Schizophrenia**, Nature Publishing Group, v. 1, n. 1, p. 1–8, 2015. Citation on page 37.

CHRISTIAN, S. T.; HARRISON, R.; QUAYLE, E.; PAGEL, J.; MONTI, J. The in vitro identification of dimethyltryptamine (dmt) in mammalian brain and its characterization as a possible endogenous neuroregulatory agent. **Biochemical medicine**, Elsevier, v. 18, n. 2, p. 164–183, 1977. Citation on page 80.

CIPRIANI, A.; FURUKAWA, T. A.; SALANTI, G.; CHAIMANI, A.; ATKINSON, L. Z.; OGAWA, Y.; LEUCHT, S.; RUHE, H. G.; TURNER, E. H.; HIGGINS, J. P. *et al.* Comparative efficacy and acceptability of 21 antidepressant drugs for the acute treatment of adults with major depressive disorder: a systematic review and network meta-analysis. **Focus**, Am Psychiatric Assoc, v. 16, n. 4, p. 420–429, 2018. Citation on page 36.

CLAUSET, A.; NEWMAN, M. E.; MOORE, C. Finding community structure in very large networks. **Physical review E**, APS, v. 70, n. 6, p. 066111, 2004. Citations on pages 63, 88, 109, and 131.

CLERY, H.; ANDERSSON, F.; BONNET-BRILHAULT, F.; PHILIPPE, A.; WICKER, B.; GOMOT, M. fmri investigation of visual change detection in adults with autism. **NeuroImage: Clinical**, Elsevier, v. 2, p. 303–312, 2013. Citation on page 119.

COBIA, D. J.; SMITH, M. J.; WANG, L.; CSERNANSKY, J. G. Longitudinal progression of frontal and temporal lobe changes in schizophrenia. **Schizophrenia research**, Elsevier, v. 139, n. 1-3, p. 1–6, 2012. Citation on page 96.

COMIN, C. H.; PERON, T.; SILVA, F. N.; AMANCIO, D. R.; RODRIGUES, F. A.; COSTA, L. d. F. Complex systems: Features, similarity and connectivity. **Physics Reports**, Elsevier, v. 861, p. 1–41, 2020. Citation on page 48.

CONINCK, J. C.; FERRARI, F. A.; REIS, A. S.; IAROSZ, K. C.; CALDAS, I. L.; BATISTA, A. M.; VIANA, R. L. Network properties of healthy and alzheimer brains. **Physica A: Statistical Mechanics and its Applications**, Elsevier, v. 547, p. 124475, 2020. Citation on page 76.

COPE, T. E.; RITTMAN, T.; BORCHERT, R. J.; JONES, P. S.; VATANSEVER, D.; ALLINSON, K.; PASSAMONTI, L.; RODRIGUEZ, P. V.; BEVAN-JONES, W. R.; O'BRIEN, J. T. *et al.* Tau burden and the functional connectome in alzheimer's disease and progressive supranuclear palsy. **Brain**, Oxford University Press, v. 141, n. 2, p. 550–567, 2018. Citation on page 74.

COSTA, L. d. F.; RODRIGUES, F. A.; TRAVIESO, G.; BOAS, P. R. V. Characterization of complex networks: A survey of measurements. **Advances in Physics**, Taylor & Francis, v. 56, n. 1, p. 167–242, 2007. Citation on page 45.

COSTA, L. da F.; BOAS, P. V.; SILVA, F.; RODRIGUES, F. A pattern recognition approach to complex networks. **Journal of Statistical Mechanics: Theory and Experiment**, IOP Publishing, v. 2010, n. 11, p. P11015, 2010. Citation on page 45.

CSARDI, G.; NEPUSZ, T. *et al.* The igraph software package for complex network research. **InterJournal, complex systems**, v. 1695, n. 5, p. 1–9, 2006. Citation on page 87.

DAFTARI, C.; SHAH, J.; SHAH, M. Detection of epileptic seizure disorder using eeg signals. In: **Artificial Intelligence-Based Brain-Computer Interface**. [S.l.]: Elsevier, 2022. p. 163–188. Citation on page 86.

DAIANU, M.; JAHANSHAD, N.; NIR, T. M.; TOGA, A. W.; JR, C. R. J.; WEINER, M. W.; THOMPSON FOR THE ALZHEIMER'S DISEASE NEUROIMAGING INITIATIVE, P. M. Breakdown of brain connectivity between normal aging and alzheimer's disease: a structural k-core network analysis. **Brain connectivity**, Mary Ann Liebert, Inc. 140 Huguenot Street, 3rd Floor New Rochelle, NY 10801 USA, v. 3, n. 4, p. 407–422, 2013. Citation on page 120.

DAS, S.; PUTHANKATTIL, S. D. Complex network analysis of mci-ad eeg signals under cognitive and resting state. **Brain Research**, Elsevier, v. 1735, p. 146743, 2020. Citation on page 82.

DAUMANN, J.; HEEKEREN, K.; NEUKIRCH, A.; THIEL, C. M.; MÖLLER-HARTMANN, W.; GOUZOULIS-MAYFRANK, E. Pharmacological modulation of the neural basis underlying inhibition of return (ior) in the human 5-ht2a agonist and nmda antagonist model of psychosis. **Psychopharmacology**, Springer, v. 200, n. 4, p. 573–583, 2008. Citation on page 82.

DAUWELS, J.; VIALATTE, F.; CICHOCKI, A. Diagnosis of alzheimer's disease from eeg signals: where are we standing? **Current Alzheimer Research**, Bentham Science Publishers, v. 7, n. 6, p. 487–505, 2010. Citation on page 44.

DAVIS, A. K.; SO, S.; LANCELOTTA, R.; BARSUGLIA, J. P.; GRIFFITHS, R. R. 5-methoxy-n, n-dimethyltryptamine (5-meo-dmt) used in a naturalistic group setting is associated with unintended improvements in depression and anxiety. **The American journal of drug and alcohol abuse**, Taylor & Francis, v. 45, n. 2, p. 161–169, 2019. Citations on pages 82 and 97.

DEHMER, M.; MOWSHOWITZ, A. A history of graph entropy measures. **Information Sciences**, Elsevier, v. 181, n. 1, p. 57–78, 2011. Citations on pages 63, 87, 109, and 131.

DELGADO-GARCÍA, J. Estructura y función del cerebelo. **Rev Neurol**, v. 33, n. 7, p. 635–642, 2001. Citation on page 120.

DERAMUS, T. P.; BLACK, B. S.; PENNICK, M. R.; KANA, R. K. Enhanced parietal cortex activation during location detection in children with autism. **Journal of neurodevelopmental disorders**, Springer, v. 6, n. 1, p. 1–10, 2014. Citation on page 102.

DEVI, B.; KUMAR, S.; SHANKAR, V. G. *et al.* Anadata: A novel approach for data analytics using random forest tree and svm. In: **Computing, Communication and Signal Processing**. [S.l.]: Springer, 2019. p. 511–521. Citation on page 104.

DEY, S.; RAO, A. R.; SHAH, M. Attributed graph distance measure for automatic detection of attention deficit hyperactive disordered subjects. **Frontiers in neural circuits**, Frontiers, v. 8, p. 64, 2014. Citations on pages 59 and 83.

DIJK, K. R. V.; HEDDEN, T.; VENKATARAMAN, A.; EVANS, K. C.; LAZAR, S. W.; BUCKNER, R. L. Intrinsic functional connectivity as a tool for human connectomics: theory, properties, and optimization. **Journal of neurophysiology**, Am Physiological Soc, v. 103, n. 1, p. 297–321, 2010. Citation on page 82.

DING, Y.; SOHN, J. H.; KAWCZYNSKI, M. G.; TRIVEDI, H.; HARNISH, R.; JENKINS, N. W.; LITUIEV, D.; COPELAND, T. P.; ABOIAN, M. S.; APARICI, C. M. *et al.* A deep learning model to predict a diagnosis of alzheimer disease by using 18f-fdg pet of the brain. **Radiology**, Radiological Society of North America, v. 290, n. 2, p. 456–464, 2019. Citation on page 44.

DIYKH, M.; LI, Y.; WEN, P. Classify epileptic eeg signals using weighted complex networks based community structure detection. **Expert Systems with Applications**, Elsevier, v. 90, p. 87–100, 2017. Citations on pages 45, 59, 82, and 83.

DOKE, P.; SHRIVASTAVA, D.; PAN, C.; ZHOU, Q.; ZHANG, Y.-D. Using cnn with bayesian optimization to identify cerebral micro-bleeds. **Machine Vision and Applications**, Springer, v. 31, p. 1–14, 2020. Citation on page 48.

DOLGIN, E. How to defeat dementia. **Nature News**, v. 539, n. 7628, p. 156, 2016. Citation on page 44.

DONG, D.; WANG, Y.; CHANG, X.; LUO, C.; YAO, D. Dysfunction of large-scale brain networks in schizophrenia: a meta-analysis of resting-state functional connectivity. **Schizophrenia bulletin**, Oxford University Press US, v. 44, n. 1, p. 168–181, 2018. Citation on page 125.

DOYLE, J.; GRAVER, J. Mean distance in a graph. **Discrete Mathematics**, Elsevier, v. 17, n. 2, p. 147–154, 1977. Citations on pages 63, 87, 109, and 131.

DOYON, J.; MILNER, B. Right temporal-lobe contribution to global visual processing. **Neuropsychologia**, Elsevier, v. 29, n. 5, p. 343–360, 1991. Citation on page 96.

DUFF, B. J.; MACRITCHIE, K. A.; MOORHEAD, T. W.; LAWRIE, S. M.; BLACKWOOD, D. H. Human brain imaging studies of disc1 in schizophrenia, bipolar disorder and depression: a systematic review. **Schizophrenia research**, Elsevier, v. 147, n. 1, p. 1–13, 2013. Citation on page 143.

DUFFAU, H.; CAPELLE, L.; DENVIL, D.; GATIGNOL, P.; SICHEZ, N.; LOPES, M.; SICHEZ, J.-P.; EFFENTERRE, R. V. The role of dominant premotor cortex in language: a study using intraoperative functional mapping in awake patients. **Neuroimage**, Elsevier, v. 20, n. 4, p. 1903–1914, 2003. Citation on page 139.

DUKART, J.; WEIS, S.; GENON, S.; EICKHOFF, S. B. Towards increasing the clinical applicability of machine learning biomarkers in psychiatry. **Nature Human Behaviour**, Nature Publishing Group, v. 5, n. 4, p. 431–432, 2021. Citations on pages 60, 89, 108, and 130.

DUNEJA, A.; PUYALNITHI, T.; VANKADARA, M. V.; CHILAMKURTI, N. Analysis of inter-concept dependencies in disease diagnostic cognitive maps using recurrent neural network and genetic algorithms in time series clinical data for targeted treatment. **Journal of Ambient Intelligence and Humanized Computing**, Springer, v. 10, n. 10, p. 3915–3923, 2019. Citation on page 46.

D'SOUZA, R. N.; HUANG, P.-Y.; YEH, F.-C. Structural analysis and optimization of convolutional neural networks with a small sample size. **Scientific reports**, Nature Publishing Group, v. 10, n. 1, p. 1–13, 2020. Citation on page 103.

EBADI, A.; ROCHA, J. L. Dalboni da; NAGARAJU, D. B.; TOVAR-MOLL, F.; BRAMATI, I.; COUTINHO, G.; SITARAM, R.; RASHIDI, P. Ensemble classification of alzheimer's disease and mild cognitive impairment based on complex graph measures from diffusion tensor images. **Frontiers in neuroscience**, Frontiers, v. 11, p. 56, 2017. Citation on page 74.

EKANAYAKE, I.; MEDDAGE, D.; RATHNAYAKE, U. A novel approach to explain the black-box nature of machine learning in compressive strength predictions of concrete using shapley additive explanations (shap). **Case Studies in Construction Materials**, Elsevier, p. e01059, 2022. Citations on pages 38, 83, and 103.

ELBERT, T.; LUTZENBERGER, W.; ROCKSTROH, B.; BERG, P.; COHEN, R. Physical aspects of the eeg in schizophrenics. **Biological psychiatry**, Elsevier, v. 32, n. 7, p. 595–606, 1992. Citation on page 132.

EPPSTEIN, D.; PATERSON, M. S.; YAO, F. F. On nearest-neighbor graphs. **Discrete & Computational Geometry**, Springer, v. 17, n. 3, p. 263–282, 1997. Citations on pages 63, 87, 109, and 131.

ESTEVA, A.; ROBICQUET, A.; RAMSUNDAR, B.; KULESHOV, V.; DEPRISTO, M.; CHOU, K.; CUI, C.; CORRADO, G.; THRUN, S.; DEAN, J. A guide to deep learning in healthcare. **Nature medicine**, Nature Publishing Group, v. 25, n. 1, p. 24–29, 2019. Citation on page 38.

EUSTON, D. R.; GRUBER, A. J.; MCNAUGHTON, B. L. The role of medial prefrontal cortex in memory and decision making. **Neuron**, Elsevier, v. 76, n. 6, p. 1057–1070, 2012. Citation on page 102.

EZPELETA, L.; NAVARRO, J. B.; OSA, N. de la; TREPAT, E.; PENELO, E. Life conditions during covid-19 lockdown and mental health in spanish adolescents. **International journal of**

environmental research and public health, MDPI, v. 17, n. 19, p. 7327, 2020. Citation on page 35.

FALK, T. H.; FRAGA, F. J.; TRAMBAIOLLI, L.; ANGHINAH, R. Eeg amplitude modulation analysis for semi-automated diagnosis of alzheimer's disease. **EURASIP Journal on Advances in Signal Processing**, Springer, v. 2012, n. 1, p. 1–9, 2012. Citation on page 44.

FALLANI, F. D. V.; RODRIGUES, F. A.; COSTA, L. da F.; ASTOLFI, L.; CINCOTTI, F.; MATTIA, D.; SALINARI, S.; BABILONI, F. Multiple pathways analysis of brain functional networks from eeg signals: an application to real data. **Brain Topography**, Springer, v. 23, n. 4, p. 344–354, 2011. Citation on page 53.

____. Multiple pathways analysis of brain functional networks from eeg signals: an application to real data. **Brain topography**, Springer, v. 23, n. 4, p. 344–354, 2011. Citations on pages 87, 103, and 126.

FARNES, N.; JUEL, B. E.; NILSEN, A. S.; ROMUNDSTAD, L. G.; STORM, J. F. Increased signal diversity/complexity of spontaneous eeg, but not evoked eeg responses, in ketamine-induced psychedelic state in humans. **Plos one**, Public Library of Science San Francisco, CA USA, v. 15, n. 11, p. e0242056, 2020. Citations on pages 99 and 149.

FEKETE, T.; ZACH, N.; MUJICA-PARODI, L. R.; TURNER, M. R. Multiple kernel learning captures a systems-level functional connectivity biomarker signature in amyotrophic lateral sclerosis. **PloS one**, Public Library of Science San Francisco, USA, v. 8, n. 12, p. e85190, 2013. Citations on pages 57 and 82.

FELICIAN, O.; ROMAIGUÈRE, P.; ANTON, J.-L.; NAZARIAN, B.; ROTH, M.; PONCET, M.; ROLL, J.-P. The role of human left superior parietal lobule in body part localization. **Annals of Neurology: Official Journal of the American Neurological Association and the Child Neurology Society**, Wiley Online Library, v. 55, n. 5, p. 749–751, 2004. Citation on page 140.

FERGUSON, A. R.; NIELSON, J. L.; CRAGIN, M. H.; BANDROWSKI, A. E.; MARTONE, M. E. Big data from small data: data-sharing in the'long tail'of neuroscience. **Nature neuroscience**, Nature Publishing Group, v. 17, n. 11, p. 1442–1447, 2014. Citation on page 103.

FERNÁNDEZ, X.; FÁBREGAS, J. M. Experience of treatment with ayahuasca for drug addiction in the brazilian amazon. In: **The therapeutic use of ayahuasca**. [S.l.]: Springer, 2014. p. 161–182. Citation on page 57.

FERRARI, A. J.; NORMAN, R. E.; FREEDMAN, G.; BAXTER, A. J.; PIRKIS, J. E.; HARRIS, M. G.; PAGE, A.; CARNAHAN, E.; DEGENHARDT, L.; VOS, T. *et al.* The burden attributable to mental and substance use disorders as risk factors for suicide: findings from the global burden of disease study 2010. **PloS one**, Public Library of Science, v. 9, n. 4, p. e91936, 2014. Citations on pages 35 and 192.

FLEISCHHACKER, W. W.; ARANGO, C.; ARTEEL, P.; BARNES, T. R.; CARPENTER, W.; DUCKWORTH, K.; GALDERISI, S.; HALPERN, L.; KNAPP, M.; MARDER, S. R. *et al.* Schizophrenia—time to commit to policy change. **Schizophrenia bulletin**, Oxford University Press US, v. 40, n. Suppl_3, p. S165–S194, 2014. Citation on page 44.

FONG, R. C.; SCHEIRER, W. J.; COX, D. D. Using human brain activity to guide machine learning. **Scientific reports**, Nature Publishing Group, v. 8, n. 1, p. 1–10, 2018. Citations on pages 38 and 83.

FORMISANO, E.; KIM, D.-S.; SALLE, F. D.; MOORTELE, P.-F. Van de; UGURBIL, K.; GOEBEL, R. Mirror-symmetric tonotopic maps in human primary auditory cortex. **Neuron**, Elsevier, v. 40, n. 4, p. 859–869, 2003. Citations on pages 103 and 126.

FORNITO, A.; ZALESKY, A.; BULLMORE, E. **Fundamentals of brain network analysis**. [S.l.]: Academic Press, 2016. Citation on page 82.

FRANCISCO, P. M. S. B.; DONALISIO, M. R.; BARROS, M. B. d. A.; CESAR, C. L. G.; CARANDINA, L.; GOLDBAUM, M. Medidas de associação em estudo transversal com delineamento complexo: razão de chances e razão de prevalência. **Revista Brasileira de Epidemiologia**, SciELO Public Health, v. 11, p. 347–355, 2008. Citation on page 36.

FRANZMEIER, N.; NEITZEL, J.; RUBINSKI, A.; SMITH, R.; STRANDBERG, O.; OSSENKOPPELE, R.; HANSSON, O.; EWERS, M. Functional brain architecture is associated with the rate of tau accumulation in alzheimer's disease. **Nature communications**, Nature Publishing Group, v. 11, n. 1, p. 1–17, 2020. Citation on page 37.

FRECSKA, E.; BOKOR, P.; WINKELMAN, M. The therapeutic potentials of ayahuasca: possible effects against various diseases of civilization. **Frontiers in pharmacology**, Frontiers, v. 7, p. 35, 2016. Citations on pages 57 and 76.

FREEMAN, L. C. A set of measures of centrality based on betweenness. **Sociometry**, JSTOR, p. 35–41, 1977. Citations on pages 63, 87, 109, and 131.

____. Centrality in social networks conceptual clarification. **Social networks**, North-Holland, v. 1, n. 3, p. 215–239, 1978. Citations on pages 63, 74, 87, 97, 109, and 131.

FRIED, E. I.; BORKULO, C. D. van; CRAMER, A. O.; BOSCHLOO, L.; SCHOEVERS, R. A.; BORSBOOM, D. Mental disorders as networks of problems: a review of recent insights. **Social Psychiatry and Psychiatric Epidemiology**, Springer, v. 52, n. 1, p. 1–10, 2017. Citations on pages 37 and 44.

FRIEDMAN, J. H. Greedy function approximation: a gradient boosting machine. **Annals of statistics**, JSTOR, p. 1189–1232, 2001. Citations on pages 60 and 194.

FRIEDMAN, N.; GEIGER, D.; GOLDSZMIDT, M. Bayesian network classifiers. **Machine learning**, Springer, v. 29, n. 2, p. 131–163, 1997. Citations on pages 60, 108, and 194.

FRISTON, K. J.; FRITH, C. D. Schizophrenia: a disconnection syndrome. **Clinical Neuroscience**, v. 3, n. 2, p. 89–97, 1995. Citation on page 125.

FROHLICH, J.; REITER, L. T.; SARAVANAPANDIAN, V.; DISTEFANO, C.; HUBERTY, S.; HYDE, C.; CHAMBERLAIN, S.; BEARDEN, C. E.; GOLSHANI, P.; IRIMIA, A. *et al.* Mechanisms underlying the eeg biomarker in dup15q syndrome. **Molecular autism**, BioMed Central, v. 10, n. 1, p. 1–15, 2019. Citation on page 149.

FROHLICH, J.; TOKER, D.; MONTI, M. M. Consciousness among delta waves: a paradox? **Brain**, Oxford University Press, v. 144, n. 8, p. 2257–2277, 2021. Citation on page 95.

FROOD, A. Ayahuasca psychedelic tested for depression. **Nature News**, 2015. Citation on page 57.

GAINOTTI, G. Face familiarity feelings, the right temporal lobe and the possible underlying neural mechanisms. **Brain research reviews**, Elsevier, v. 56, n. 1, p. 214–235, 2007. Citation on page 96.

GARRITY, A. G.; PEARLSON, G. D.; MCKIERNAN, K.; LLOYD, D.; KIEHL, K. A.; CALHOUN, V. D. Aberrant "default mode" functional connectivity in schizophrenia. **American journal of psychiatry**, Am Psychiatric Assoc, v. 164, n. 3, p. 450–457, 2007. Citation on page 37.

GAUJAC, A.; FORD, J. L.; DEMPSTER, N. M.; ANDRADE, J. B. de; BRANDT, S. D. Investigations into the polymorphic properties of n, n-dimethyltryptamine by x-ray diffraction and differential scanning calorimetry. **Microchemical Journal**, Elsevier, v. 110, p. 146–157, 2013. Citation on page 81.

GEERLIGS, L.; HENSON, R. N. *et al.* Functional connectivity and structural covariance between regions of interest can be measured more accurately using multivariate distance correlation. **NeuroImage**, Elsevier, v. 135, p. 16–31, 2016. Citation on page 38.

GIOVANNETTI, C.; ARCE, S. G.; RUSH, B.; MENDIVE, F. Pilot evaluation of a residential drug addiction treatment combining traditional amazonian medicine, ayahuasca and psychotherapy on depression and anxiety. **Journal of Psychoactive Drugs**, Taylor & Francis, v. 52, n. 5, p. 472–481, 2020. Citation on page 57.

GIRN, M.; MILLS, C.; ROSEMAN, L.; CARHART-HARRIS, R. L.; CHRISTOFF, K. Updating the dynamic framework of thought: creativity and psychedelics. **Neuroimage**, Elsevier, v. 213, p. 116726, 2020. Citation on page 82.

GIRVAN, M.; NEWMAN, M. E. Community structure in social and biological networks. **Proceedings of the national academy of sciences**, National Acad Sciences, v. 99, n. 12, p. 7821–7826, 2002. Citations on pages 63, 65, 88, 109, and 131.

GOLBECK, J. **Analyzing the social web**. [S.l.]: Newnes, 2013. Citation on page 144.

GOMEZ-PILAR, J.; LUIS-GARCÍA, R. de; LUBEIRO, A.; URIBE, N. de; POZA, J.; NÚÑEZ, P.; AYUSO, M.; HORNERO, R.; MOLINA, V. Deficits of entropy modulation in schizophrenia are predicted by functional connectivity strength in the theta band and structural clustering. **NeuroImage: Clinical**, Elsevier, v. 18, p. 382–389, 2018. Citation on page 143.

GOÑI, J.; AVENA-KOENIGSBERGER, A.; MENDIZABAL, N. Velez de; HEUVEL, M. P. van den; BETZEL, R. F.; SPORNS, O. Exploring the morphospace of communication efficiency in complex networks. **PLoS One**, Public Library of Science San Francisco, USA, v. 8, n. 3, p. e58070, 2013. Citation on page 87.

GOODFELLOW, I.; BENGIO, Y.; COURVILLE, A. **Deep learning**. [S.l.]: MIT press, 2016. Citations on pages 45, 48, and 209.

GOTTESMAN, I. I.; SHIELDS, J. **Schizophrenia**. [S.l.]: CUP Archive, 1982. Citation on page 44.

GRAMFORT, A.; LUESSI, M.; LARSON, E.; ENGEMANN, D. A.; STROHMEIER, D.; BRODBECK, C.; GOJ, R.; JAS, M.; BROOKS, T.; PARKKONEN, L. *et al.* Meg and eeg data analysis with mne-python. **Frontiers in neuroscience**, Frontiers, v. 7, p. 267, 2013. Citations on pages 22, 86, and 197.

GRANGER, C. W. Investigating causal relations by econometric models and cross-spectral methods. **Econometrica: journal of the Econometric Society**, JSTOR, p. 424–438, 1969. Citations on pages 47, 106, and 129.

GREICIUS, M. D.; FLORES, B. H.; MENON, V.; GLOVER, G. H.; SOLVASON, H. B.; KENNA, H.; REISS, A. L.; SCHATZBERG, A. F. Resting-state functional connectivity in major depression: abnormally increased contributions from subgenual cingulate cortex and thalamus. **Biological psychiatry**, Elsevier, v. 62, n. 5, p. 429–437, 2007. Citation on page 37.

GREICIUS, M. D.; SRIVASTAVA, G.; REISS, A. L.; MENON, V. Default-mode network activity distinguishes alzheimer's disease from healthy aging: evidence from functional mri. **Proceedings of the National Academy of Sciences**, National Acad Sciences, v. 101, n. 13, p. 4637–4642, 2004. Citation on page 37.

GRIFFA, A.; BAUMANN, P. S.; FERRARI, C.; DO, K. Q.; CONUS, P.; THIRAN, J.-P.; HAGMANN, P. Characterizing the connectome in schizophrenia with diffusion spectrum imaging. **Human brain mapping**, Wiley Online Library, v. 36, n. 1, p. 354–366, 2015. Citation on page 144.

GUERRA, A. D.; AHMAD, S.; AVRAM, M.; BELCARI, N.; BERNEKING, A.; BIAGI, L.; BISOGNI, M. G.; BRANDL, F.; CABELLO, J.; CAMARLINGHI, N. *et al.* Trimage: A dedicated trimodality (pet/mr/eeg) imaging tool for schizophrenia. **European Psychiatry**, Cambridge University Press, v. 50, p. 7–20, 2018. Citation on page 44.

HABIBABAD, A. S.; MAHDINEJAD, J.-e.-D.; AZEMATI, H.; MATRACCHI, P. Using neurology sciences to investigate the color component and its effect on promoting the sense of spirituality in the interior space of the vakil mosque of shiraz (using quantitative electroencephalography wave recording). **Journal of Religion and Health**, Springer, p. 1–18, 2019. Citation on page 95.

HACK, L. M.; ZHANG, X.; WILLIAMS, L. M. Striato-cortical neuroimaging markers in the reward network distinguish melancholic depression and response to treatment: An ispot-d report. **Biological Psychiatry**, Elsevier, v. 89, n. 9, p. S270, 2021. Citation on page 110.

HAFKEMEIJER, A.; GROND, J. van der; ROMBOUTS, S. A. Imaging the default mode network in aging and dementia. **Biochimica et Biophysica Acta (BBA)-Molecular Basis of Disease**, Elsevier, v. 1822, n. 3, p. 431–441, 2012. Citation on page 37.

HAGE, P.; HARARY, F. Eccentricity and centrality in networks. **Social networks**, Elsevier, v. 17, n. 1, p. 57–63, 1995. Citations on pages 63, 87, 109, and 131.

HAGMANN, P.; CAMMOUN, L.; GIGANDET, X.; MEULI, R.; HONEY, C. J.; WEDEEN, V. J.; SPORNS, O. Mapping the structural core of human cerebral cortex. **PLoS biology**, Public Library of Science San Francisco, USA, v. 6, n. 7, p. e159, 2008. Citation on page 120.

HAJEBRAHIMI, F.; VELIOGLU, H. A.; BAYRAKTAROGLU, Z.; YILMAZ, N. H.; HANOGLU, L. Clinical evaluation and resting state fmri analysis of virtual reality based training in parkinson's disease through a randomized controlled trial. **Scientific Reports**, Nature Publishing Group, v. 12, n. 1, p. 1–13, 2022. Citation on page 110.

HAMILTON, J. P.; SACCHET, M. D.; HJØRNEVIK, T.; CHIN, F. T.; SHEN, B.; KÄMPE, R.; PARK, J. H.; KNUTSON, B. D.; WILLIAMS, L. M.; BORG, N. *et al.* Striatal dopamine deficits predict reductions in striatal functional connectivity in major depression: A concurrent

11 c-raclopride positron emission tomography and functional magnetic resonance imaging investigation. **Translational psychiatry**, Nature Publishing Group, v. 8, n. 1, p. 1–10, 2018. Citation on page 37.

HAN, C.; SUN, X.; YANG, Y.; CHE, Y.; QIN, Y. Brain complex network characteristic analysis of fatigue during simulated driving based on electroencephalogram signals. **Entropy**, Multidisciplinary Digital Publishing Institute, v. 21, n. 4, p. 353, 2019. Citations on pages 63 and 87.

HANNUN, A. Y.; RAJPURKAR, P.; HAGHPANAHI, M.; TISON, G. H.; BOURN, C.; TURAKHIA, M. P.; NG, A. Y. Cardiologist-level arrhythmia detection and classification in ambulatory electrocardiograms using a deep neural network. **Nature medicine**, Nature Publishing Group, v. 25, n. 1, p. 65–69, 2019. Citations on pages 60, 89, and 108.

HARDOON, D. R.; SHAWE-TAYLOR, J. Sparse canonical correlation analysis. **Machine Learning**, Springer, v. 83, n. 3, p. 331–353, 2011. Citations on pages 107 and 129.

HAYASHIDA, M.; AKUTSU, T. Complex network-based approaches to biomarker discovery. **Biomarkers in medicine**, Future Medicine, v. 10, n. 6, p. 621–632, 2016. Citations on pages 57 and 82.

HENSHALL, K. R.; SERGEJEW, A. A.; RANCE, G.; MCKAY, C. M.; COPOLOV, D. L. Interhemispheric eeg coherence is reduced in auditory cortical regions in schizophrenia patients with auditory hallucinations. **International journal of psychophysiology**, Elsevier, v. 89, n. 1, p. 63–71, 2013. Citation on page 141.

HERNANDEZ, L. M.; RUDIE, J. D.; GREEN, S. A.; BOOKHEIMER, S.; DAPRETTO, M. Neural signatures of autism spectrum disorders: insights into brain network dynamics. **Neuropsychopharmacology**, Nature Publishing Group, v. 40, n. 1, p. 171–189, 2015. Citation on page 37.

HEUVEL, M. P. V. D.; POL, H. E. H. Exploring the brain network: a review on resting-state fmri functional connectivity. **European neuropsychopharmacology**, Elsevier, v. 20, n. 8, p. 519–534, 2010. Citation on page 37.

HILGETAG, C.-C.; BURNS, G. A.; O'NEILL, M. A.; SCANNELL, J. W.; YOUNG, M. P. Anatomical connectivity defines the organization of clusters of cortical areas in the macaque and the cat. **Philosophical Transactions of the Royal Society of London B: Biological Sciences**, The Royal Society, v. 355, n. 1393, p. 91–110, 2000. Citation on page 82.

HINTON, G.; RUMELHART, D.; WILLIAMS, R. Learning internal representations by error propagation. **Parallel distributed processing**, MIT Press, v. 1, p. 318–362, 1986. Citations on pages 60, 108, and 194.

HJORTH, B. Eeg analysis based on time domain properties. **Electroencephalography and clinical neurophysiology**, Elsevier, v. 29, n. 3, p. 306–310, 1970. Citation on page 143.

____. Time domain descriptors and their relation to a particular model for generation of eeg activity. **CEAN-Computerized EEG analysis**, p. 3–8, 1975. Citation on page 132.

____. Physical aspects of eeg data as a basis for topographic mapping. **Topographic mapping of brain electrical activity**, Butterworths Boston, p. 175–194, 1986. Citation on page 132.

HOCHREITER, S.; SCHMIDHUBER, J. Long short-term memory. **Neural computation**, MIT Press, v. 9, n. 8, p. 1735–1780, 1997. Citation on page 130.

HOERTEL, N.; FRANCO, S.; WALL, M.; OQUENDO, M.; KERRIDGE, B.; LIMOSIN, F.; BLANCO, C. Mental disorders and risk of suicide attempt: a national prospective study. **Molecular psychiatry**, Nature Publishing Group, v. 20, n. 6, p. 718, 2015. Citation on page 35.

HOSOZAWA, M.; SACKER, A.; CABLE, N. Timing of diagnosis, depression and self-harm in adolescents with autism spectrum disorder. **Autism**, SAGE Publications Sage UK: London, England, v. 25, n. 1, p. 70–78, 2021. Citation on page 102.

HOSSEINI, A.; CHEN, T.; WU, W.; SUN, Y.; SARRAFZADEH, M. Heteromed: Heterogeneous information network for medical diagnosis. In: ACM. **Proceedings of the 27th ACM International Conference on Information and Knowledge Management**. [S.l.], 2018. p. 763–772. Citation on page 38.

HUBEL, D. H.; WIESEL, T. N. Receptive fields, binocular interaction and functional architecture in the cat's visual cortex. **The Journal of Physiology**, Wiley-Blackwell, v. 160, n. 1, p. 106, 1962. Citation on page 48.

HUFFMAN, D. A. A method for the construction of minimum-redundancy codes. **Proceedings of the IRE**, IEEE, v. 40, n. 9, p. 1098–1101, 1952. Citation on page 65.

HUHN, M.; NIKOLAKOPOULOU, A.; SCHNEIDER-THOMA, J.; KRAUSE, M.; SAMARA, M.; PETER, N.; ARNDT, T.; BÄCKERS, L.; ROTHE, P.; CIPRIANI, A. *et al.* Comparative efficacy and tolerability of 32 oral antipsychotics for the acute treatment of adults with multi-episode schizophrenia: a systematic review and network meta-analysis. **The Lancet**, Elsevier, v. 394, n. 10202, p. 939–951, 2019. Citation on page 125.

HUTTER, F.; LÜCKE, J.; SCHMIDT-THIEME, L. Beyond manual tuning of hyperparameters. **KI-Künstliche Intelligenz**, Springer, v. 29, n. 4, p. 329–337, 2015. Citation on page 48.

HYDE, K. K.; NOVACK, M. N.; LAHAYE, N.; PARLETT-PELLERITI, C.; ANDEN, R.; DIXON, D. R.; LINSTEAD, E. Applications of supervised machine learning in autism spectrum disorder research: a review. **Review Journal of Autism and Developmental Disorders**, Springer, v. 6, n. 2, p. 128–146, 2019. Citations on pages 25, 103, and 104.

ILYASOVA, N.; KUPRIYANOV, A.; PARINGER, R.; KIRSH, D. Particular use of big data in medical diagnostic tasks. **Pattern Recognition and Image Analysis**, Springer, v. 28, n. 1, p. 114–121, 2018. Citations on pages 38, 58, and 82.

ISLAM, J.; ZHANG, Y. Brain mri analysis for alzheimer's disease diagnosis using an ensemble system of deep convolutional neural networks. **Brain informatics**, Springer, v. 5, n. 2, p. 1–14, 2018. Citation on page 46.

ITO, Y.; UNAGAMI, M.; YAMABE, F.; MITSUI, Y.; NAKAJIMA, K.; NAGAO, K.; KOBAYASHI, H. A method for utilizing automated machine learning for histopathological classification of testis based on johnsen scores. **Scientific reports**, Nature Publishing Group, v. 11, n. 1, p. 1–11, 2021. Citations on pages 60, 89, 108, and 130.

JAHMUNAH, V.; OH, S. L.; RAJINIKANTH, V.; CIACCIO, E. J.; CHEONG, K. H.; ARUNKUMAR, N.; ACHARYA, U. R. Automated detection of schizophrenia using nonlinear signal processing methods. **Artificial intelligence in medicine**, Elsevier, v. 100, p. 101698, 2019. Citation on page 44.

JALILI, M. Functional brain networks: does the choice of dependency estimator and binarization method matter? **Scientific reports**, Nature Publishing Group, v. 6, n. 1, p. 1–12, 2016. Citations on pages 63 and 87.

JANGHEL, R.; RATHORE, Y. Deep convolution neural network based system for early diagnosis of alzheimer's disease. **IRBM**, Elsevier, v. 42, n. 4, p. 258–267, 2021. Citation on page 53.

JAWORSKA, N.; SALLE, S. De la; IBRAHIM, M.-H.; BLIER, P.; KNOTT, V. Leveraging machine learning approaches for predicting antidepressant treatment response using electroencephalography (eeg) and clinical data. **Frontiers in psychiatry**, Frontiers Media SA, v. 9, p. 768, 2019. Citation on page 149.

JAYARATHNE, I.; COHEN, M.; AMARAKEERTHI, S. Person identification from eeg using various machine learning techniques with inter-hemispheric amplitude ratio. **PloS one**, Public Library of Science San Francisco, CA USA, v. 15, n. 9, p. e0238872, 2020. Citation on page 58.

JEREMY, D.; SCHMAHMANN, J. The cerebellum and cognition. **Neuroscience Letters**, v. 688, p. 62–75, 2019. Citation on page 120.

JIE, B.; LIU, M.; LIAN, C.; SHI, F.; SHEN, D. Designing weighted correlation kernels in convolutional neural networks for functional connectivity based brain disease diagnosis. **Medical image analysis**, Elsevier, v. 63, p. 101709, 2020. Citation on page 104.

JIMÉNEZ-GARRIDO, D. F.; GÓMEZ-SOUSA, M.; ONA, G.; SANTOS, R. G. D.; HALLAK, J. E.; ALCÁZAR-CÓRCOLES, M. Á.; BOUSO, J. C. Effects of ayahuasca on mental health and quality of life in naïve users: A longitudinal and cross-sectional study combination. **Scientific reports**, Nature Publishing Group, v. 10, n. 1, p. 1–12, 2020. Citations on pages 57 and 72.

JOHNSON, M. W.; RICHARDS, W. A.; GRIFFITHS, R. R. Human hallucinogen research: guidelines for safety. **Journal of psychopharmacology**, Sage Publications Sage UK: London, England, v. 22, n. 6, p. 603–620, 2008. Citation on page 59.

JONES, P. J.; HEEREN, A.; MCNALLY, R. J. Commentary: A network theory of mental disorders. **Frontiers in psychology**, Frontiers, v. 8, p. 1305, 2017. Citation on page 37.

JR, C. R. J.; LOWE, V. J.; WEIGAND, S. D.; WISTE, H. J.; SENJEM, M. L.; KNOPMAN, D. S.; SHIUNG, M. M.; GUNTER, J. L.; BOEVE, B. F.; KEMP, B. J. *et al.* Serial pib and mri in normal, mild cognitive impairment and alzheimer's disease: implications for sequence of pathological events in alzheimer's disease. **Brain**, Oxford University Press, v. 132, n. 5, p. 1355–1365, 2009. Citation on page 44.

JUNG, T.-P.; MAKEIG, S.; HUMPHRIES, C.; LEE, T.-W.; MCKEOWN, M. J.; IRAGUI, V.; SEJNOWSKI, T. J. Removing electroencephalographic artifacts by blind source separation. **Psychophysiology**, Cambridge University Press, v. 37, n. 2, p. 163–178, 2000. Citation on page 86.

KAISER, R. H.; WHITFIELD-GABRIELI, S.; DILLON, D. G.; GOER, F.; BELTZER, M.; MINKEL, J.; SMOSKI, M.; DICHTER, G.; PIZZAGALLI, D. A. Dynamic resting-state functional connectivity in major depression. **Neuropsychopharmacology**, Nature Publishing Group, v. 41, n. 7, p. 1822–1830, 2016. Citation on page 37.

KASHIPAREKH, K.; NARWARIYA, J.; MALHOTRA, P.; VIG, L.; SHROFF, G. Convtimenet: A pre-trained deep convolutional neural network for time series classification. In: IEEE. **2019 International Joint Conference on Neural Networks (IJCNN)**. [S.l.], 2019. p. 1–8. Citation on page 46.

KATCHBORIAN-NETO, A.; SANTOS, W. T.; NICÁCIO, K. J.; CORRÊA, J. O.; MURGU, M.; MARTINS, T. M.; GOMES, D. A.; GOES, A. M.; SOARES, M. G.; DIAS, D. F. *et al.* Neuroprotective potential of ayahuasca and untargeted metabolomics analyses: applicability to parkinson's disease. **Journal of ethnopharmacology**, Elsevier, v. 255, p. 112743, 2020. Citation on page 57.

KAUFMANN, T.; ALNÆS, D.; DOAN, N. T.; BRANDT, C. L.; ANDREASSEN, O. A.; WESTLYE, L. T. Delayed stabilization and individualization in connectome development are related to psychiatric disorders. **Nature neuroscience**, Nature Publishing Group, v. 20, n. 4, p. 513–515, 2017. Citation on page 38.

KAWAMOTO, T.; KABASHIMA, Y. Cross-validation estimate of the number of clusters in a network. **Scientific reports**, Nature Publishing Group, v. 7, n. 1, p. 1–17, 2017. Citations on pages 60, 88, 108, and 130.

KEANE, P. A.; TOPOL, E. J. **With an eye to AI and autonomous diagnosis**. [S.l.]: Nature Publishing Group, 2018. Citation on page 82.

KELLER, T. A.; KANA, R. K.; JUST, M. A. A developmental study of the structural integrity of white matter in autism. **Neuroreport**, LWW, v. 18, n. 1, p. 23–27, 2007. Citation on page 103.

KENNEDY, D. P.; REDCAY, E.; COURCHESNE, E. Failing to deactivate: resting functional abnormalities in autism. **Proceedings of the National Academy of Sciences**, National Acad Sciences, v. 103, n. 21, p. 8275–8280, 2006. Citations on pages 102 and 103.

KHAJEHPOUR, H.; MAKKIABADI, B.; EKHTIARI, H.; BAKHT, S.; NOROOZI, A.; MOHAGHEGHIAN, F. Disrupted resting-state brain functional network in methamphetamine abusers: A brain source space study by eeg. **PloS one**, Public Library of Science San Francisco, CA USA, v. 14, n. 12, p. e0226249, 2019. Citation on page 58.

KIM, J.; LEE, J.; PARK, E.; HAN, J. A deep learning model for detecting mental illness from user content on social media. **Scientific reports**, Nature Publishing Group, v. 10, n. 1, p. 1–6, 2020. Citations on pages 60, 89, 108, and 130.

KIM, J.; LEE, J.-G. Community detection in multi-layer graphs: A survey. **ACM SIGMOD Record**, ACM New York, NY, USA, v. 44, n. 3, p. 37–48, 2015. Citations on pages 57, 88, 109, and 131.

KLEINBERG, J. M. Hubs, authorities, and communities. **ACM computing surveys (CSUR)**, ACM New York, NY, USA, v. 31, n. 4es, p. 5–es, 1999. Citations on pages 63, 87, 109, and 131.

KLUG, M.; GRAMANN, K. Identifying key factors for improving ica-based decomposition of eeg data in mobile and stationary experiments. **European Journal of Neuroscience**, Wiley Online Library, v. 54, n. 12, p. 8406–8420, 2021. Citation on page 86.

KOENIGS, M.; BARBEY, A. K.; POSTLE, B. R.; GRAFMAN, J. Superior parietal cortex is critical for the manipulation of information in working memory. **Journal of Neuroscience**, Soc Neuroscience, v. 29, n. 47, p. 14980–14986, 2009. Citation on page 140.

KOH, H. C.; TAN, G. *et al.* Data mining applications in healthcare. **Journal of healthcare information management**, Citeseer, v. 19, n. 2, p. 65, 2011. Citation on page 38.

KORA, P.; MEENAKSHI, K.; SWARAJA, K.; RAJANI, A.; RAJU, M. S. Eeg based interpretation of human brain activity during yoga and meditation using machine learning: A systematic review. **Complementary Therapies in Clinical Practice**, Elsevier, v. 43, p. 101329, 2021. Citation on page 95.

KRAGEL, P. A.; LABAR, K. S. Decoding the nature of emotion in the brain. **Trends in cognitive sciences**, Elsevier, v. 20, n. 6, p. 444–455, 2016. Citations on pages 38 and 83.

KRASKOV, A.; STÖGBAUER, H.; GRASSBERGER, P. Estimating mutual information. **Physical review E**, APS, v. 69, n. 6, p. 066138, 2004. Citations on pages 107 and 129.

KRITTANAWONG, C.; VIRK, H. U. H.; KUMAR, A.; AYDAR, M.; WANG, Z.; STEWART, M. P.; HALPERIN, J. L. Machine learning and deep learning to predict mortality in patients with spontaneous coronary artery dissection. **Scientific reports**, Nature Publishing Group, v. 11, n. 1, p. 1–10, 2021. Citations on pages 60, 89, 108, and 130.

KUMAR, A.; NAYAR, K. R. **COVID 19 and its mental health consequences**. [S.l.]: Taylor & Francis, 2021. 1–2 p. Citation on page 35.

KUMAR, P.; SAINI, R.; ROY, P. P.; DOGRA, D. P. A bio-signal based framework to secure mobile devices. **Journal of Network and Computer Applications**, Elsevier, v. 89, p. 62–71, 2017. Citation on page 86.

LAIDI, C.; BOISGONTIER, J.; PIERREFEU, A. de; DUCHESNAY, E.; HOTIER, S.; D'ALBIS, M.-A.; DELORME, R.; BOLOGNANI, F.; CZECH, C.; BOUQUET, C. *et al.* Decreased cortical thickness in the anterior cingulate cortex in adults with autism. **Journal of Autism and Developmental Disorders**, Springer, v. 49, n. 4, p. 1402–1409, 2019. Citation on page 119.

LASHGARI, E.; LIANG, D.; MAOZ, U. Data augmentation for deep-learning-based electroencephalography. **Journal of Neuroscience Methods**, Elsevier, v. 346, p. 108885, 2020. Citation on page 104.

LATORA, V.; MARCHIORI, M. Economic small-world behavior in weighted networks. **The European Physical Journal B-Condensed Matter and Complex Systems**, Springer, v. 32, n. 2, p. 249–263, 2003. Citations on pages 63, 87, 109, and 131.

LAU, W. K.; LEUNG, M.-K.; ZHANG, R. Hypofunctional connectivity between the posterior cingulate cortex and ventromedial prefrontal cortex in autism: Evidence from coordinate-based imaging meta-analysis. **Progress in Neuro-Psychopharmacology and Biological Psychiatry**, Elsevier, v. 103, p. 109986, 2020. Citation on page 119.

LECUN, Y.; BENGIO, Y.; HINTON, G. Deep learning. **Nature**, Nature Publishing Group, v. 521, n. 7553, p. 436–444, 2015. Citations on pages 38 and 48.

LECUN, Y. *et al.* Generalization and network design strategies. **Connectionism in perspective**, Elsevier Zurich, Switzerland, v. 19, p. 143–155, 1989. Citation on page 48.

LEDOIT, O.; WOLF, M. Nonlinear shrinkage estimation of large-dimensional covariance matrices. **The Annals of Statistics**, Institute of Mathematical Statistics, v. 40, n. 2, p. 1024–1060, 2012. Citations on pages 107 and 129.

LEECH, R.; BRAGA, R.; SHARP, D. J. Echoes of the brain within the posterior cingulate cortex. **Journal of Neuroscience**, Soc Neuroscience, v. 32, n. 1, p. 215–222, 2012. Citation on page 138.

LEECH, R.; SHARP, D. J. The role of the posterior cingulate cortex in cognition and disease. **Brain**, Oxford University Press, v. 137, n. 1, p. 12–32, 2014. Citations on pages 119 and 138.

LEITE, I. d. C.; VALENTE, J. G.; SCHRAMM, J. M. d. A.; DAUMAS, R. P.; RODRIGUES, R. d. N.; SANTOS, M. d. F.; OLIVEIRA, A. F. d.; SILVA, R. S. d.; CAMPOS, M. R.; MOTA, J. C. d. Burden of disease in brazil and its regions, 2008. **Cadernos de saude publica**, SciELO Brasil, v. 31, n. 7, p. 1551–1564, 2015. Citation on page 191.

LEMPEL, A.; ZIV, J. On the complexity of finite sequences. **IEEE Transactions on information theory**, IEEE, v. 22, n. 1, p. 75–81, 1976. Citation on page 132.

LI, H.; ZHANG, R.; ZHAO, Z.; LIU, X. Lpa-mni: an improved label propagation algorithm based on modularity and node importance for community detection. **Entropy**, MDPI, v. 23, n. 5, p. 497, 2021. Citation on page 65.

LI, R.; SHINDE, A.; LIU, A.; GLASER, S.; LYOU, Y.; YUH, B.; WONG, J.; AMINI, A. Machine learning–based interpretation and visualization of nonlinear interactions in prostate cancer survival. **JCO Clinical Cancer Informatics**, American Society of Clinical Oncology, v. 4, p. 637–646, 2020. Citations on pages 38 and 83.

LI, R. C.; ASCH, S. M.; SHAH, N. H. Developing a delivery science for artificial intelligence in healthcare. **NPJ digital medicine**, Nature Publishing Group, v. 3, n. 1, p. 1–3, 2020. Citations on pages 58, 60, 89, 108, and 130.

LI, Y.; NOWAK, C. M.; PHAM, U.; NGUYEN, K.; BLERIS, L. Cell morphology-based machine learning models for human cell state classification. **NPJ systems biology and applications**, Nature Publishing Group, v. 7, n. 1, p. 1–9, 2021. Citations on pages 60, 89, 108, and 130.

LI, Y.; YANG, H.; LI, J.; CHEN, D.; DU, M. Eeg-based intention recognition with deep recurrent-convolution neural network: Performance and channel selection by grad-cam. **Neurocomputing**, Elsevier, v. 415, p. 225–233, 2020. Citation on page 104.

LINGNAU, A.; DOWNING, P. E. The lateral occipitotemporal cortex in action. **Trends in cognitive sciences**, Elsevier, v. 19, n. 5, p. 268–277, 2015. Citation on page 96.

LIU, J.; CHEN, H.; GAO, X.; CUI, M.; MA, L.; ZHENG, X.; GUAN, B.; MA, X. Surgical treatment of diffuse and multi-lobes involved glioma with the assistance of a multimodal technique. **Scientific Reports**, Nature Publishing Group, v. 12, n. 1, p. 1–12, 2022. Citation on page 110.

LIU, J. J.; BAO, Y.; HUANG, X.; SHI, J.; LU, L. Mental health considerations for children quarantined because of covid-19. **The Lancet Child & Adolescent Health**, Elsevier, v. 4, n. 5, p. 347–349, 2020. Citation on page 35.

LIU, Y.; LIANG, M.; ZHOU, Y.; HE, Y.; HAO, Y.; SONG, M.; YU, C.; LIU, H.; LIU, Z.; JIANG, T. Disrupted small-world networks in schizophrenia. **Brain**, Oxford University Press, v. 131, n. 4, p. 945–961, 2008. Citations on pages 37 and 125.

LOIWAL, M. 20% increase in patients with mental illness since coronavirus outbreak: Survey. **India Today**, v. 31, 2020. Citation on page 35.

LOPES, E. d. O. *et al.* Análise de medidas em grafos para conectividade funcional em redes de modo padrão na demência da doença de alzheimer leve utilizando técnicas de aprendizado de máquina. [sn], 2016. Citation on page 126.

LOPEZ, A. D.; MURRAY, C. C. The global burden of disease, 1990–2020. **Nature medicine**, Nature Publishing Group, v. 4, n. 11, p. 1241, 1998. Citation on page 191.

LÓPEZ-RISUEÑO, G.; GRAJAL, J.; HAYKIN, S.; DÍAZ-OLIVER, R. Convolutional neural networks for radar detection. In: SPRINGER. **International Conference on Artificial Neural Networks**. [S.l.], 2002. p. 1150–1155. Citation on page 48.

LORD, C.; BRUGHA, T. S.; CHARMAN, T.; CUSACK, J.; DUMAS, G.; FRAZIER, T.; JONES, E. J.; JONES, R. M.; PICKLES, A.; STATE, M. W. *et al.* Autism spectrum disorder. **Nature reviews Disease primers**, Nature Publishing Group, v. 6, n. 1, p. 1–23, 2020. Citation on page 102.

LOUWERSE, M.; HUTCHINSON, S. Neurological evidence linguistic processes precede perceptual simulation in conceptual processing. **Frontiers in psychology**, Frontiers, v. 3, p. 385, 2012. Citation on page 86.

LUBINSKI, D. Introduction to the special section on cognitive abilities: 100 years after spearman's (1904)"'general intelligence,'objectively determined and measured". **Journal of personality and social psychology**, American Psychological Association, v. 86, n. 1, p. 96, 2004. Citations on pages 47, 106, and 129.

LUNDBERG, S. M.; LEE, S.-I. A unified approach to interpreting model predictions. In: **Proceedings of the 31st international conference on neural information processing systems**. [S.l.: s.n.], 2017. p. 4768–4777. Citations on pages 38, 61, 83, and 103.

LUNG, R. I.; SUCIU, M.; MESZLÉNYI, R.; BUZA, K.; GASKÓ, N. Community structure detection for the functional connectivity networks of the brain. In: SPRINGER. **International Conference on Parallel Problem Solving from Nature**. [S.l.], 2016. p. 633–643. Citation on page 58.

LUO, W.; GREENE, A. S.; CONSTABLE, R. T. Within node connectivity changes, not simply edge changes, influence graph theory measures in functional connectivity studies of the brain. **NeuroImage**, Elsevier, v. 240, p. 118332, 2021. Citations on pages 98 and 144.

LUO, Y.; SUN, T.; MA, C.; ZHANG, X.; JI, Y.; FU, X.; NI, H. Alterations of brain networks in alzheimer's disease and mild cognitive impairment: A resting state fmri study based on a population-specific brain template. **Neuroscience**, Elsevier, v. 452, p. 192–207, 2021. Citation on page 76.

LUO, Y.; ZHU, L.-Z.; WAN, Z.-Y.; LU, B.-L. Data augmentation for enhancing eeg-based emotion recognition with deep generative models. **Journal of Neural Engineering**, IOP Publishing, v. 17, n. 5, p. 056021, 2020. Citation on page 104.

LUPPI, A. I.; CARHART-HARRIS, R. L.; ROSEMAN, L.; PAPPAS, I.; MENON, D. K.; STAMATAKIS, E. A. Lsd alters dynamic integration and segregation in the human brain. **NeuroImage**, Elsevier, v. 227, p. 117653, 2021. Citation on page 96.

LUSCH, B.; MAIA, P. D.; KUTZ, J. N. Inferring connectivity in networked dynamical systems: Challenges using granger causality. **Physical Review E**, APS, v. 94, n. 3, p. 032220, 2016. Citation on page 48.

LY, C.; GREB, A. C.; CAMERON, L. P.; WONG, J. M.; BARRAGAN, E. V.; WILSON, P. C.; BURBACH, K. F.; ZARANDI, S. S.; SOOD, A.; PADDY, M. R. *et al.* Psychedelics promote structural and functional neural plasticity. **Cell reports**, Elsevier, v. 23, n. 11, p. 3170–3182, 2018. Citation on page 81.

LYNCH, C. J.; LISTON, C. New machine-learning technologies for computer-aided diagnosis. **Nature medicine**, Nature Publishing Group, v. 24, n. 9, p. 1304–1305, 2018. Citation on page 82.

LYNN, C. W.; BASSETT, D. S. The physics of brain network structure, function and control. **Nature Reviews Physics**, Nature Publishing Group, v. 1, n. 5, p. 318–332, 2019. Citation on page 53.

MANSKE, R. H. A synthesis of the methyltryptamines and some derivatives. **Canadian Journal of Research**, NRC Research Press Ottawa, Canada, v. 5, n. 5, p. 592–600, 1931. Citation on page 81.

MARIËN, P.; BORGATTI, R. Language and the cerebellum. **Handbook of clinical neurology**, Elsevier, v. 154, p. 181–202, 2018. Citation on page 120.

MARTÍNEZ, K.; MARTÍNEZ-GARCÍA, M.; MARCOS-VIDAL, L.; JANSSEN, J.; CASTELLANOS, F. X.; PRETUS, C.; VILLARROYA, Ó.; PINA-CAMACHO, L.; DÍAZ-CANEJA, C. M.; PARELLADA, M. *et al.* Sensory-to-cognitive systems integration is associated with clinical severity in autism spectrum disorder. **Journal of the American Academy of Child & Adolescent Psychiatry**, Elsevier, v. 59, n. 3, p. 422–433, 2020. Citation on page 119.

MAZAHERI, A.; COFFEY-CORINA, S.; MANGUN, G. R.; BEKKER, E. M.; BERRY, A. S.; CORBETT, B. A. Functional disconnection of frontal cortex and visual cortex in attention-deficit/hyperactivity disorder. **Biological psychiatry**, Elsevier, v. 67, n. 7, p. 617–623, 2010. Citation on page 37.

MAZROOYISEBDANI, M.; NAIR, V. A.; GARCIA-RAMOS, C.; MOHANTY, R.; MEYERAND, E.; HERMANN, B.; PRABHAKARAN, V.; AHMED, R. Graph theory analysis of functional connectivity combined with machine learning approaches demonstrates widespread network differences and predicts clinical variables in temporal lobe epilepsy. **Brain connectivity**, Mary Ann Liebert, Inc., publishers 140 Huguenot Street, 3rd Floor New . . . , v. 10, n. 1, p. 39–50, 2020. Citations on pages 59 and 83.

MCBRIDE, J. C.; ZHAO, X.; MUNRO, N. B.; JICHA, G. A.; SCHMITT, F. A.; KRYSCIO, R. J.; SMITH, C. D.; JIANG, Y. Sugihara causality analysis of scalp eeg for detection of early alzheimer's disease. **NeuroImage: Clinical**, Elsevier, v. 7, p. 258–265, 2015. Citations on pages 103, 104, and 121.

MCGRATH, J.; JOHNSON, K.; O'HANLON, E.; GARAVAN, H.; LEEMANS, A.; GALLAGHER, L. Abnormal functional connectivity during visuospatial processing is associated with disrupted organisation of white matter in autism. **Frontiers in human neuroscience**, Frontiers Media SA, v. 7, p. 434, 2013. Citation on page 119.

MCKENNA, M. T.; MICHAUD, C. M.; MURRAY, C. J.; MARKS, J. S. Assessing the burden of disease in the united states using disability-adjusted life years. **American journal of preventive medicine**, Elsevier, v. 28, n. 5, p. 415–423, 2005. Citation on page 191.

MENON, V.; CROTTAZ-HERBETTE, S. Combined eeg and fmri studies of human brain function. **Int Rev Neurobiol**, v. 66, n. 05, p. 291–321, 2005. Citations on pages 103 and 126.

METZNER, R. Hallucinogenic drugs and plants in psychotherapy and shamanism. **Journal of psychoactive drugs**, Taylor & Francis, v. 30, n. 4, p. 333–341, 1998. Citation on page 56.

MICHEL, C. M.; BRUNET, D. Eeg source imaging: a practical review of the analysis steps. **Frontiers in neurology**, Frontiers, v. 10, p. 325, 2019. Citations on pages 17, 19, 22, 70, 73, 93, and 144.

MICHELOYANNIS, S.; PACHOU, E.; STAM, C. J.; VOURKAS, M.; ERIMAKI, S.; TSIRKA, V. Using graph theoretical analysis of multi channel eeg to evaluate the neural efficiency hypothesis. **Neuroscience letters**, Elsevier, v. 402, n. 3, p. 273–277, 2006. Citation on page 125.

MIJALKOV, M.; KAKAEI, E.; PEREIRA, J. B.; WESTMAN, E.; VOLPE, G.; INITIATIVE, A. D. N. Braph: a graph theory software for the analysis of brain connectivity. **PloS one**, Public Library of Science San Francisco, CA USA, v. 12, n. 8, p. e0178798, 2017. Citations on pages 17, 19, 20, 22, 70, 73, 93, 114, and 144.

MILLSTEIN, F. **Convolutional Neural Networks In Python: Beginner's Guide To Convolutional Neural Networks In Python**. [S.l.]: Frank Millstein, 2020. Citation on page 48.

MINCHOLÉ, A.; RODRIGUEZ, B. Artificial intelligence for the electrocardiogram. **Nature medicine**, Nature Publishing Group, v. 25, n. 1, p. 22–23, 2019. Citations on pages 60, 89, 108, and 130.

MIOTTO, R.; WANG, F.; WANG, S.; JIANG, X.; DUDLEY, J. T. Deep learning for healthcare: review, opportunities and challenges. **Briefings in bioinformatics**, Oxford University Press, v. 19, n. 6, p. 1236–1246, 2017. Citation on page 38.

MITCHELL, J. M.; BOGENSCHUTZ, M.; LILIENSTEIN, A.; HARRISON, C.; KLEIMAN, S.; PARKER-GUILBERT, K.; G, M. O.; GARAS, W.; PALEOS, C.; GORMAN, I. *et al.* Mdma-assisted therapy for severe ptsd: a randomized, double-blind, placebo-controlled phase 3 study. **Nature Medicine**, Nature Publishing Group, v. 27, n. 6, p. 1025–1033, 2021. Citations on pages 39 and 81.

MOLINA, V.; LUBEIRO, A.; GARCIA, R. de L.; GOMEZ-PILAR, J.; MARTÍN-SANTIAGO, O.; IGLESIAS-TEJEDOR, M.; HOLGADO-MADERA, P.; SEGARRA-ECHEVERRÍA, R.; RECIO-BARBERO, M.; NÚÑEZ, P. *et al.* Deficits of entropy modulation of the eeg: A biomarker for altered function in schizophrenia and bipolar disorder? **Journal of Psychiatry and Neuroscience**, Journal of Psychiatry and Neuroscience, v. 45, n. 5, p. 322–333, 2020. Citation on page 143.

MOLNAR, C. **Interpretable machine learning**. [S.l.]: Lulu. com, 2020. Citation on page 90.

MORALES-GARCÍA, J. A.; REVENGA, M. de la F.; ALONSO-GIL, S.; RODRÍGUEZ-FRANCO, M. I.; FEILDING, A.; PEREZ-CASTILLO, A.; RIBA, J. The alkaloids of banisteriopsis caapi, the plant source of the amazonian hallucinogen ayahuasca, stimulate adult neurogenesis in vitro. **Scientific reports**, Nature Publishing Group, v. 7, n. 1, p. 1–13, 2017. Citation on page 57.

MOSTOFSKY, S. H.; BURGESS, M. P.; LARSON, J. C. G. Increased motor cortex white matter volume predicts motor impairment in autism. **Brain**, Oxford University Press, v. 130, n. 8, p. 2117–2122, 2007. Citation on page 120.

MOTA, N. B.; VASCONCELOS, N. A.; LEMOS, N.; PIERETTI, A. C.; KINOUCHI, O.; CECCHI, G. A.; COPELLI, M.; RIBEIRO, S. Speech graphs provide a quantitative measure of thought disorder in psychosis. **PloS one**, Public Library of Science San Francisco, USA, v. 7, n. 4, p. e34928, 2012. Citation on page 139.

MOZAFFARINYA, M.; SHAHRIYARI, A. R.; BAHADORI, M. K.; GHAZVINI, A.; ATHARI, S. S.; VAHEDI, G. A data-mining algorithm to assess key factors in asthma diagnosis. **Revue Française d'Allergologie**, Elsevier, 2019. Citations on pages 38, 58, and 82.

MUNIASAMY, A.; TABASSAM, S.; HUSSAIN, M. A.; SULTANA, H.; MUNIASAMY, V.; BHATNAGAR, R. Deep learning for predictive analytics in healthcare. In: SPRINGER. **International Conference on Advanced Machine Learning Technologies and Applications**. [S.l.], 2019. p. 32–42. Citation on page 38.

MURRAY, C. J.; EZZATI, M.; FLAXMAN, A. D.; LIM, S.; LOZANO, R.; MICHAUD, C.; NAGHAVI, M.; SALOMON, J. A.; SHIBUYA, K.; VOS, T. *et al.* Gbd 2010: design, definitions, and metrics. **The Lancet**, Elsevier, v. 380, n. 9859, p. 2063–2066, 2012. Citations on pages 191 and 192.

NAGHAVI, M.; ABAJOBIR, A. A.; ABBAFATI, C.; ABBAS, K. M.; ABD-ALLAH, F.; ABERA, S. F.; ABOYANS, V.; ADETOKUNBOH, O.; AFSHIN, A.; AGRAWAL, A. *et al.* Global, regional, and national age-sex specific mortality for 264 causes of death, 1980–2016: a systematic analysis for the global burden of disease study 2016. **The Lancet**, Elsevier, v. 390, n. 10100, p. 1151–1210, 2017. Citation on page 35.

NAGHAVI, M.; ABOLHASSANI, F.; POURMALEK, F.; LAKEH, M. M.; JAFARI, N.; VASEGHI, S.; HEZAVEH, N. M.; KAZEMEINI, H. The burden of disease and injury in iran 2003. **Population health metrics**, BioMed Central, v. 7, n. 1, p. 9, 2009. Citation on page 191.

NAJAFABADI, M. M.; KHOSHGOFTAAR, T. M.; VILLANUSTRE, F.; HOLT, J. Large-scale distributed l-bfgs. **Journal of Big Data**, SpringerOpen, v. 4, n. 1, p. 1–17, 2017. Citation on page 108.

NASRABADI, A. M.; ALLAHVERDY, A.; SAMAVATI, M.; MOHAMMADI, M. R. **EEG data for ADHD / Control children**. IEEE Dataport, 2020. Available: <https://dx.doi.org/10.21227/rzfh-zn36>. Citation on page 149.

NEBEL, M. B.; JOEL, S. E.; MUSCHELLI, J.; BARBER, A. D.; CAFFO, B. S.; PEKAR, J. J.; MOSTOFSKY, S. H. Disruption of functional organization within the primary motor cortex in children with autism. **Human brain mapping**, Wiley Online Library, v. 35, n. 2, p. 567–580, 2014. Citation on page 120.

NEWMAN, M. **Networks: an introduction**. [S.l.]: Oxford university press, 2010. Citations on pages 63, 87, 109, and 131.

NEWMAN, M. E. Assortative mixing in networks. **Physical review letters**, APS, v. 89, n. 20, p. 208701, 2002. Citations on pages 63, 74, 87, 109, and 131.

____. The structure and function of complex networks. **SIAM review**, SIAM, v. 45, n. 2, p. 167–256, 2003. Citations on pages 63, 87, 109, and 131.

____. Finding community structure in networks using the eigenvectors of matrices. **Physical review E**, APS, v. 74, n. 3, p. 036104, 2006. Citations on pages 65, 88, 109, and 131.

____. Communities, modules and large-scale structure in networks. **Nature physics**, Nature Publishing Group, v. 8, n. 1, p. 25–31, 2012. Citations on pages 57, 88, 109, and 131.

NEWMAN, M. E.; WATTS, D. J.; STROGATZ, S. H. Random graph models of social networks. **Proceedings of the National Academy of Sciences**, National Acad Sciences, v. 99, n. suppl 1, p. 2566–2572, 2002. Citations on pages 63, 87, 109, and 131.

NICHOLS, D. E. N, n-dimethyltryptamine and the pineal gland: Separating fact from myth. **Journal of Psychopharmacology**, SAGE Publications Sage UK: London, England, v. 32, n. 1, p. 30–36, 2018. Citation on page 81.

____. Psilocybin: from ancient magic to modern medicine. **The Journal of antibiotics**, Nature Publishing Group, v. 73, n. 10, p. 679–686, 2020. Citations on pages 39 and 81.

NICHOLS, D. E.; JOHNSON, M. W.; NICHOLS, C. D. Psychedelics as medicines: an emerging new paradigm. **Clinical Pharmacology & Therapeutics**, Wiley Online Library, v. 101, n. 2, p. 209–219, 2017. Citations on pages 82 and 98.

NIELSEN, J. A.; ZIELINSKI, B. A.; FLETCHER, P. T.; ALEXANDER, A. L.; LANGE, N.; BIGLER, E. D.; LAINHART, J. E.; ANDERSON, J. S. Multisite functional connectivity mri classification of autism: Abide results. **Frontiers in human neuroscience**, Frontiers Media SA, v. 7, p. 599, 2013. Citation on page 105.

NIERENBERG, J.; SALISBURY, D. F.; LEVITT, J. J.; DAVID, E. A.; MCCARLEY, R. W.; SHENTON, M. E. Reduced left angular gyrus volume in first-episode schizophrenia. **American Journal of Psychiatry**, Am Psychiatric Assoc, v. 162, n. 8, p. 1539–1541, 2005. Citation on page 125.

NIZNIKIEWICZ, M.; DONNINO, R.; MCCARLEY, R. W.; NESTOR, P. G.; IOSIFESCU, D. V.; O'DONNELL, B.; LEVITT, J.; SHENTON, M. E. Abnormal angular gyrus asymmetry in schizophrenia. **American Journal of Psychiatry**, Am Psychiatric Assoc, v. 157, n. 3, p. 428–437, 2000. Citation on page 125.

NUNES, A. S.; VAKORIN, V. A.; KOZHEMIAKO, N.; PEATFIELD, N.; RIBARY, U.; DOESBURG, S. M. Atypical age-related changes in cortical thickness in autism spectrum disorder. **Scientific reports**, Nature Publishing Group, v. 10, n. 1, p. 1–15, 2020. Citation on page 104.

OH, S. L.; HAGIWARA, Y.; RAGHAVENDRA, U.; YUVARAJ, R.; ARUNKUMAR, N.; MURUGAPPAN, M.; ACHARYA, U. R. A deep learning approach for parkinson's disease diagnosis from eeg signals. **Neural Computing and Applications**, Springer, p. 1–7, 2018. Citation on page 46.

OH, S. L.; VICNESH, J.; CIACCIO, E. J.; YUVARAJ, R.; ACHARYA, U. R. Deep convolutional neural network model for automated diagnosis of schizophrenia using eeg signals. **Applied Sciences**, Multidisciplinary Digital Publishing Institute, v. 9, n. 14, p. 2870, 2019. Citations on pages 45, 48, and 54.

OLDEHINKEL, M.; MENNES, M.; MARQUAND, A.; CHARMAN, T.; TILLMANN, J.; ECKER, C.; DELL'ACQUA, F.; BRANDEIS, D.; BANASCHEWSKI, T.; BAUMEISTER, S. *et al.* Altered connectivity between cerebellum, visual, and sensory-motor networks in autism

spectrum disorder: results from the eu-aims longitudinal european autism project. **Biological Psychiatry: Cognitive Neuroscience and Neuroimaging**, Elsevier, v. 4, n. 3, p. 260–270, 2019. Citation on page 120.

ORGANIZATION, W. H. **The World Health Report 2001: Mental health: new understanding, new hope**. [S.l.]: World Health Organization, 2001. Citation on page 37.

____. **Neurological disorders: public health challenges**. [S.l.]: World Health Organization, 2006. Citation on page 44.

OSÓRIO, F. de L.; MACEDO, L. R. H. de; SOUSA, J. P. M. de; PINTO, J. P.; QUEVEDO, J.; CRIPPA, J. A. de S.; HALLAK, J. E. C. The therapeutic potential of harmine and ayahuasca in depression: Evidence from exploratory animal and human studies. **The ethnopharmacology of ayahuasca**, Transworld Research Network Trivandrum, India, v. 75, p. 85, 2011. Citation on page 57.

OTT, J. Pharmahuasca: human pharmacology of oral dmt plus harmine. **Journal of psychoactive drugs**, Taylor & Francis, v. 31, n. 2, p. 171–177, 1999. Citation on page 81.

OVERWALLE, F. V.; MANTO, M.; CATTANEO, Z.; CLAUSI, S.; FERRARI, C.; GABRIELI, J. D.; GUELL, X.; HELEVEN, E.; LUPO, M.; MA, Q. *et al.* Consensus paper: cerebellum and social cognition. **The Cerebellum**, Springer, v. 19, n. 6, p. 833–868, 2020. Citation on page 120.

PALHANO-FONTES, F.; BARRETO, D.; ONIAS, H.; ANDRADE, K. C.; NOVAES, M. M.; PESSOA, J. A.; MOTA-ROLIM, S. A.; OSÓRIO, F. L.; SANCHES, R.; SANTOS, R. G. D. *et al.* Rapid antidepressant effects of the psychedelic ayahuasca in treatment-resistant depression: a randomized placebo-controlled trial. **Psychological medicine**, Cambridge University Press, v. 49, n. 4, p. 655–663, 2019. Citation on page 57.

PALHANO-FONTES, F.; MOTA-ROLIM, S.; LOBÃO-SOARES, B.; GALVÃO-COELHO, N.; MAIA-OLIVEIRA, J. P.; ARAÚJO, D. B. Recent evidence on the antidepressant effects of ayahuasca. **Ayahuasca Healing and Science**, Springer Nature, p. 21, 2021. Citation on page 57.

PALLAVICINI, C.; CAVANNA, F.; ZAMBERLAN, F.; FUENTE, L. A. de la; ARIAS, M.; ROMERO, M. C.; CARHART-HARRIS, R.; TIMMERMANN, C.; TAGLIAZUCCHI, E. Neural and subjective effects of inhaled dmt in natural settings. **bioRxiv**, Cold Spring Harbor Laboratory, 2020. Citations on pages 77 and 95.

PALLAVICINI, C.; CAVANNA, F.; ZAMBERLAN, F.; FUENTE, L. A. de la; ILKSOY, Y.; PERL, Y. S.; ARIAS, M.; ROMERO, C.; CARHART-HARRIS, R.; TIMMERMANN, C. *et al.* Neural and subjective effects of inhaled n, n-dimethyltryptamine in natural settings. **Journal of Psychopharmacology**, Sage Publications Sage UK: London, England, v. 35, n. 4, p. 406–420, 2021. Citations on pages 84, 94, 95, and 96.

PAPO, D. Commentary: The entropic brain: a theory of conscious states informed by neuroimaging research with psychedelic drugs. **Frontiers in human neuroscience**, Frontiers, p. 423, 2016. Citation on page 77.

PARK, Y.; KELLIS, M. Deep learning for regulatory genomics. **Nature biotechnology**, Nature Publishing Group, v. 33, n. 8, p. 825–826, 2015. Citations on pages 60, 89, 108, and 130.

PARRACHINO, I. **Cooperative game theory and its application to natural, environmental and water resource issues**. [S.l.]: World Bank Publications, 2012. Citation on page 90.

PATEL, A.; BISO, G. M. N. R.; FOWLER, J. B. Neuroanatomy, temporal lobe. In: **StatPearls [Internet]**. [S.l.]: StatPearls Publishing, 2021. Citation on page 141.

PATEL, D.; KHER, V.; DESAI, B.; LEI, X.; CEN, S.; NANDA, N.; GHOLAMREZANEZHAD, A.; DUDDALWAR, V.; VARGHESE, B.; OBERAI, A. A. Machine learning based predictors for covid-19 disease severity. **Scientific Reports**, Nature Publishing Group, v. 11, n. 1, p. 1–7, 2021. Citations on pages 60, 89, 96, 108, and 130.

PATEL, P.; AGGARWAL, P.; GUPTA, A. Classification of schizophrenia versus normal subjects using deep learning. In: **Proceedings of the Tenth Indian Conference on Computer Vision, Graphics and Image Processing**. [S.l.: s.n.], 2016. p. 1–6. Citation on page 126.

PERAZA, L. R.; DÍAZ-PARRA, A.; KENNION, O.; MORATAL, D.; TAYLOR, J.-P.; KAISER, M.; BAUER, R.; INITIATIVE, A. D. N. *et al.* Structural connectivity centrality changes mark the path toward alzheimer's disease. **Alzheimer's & Dementia: Diagnosis, Assessment & Disease Monitoring**, Elsevier, v. 11, p. 98–107, 2019. Citation on page 74.

PEREIRA, J. B.; MIJALKOV, M.; KAKAEI, E.; MECOCCI, P.; VELLAS, B.; TSOLAKI, M.; KŁOSZEWSKA, I.; SOININEN, H.; SPENGER, C.; LOVESTONE, S. *et al.* Disrupted network topology in patients with stable and progressive mild cognitive impairment and alzheimer's disease. **Cerebral Cortex**, Oxford University Press, v. 26, n. 8, p. 3476–3493, 2016. Citation on page 74.

PERKINS, D.; SARRIS, J.; ROSSELL, S.; BONOMO, Y.; FORBES, D.; DAVEY, C.; HOYER, D.; LOO, C.; MURRAY, G.; HOOD, S. *et al.* Medicinal psychedelics for mental health and addiction: Advancing research of an emerging paradigm. **Australian & New Zealand Journal of Psychiatry**, SAGE Publications Sage UK: London, England, v. 55, n. 12, p. 1127–1133, 2021. Citations on pages 39 and 81.

PEROVNIK, M.; TOMŠE, P.; JAMŠEK, J.; EMERŠIČ, A.; TANG, C.; EIDELBERG, D.; TROŠT, M. Identification and validation of alzheimer's disease-related metabolic brain pattern in biomarker confirmed alzheimer's dementia patients. **Scientific Reports**, Nature Publishing Group, v. 12, n. 1, p. 1–11, 2022. Citation on page 110.

PETERS, J. M.; TAQUET, M.; VEGA, C.; JESTE, S. S.; FERNÁNDEZ, I. S.; TAN, J.; NELSON, C. A.; SAHIN, M.; WARFIELD, S. K. Brain functional networks in syndromic and non-syndromic autism: a graph theoretical study of eeg connectivity. **BMC medicine**, BioMed Central, v. 11, n. 1, p. 1–16, 2013. Citation on page 37.

PIERNO, A. C.; TUBALDI, F.; TURELLA, L.; GROSSI, P.; BARACHINO, L.; GALLO, P.; CASTIELLO, U. Neurofunctional modulation of brain regions by the observation of pointing and grasping actions. **Cerebral Cortex**, Oxford University Press, v. 19, n. 2, p. 367–374, 2009. Citation on page 96.

PINAYA, W. H.; GADELHA, A.; DOYLE, O. M.; NOTO, C.; ZUGMAN, A.; CORDEIRO, Q.; JACKOWSKI, A. P.; BRESSAN, R. A.; SATO, J. R. Using deep belief network modelling to characterize differences in brain morphometry in schizophrenia. **Scientific reports**, Nature Publishing Group, v. 6, p. 38897, 2016. Citation on page 38.

PINEDA, A.; ALVES, C. Alzheimer's disease and Schizophrenia. 1 2022. Available: <https://figshare.com/articles/dataset/Alzheimer_s_disease_and_Schizophrenia/19091771>. Citation on page 47.

PINEDA, A. M.; RAMOS, F. M.; BETTING, L. E.; CAMPANHARO, A. S. Quantile graphs for eeg-based diagnosis of alzheimer's disease. **Plos one**, Public Library of Science San Francisco, CA USA, v. 15, n. 6, p. e0231169, 2020. Citations on pages 45, 47, 57, 58, and 82.

PISNER, D. A.; SCHNYER, D. M. Support vector machine. In: **Machine learning**. [S.l.]: Elsevier, 2020. p. 101–121. Citation on page 83.

PIUBELLI, L.; POLLEGIONI, L.; RABATTONI, V.; MAURI, M.; CARIDDI, L. P.; VERSINO, M.; SACCHI, S. Serum d-serine levels are altered in early phases of alzheimer's disease: towards a precocious biomarker. **Translational Psychiatry**, Nature Publishing Group, v. 11, n. 1, p. 1–8, 2021. Citation on page 44.

POLLI, A.; WEIS, L.; BIUNDO, R.; THACKER, M.; TUROLLA, A.; KOUTSIKOS, K.; CHAUDHURI, K. R.; ANTONINI, A. Anatomical and functional correlates of persistent pain in parkinson's disease. **Movement Disorders**, Wiley Online Library, v. 31, n. 12, p. 1854–1864, 2016. Citation on page 110.

PONDÉ, M. P. A crise do diagnóstico em psiquiatria e os manuais diagnósticos. **Revista Latinoamericana de Psicopatologia Fundamental**, Associação Universitária de Pesquisa em Psicopatologia Fundamental, v. 21, n. 1, p. 145–166, 2018. Citation on page 37.

PORTNOVA, G. V.; ATANOV, M. S. Nonlinear eeg parameters of emotional perception in patients with moderate traumatic brain injury, coma, stroke and schizophrenia. **AIMS neuroscience**, AIMS Press, v. 5, n. 4, p. 221, 2018. Citation on page 143.

PRITCHARD, W. S.; DUKE, D. W.; COBURN, K. L. Altered eeg dynamical responsivity associated with normal aging and probable alzheimer's disease. **Dementia and Geriatric Cognitive Disorders**, Karger Publishers, v. 2, n. 2, p. 102–105, 1991. Citation on page 47.

QIAN, X.; LOO, B. R. Y.; CASTELLANOS, F. X.; LIU, S.; KOH, H. L.; POH, X. W. W.; KRISHNAN, R.; FUNG, D.; CHEE, M. W.; GUAN, C. *et al.* Brain-computer-interface-based intervention re-normalizes brain functional network topology in children with attention deficit/hyperactivity disorder. **Translational psychiatry**, Nature Publishing Group, v. 8, n. 1, p. 1–11, 2018. Citation on page 37.

QIANG, N.; DONG, Q.; LIANG, H.; GE, B.; ZHANG, S.; SUN, Y.; ZHANG, C.; ZHANG, W.; GAO, J.; LIU, T. Modeling and augmenting of fmri data using deep recurrent variational auto-encoder. **Journal of Neural Engineering**, IOP Publishing, v. 18, n. 4, p. 0460b6, 2021. Citation on page 104.

QURESHI, M. N. I.; OH, J.; CHO, D.; JO, H. J.; LEE, B. Multimodal discrimination of schizophrenia using hybrid weighted feature concatenation of brain functional connectivity and anatomical features with an extreme learning machine. **Frontiers in neuroinformatics**, Frontiers Media SA, v. 11, p. 59, 2017. Citation on page 126.

RAGHAVAN, U. N.; ALBERT, R.; KUMARA, S. Near linear time algorithm to detect community structures in large-scale networks. **Physical review E**, APS, v. 76, n. 3, p. 036106, 2007. Citations on pages 65, 88, 109, and 131.

RAJULA, H. S. R.; VERLATO, G.; MANCHIA, M.; ANTONUCCI, N.; FANOS, V. Comparison of conventional statistical methods with machine learning in medicine: diagnosis, drug development, and treatment. **Medicina**, Multidisciplinary Digital Publishing Institute, v. 56, n. 9, p. 455, 2020. Citations on pages 38 and 83.

RANGAPRAKASH, D.; DRETSCH, M. N.; KATZ, J. S.; JR, T. S. D.; DESHPANDE, G. Dynamics of segregation and integration in directional brain networks: illustration in soldiers with ptsd and neurotrauma. **Frontiers in neuroscience**, Frontiers, p. 803, 2019. Citations on pages 98 and 144.

RASCHKA, S.; MIRJALILI, V. **Python machine learning: Machine learning and deep learning with Python, scikit-learn, and TensorFlow 2**. [S.l.]: Packt Publishing Ltd, 2019. Citation on page 133.

RASHIDI, H. H.; SEN, S.; PALMIERI, T. L.; BLACKMON, T.; WAJDA, J.; TRAN, N. K. Early recognition of burn-and trauma-related acute kidney injury: a pilot comparison of machine learning techniques. **Scientific reports**, Nature Publishing Group, v. 10, n. 1, p. 1–9, 2020. Citations on pages 60, 89, 108, and 130.

REFAEILZADEH, P.; TANG, L.; LIU, H. Cross-validation. **Encyclopedia of database systems**, Springer, v. 5, p. 532–538, 2009. Citations on pages 60 and 88.

REHM, J.; SHIELD, K. D. Global burden of disease and the impact of mental and addictive disorders. **Current psychiatry reports**, Springer, v. 21, n. 2, p. 10, 2019. Citation on page 35.

REICHARDT, J.; BORNHOLDT, S. Statistical mechanics of community detection. **Physical review E**, APS, v. 74, n. 1, p. 016110, 2006. Citations on pages 65, 88, 109, and 131.

RIBA, J.; ROMERO, S.; GRASA, E.; MENA, E.; CARRIÓ, I.; BARBANOJ, M. J. Increased frontal and paralimbic activation following ayahuasca, the pan-amazonian inebriant. **Psychopharmacology**, Springer, v. 186, n. 1, p. 93–98, 2006. Citation on page 72.

RICHENS, J. G.; LEE, C. M.; JOHRI, S. Improving the accuracy of medical diagnosis with causal machine learning. **Nature communications**, Nature Publishing Group, v. 11, n. 1, p. 1–9, 2020. Citation on page 82.

RITCHIE, H.; ROSER, M. Mental health. **Our World in Data**, 2019. Https://ourworldindata.org/mental-health. Citations on pages 15 and 36.

ROCCA, M. L.; GARNER, R.; AMOROSO, N.; LUTKENHOFF, E. S.; MONTI, M. M.; VESPA, P.; TOGA, A. W.; DUNCAN, D. Multiplex networks to characterize seizure development in traumatic brain injury patients. **Frontiers in neuroscience**, Frontiers, v. 14, p. 1238, 2020. Citation on page 45.

RODRIGUES, F. A.; COSTA, L. da F. A structure–dynamic approach to cortical organization: Number of paths and accessibility. **Journal of Neuroscience Methods**, Elsevier, v. 183, n. 1, p. 57–62, 2009. Citation on page 53.

RODRIGUEZ, E.; GEORGE, N.; LACHAUX, J.-P.; MARTINERIE, J.; RENAULT, B.; VARELA, F. J. Perception's shadow: long-distance synchronization of human brain activity. **Nature**, Nature Publishing Group, v. 397, n. 6718, p. 430–433, 1999. Citation on page 73.

RODRÍGUEZ-PÉREZ, R.; BAJORATH, J. Interpretation of compound activity predictions from complex machine learning models using local approximations and shapley values. **Journal of Medicinal Chemistry**, ACS Publications, v. 63, n. 16, p. 8761–8777, 2019. Citations on pages 38, 58, 61, 83, 104, and 126.

____. Interpretation of machine learning models using shapley values: application to compound potency and multi-target activity predictions. **Journal of computer-aided molecular design**, Springer, v. 34, n. 10, p. 1013–1026, 2020. Citation on page 89.

RODRIGUEZ, S.; HUG, C.; TODOROV, P.; MORET, N.; BOSWELL, S. A.; EVANS, K.; ZHOU, G.; JOHNSON, N. T.; HYMAN, B. T.; SORGER, P. K. *et al.* Machine learning identifies candidates for drug repurposing in alzheimer's disease. **Nature Communications**, Nature Publishing Group, v. 12, n. 1, p. 1–13, 2021. Citation on page 44.

ROJAS, G. M.; ALVAREZ, C.; MONTOYA, C. E.; IGLESIA-VAYÁ, M. de la; CISTERNAS, J. E.; GÁLVEZ, M. Study of resting-state functional connectivity networks using eeg electrodes position as seed. **Frontiers in neuroscience**, Frontiers, v. 12, p. 235, 2018. Citations on pages 63 and 87.

ROMBOUTS, S. A.; DAMOISEAUX, J. S.; GOEKOOP, R.; BARKHOF, F.; SCHELTENS, P.; SMITH, S. M.; BECKMANN, C. F. Model-free group analysis shows altered bold fmri networks in dementia. **Human brain mapping**, Wiley Online Library, v. 30, n. 1, p. 256–266, 2009. Citation on page 37.

ROSTAMIZADEH, A.; TALWALKAR, A.; DESALVO, G.; JAMIESON, K.; LI, L. Efficient hyperparameter optimization and infinitely many armed bandits. In: **5th International Conference on Learning Representations**. [S.l.: s.n.], 2017. Citation on page 48.

ROSVALL, M.; AXELSSON, D.; BERGSTROM, C. T. The map equation. **The European Physical Journal Special Topics**, Springer, v. 178, n. 1, p. 13–23, 2009. Citations on pages 65, 88, 109, and 131.

RUBINOV, M.; KNOCK, S. A.; STAM, C. J.; MICHELOYANNIS, S.; HARRIS, A. W.; WILLIAMS, L. M.; BREAKSPEAR, M. Small-world properties of nonlinear brain activity in schizophrenia. **Human brain mapping**, Wiley Online Library, v. 30, n. 2, p. 403–416, 2009. Citation on page 125.

RUBINOV, M.; SPORNS, O. Complex network measures of brain connectivity: uses and interpretations. **Neuroimage**, Elsevier, v. 52, n. 3, p. 1059–1069, 2010. Citations on pages 74, 87, and 97.

RUDIN, C. Stop explaining black box machine learning models for high stakes decisions and use interpretable models instead. **Nature Machine Intelligence**, Nature Publishing Group, v. 1, n. 5, p. 206–215, 2019. Citations on pages 38, 83, and 103.

RYU, S.; LEE, H.; LEE, D.-K.; NAM, H. J.; CHUNG, Y.-C.; KIM, S.-W. Network structures of social functioning domains in schizophrenia and bipolar disorder: A preliminary study. **Clinical Psychopharmacology and Neuroscience**, Korean College of Neuropsychopharmacology, v. 18, n. 4, p. 571, 2020. Citation on page 142.

SANCHES, R. F.; OSÓRIO, F. de L.; SANTOS, R. G. D.; MACEDO, L. R.; OLIVEIRA, J. P. Maia-de; WICHERT-ANA, L.; ARAUJO, D. B. de; RIBA, J.; CRIPPA, J. A. S.; HALLAK, J. E. Antidepressant effects of a single dose of ayahuasca in patients with recurrent depression: a spect

study. **Journal of clinical psychopharmacology**, LWW, v. 36, n. 1, p. 77–81, 2016. Citation on page 57.

SANTOS, R. G. D.; HALLAK, J. E. Effects of the natural β-carboline alkaloid harmine, a main constituent of ayahuasca, in memory and in the hippocampus: A systematic literature review of preclinical studies. **Journal of psychoactive drugs**, Taylor & Francis, v. 49, n. 1, p. 1–10, 2017. Citation on page 57.

SANTOS, R. G. D.; HALLAK, J. E. C. Ayahuasca, an ancient substance with traditional and contemporary use in neuropsychiatry and neuroscience. **Epilepsy & Behavior**, Elsevier, v. 121, p. 106300, 2021. Citation on page 73.

SANTOS, R. G. D.; OSÓRIO, F. L.; CRIPPA, J. A. S.; RIBA, J.; ZUARDI, A. W.; HALLAK, J. E. Antidepressive, anxiolytic, and antiaddictive effects of ayahuasca, psilocybin and lysergic acid diethylamide (lsd): a systematic review of clinical trials published in the last 25 years. **Therapeutic advances in psychopharmacology**, Sage Publications Sage UK: London, England, v. 6, n. 3, p. 193–213, 2016. Citations on pages 57 and 72.

SANZ-ARIGITA, E. J.; SCHOONHEIM, M. M.; DAMOISEAUX, J. S.; ROMBOUTS, S. A.; MARIS, E.; BARKHOF, F.; SCHELTENS, P.; STAM, C. J. Loss of 'small-world'networks in alzheimer's disease: graph analysis of fmri resting-state functional connectivity. **PloS one**, Public Library of Science, v. 5, n. 11, p. e13788, 2010. Citation on page 37.

SATO, M.; MORIMOTO, K.; KAJIHARA, S.; TATEISHI, R.; SHIINA, S.; KOIKE, K.; YATOMI, Y. Machine-learning approach for the development of a novel predictive model for the diagnosis of hepatocellular carcinoma. **Scientific reports**, Nature Publishing Group, v. 9, n. 1, p. 1–7, 2019. Citations on pages 60, 89, 108, and 130.

SAÚDE, O. M. da. **CID-10: Classificação Estatística Internacional de Doenças com disquete Vol. 1**. [S.l.]: Edusp, 1994. Citation on page 192.

SAVIO, A.; GRAÑA, M. Local activity features for computer aided diagnosis of schizophrenia on resting-state fmri. **Neurocomputing**, Elsevier, v. 164, p. 154–161, 2015. Citation on page 126.

SCANNELL, J.; BURNS, G.; HILGETAG, C.; O'NEIL, M.; YOUNG, M. P. The connectional organization of the cortico-thalamic system of the cat. **Cerebral Cortex**, Oxford University Press, v. 9, n. 3, p. 277–299, 1999. Citation on page 82.

SCHARTNER, M. M.; TIMMERMANN, C. Neural network models for dmt-induced visual hallucinations. **Neuroscience of Consciousness**, Oxford University Press, v. 2020, n. 1, p. niaa024, 2020. Citation on page 81.

SCHAUMBERG, A. J.; RUBIN, M. A.; FUCHS, T. J. H&e-stained whole slide image deep learning predicts spop mutation state in prostate cancer. **BioRxiv**, Cold Spring Harbor Laboratory, p. 064279, 2018. Citations on pages 38 and 39.

SCHENBERG, E. E.; ALEXANDRE, J. F. M.; FILEV, R.; CRAVO, A. M.; SATO, J. R.; MUTHUKUMARASWAMY, S. D.; YONAMINE, M.; WAGUESPACK, M.; LOMNICKA, I.; BARKER, S. A. *et al.* Acute biphasic effects of ayahuasca. **PloS one**, Public Library of Science San Francisco, CA USA, v. 10, n. 9, p. e0137202, 2015. Citations on pages 57, 59, and 61.

SCHREIBER, T. Measuring information transfer. **Physical review letters**, APS, v. 85, n. 2, p. 461, 2000. Citations on pages 107 and 129.

SCHÜRMANN, M.; JÄRVELÄINEN, J.; AVIKAINEN, S.; CANNON, T. D.; LÖNNQVIST, J.; HUTTUNEN, M.; RIITTA, H. Manifest disease and motor cortex reactivity in twins discordant for schizophrenia. **The British Journal of Psychiatry**, Cambridge University Press, v. 191, n. 2, p. 178–179, 2007. Citation on page 125.

SCRIVENER, C. L.; READER, A. T. Variability of eeg electrode positions and their underlying brain regions: visualizing gel artifacts from a simultaneous eeg-fmri dataset. **Brain and Behavior**, Wiley Online Library, p. e2476, 2022. Citations on pages 22, 95, 140, and 144.

SEGHIER, M. L. The angular gyrus: multiple functions and multiple subdivisions. **The Neuroscientist**, Sage Publications Sage CA: Los Angeles, CA, v. 19, n. 1, p. 43–61, 2013. Citation on page 139.

SEIDMAN, S. B. Network structure and minimum degree. **Social networks**, Elsevier, v. 5, n. 3, p. 269–287, 1983. Citations on pages 63, 87, 109, and 131.

SERRANO-DUEÑAS, M.; CARDOZO-PELAEZ, F.; SÁNCHEZ-RAMOS, J. R. Effects of banisteriopsis caapi extract on parkinson's disease. **The Scientific Review of Alternative Medicine**, v. 5, n. 3, p. 127–132, 2001. Citation on page 57.

SETH, A. K.; BARRETT, A. B.; BARNETT, L. Granger causality analysis in neuroscience and neuroimaging. **Journal of Neuroscience**, Soc Neuroscience, v. 35, n. 8, p. 3293–3297, 2015. Citations on pages 46 and 48.

SHAH, A. A.; KHAN, Y. D. Identification of 4-carboxyglutamate residue sites based on position based statistical feature and multiple classification. **Scientific Reports**, Nature Publishing Group, v. 10, n. 1, p. 1–10, 2020. Citations on pages 60, 88, 108, and 130.

SHANDILYA, S. G.; TIMME, M. Inferring network topology from complex dynamics. **New Journal of Physics**, IOP Publishing, v. 13, n. 1, p. 013004, 2011. Citation on page 48.

SHAPLEY, L. S. **A value for n-person games, Contributions to the Theory of Games, 2, 307–317**. [S.l.]: Princeton University Press, Princeton, NJ, USA, 1953. Citation on page 89.

SIEGEL, A. N.; MESHKAT, S.; BENITAH, K.; LIPSITZ, O.; GILL, H.; LUI, L. M.; TEOPIZ, K. M.; MCINTYRE, R. S.; ROSENBLAT, J. D. Registered clinical studies investigating psychedelic drugs for psychiatric disorders. **Journal of Psychiatric Research**, Elsevier, v. 139, p. 71–81, 2021. Citations on pages 39 and 81.

SIGURDSSON, T.; STARK, K. L.; KARAYIORGOU, M.; GOGOS, J. A.; GORDON, J. A. Impaired hippocampal–prefrontal synchrony in a genetic mouse model of schizophrenia. **Nature**, Nature Publishing Group, v. 464, n. 7289, p. 763–767, 2010. Citation on page 37.

SILVA, M. G. da; DAROS, G. C.; BITENCOURT, R. M. de. Anti-inflammatory activity of ayahuasca and its implications for the treatment of neurological and psychiatric diseases. **Behavioural Brain Research**, Elsevier, p. 113003, 2020. Citation on page 57.

SMITH, R.; SCHÖLL, M.; LONDOS, E.; OHLSSON, T.; HANSSON, O. 18 f-av-1451 in parkinson's disease with and without dementia and in dementia with lewy bodies. **Scientific reports**, Nature Publishing Group, v. 8, n. 1, p. 1–6, 2018. Citation on page 73.

SMITH, R. L.; CANTON, H.; BARRETT, R. J.; SANDERS-BUSH, E. Agonist properties of n, n-dimethyltryptamine at serotonin 5-ht2a and 5-ht2c receptors. **Pharmacology Biochemistry and Behavior**, Elsevier, v. 61, n. 3, p. 323–330, 1998. Citation on page 81.

SMYTHIES, J. R.; MORIN, R.; BROWN, G. Identification of dimethyltryptamine and o-methylbufotenin in human cerebrospinal fluid by combined gas chromatography/mass spectrometry. **Biological psychiatry**, v. 14, n. 3, p. 549–556, 1979. Citation on page 80.

SNIJDERS, T. A. The degree variance: an index of graph heterogeneity. **Social networks**, Elsevier, v. 3, n. 3, p. 163–174, 1981. Citations on pages 63, 87, 109, and 131.

SOJOUDI, S. Equivalence of graphical lasso and thresholding for sparse graphs. **The Journal of Machine Learning Research**, JMLR. org, v. 17, n. 1, p. 3943–3963, 2016. Citations on pages 107 and 129.

SONG, C.-W.; JUNG, H.; CHUNG, K. Development of a medical big-data mining process using topic modeling. **Cluster Computing**, Springer, v. 22, n. 1, p. 1949–1958, 2019. Citations on pages 38, 58, and 82.

SPADON, G.; CARVALHO, A. C. de; RODRIGUES-JR, J. F.; ALVES, L. G. Reconstructing commuters network using machine learning and urban indicators. **Scientific reports**, Nature Publishing Group, v. 9, n. 1, p. 1–13, 2019. Citations on pages 38, 58, 61, 67, 83, 91, 104, 112, 126, and 134.

SPORNS, O. Network analysis, complexity, and brain function. **Complexity**, Wiley Online Library, v. 8, n. 1, p. 56–60, 2002. Citations on pages 45, 76, and 97.

____. **Networks of the Brain**. [S.l.]: MIT press, 2010. Citation on page 125.

____. The human connectome: a complex network. **Annals of the New York Academy of Sciences**, Wiley Online Library, v. 1224, n. 1, p. 109–125, 2011. Citation on page 37.

____. Network attributes for segregation and integration in the human brain. **Current opinion in neurobiology**, Elsevier, v. 23, n. 2, p. 162–171, 2013. Citation on page 97.

____. Graph theory methods: applications in brain networks. **Dialogues in clinical neuroscience**, Les Laboratoires Servier, v. 20, n. 2, p. 111, 2018. Citations on pages 57 and 82.

SPORNS, O.; ZWI, J. D. The small world of the cerebral cortex. **Neuroinformatics**, Springer, v. 2, n. 2, p. 145–162, 2004. Citation on page 82.

SRITHARAN, A.; LINE, P.; SERGEJEW, A.; SILBERSTEIN, R.; EGAN, G.; COPOLOV, D. Eeg coherence measures during auditory hallucinations in schizophrenia. **Psychiatry research**, Elsevier, v. 136, n. 2-3, p. 189–200, 2005. Citation on page 141.

SRIVASTAVA, N.; HINTON, G.; KRIZHEVSKY, A.; SUTSKEVER, I.; SALAKHUTDINOV, R. Dropout: a simple way to prevent neural networks from overfitting. **The journal of machine learning research**, JMLR. org, v. 15, n. 1, p. 1929–1958, 2014. Citations on pages 49 and 209.

STAM, C. J. Modern network science of neurological disorders. **Nature reviews. Neuroscience**, v. 15 10, p. 683–95, 2014. Citation on page 37.

STEVENSON, N. J.; TAPANI, K.; LAURONEN, L.; VANHATALO, S. A dataset of neonatal eeg recordings with seizure annotations. **Scientific data**, Nature Publishing Group, v. 6, n. 1, p. 1–8, 2019. Citation on page 86.

STEYERBERG, E. W.; EIJKEMANS, M. J.; JR, F. E. H.; HABBEMA, J. D. F. Prognostic modelling with logistic regression analysis: a comparison of selection and estimation methods in small data sets. **Statistics in medicine**, Wiley Online Library, v. 19, n. 8, p. 1059–1079, 2000. Citation on page 103.

STOODLEY, C. J. The cerebellum and neurodevelopmental disorders. **The Cerebellum**, Springer, v. 15, n. 1, p. 34–37, 2016. Citation on page 120.

STRASSMAN, R. Dmt: the spirit molecule. rochester, vt at< http://scroungehound. com/sell-sheets. **B0145_DMT. pdf**, 2001. Citation on page 81.

STRASSMAN, R. J.; QUALLS, C. R.; UHLENHUTH, E. H.; KELLNER, R. Dose-response study of n, n-dimethyltryptamine in humans: Ii. subjective effects and preliminary results of a new rating scale. **Archives of general psychiatry**, American Medical Association, v. 51, n. 2, p. 98–108, 1994. Citation on page 81.

STURZBECHER, M. J. **Detecção e caracterização da resposta hemodinâmica pelo desenvolvimento de novos métodos de processamento de imagens funcionais por ressonância magnética**. Phd Thesis (PhD Thesis) — Universidade de São Paulo, 2006. Citations on pages 103 and 126.

SUBAH, F. Z.; DEB, K.; DHAR, P. K.; KOSHIBA, T. A deep learning approach to predict autism spectrum disorder using multisite resting-state fmri. **Applied Sciences**, MDPI, v. 11, n. 8, p. 3636, 2021. Citations on pages 104, 105, and 128.

SZARA, S. Dimethyltryptamin: Its metabolism in man; the relation of its psychotic effect to the serotonin metabolism. **Experientia**, Springer, v. 12, n. 11, p. 441–442, 1956. Citation on page 81.

TAGLIAZUCCHI, E.; ZAMBERLAN, F.; CAVANNA, F.; FUENTE, L. D. L.; ROMERO, C.; PERL, Y. S.; PALLAVICINI, C. Baseline power of theta oscillations predicts mystical-type experiences induced by dmt in a natural setting. **Frontiers in Psychiatry**, Frontiers Media SA, v. 12, 2021. Citation on page 82.

TAIT, L.; TAMAGNINI, F.; STOTHART, G.; BARVAS, E.; MONALDINI, C.; FRUSCIANTE, R.; VOLPINI, M.; GUTTMANN, S.; COULTHARD, E.; BROWN, J. T. *et al.* Eeg microstate complexity for aiding early diagnosis of alzheimer's disease. **Scientific Reports**, Nature Publishing Group, v. 10, n. 1, p. 1–10, 2020. Citation on page 44.

TAKAHASHI, T.; CHO, R. Y.; MIZUNO, T.; KIKUCHI, M.; MURATA, T.; TAKAHASHI, K.; WADA, Y. Antipsychotics reverse abnormal eeg complexity in drug-naive schizophrenia: a multiscale entropy analysis. **Neuroimage**, Elsevier, v. 51, n. 1, p. 173–182, 2010. Citation on page 143.

TAN, H.-Y.; SUST, S.; BUCKHOLTZ, J. W.; MATTAY, V. S.; MEYER-LINDENBERG, A.; EGAN, M. F.; WEINBERGER, D. R.; CALLICOTT, J. H. Dysfunctional prefrontal regional specialization and compensation in schizophrenia. **American Journal of Psychiatry**, Am Psychiatric Assoc, v. 163, n. 11, p. 1969–1977, 2006. Citation on page 125.

THOMAS, J. B.; BRIER, M. R.; ORTEGA, M.; BENZINGER, T. L.; ANCES, B. M. Weighted brain networks in disease: centrality and entropy in human immunodeficiency virus and aging. **Neurobiology of aging**, Elsevier, v. 36, n. 1, p. 401–412, 2015. Citation on page 144.

TIAN, Y.; ZHANG, H.; XU, W.; ZHANG, H.; YANG, L.; ZHENG, S.; SHI, Y. Spectral entropy can predict changes of working memory performance reduced by short-time training in the delayed-match-to-sample task. **Frontiers in human neuroscience**, Frontiers Media SA, v. 11, p. 437, 2017. Citation on page 132.

TIMMERMANN, C.; ROSEMAN, L.; SCHARTNER, M.; MILLIERE, R.; WILLIAMS, L. T.; ERRITZOE, D.; MUTHUKUMARASWAMY, S.; ASHTON, M.; BENDRIOUA, A.; KAUR, O. *et al.* Neural correlates of the dmt experience assessed with multivariate eeg. **Scientific reports**, Nature Publishing Group, v. 9, n. 1, p. 1–13, 2019. Citations on pages 82 and 94.

TIMMERMANN, C.; ROSEMAN, L.; WILLIAMS, L.; ERRITZOE, D.; MARTIAL, C.; CASSOL, H.; LAUREYS, S.; NUTT, D.; CARHART-HARRIS, R. Dmt models the near-death experience. **Frontiers in psychology**, Frontiers, p. 1424, 2018. Citation on page 81.

TOKARIEV, A.; ROBERTS, J. A.; ZALESKY, A.; ZHAO, X.; VANHATALO, S.; BREAKSPEAR, M.; COCCHI, L. Large-scale brain modes reorganize between infant sleep states and carry prognostic information for preterms. **Nature communications**, Nature Publishing Group, v. 10, n. 1, p. 1–9, 2019. Citations on pages 63 and 87.

TOLKACH, Y.; DOHMGÖRGEN, T.; TOMA, M.; KRISTIANSEN, G. High-accuracy prostate cancer pathology using deep learning. **Nature Machine Intelligence**, Nature Publishing Group, v. 2, n. 7, p. 411–418, 2020. Citations on pages 60, 89, 108, and 130.

TOLLES, J.; MEURER, W. J. Logistic regression: relating patient characteristics to outcomes. **Jama**, American Medical Association, v. 316, n. 5, p. 533–534, 2016. Citation on page 60.

TONONI, G.; SPORNS, O.; EDELMAN, G. M. A measure for brain complexity: relating functional segregation and integration in the nervous system. **Proceedings of the National Academy of Sciences**, National Acad Sciences, v. 91, n. 11, p. 5033–5037, 1994. Citations on pages 76 and 97.

TRAMBAIOLLI, L. R.; FALK, T. H.; FRAGA, F. J.; ANGHINAH, R.; LORENA, A. C. Eeg spectro-temporal modulation energy: a new feature for automated diagnosis of alzheimer's disease. In: IEEE. **2011 Annual International Conference of the IEEE Engineering in Medicine and Biology Society**. [S.l.], 2011. p. 3828–3831. Citation on page 44.

TRAPP, C.; VAKAMUDI, K.; POSSE, S. On the detection of high frequency correlations in resting state fmri. **Neuroimage**, Elsevier, v. 164, p. 202–213, 2018. Citation on page 105.

TYAGI, A.; SINGH, V. P.; GORE, M. M. Towards artificial intelligence in mental health: a comprehensive survey on the detection of schizophrenia. **Multimedia Tools and Applications**, Springer, p. 1–63, 2022. Citation on page 125.

VANLUCHENE, A. L.; VEREECKE, H.; THAS, O.; MORTIER, E. P.; SHAFER, S. L.; STRUYS, M. M. Spectral entropy as an electroencephalographic measure of anesthetic drug effect: a comparison with bispectral index and processed midlatency auditory evoked response. **The Journal of the American Society of Anesthesiologists**, The American Society of Anesthesiologists, v. 101, n. 1, p. 34–42, 2004. Citation on page 132.

VARLEY, T. F.; CRAIG, M.; ADAPA, R.; FINOIA, P.; WILLIAMS, G.; ALLANSON, J.; PICKARD, J.; MENON, D. K.; STAMATAKIS, E. A. Fractal dimension of cortical functional connectivity networks & severity of disorders of consciousness. **PLoS One**, Public Library of Science San Francisco, CA USA, v. 15, n. 2, p. e0223812, 2020. Citation on page 58.

VEAGUE, H. B.; COLLINS, C. E. **Personality disorders**. [S.l.]: Infobase Publishing, 2007. Citation on page 124.

VIGO, D.; THORNICROFT, G.; ATUN, R. Estimating the true global burden of mental illness. **The Lancet Psychiatry**, Elsevier, v. 3, n. 2, p. 171–178, 2016. Citation on page 35.

VIOL, A.; PALHANO-FONTES, F.; ONIAS, H.; ARAUJO, D. B. de; VISWANATHAN, G. Shannon entropy of brain functional complex networks under the influence of the psychedelic ayahuasca. **Scientific reports**, Nature Publishing Group, v. 7, n. 1, p. 1–13, 2017. Citations on pages 76, 82, and 97.

WALHOVD, K.; FJELL, A.; BREWER, J.; MCEVOY, L.; FENNEMA-NOTESTINE, C.; HAGLER, D.; JENNINGS, R.; KAROW, D.; DALE, A.; INITIATIVE, A. D. N. *et al.* Combining mr imaging, positron-emission tomography, and csf biomarkers in the diagnosis and prognosis of alzheimer disease. **American Journal of Neuroradiology**, Am Soc Neuroradiology, v. 31, n. 2, p. 347–354, 2010. Citation on page 44.

WALTHER, S.; SCHÄPPI, L.; FEDERSPIEL, A.; BOHLHALTER, S.; WIEST, R.; STRIK, W.; STEGMAYER, K. Resting-state hyperperfusion of the supplementary motor area in catatonia. **Schizophrenia bulletin**, Oxford University Press US, v. 43, n. 5, p. 972–981, 2017. Citation on page 139.

WAN, Z.; YANG, R.; HUANG, M.; ZENG, N.; LIU, X. A review on transfer learning in eeg signal analysis. **Neurocomputing**, Elsevier, v. 421, p. 1–14, 2021. Citation on page 121.

WANG, H.; ZENG, L.-L.; CHEN, Y.; YIN, H.; TAN, Q.; HU, D. Evidence of a dissociation pattern in default mode subnetwork functional connectivity in schizophrenia. **Scientific reports**, Nature Publishing Group, v. 5, n. 1, p. 1–10, 2015. Citation on page 37.

WANG, J.; DING, H.; BIDGOLI, F. A.; ZHOU, B.; IRIBARREN, C.; MOLLOI, S.; BALDI, P. Detecting cardiovascular disease from mammograms with deep learning. **IEEE transactions on medical imaging**, IEEE, v. 36, n. 5, p. 1172–1181, 2017. Citation on page 38.

WANG, L.; WANG, W.; YAN, T.; SONG, J.; YANG, W.; WANG, B.; GO, R.; HUANG, Q.; WU, J. Beta-band functional connectivity influences audiovisual integration in older age: an eeg study. **Frontiers in aging neuroscience**, Frontiers, v. 9, p. 239, 2017. Citations on pages 63 and 87.

WANG, S. S.-H.; KLOTH, A. D.; BADURA, A. The cerebellum, sensitive periods, and autism. **Neuron**, Elsevier, v. 83, n. 3, p. 518–532, 2014. Citation on page 120.

WANG, Y.; LI, Y.; CAO, H.; XIONG, M.; SHUGART, Y. Y.; JIN, L. Efficient test for nonlinear dependence of two continuous variables. **BMC bioinformatics**, Springer, v. 16, n. 1, p. 1–8, 2015. Citation on page 117.

WANG, Y.-H.; SAMOYLENKO, V.; TEKWANI, B. L.; KHAN, I. A.; MILLER, L. S.; CHAURASIYA, N. D.; RAHMAN, M. M.; TRIPATHI, L. M.; KHAN, S. I.; JOSHI, V. C. *et al.* Composition, standardization and chemical profiling of banisteriopsis caapi, a plant for the treatment of neurodegenerative disorders relevant to parkinson's disease. **Journal of ethnopharmacology**, Elsevier, v. 128, n. 3, p. 662–671, 2010. Citation on page 57.

WATTS, D. J.; STROGATZ, S. H. Collective dynamics of 'small-world'networks. **Nature**, Nature Publishing Group, v. 393, n. 6684, p. 440–442, 1998. Citations on pages 37, 63, 82, 87, 109, and 131.

WELCHEW, D. E.; ASHWIN, C.; BERKOUK, K.; SALVADOR, R.; SUCKLING, J.; BARON-COHEN, S.; BULLMORE, E. Functional disconnectivity of the medial temporal lobe in asperger's syndrome. **Biological psychiatry**, Elsevier, v. 57, n. 9, p. 991–998, 2005. Citation on page 37.

WELNIARZ, Q.; GALLEA, C.; LAMY, J.-C.; MÉNERET, A.; POPA, T.; VALABREGUE, R.; BÉRANGER, B.; BROCHARD, V.; FLAMAND-ROZE, C.; TROUILLARD, O. *et al.* The supplementary motor area modulates interhemispheric interactions during movement preparation. **Human brain mapping**, Wiley Online Library, v. 40, n. 7, p. 2125–2142, 2019. Citation on page 139.

WHITE, J. G.; SOUTHGATE, E.; THOMSON, J. N.; BRENNER, S. The structure of the nervous system of the nematode caenorhabditis elegans: the mind of a worm. **Philosophical Transactions of the Royal Society of London**, v. 314, p. 1–340, 1986. Citation on page 82.

WHITEFORD, H.; FERRARI, A.; DEGENHARDT, L. Global burden of disease studies: implications for mental and substance use disorders. **Health Affairs**, v. 35, n. 6, p. 1114–1120, 2016. Citations on pages 15 and 36.

WHITEFORD, H. A.; DEGENHARDT, L.; REHM, J.; BAXTER, A. J.; FERRARI, A. J.; ERSKINE, H. E.; CHARLSON, F. J.; NORMAN, R. E.; FLAXMAN, A. D.; JOHNS, N. *et al.* Global burden of disease attributable to mental and substance use disorders: findings from the global burden of disease study 2010. **The Lancet**, Elsevier, v. 382, n. 9904, p. 1575–1586, 2013. Citation on page 35.

WILCOX, R. R. **Introduction to robust estimation and hypothesis testing**. [S.l.]: Academic press, 2011. Citations on pages 107 and 129.

WILLIAM, S. The probable error of a mean. **Biometrika**, v. 6, n. 1, p. 1–25, 1908. Citation on page 110.

WINDISCHBERGER, C.; LAMM, C.; BAUER, H.; MOSER, E. Human motor cortex activity during mental rotation. **NeuroImage**, Elsevier, v. 20, n. 1, p. 225–232, 2003. Citation on page 139.

WISE, T.; MARWOOD, L.; PERKINS, A.; HERANE-VIVES, A.; JOULES, R.; LYTHGOE, D.; LUH, W.; WILLIAMS, S.; YOUNG, A.; CLEARE, A. *et al.* Instability of default mode network connectivity in major depression: a two-sample confirmation study. **Translational psychiatry**, Nature Publishing Group, v. 7, n. 4, p. e1105–e1105, 2017. Citation on page 37.

XU, Y.; ZHU, J.-Y.; ERIC, I.; CHANG, C.; LAI, M.; TU, Z. Weakly supervised histopathology cancer image segmentation and classification. **Medical image analysis**, Elsevier, v. 18, n. 3, p. 591–604, 2014. Citations on pages 38 and 39.

XU, Y.; ZOMER, S.; BRERETON, R. G. Support vector machines: a recent method for classification in chemometrics. **Critical Reviews in Analytical Chemistry**, Taylor & Francis, v. 36, n. 3-4, p. 177–188, 2006. Citation on page 88.

YAMAGATA, B.; ITAHASHI, T.; FUJINO, J.; OHTA, H.; NAKAMURA, M.; KATO, N.; MIMURA, M.; HASHIMOTO, R.-i.; AOKI, Y. Machine learning approach to identify a resting-state functional connectivity pattern serving as an endophenotype of autism spectrum disorder. **Brain imaging and behavior**, Springer, v. 13, n. 6, p. 1689–1698, 2019. Citations on pages 103, 104, and 121.

YANG, J.; SHU, H. The role of the premotor cortex and the primary motor cortex in action verb comprehension: Evidence from granger causality analysis. **Brain research bulletin**, Elsevier, v. 88, n. 5, p. 460–466, 2012. Citation on page 139.

YANG, S.; KWEON, J.; ROH, J.-H.; LEE, J.-H.; KANG, H.; PARK, L.-J.; KIM, D. J.; YANG, H.; HUR, J.; KANG, D.-Y. *et al.* Deep learning segmentation of major vessels in x-ray coronary angiography. **Scientific reports**, Nature Publishing Group, v. 9, n. 1, p. 1–11, 2019. Citations on pages 60, 89, and 108.

YANG, X.; ZHANG, N.; SCHRADER, P. A study of brain networks for autism spectrum disorder classification using resting-state functional connectivity. **Machine Learning with Applications**, Elsevier, v. 8, p. 100290, 2022. Citations on pages 105 and 129.

YILDIRIM, Ö.; BALOGLU, U. B.; ACHARYA, U. R. A deep convolutional neural network model for automated identification of abnormal eeg signals. **Neural Computing and Applications**, Springer, p. 1–12, 2018. Citation on page 46.

YU, X.; PANG, W.; XU, Q.; LIANG, M. Mammographic image classification with deep fusion learning. **Scientific Reports**, Nature Publishing Group, v. 10, n. 1, p. 1–11, 2020. Citations on pages 60, 89, 108, and 130.

ZENG, L.-L.; WANG, H.; HU, P.; YANG, B.; PU, W.; SHEN, H.; CHEN, X.; LIU, Z.; YIN, H.; TAN, Q. *et al.* Multi-site diagnostic classification of schizophrenia using discriminant deep learning with functional connectivity mri. **EBioMedicine**, Elsevier, v. 30, p. 74–85, 2018. Citation on page 126.

ZHANG, L. Eeg signals classification using machine learning for the identification and diagnosis of schizophrenia. In: IEEE. **2019 41st Annual International Conference of the IEEE Engineering in Medicine and Biology Society (EMBC)**. [S.l.], 2019. p. 4521–4524. Citation on page 149.

ZHANG, T. Solving large scale linear prediction problems using stochastic gradient descent algorithms. In: **Proceedings of the twenty-first international conference on Machine learning**. [S.l.: s.n.], 2004. p. 116. Citation on page 60.

ZHANG, Y.-j.; PU, C.-c.; WANG, Y.-m.; ZHANG, R.-t.; CAI, X.-l.; ZHOU, S.-z.; MA, Y.-t.; WANG, Y.; CHEUNG, E. F.; LUI, S. S. *et al.* Social brain network correlates with real-life social network in individuals with schizophrenia and social anhedonia. **Schizophrenia Research**, Elsevier, v. 232, p. 77–84, 2021. Citation on page 125.

ZHAO, X.; LIANG, J.; WANG, J. A community detection algorithm based on graph compression for large-scale social networks. **Information Sciences**, Elsevier, v. 551, p. 358–372, 2021. Citations on pages 57, 88, 109, and 131.

ZHONG, Z.; YUAN, X.; LIU, S.; YANG, Y.; LIU, F. Machine learning prediction models for prognosis of critically ill patients after open-heart surgery. **Scientific Reports**, Nature Publishing Group, v. 11, n. 1, p. 1–10, 2021. Citations on pages 60, 89, 108, and 130.

APPENDIX

A

GLOBAL DISEASE BURDEN STUDY METRICS

The Global Burden of Disease (GBD) Study fwas started in 1992 and is a collaboration between the Harvard School of Public Health, the World Health Organization (WHO) and the World Bank (WB) that seeks to meet the public health challenge of finding reliable and complete metrics capable of globally assessing health conditions and the causes of illness and injury to guide public policies in the next century (LOPEZ; MURRAY, 1998). This study, initially coordinated by WHO and, since 2007, by Institute for Health Metrics and Evaluation (IHME), University of Washington (United States of America - USA), presents a standardized disease analysis methodology and is therefore comparable across countries (MURRAY *et al.*, 2012).

One of the metrics used in the GBD and which was adopted by the WHO and the WB (LEITE *et al.*, 2015) was the Disability Adjusted Life Years (DALY). This synthetic measure combines information on mortality and morbidity and was originally calculated for a list of more than 100 diseases and conditions (NAGHAVI *et al.*, 2009); it also allows measuring the impact of each disease or condition on the population's health status, constituting a fundamental tool for the elaboration of policies aimed at reducing the burden of disease (MCKENNA *et al.*, 2005).

In practical terms, a DALY represents a healthy year of life lost, being calculated as the sum of two components: that of mortality, represented by the years of life lost (YLL) due to premature death, and morbidity, characterized by years of healthy life lost due to disability (YLD) (BARENDREGT; BONNEUX; MAAS, 1996). Mathematically, this metric is given by the equation A.1.

$$DALY = YLL + YLD \tag{A.1}$$

The YLL for a given cause of death is calculated as the product between the number of deaths related to that cause and the estimated life expectancy for the age at which the death occurred, according to (LEITE *et al.*, 2015) the YLL can be mathematically given by the equation

A.2.

$$YLL(c,i,s) = N(c,i,s)XE(i,s), \tag{A.2}$$

Being $N(c,i,s)$ is the number of deaths due to the cause c for the age i and sex s; while $E(i,s)$ understands life expectancy at age i and sex s. On the other hand, considering that mortality is an incident event, the YLD is calculated based on the new cases of a given disease that occurred in a specific year (MURRAY *et al.*, 2012) and can be calculated by the equation A.3.

$$YLD(c,i,s) = I(c,i,s)XD(c,i,s)XP(c,i,s), \tag{A.3}$$

where $I(c,i,s)$ is the number of incident cases due to the cause c, para a idade i and sex s; $D(c,i,s)$ refers to the average duration of disability resulting from the cause c, for the age i and sex s; and $P(c,i,s)$ understands the weight of disability related to the cause c, for age i and sex s.

An important study for mental disorders was 2015 GBD (FERRARI *et al.*, 2014), in which these disorders were defined according to the diagnostic criteria described in the International Statistical Classification of Diseases and Related Health Problems (ICD-10) (SAÚDE, 1994) or in the Diagnostic and Statistical Manual of Mental Disorders (DSM–5). These disorders total 19 groups listed below:

1. Neurodevelopmental disorders;
2. Schizophrenia spectrum and other psychotic disorders;
3. Bipolar and related disordersr;
4. Depressive disorders;
5. Anxiety disorders;
6. Obsessive-compulsive and related disorders;
7. Trauma- and stressor-related disorders;
8. Dissociative disorders;
9. Somatic symptom and related disorders;
10. Feeding and eating disorders;
11. Elimination disorders;
12. Sleep–wake disorder;
13. Sexual dysfunctions;

14. Gender dysphoria;
15. Disruptive, impulse-control, and conduct disorders;
16. Substance-related and addictive disorders;
17. Neurocognitive disorders;
18. Personality disorders;
19. Paraphilic disorders;

A.1 Machine learning algorithms for a small data set

Due to the fact that our data sets are very small since we cannot find more data in the available literature, and that CNN may suffer from this lack of data, in this section, we aim to try other classifiers that work more efficiently with small data sets.

For our best AD results using Pearson's correlation and SZ using Granger causality, we compared the following machine learning methods to classify: Support Vector Machine (SVM) (BOTTOU; LIN, 2007), Random Forest (RF) (BREIMAN, 2001), Naive Bayes (NB) (FRIEDMAN; GEIGER; GOLDSZMIDT, 1997), Multilayer Perceptron (MLP) (HINTON; RUMELHART; WILLIAMS, 1986) and extreme Gradient Boosting classifier (FRIEDMAN, 2001) (XGBoost). We used the same resampling described used with CNN model with a hyperparametric optimization called grid search whose values used for each classifier model can be found in Table 24.

We can see in the Tables 21, 22 the results of all classifiers and to AD (using the Pearson's correlation) and SZ (using the Granger causality), respectively. Note that there are no cases indicating overfitting. We can observe in Table 21 that all classifiers are able to differentiate between patients in different health conditions, as opposed to the results in Table 22 that this cannot be verified (since all classifiers performed similarly to a random classifier). Therefore, CNN was able to differentiate both cases with better performance.

Table 21 – Classification results for AD using the Pearson's correlation.

Classifier	subset	AUC	Acc.	F1 score	Rec.	Pre.
SVM	**Train**	0.95	0.95	0.95	0.95	0.95
	Test	0.91	0.91	0.91	0.91	0.92
NB	**Train**	0.76	0.76	0.76	0.76	0.77
	Test	0.70	0.69	0.69	0.70	0.70
RF	**Train**	0.98	0.98	0.98	0.98	0.98
	Test	0.96	0.96	0.96	0.96	0.96
MLP	**Train**	1.00	1.00	1.00	1.00	1.00
	Test	0.97	0.97	0.97	0.97	0.97
GBC	**Train**	0.96	0.96	0.96	0.96	0.96
	Test	0.92	0.93	0.93	0.92	0.94

Table 22 – Classification results for schizophrenia using the Granger causality.

Classifier	subset	AUC	Acc.	F1	Rec.	Pre.
SVM	**Train**	0.56	0.56	0.53	0.56	0.57
	Test	0.55	0.56	0.54	0.55	0.56
NB	**Train**	0.57	0.57	0.55	0.57	0.58
	Test	0.52	0.52	0.50	0.52	0.52
RF	**Train**	0.67	0.66	0.66	0.67	0.67
	Test	0.52	0.52	0.52	0.52	0.52
MLP	**Train**	0.64	0.63	0.60	0.64	0.72
	Test	0.59	0.59	0.56	0.59	0.61
GBC	**Train**	0.50	0.50	0.33	0.50	0.25
	Test	0.50	0.48	0.32	0.50	0.24

Table 23 – Table containing the hyper-parameters for each classifier using the Grid search optimizer.

Classifier	Hyperparameters and description	Values
RF	- max_depth: The maximum depth of the tree.	[1,2,5,10,20,80]
	- max_features: The number of features to consider when looking for the best split.	[2, 3,5,10]
	- min_samples_leaf : The minimum number of samples required to be at a leaf node.	[1,2,3, 4, 5]
	- min_samples_split: The minimum number of samples required to split an internal node.	[1,2,8, 10, 12,20]
	- n_estimators: The number of trees in the forest.	[1,2,3,5,10, 30,50,100, 200, 300,500]
SVM	-kernel: Specifies the kernel type to be used in the algorithm.	[rbf, linear]
	-gamma: Kernel coefficient.	[1e-3, 1e-4]
	-C: Regularization parameter.	[1, 10, 100, 1000]
NB	-var_smoothin:Portion of the largest variance of all features that is added to variances for calculation stability.	range 1e-09 to 1
MLP	- activation: Activation function for the hidden layer.	[identity, logistic, tanh, relu]
	- solver: The solver for weight optimization.	[lbfgs, sgd, adam]
	- alpha: L2 penalty (regularization term) parameter.	[0.0001,1e-5,0.01,0.001]
	- batch_size: Size of minibatches for stochastic optimizers.	[1000,5000]
	- learning_rate: Learning rate schedule for weight updates.	[constant, invscaling, adaptive]
	- learning_rate_init: The initial learning rate used.	[0.001,0.01,0.1,0.2,0.3]
XGBoost	- learning_rate: Learning rate shrinks the contribution of each tree.	[0.01, 0.025, 0.05, 0.075, 0.1, 0.15, 0.2]
	- min_samples_split: The minimum number of samples required to split an internal node.	range 0.1 to 0.5
	- min_samples_leaf: The minimum number of samples required to be at a leaf node.	range 0.1 to 0.5
	- max_depth: The maximum depth of the individual r egression estimators.	[3,5,8]
	- max_features: The number of features to consider when looking for the best split.	[log2, sqrt]
	- criterion: The function to measure the quality of a split.	[friedman_mse, mae],
	- subsample: The fraction of samples to be used for fitting the individual base learners.	[0.5, 0.618, 0.8, 0.85, 0.9, 0.95, 1.0],
	-n_estimators: The number of boosting stages to perform.	[10, 100. 1000, 10000]

We also vary the validation sample size, including 10% to 50% of the observation in the test set. Notice that we consider 10% of the elements in the test set to generate our results shown before. As we can see in figure 50, regardless of the sample size, the obtained AUC is higher than 0.90. We also included a k-fold cross-validation analysis for two different values of

k, namely k=4 and k=12. For AD, considering k=4, the AUC train is 0.99 and k=12, the AUC train is 0.91. Therefore, we can see that we can predict the mental disorders with high accuracy, independent of the test size and using the k-fold cross-validation technique.

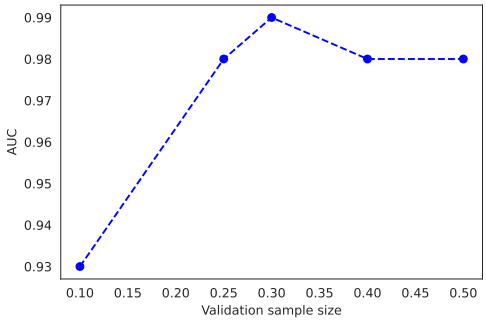

Figure 50 – The AUC according to the test size for AD.

A.2 EEG database electrodes

Figure 51 showing the head model schematic with electrodes from the EEG database used in this paper.

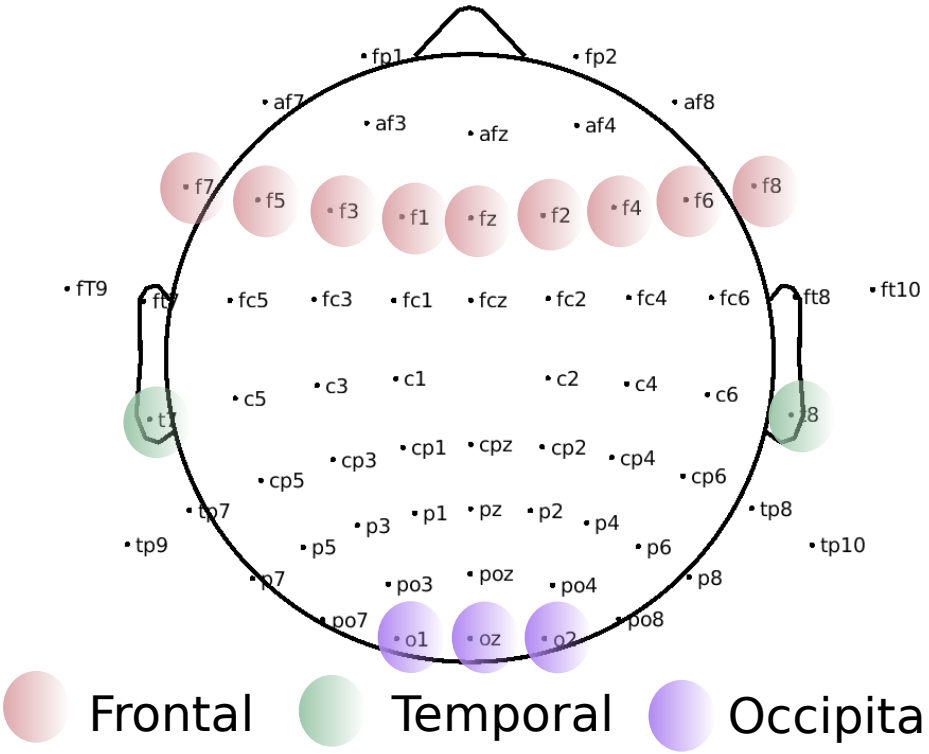

Figure 51 – **Head model for all electrodes used in the present work.** The brain regions modulated after using ayahuasca, according to literature, are the frontal, temporal, and occipital lobes, highlighted in the Fig in pink, green and purple, respectively. Developed by the authors using MNE-Python (GRAMFORT *et al.*, 2013).

A.3 Hyperparameter values of Grid Search classifier

We used grid search as an optimization method to achieve good performance, which is a method that exhaustively tests all possible combinations of values for each hyperparameter considered—the Table 24 containing each classifier, the hyperparameters, and the values used in the grid search tunning.

Table 24 – Table containing the hyperparameters for each classifier using the Grid search optimizer.

Classifier	Hyperparameters and description	Values
RF	- max_depth: The maximum depth of the tree.	[1,2,5,10,20,80]
	- max_features: The number of features to consider when looking for the best split.	[2, 3,5,10]
	- min_samples_leaf : The minimum number of samples required to be at a leaf node.	[1,2,3, 4, 5]
	- min_samples_split: The minimum number of samples required to split an internal node.	[1,2,8, 10, 12,20]
	- n_estimators: The number of trees in the forest.	[1,2,3,5,10, 30,50,100, 200, 300,500]
SVM	-kernel: Specifies the kernel type to be used in the algorithm.	[rbf, linear]
	-gamma: Kernel coefficient.	[1e-3, 1e-4]
	-C: Regularization parameter.	[1, 10, 100, 1000]
NB	-var_smoothin:Portion of the largest variance of all features that is added to variances for calculation stability.	range 1e-09 to 1
MLP	- activation: Activation function for the hidden layer.	[identity, logistic, tanh, relu]
	- solver: The solver for weight optimization.	[lbfgs, sgd, adam]
	- alpha: L2 penalty (regularization term) parameter.	[0.0001,1e-5,0.01,0.001]
	- batch_size: Size of minibatches for stochastic optimizers.	[1000,5000]
	- learning_rate: Learning rate schedule for weight updates.	[constant, invscaling, adaptive]
	- learning_rate_init: The initial learning rate used.	[0.001,0.01,0.1,0.2,0.3]
SGD	- loss: The loss function to be used	[hinge, log, squared_hinge, modified_huber]
	- alpha: Constant that multiplies the regularization term. The higher the value, the stronger the regularization.	[0.0001, 0.001, 0.01, 0.1]
	- penalty: The penalty (regularization term) to be used.	[l2, l1, none]
LR	- C: Each of the values in Cs describes the inverse of r egularization strength.	range 0.001 to 1000
	- penalty: Specify the norm of the penalty.	[l1, l2]
XGBoost	- learning_rate: Learning rate shrinks the contribution of each tree.	[0.01, 0.025, 0.05, 0.075, 0.1, 0.15, 0.2]
	- min_samples_split: The minimum number of samples required to split an internal node.	range 0.1 to 0.5
	- min_samples_leaf: The minimum number of samples required to be at a leaf node.	range 0.1 to 0.5
	- max_depth: The maximum depth of the individual r egression estimators.	[3,5,8]
	- max_features: The number of features to consider when looking for the best split.	[log2, sqrt]
	- criterion: The function to measure the quality of a split.	[friedman_mse, mae],
	- subsample: The fraction of samples to be used for fitting the individual base learners.	[0.5, 0.618, 0.8, 0.85, 0.9, 0.95, 1.0],
	-n_estimators: The number of boosting stages to perform.	[10, 100. 1000, 10000]

A.4 Results of all classifier in the complex network measures

In the present study, we tested several machine learning algorithms whose performance is shown in the Table 25.

Table 25 – Performance of all classifiers applied to the network measurements. In bold the best performance referring to the SVM classifier.

Classifier	Subset	AUC	Acc.	F1 score	Recall	Precision
RF	**Train**	0.69	0.75	0.70	0.69	0.72
	Test	0.44	0.58	0.37	0.44	0.32
SVM	**Train**	**0.79**	**0.81**	**0.78**	**0.79**	**0.79**
	Test	**0.75**	**0.83**	**0.79**	**0.75**	**0.90**
NB	**Train**	0.83	0.86	0.84	0.83	0.85
	Test	0.50	0.67	0.40	0.50	0.33
MLP	**Train**	1.00	1.00	1.00	1.00	1.00
	Test	0.50	0.67	0.40	0.50	0.33
SGD	**Train**	0.75	0.78	0.75	0.75	0.75
	Test	0.56	0.67	0.55	0.56	0.60
LR	**Train**	0.83	0.86	0.84	0.83	0.85
	Test	0.63	0.75	0.62	0.63	0.86
XGBoost	**Train**	0.98	0.97	0.97	0.98	0.96
	Test	0.38	0.50	0.33	0.38	0.3

A.5 Deep learning results

Additionally, Pearson's connectivity matrix was used as an input to the deep learning algorithm implemented in (ALVES *et al.*, 2022b) with random research tuning. The results are shown in Table 26 and Fig 52, in which it can be seen that it was possible to capture the alteration due to ayahuasca without an indication of underfitting and overfitting. Also, the python code used for the analysis is available at: <https://github.com/Carol180619/Paper-ayahuasca.git>.

Table 26 – Results were obtained by the use of the deep learning model.

Subset	AUC	Acc.	F1 score	Recall	Precision
Train	1.00	1.00	1.00	1.00	1.00
Test	0.96	0.94	0.94	0.94	0.94

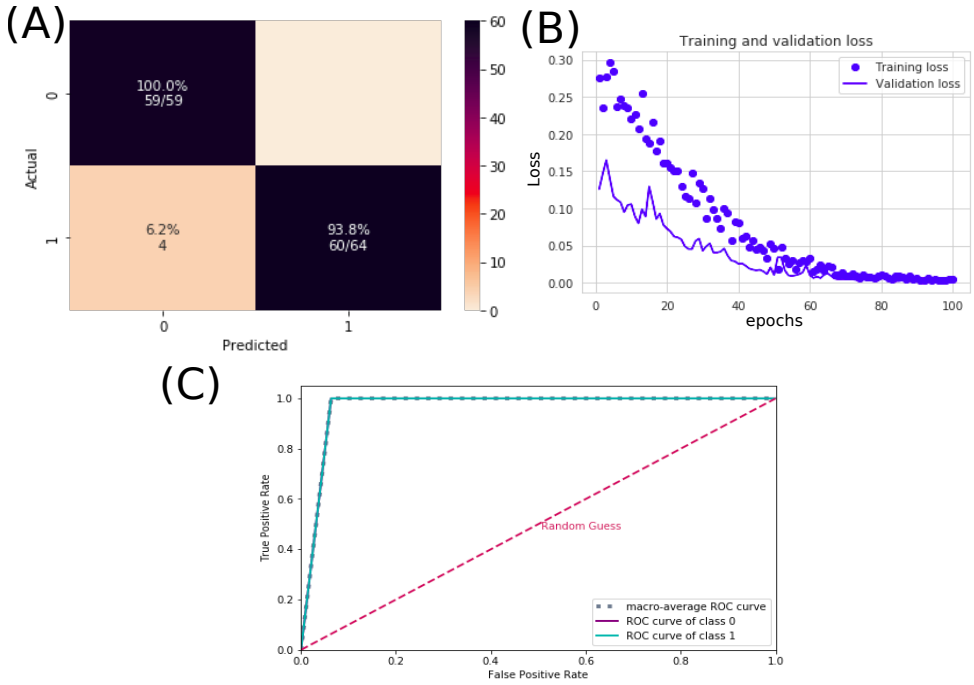

Figure 52 – **Results were obtained by the use of the deep learning model.** A) The confusion matrix indicates a true negative rate of 93.8% (blue according to the color bar) and a true positive rate of 100.0% (blue according to the color bar). B) Loss value over the training data (blue dots points) and validation data (blue line) after each epoch; in this curve, the error loss decreases, indicating no underfitting or overfitting. C) ROC curve of class 0 (without ayahuasca) and class 1 (with ayahuasca). The gray dotted curve is the macro-average accuracy (area under curve = 0.96), and the pink one is the random classifier.

A.6 Grid search hyperparameter tuning

Figure 53 contains the values used in the present work where for one of the models (considering all frequencies and comparison of DMT and open eyes control), the combination of hyperparameter values and the grid search was plotted concerning the AUC metric.

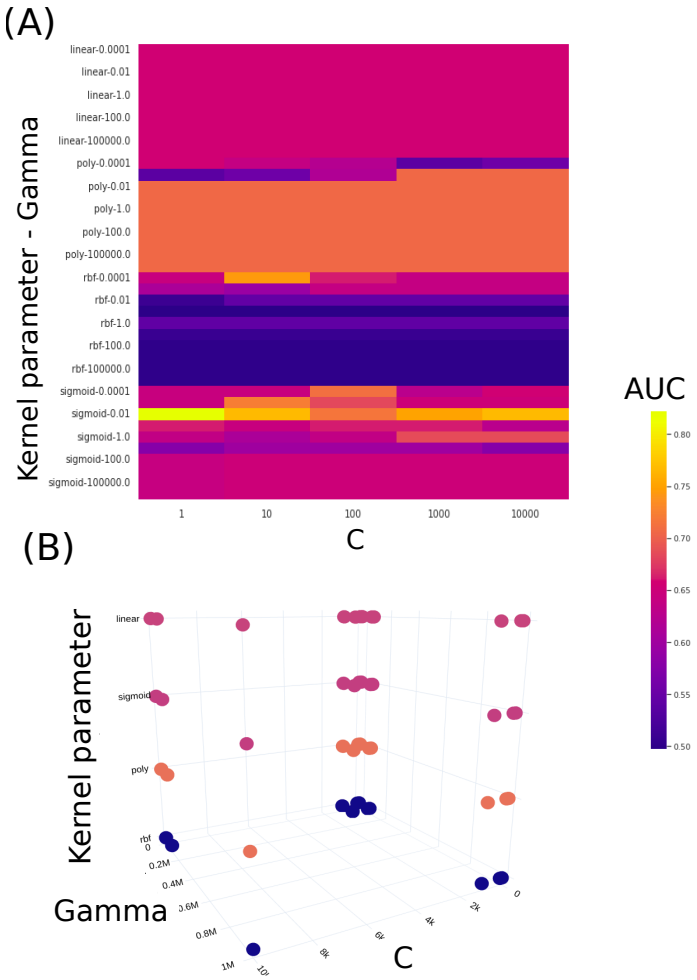

Figure 53 – Figure containing the values of each hyperparameter of the SVM varied with the grid search. In (A), for the model considering all frequencies and comparing the subject DMT and without DMT with the eye closed, the two-dimensional plot with the x-axis being the values of the parameter C and the y-axis being the values of the kernel and gamma function. For each combination of values and hyperparameters, AUC performance was obtained (whose obtained values are illustrated in the color table). In (B), the three-dimensional plot of (A) in which each hyperparameter corresponds to an axis.

A.7 Results comparing different band frequencies

Table 27 – The table contains results considering different band frequencies.

Band frequencies	Subset	AUC	Acc.	F1 score	Recall	Precision
All frequencies	**Train**	0.90	0.90	0.90	0.90	0.90
	Test	0.67	0.67	0.67	0.67	0.68
Low alpha	**Train**	1.00	1.00	1.00	1.00	1.00
	Test	0.67	0.67	0.67	0.67	0.67
High alpha	**Train**	**1.00**	**1.00**	**1.00**	**1.00**	**1.00**
	Test	**0.72**	**0.72**	**0.72**	**0.72**	**0.73**
Low beta	**Train**	**0.98**	**0.98**	**0.98**	**0.98**	**0.98**
	Test	**0.78**	**0.78**	**0.78**	**0.78**	**0.78**
Mid beta	**Train**	0.98	0.98	0.97	0.98	0.98
	Test	0.45	0.47	0.40	0.45	0.42
High beta	**Train**	1.00	1.00	1.00	1.00	1.00
	Test	0.56	0.56	0.45	0.56	0.76
Gamma	**Train**	0.67	0.67	0.67	0.67	0.67
	Test	0.44	0.44	0.42	0.44	0.43
Delta	**Train**	**1.00**	**1.00**	**1.00**	**1.00**	**1.00**
	Test	**0.72**	**0.72**	**0.72**	**0.72**	**0.73**
Theta	**Train**	0.61	0.61	0.61	0.61	0.61
	Test	0.50	0.50	0.50	0.50	0.50

A.8 Results considering complex network measures and different frequencies band

Table 28 – The table contains results considering complex network measures and different band frequencies.

Band frequencies	AUC	Acc.	F1 score	Recall	Precision	
All frequencies	**Train**	1.00	1.00	1.00	1.00	1.00
	Test	0.69	0.69	0.68	0.69	0.73
Low alpha	**Train**	1.00	1.00	1.00	1.00	1.00
	Test	0.72	0.72	0.70	0.72	0.82
High alpha	**Train**	1.00	1.00	1.00	1.00	1.00
	Test	0.61	0.61	0.54	0.61	0.76
Low beta	**Train**	1.00	1.00	1.00	1.00	1.00
	Test	0.56	0.56	0.56	0.56	0.56
Mid beta	**Train**	0.98	0.98	0.98	0.98	0.98
	Test	0.45	0.47	0.40	0.45	0.42
High beta	**Train**	1.00	1.00	1.00	1.00	1.00
	Test	0.56	0.56	0.45	0.56	0.76
Gamma	**Train**	1.00	1.00	1.00	1.00	1.00
	Test	0.17	0.17	0.14	0.17	0.13
Delta	**Train**	**1.00**	**1.00**	**1.00**	**1.00**	**1.00**
	Test	**0.89**	**0.89**	**0.88**	**0.88**	**0.91**
Theta	**Train**	1.00	1.00	1.00	1.00	1.00
	Test	0.50	0.50	0.33	0.50	0.25

A.9 Similarity of results obtained for each frequency

The SHAP value calculated for each frequency band was also considered. For each band, a vector of connection between electrode pairs and its respective SHAP value found by the model is generated. For each of these vectors, the Euclidean distance between them is then calculated, generating a distance matrix of these vectors. This aims to quantify how close the resulting vectors are. The distance matrix is displayed as a cluster map, see Figure 54, where vectors with a distance less than 0.2 are connected hierarchically in a dendrogram indicating clusters. Here, the cluster is most prominent between the low beta and the delta frequency band vector.

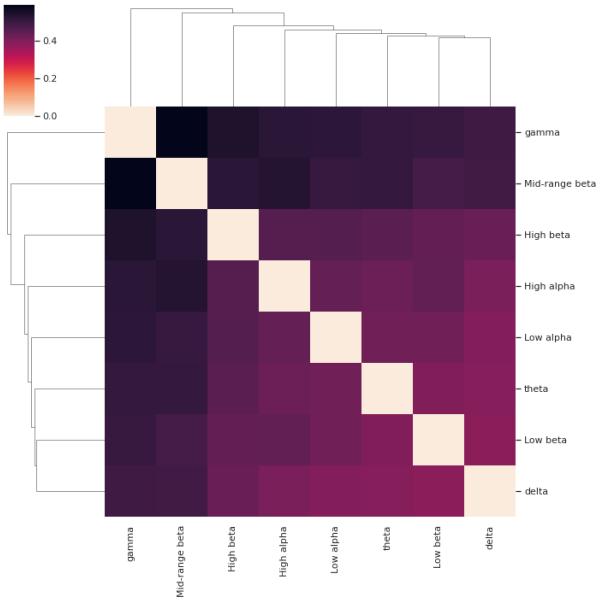

Figure 54 – Cluster map with the Euclidean distance of each band SHAP value vector. The delta bands and low beta frequencies are the closest frequencies, forming in the cluster map a connection.

The same was made for the complex network measure, and then, a cluster map with the Euclidean distance between vectors containing SHAP values for each complex network measure is generated (see Figure 55). All vectors, except low beta, are very close to each other. This proximity indicates that the results obtained were similar; in other words, the connections between the electrodes and their respective SHAP value were similar for all frequency bands. Thus, it can be seen that the results of the SHAP value vectors of each frequency, except for the low beta frequency, were very close, showing remarkable similarities between them.

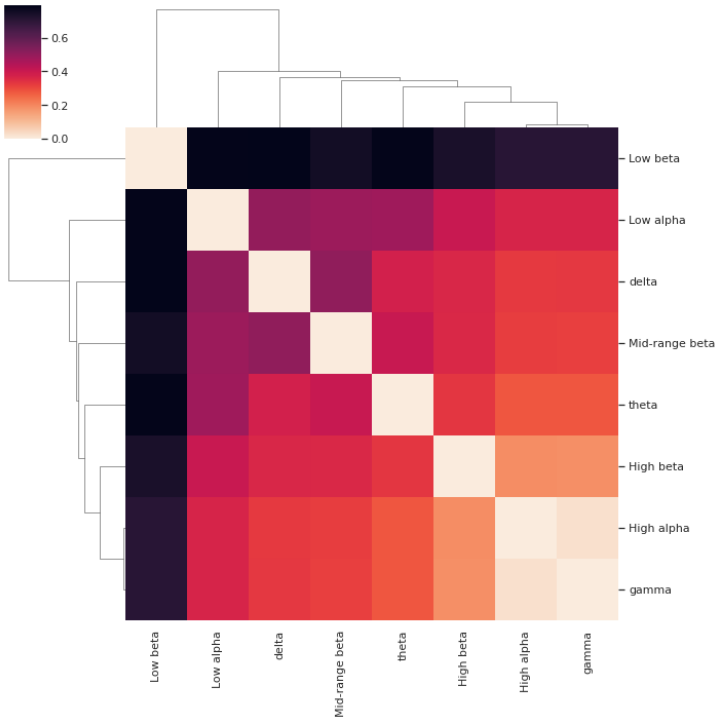

Figure 55 – Cluster map showing the Euclidean distance of the SHAP value vectors for different frequency bands. Frequency band vectors, except low beta, are very close to each other, indicating remarkable similarity.

A.10 Boxplot with the best measures of complex networks

Figure 56 contains the best measurements of complex networks using the SHAP value method. Further, a Wilcoxon test with Bonferroni correction was also used to compare the measurements before and after DMT, and the following symbols represent the statistical significance:

- ns: $5.00e-02 < p <= 1.00e+00$
- *: $1.00e-02 < p <= 5.00e-02$
- **: $1.00e-03 < p <= 1.00e-02$
- ***: $1.00e-04 < p <= 1.00e-03$
- ****: $p <= 1.00e-04$

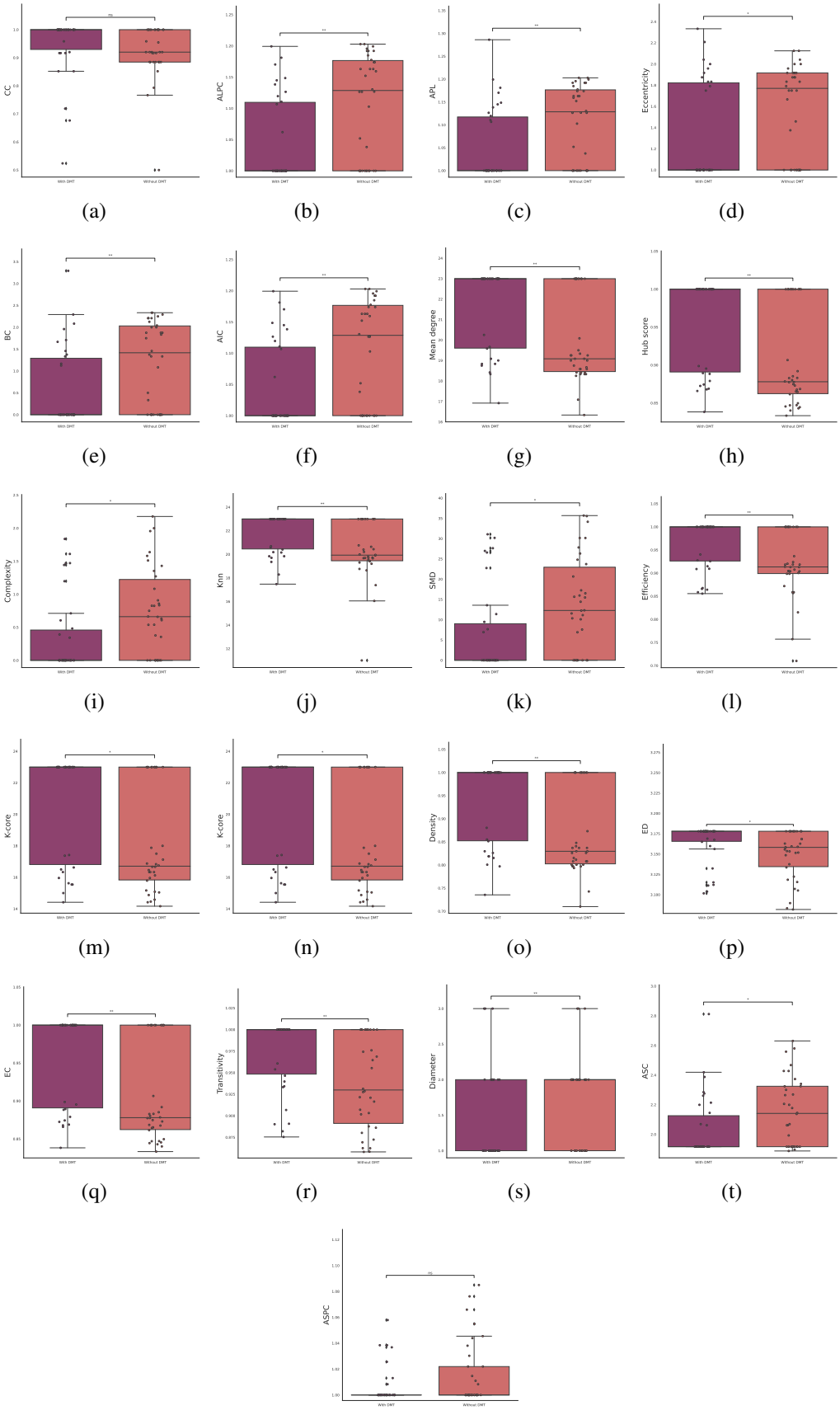

(a) (b) (c) (d)

(e) (f) (g) (h)

(i) (j) (k) (l)

(m) (n) (o) (p)

(q) (r) (s) (t)

(u)

Figure 56 – Boxplot showing the best complex network measures. A Wilcoxon test with Bonferroni correction was also used to compare the measurements before (in pink) and after DMT (in purple).

A.11 fMRI best pairwise metrics

Table 29 contains the all pairwise metrics results.

Table 29 – Results were obtained regarding the metrics used to obtain the connectivity matrix. The best metric was TE, whose performance is highlighted.

Data abstraction level	Subset	AUC	Acc.	Recall	Precision
time series	**Train**	0.50	0.50	0.40	0.30
	Test	0.50	0.51	0.50	0.26
PC	**Train**	0.57	0.57	0.59	0.56
	Test	0.42	0.43	0.43	0.41
SC	**Train**	0.57	0.56	0.57	0.58
	Test	0.35	0.35	0.35	0.35
GC	**Train**	0.48	0.47	0.36	0.43
	Test	0.40	0.40	0.40	0.37
SCC	**Train**	0.49	0.47	0.35	0.40
	Test	0.45	0.46	0.45	0.37
LW	**Train**	0.45	0.43	0.31	0.34
	Test	0.56	0.57	0.56	0.57
CC	**Train**	0.71	0.71	0.71	0.74
	Test	0.68	0.67	0.68	0.68
MI	**Train**	0.50	0.50	0.40	0.26
	Test	0.50	0.51	0.50	0.26
TE	**Train**	**0.99**	**0.99**	**1.00**	**0.99**
	Test	**0.92**	**0.92**	**0.92**	**0.92**

A.12 Deep Learning architetrure

Two approaches for the CNN architectures are proposed here, one using a Random Search tuning method (CNN_{tuned}) and another without this optimization step ($CNN_{untuned}$). Tuning is an optimization approach for determining hyperparameter values to improve the performance of the CNN model (GOODFELLOW; BENGIO; COURVILLE, 2016).

In the CNN_{tuned} model, the dropout regularization technique is employed to avoid overfitting (SRIVASTAVA *et al.*, 2014). The layers and range used for hyperparameters are presented in table 30. The best CNN_{tuned} architectures tuned for each data set are depicted in table 31. The $CNN_{untuned}$ model presents fewer layers and, therefore, lower computational costs. The parameters used in our analysis are described in table 32.

Table 30 – Best hyperparameters and layer configurations obtained for the CNN_{tuned} model.

Type of Layer	**Tuning hyperparameter**	**Value**
Convolutional	—	—
Convolutional	dropout	[0.00, 0.05, 0.10, 0.15, 0.20, 0.25, 0.30, 0.35, 0.40, 0.45, 0.50]
Convolutional	—	—
Convolutional	number of filters	[32, 64]
Max Pooling	dropout	[0.00, 0.50, 0.10, 0.15, 0.20]
Flatten	—	—
Dense	- units -activation	[32, 64, 96....512] [relu, tanh, sigmoid]
Dropout	rate	[0.00, 0.50, 0.10, 0.15, 0.20]
Adam optimization compile	learning rate	$min - value = 1e^{-4}$ $max - value = 1e^{-2}$ sampling= LOG

The learning curve and ROC curve obtained for the $CNN_{untuned}$ model are found in Figure 57.

Furthermore, the LSTM parameters used in our analysis are described in table 33.

The learning curve and ROC curve obtained for the LSTM model are found in Figure 58.

Table 31 – The CNN_{tuned} model used in the SCZ dataset is the network architecture.

Type of Layer	Output Shape (AD)		Parameter
Convolutional	(None, 122, 122, 1)	160	
Convolutional	(None, 119, 119, 32)	2320	
max-pooling	(None, 59, 59, 32)	0	
dropout	(None, 56, 56, 16)	0	
Convolutional	(None, 28, 28, 16)	4640	
Convolutional	(None, 2, 2, 32)	9248	
max-pooling	(None, 1, 1, 32)	0	
dropout	(None, 1, 1, 32)	0	
flatten	(None, 32)	0	
dense	(None, 160)	5280	
dropout	(None, 160)	0	
dense	(None, 2)	3	

Table 32 – The network architecture for the $CNN_{untuned}$ model used in the SCZ dataset.

Type of Layer	Output Layer	Kernel
Input Layer	(None, 122, 122, 1)	0
Convolution	(None, 119, 119, 32)	544
Max pooling	(None, 59, 59, 32)	0
Convolution	(None, 56, 56, 16)	8208
Max pooling	(None, 28, 28, 16)	0
Flatten	(None, 12544)	0
Fully connected	(None, 10)	125450
Fully connected	(None, 1)	11

Table 33 – The network architecture for the LSTM model used in the SCZ dataset.

Type of Layer	Output Layer	Param
LSTM	(None, 122, 70)	54040
LSTM	(None, 122, 60)	31440
LSTM	(None, 122, 50)	22200
LSTM	(None, 40)	14560
Dense	(None, 2)	82

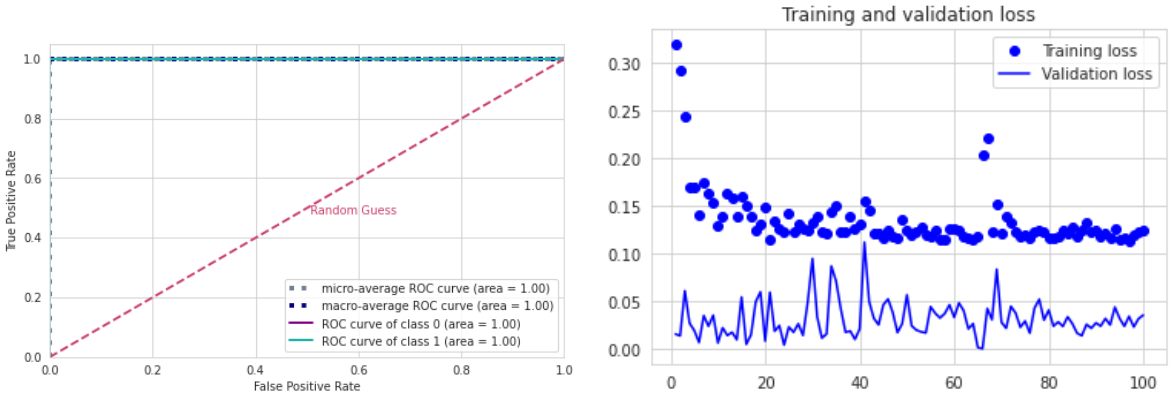

Figure 57 – CNN$_{untuned}$ model results using fMRI connectivity matrices. (a) ROC curve with class 0 (control) and class 1 (with SCZ). (b) Each epoch loses the training (blue dots) and validation (blue line).

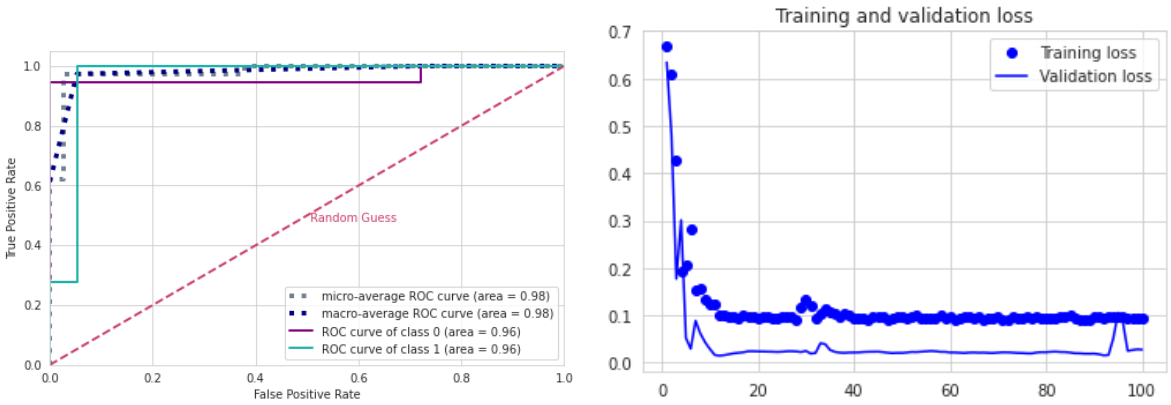

Figure 58 – LSTM model results using fMRI connectivity matrices. a) ROC curve with class 0 (control) and class 1 (with SCZ). (b) Each epoch loses the training (blue dots) and validation (blue line).


ICMC
USP
SÃO CARLOS